Studying the Physical Stability of BSA at the Bulk Solution and Oil/Water Interface

Paulina Guzman Fuhrer

(Pharmaceutical Chemistry, University of Chile)

A thesis submitted for the degree of
Doctor of Philosophy
University of Otago, Dunedin, New Zealand

In collaboration with University of Copenhagen, Denmark

September, 2014

To my family

PREFACE

"Don't worry about a thing,
'Cause every little thing gonna be alright.
Singing' "Don't worry about a thing,
'Cause every little thing gonna be alright!"

Rise up this mornin',
Smiled with the risin' sun,
Three little birds
Pitch by my doorstep
Singin' sweet songs
Of melodies pure and true,
Saying', ("This is my message to you")

"Don't worry about a thing,
'Cause every little thing gonna be alright.
Singing' "Don't worry about a thing,
'Cause every little thing gonna be alright!"

Three little birds
Bob Marley

ABSTRACT

Proteins are being used as therapeutic active components by the pharmaceutical industry. However, protein drugs may suffer physical and chemical degradation as results of protein purification and formulation. The physical stability of proteins in solution may be affected by the interaction of proteins with surrounding molecules at the bulk phase (i.e. protein-protein, protein-water, protein-excipients), as well as protein adsorption to interfaces (i.e. solid-liquid, liquid-liquid and air-liquid). The objective of this thesis was to study the physical stability of proteins, at the bulk solution and oil-water interface, using bovine serum albumin (BSA). In particular, two hypotheses were stated, defining the specific objectives of the study: 1) spectroscopy and multivariate analysis (MVA) could be used to develop methods of protein characterization and quantification, able to detect small amount of unfolded proteins in the bulk solution, and 2) the adsorption of native protein to liquid-liquid interfaces is affected by the presence of unfolded proteins and excipients in the bulk solution.

BSA was dissolved in distilled water to prepare native BSA solutions at 1% w/w and 5% w/w. Samples were heated at 90°C for 30 minutes to prepare heat-denatured BSA solutions. Binary mixtures of native and heat-denatured BSA were prepared over the range of 100% to 50% w/w native BSA. These solutions were analysed using spectroscopy and chromatography methods. FTIR and fluorescence spectra were modified using diverse pre-processing methods like the second derivative (2^{nd}D), area normalization (AN), baseline correction (BC), multiplicative scatter correction (MCS) and standard normal variate (SNV). These pre-processing techniques were used to investigate which of those techniques (or combination of techniques) help to visualise changes in the secondary and tertiary structure of proteins, as consequence of protein heat-denaturation. Additionally, these pre-processing methods were also used to study their capacity to reduce the spectral noise and increase the linearity between the spectral signal and protein concentration. These pre-processed spectra were then used to build partial least-square (PLS) regression models.

FTIR and fluorescence pre-processed spectra were used to quantify native protein concentration in the binary mixtures using PLS regression models. The quality of the PLS models was assessed by comparing the number of PLS factors, correlation coefficient (R^2), root mean square error of calibration (RMSEC) and root mean square error of prediction (RMSEP) in the calibration and prediction sets, respectively. In the case of FTIR spectroscopy, spectra were pre-processed using 2^{nd}D, BC and AN which explained the model using three PLS factors; RMSE= 0.91% and 1.64% and R^2= 0.997 and 0.991 for the calibration and prediction sets, respectively. In the case of fluorescence spectroscopy, the best PLS model was obtained for spectra pre-processed using AN and BC. This model used one PLS factor to explain the 99% of the spectra variability, RMSE% = 1.38% and 1.32% and R^2 of 0.993 and 0.994 for the calibration and prediction, respectively.

The physical stability of proteins is affected by its adsorption to interfaces. The adsorption of globular proteins like BSA to oil-water interfaces starts with protein diffusion from the bulk solution to the interface. If this interaction is favourable, proteins may undergo attachment, molecular relaxation and conformational rearrangement at the interface. At the equilibrium, the interface will be covered by a monolayer of proteins, which further evolves to a multilayer. Increases of G' and G" moduli were observed from solutions of native BSA alone, as well as from solutions of heat-denatured BSA (0.15 mM) (90°C for 30 min). The resulting maximum G' value was lower in the presence of heat-denatured protein than for the native protein alone. Addition of heat-denatured BSA (0.07 mM) to the native protein solutions decreased the maximum elastic modulus reached at equilibrium (G' 42 ± 6 mN/m) but giving similar G" (9 ± 1 mN/m) compared to native BSA alone. The delay in the protein adsorption to interfaces was attributed to differences between native and heat-denatured BSA proteins like: surface activity, protein flexibility and protein conformation (globular vs. extended), which may affect protein diffusion and adsorption to the oil-water interface.

The physical stability of proteins is also influenced by protein interaction with excipients presents in the bulk solution or at the interfaces. Excipients may prevent or increase protein adsorption to interfaces (i.e. NaCl, polymers: PBuA-PDMAEMA and PDMAEMA and phospholipids: DPPC, DSPG-Na and DSPC). NaCl at concentrations of 0.1 M and 0.5 M

increased BSA adsorption to the oil-water interface giving values of G' and G" moduli of 35 ± 20 mN/m and 90 ± 2 mN/m (0.1 M) and 25 ± 6 mN/m and 10 ± 0.2 mN/m (0.5 M), respectively. Native BSA in the presence of NaCl (1 M) showed reduced protein adsorption to the oil-water interface giving a lower value of G' (10 ± 1 mN/m) and G" (7 ± 0.5 mN/m) moduli than for native BSA alone (27 ± 2 mN/m) and 10 ± 1 mN/m, respectively. In the case of native BSA interacting with phospholipids at the interface, results show an initial increase in the G' and G" moduli followed by a progressive decrease in G' and G" moduli from 1×10^{-2} N/m to 1×10^{-4} N/m, for the highest concentration of DPPC (1×10^{-3} % w/w). In the presence of polymers, the magnitude of G' and G" moduli for native BSA alone (i.e. 27 ± 2 mN/m and 10 ± 1 mN/m, respectively) was reduced to 8 ± 3 mN/m (G' modulus) and 4 ± 1 mN/m (G" modulus) for native BSA in the presence of PDMAEMA (8.75×10^{-3} % w/v) and, 7 ± 10 mN/m (G' modulus) and 3 ± 4 mN/m (G" modulus) for native BSA in the presence of PBuA (8.75×10^{-3} % w/v). The decrease in the interfacial tension measurements (IFT) for native BSA in the presence of excipients was attributed to an increase in protein adsorption or excipient adsorption to interfaces, which was higher for native BSA in the presence of NaCl (0.5 M, 0.1 M and 1 M) than for BSA in the presence of phospholipids and polymers.

In conclusion, FTIR and fluorescence pre-processed spectra in combination with PLS regressions gave a suitable method to characterize and quantify native protein content in the bulk solution. Interfacial measurements confirmed that the kinetic and mechanism of native protein adsorption to interfaces is affected by the presence of heat-denatured BSA in the bulk solution, as well as due to the presence of excipients in the bulk phase (i.e. NaCl and polymers), or at the oil phase (i.e. phospholipids).

PUBLICATIONS

Publications that have arisen from work associated with this thesis

International peer-reviewed journals

Publications (Communication):

Guzman, P., Medlicott, N.J., Rades, T., Jorgensen, L., Baldursdottir, S.G. (2012). *Studying the adsorption of protein at the oil-water interface*. Electronic conferences in Pharmaceutical Science (ECPS).

Publications (in preparation):

Guzman, P., Medlicott, N.J., Rades, T., Jorgensen, L., Baldursdottir, S.G. (in preparation Colloid Surface B). Preventing multilayer formation using rheology and interfacial tension measurements.

Guzman, P., Medlicott, N.J., Rades, T., Jorgensen, L., Baldursdottir, S.G. (in preparation Langmuir). Characterization of protein adsorption to the oil-water interface using a rheology and interfacial tension measurements.

Guzman, P., Baldursdottir, S., Jorgensen, L., Strachan, C., Rades, T., Medlicott, N.J. (in preparation J Pharm Pharmacol). Multivariate analysis for the quantification of protein structure from FTIR and fluorescence spectroscopy.

Conferences Presentations

Poster presentations:

Guzman, P., Baldursdottir, S.G., Jorgensen, L., Strachan, C., Rades, T., Medlicott, N.J. (2012). Quantification of protein physical stability using spectroscopy and partial least square regression. *Proceedings of the American Association of Pharmaceutical Scientists (AAPS) Annual Meeting and Exposition*, Abstract ID W5315, Chicago, USA.

Guzman, P., Medlicott, N.J., Rades, T., Jorgensen, L., Baldursdottir, S.G. (2012). Adsorption of native and denatured BSA to the oil-water interface investigated using rheology and interfacial tension measurements**.** *Proceedings of the American Association of Pharmaceutical Scientists (AAPS) Annual Meeting and Exposition*, Abstract ID M1254, Chicago, USA.

Guzman, P., Medlicott, N.J., Rades, T., Jorgensen, L., Baldursdottir, S.G. (2012). Characterization of protein (BSA) adsorption to the water-oil interface. *Proceedings of the 243rd American Chemical Society National Meeting & Exposition*, Abstract ID 399, San Diego, USA.

Oral presentations:

Guzman, P., Baldursdottir, S., Jorgensen, L., Strachan, C., Rades, T., Medlicott, N.J. (2011). Prediction of Native Protein Concentration using FTIR, Fluorescence and Multivariate Analysis. *Proceedings of the 13th Annual Conference of Formulation and Delivery of Bioactives in association with the New Zealand Chapter of Controlled Release Society* , Dunedin, New Zealand.

Guzman, P., Baldursdottir, S., Jorgensen, L., Strachan, C., Rades, T., Medlicott, N.J. (2010). Multivariate analysis of protein physical stability. *Proceedings of the Australian Pharmaceutical Science Association (APSA)*. Brisbane, Australia.

Courses approved:

PhD course "Analytical Methodology in Protein Formulation Development" at Faculty of Pharmaceutical Sciences, University of Copenhagen, Denmark (14-18 November, 2011).

ACKNOWLEDGMENTS

I want to thank to my supervisors Dr. Natalie Medlicott, Dr. Stefania Baldursdottir, Professor Thomas Rades and Dr. Lene Jorgensen who have provided their guidance, support, motivation and excellent supervision through the length of this project.

I would like to thanks to the Department of Pharmacy, Faculty of Health and Medical Science, University of Copenhagen, Denmark for all the facilities to the development of Chapters 4 and 5 of this thesis as well as for the travel stipend to participate at ACS 2012. I would especially thanks to Dr. Stefania, Dr. Lene and the research groups (4^{th} and 7^{th} floors) for kindly received me and make me feel like one more of their students which make my stay at Copenhagen really enjoyable. I also wish to thanks to Sultan for her contribution with experiments of BSA protein in the presence of polymers.

At the School of Pharmacy, University of Otago, I would like to thank the academic staff, technicians and general staff as well as to all my fellow postgraduate students for their company during these years especially to Natalie's research team Emma, Farruk, Katie, Pummy and Sara.

The School of Pharmacy University of Otago is acknowledged for providing the financial support to the development of this PhD project as well as for the financial support to participate in conferences.

This PhD could not be done without the generous support and confidence of my husband Cristobal, the love of my little Vicente and the understanding and patient of my family in Chile.

TABLE OF CONTENTS

LIST OF TABLES

LIST OF FIGURES

LIST OF ABBREVIATIONS

A_{220}	Absorbance at 220 nm
AN	Area normalization
ATR	Attenuated total reflectance spectroscopy
bFGF	basic fibroblast growth factor
BC	Baseline correction
BSA	Bovine serum albumin
CaF_2	Calcium fluorure
CD	Circular dichroism spectrosocopy
CV	Coefficient of variation
DPPC	Dipalmitoylphosphatidylcholine
DSPC	Distearoylphosphatidylcholine
DSPE	Distearoylphosphatidylethanolamine
DSPG-Na	1, 2-distearoyl-sn-glycero-3-phophoglycerol sodium salt
DWR	Double wall ring geometry
FDA	Food and drug administration
FTIR	Fourier transformed infrared spectroscopy
G'	Elastic modulus
G"	Viscous modulus
HAS	Human serum albumin
Hz	Hertz
IFT	Interfacial tension
IFT_{30}	Interfacial tension at t=30 min
IFT_0	Interfacial tension at t=0 min
IR	Infrared
M	Molar
mM	milli Molar
min	Minutes
MCR-ALS	Multivariate curve resolution-alternating least squares

MSC	Multiplicative scanner correction
MVA	Multivariate analysis
mN	millinewton
mN/m	millinewton per meter
nm	nanometer
Nm	Newton meter
Ns/m	Newton second per meter
P	P-value
PBuA	PDMAEMA-PBuA$_{38700}$-PDMAEMA$_{33000}$
PDMAEMA	Poly(N,N-Dimethylaminoethyl metacrylate
PDI	Polydispersity index
pI	Isolectric point
PLS	Partial least square
PLS-DA	Protein structure determination
iPLS	Interval partial least –square
Phe	Phenylalanine
R^2	Correlation coefficient
rad/sec	radian per second
RMSEC	Root mean square error of calibration
RMSEP	Root mean square error of prediction
RT	Room temperature
SEC	Size exclusion chromatography
SNV	Standard normal variate
Tm	Melting temperature
Trp	Tryptophan
Tyr	Tyrosine
1st D	First derivative
2nd D	Second derivative
%w/w	percentage weight/weight

Chapter 1: Review of the Literature

1.1. General background

Protein drugs are an important class of therapeutic agents. In the last few years, the number of biopharmaceuticals has significantly increased to include classes of drugs such as therapeutic monoclonal antibodies and hormones as well as new vaccine antigens [1-6]. For protein drugs, however, major obstacles still exist for delivery to the body due to their large molecular size, poor permeability through biological membranes, relatively labile amide backbone, and the need to maintain conformation stability (secondary, tertiary and sometimes quaternary structures) for their biological effect [7]. For these reasons, products have typically been relatively simple solutions for parenteral administration by intravenous, intramuscular or subcutaneous routes [8-10]. Hence, a goal of drug delivery research is to allow development of a greater range of dose-concentration effect for protein bioactives [11]. To progress towards this goal understanding of interactions at the molecular level, which influence protein physical stability in dosage forms during processing, storage and use need to be explored. From new understanding, strategies or formulation excipients that maximize protein chemical and physical stability may be identified. This may provide the necessary platform on which rationale development of advanced dosage forms for protein drugs can occur.

1.2. Proteins as drugs or therapeutics

In recent years, the use of proteins as drugs have increased due to advances in the area of biotechnology and molecular biotechnology which have led to the discovery of functional proteins with therapeutic properties[12]. The European Union and FDA have approved more than 200 protein drugs from the 1980s to 2012 and this number is expected to continue growing [13-16]. So far, protein drugs are mainly based on endogenous cytokines, protein hormones and antibodies [1] and these have been used to treat diseases like cancer, diabetes, hemophilia, rheumatoid arthritis, Crohn's disease and hepatitis [13].

1.3. Proteins: definition and structure

Proteins are polymers formed by the combination of up to 20 different amino acids. The individual amino acids can be classified as polar (hydrophilic), non-polar (hydrophobic) and charged (basic or acidic amino acids) (**Table 1.1**) [7,17]. The overall protein hydrophilicity/hydrophobity has been estimated by Maldonado *et al.* (2010) from the sum of the individual amino acids [18].

Table 1.1 Classification of amino acids based on their polar, non-polar and charged amino acids [7,17].

Classification of amino acids	Amino acids residue
Polar	serine, threonine, cysteine, tyrosine, asparagine and glutamine
Non-polar	glycine, alanine, valine, leucine, isoleucine, methionine, phenylalanine, tryptophan and proline
Charged	Acidic: aspartic acid and glutamic acid Basic: lysine, arginine and histidine

The basic structure of proteins comprises on a main chain of repeating units (-N-C_α-(C=O)N-C_αHR-(C=O)-), a variable side chains (R: atoms attached to C_α) and free amino and carboxy termini at each end of the side chain (**Figure 1.1**) [19]. The side chain group confers chemically and physically characteristics to each amino acid [17].

Basic structure of proteins: NH_2-C_αHR-COOH

Acid medium ⟵ Isoelectric point ⟶ Basic medium

$^+NH_3$-C_αHRCOOH ⟵ $^+NH_3$-C_αHRCOO^- ⟶ NH_2-C_αHRCOO^-

Figure 1.1 General structure of proteins representing the ionized and unionized forms of amino acids. Proteins are overall neutral when the solution pH equals its isoelectric point [20].

1.4. Description of protein structure organization

The structure of proteins is organized into four levels: primary, secondary, tertiary and quaternary. The primary structure corresponds to the sequence of amino acids, obtained by the association between the amino terminus of one amino acid and the carboxyl terminus of the following amino acid by covalent bonds [7]. The secondary structure corresponds to the folding of amino acid chains between the amide and carbonyl groups by hydrogen bonds.

Common secondary structures include α-helix, β-sheet, β-turns, 3_{10} helix, π helix and parallel and anti-parallel β-sheets. The tertiary structure is formed by the overall folding of polypeptide chains through hydrophobic interactions between side chain groups of different amino acids as well as molecular interactions between the protein and its surrounding environment [17,21-23]. In the presence of water, most of the non polar, hydrophobic groups orientate to the internal core of the protein while polar, hydrophilic groups remain on the outer surface in direct contact with the surrounding water [17,21-23]. Hydrogen bonds, ionic bonds and disulfide bridges are other forces used by the protein to preserve its tertiary structure (**Figure 1.2**). The quaternary structure is the most complex level of protein organization and corresponds to the association between polypeptide chains to form dimers, trimers and/or higher order complexes [17,21,22].

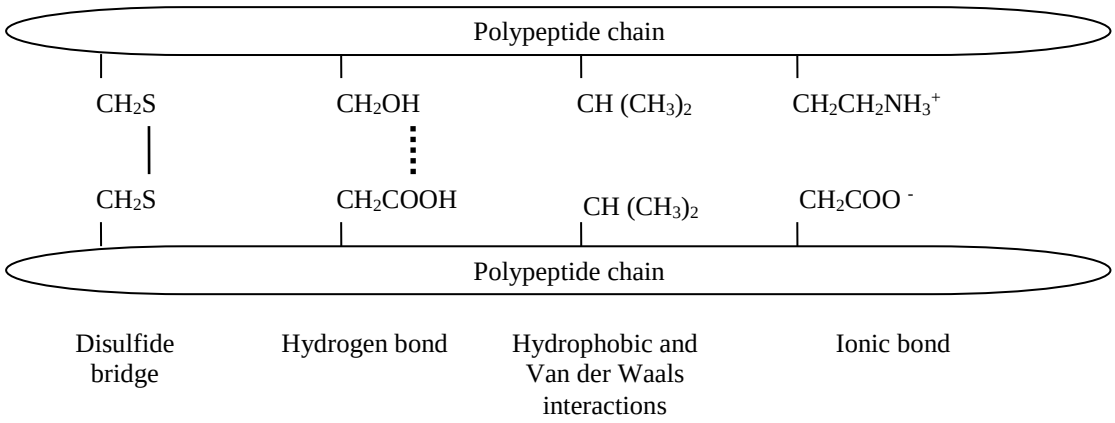

Figure 1.2 Schematic representation of forces involved in the tertiary structure of proteins. Hydrophobic interactions are the most common forces involved in folding of proteins [24]. Disulfide bridge are the strongest forces involved in folding of proteins whereas hydrogen bond, hydrophobic and Van der Waals interactions and ionic bonds form weak interactions with the side chain of proteins [17].

1.5. Protein conformation and its relevance in biological systems

Proteins in their native conformation represent the naturally occurring form under specific physical and chemical conditions. In this native conformation, globular proteins adopt an approximately spherical and compacted orientation which maintains its secondary, tertiary and quaternary structure unaltered [24] . In contrast with globular proteins, extended and non-globular proteins are long structures composed mainly of α-helix structures which do not form highly complex molecules (i.e. tertiary and quaternary structures). Moreover, the native

non-globular proteins do not have the typical hydrophobic core presents in globular proteins and can be found in fibrous proteins like collagens and keratins [25-28].

The native conformation of proteins can be altered during production into a biopharmaceutical product. Appearance of denatured or aggregated proteins is associated with immunogenicity of protein therapeutics [29-31]. As an example, insulin may produce insoluble particles (aggregated) over time which are recognized by the immune system [29] and the use of immune globulin and human growth hormone have produced antibody mediated adverse events [30]. Depending on the processing conditions and intensity of the denaturation stress, changes to protein conformation may be reversible or irreversible [24,32]. The possible relationships between unfolded, partially unfolded or aggregated proteins are summarized in **Figure 1.3** [22,33]. In a totally denatured state, proteins lose their secondary, tertiary and quaternary structures and only the polypeptide chain remains intact [24,32]. The loss of those protein structures is different for each kind of protein (i.e. globular and non-globular proteins) and may depend on protein chemical and physical resistance to environmental conditions like pressure, temperature and pH [34]. The formation of aggregates can start in just one molecule of protein due to intramolecular process (e.g. β-elimination for interleulin-1 receptor) or involve many protein molecules at the same time due to intermolecular process (e.g. thioldisulfide interchange for BSA) [24]. The transition from native to aggregated protein depends on the thermodynamic stability of the native protein. In the case of protein solutions, the native structure is thermodynamically stabilized by covalent and non-covalent forces (i.e hydrophobic interactions, hydrogen bonding, van der Waals and electrostatic interactions) [21,35-37]. In contrast with native protein, unfolded and aggregated proteins may have a reduced therapeutic activity and in some cases, aggregates may produce a toxic protein structure [22,24,38,39]. As a consequence of that, controlling the folding of proteins and preventing its aggregation during production is a crucial challenge for formulation scientists.

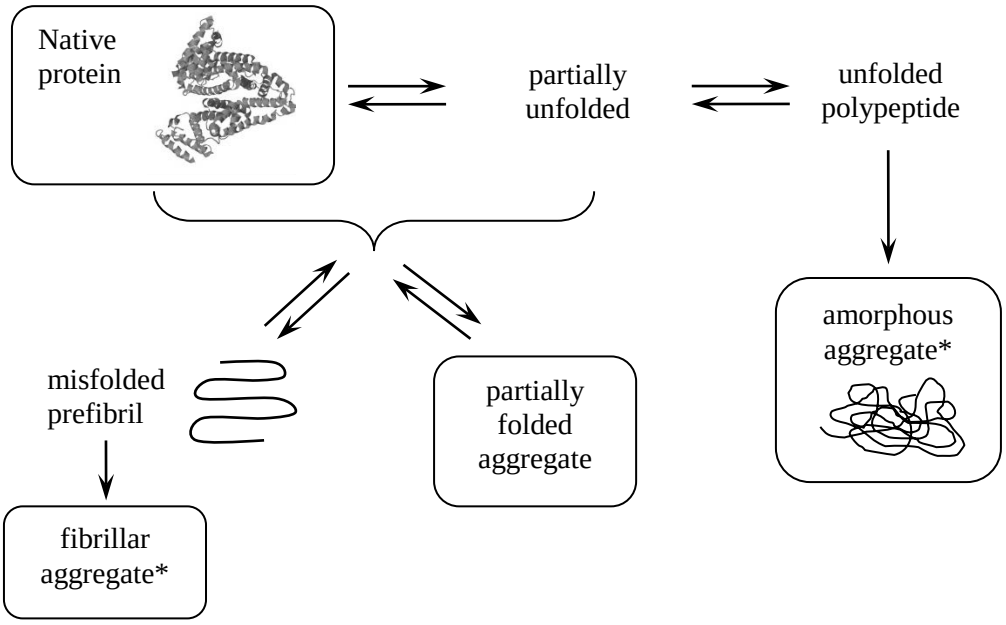

Figure 1.3 Schematic representation of protein physical degradation from native and globular protein structure to partially unfolded, unfolded and aggregated proteins modified from (Murphy and Tsai, 2006) [22,40]. Partially folded intermediates may convert to amorphous and fibrillar aggregates [41]. (* denotes an irreversible protein degradation).

1.6. Pharmaceutical formulation of proteins and their stability

Protein drugs can be prepared as liquid formulations or freeze dried solid products. Liquid formulations (i.e. solution, suspension or emulsion) are less stable than freeze dried solids but the application, processing and manipulation of liquid protein drugs formulation is simpler than for freeze dried solids [10,24,42]. It has been reported that the structure of proteins may suffer physical degradation as consequence of freeze drying process when molecules of water are removed from the core of protein. Then, freeze dried protein products need to be reconstituted in solvent/water before administration and the protein may not return to their original native conformation [23]. Studies have demonstrated this using FTIR studies [43]. Moreover, protein stability may be affected by processing [42] where the most crucial steps appear to be protein purification and formulation. In protein purification, protein solutions are tested to contain 5% or less of contaminants like proteases whereas in formulation, solubility, pI, and the study of mechanisms that promote aggregation are investigated. During formulation, solvent, pH, excipients and storage conditions are defined [22,24]. Additionally, the stability of protein in solution may be also influenced by the interaction of protein molecules with surrounding molecules dissolved at the bulk phase (i.e. protein-protein, protein-water,

protein-excipients) as well as protein adsorption to interfaces (i.e. liquid-liquid, air-liquid and solid-liquid).

1.6.1. Protein stability in bulk solution phases

Protein drugs dissolved in the bulk solution are susceptible to both, chemical and physical degradation [35,42,44]. An interaction between physical and chemical degradation has been reported for solutions heated above the protein melting temperature (T_m) where the increase in temperature may produce unfolding proteins (i.e. physical degradation) and induce protein oxidation and deamidation (i.e. chemical degradation) [32].

1.6.1.1. Protein chemical stability

Chemical degradation results in covalent modifications in the structure of protein due to reactions such as deamidation, hydrolysis, succinimidation and oxidation which can produce a change in the protein primary structure. These changes may results in forms with a greater risk of aggregation which may reduce protein biological activity [24,35,39,42]. Covalent bonds may produce soluble or insoluble aggregated proteins by two mechanisms which are the formation of new crosslink proteins or modification of the common pathway of protein aggregation.

Multiple chemical reactions may occur simultaneously which makes it difficult to study each degradation pathway independently [24]. Additionally, the protein chemical degradation pathway will depend on formulation factors like water content, presence of excipients, characteristics of the reconstituted solution (pH and temperature) and distribution of labile amino acids [24]. One method to avoid protein chemical degradation is to inhibit the principal reaction. This could be achieved by controlling the pH of the solution to avoid modifications in the protein charge and the distribution of the charge in the protein structure [39]. As an example, basic fibroblast growth factor (bFGF) is reported to degrade by a cleavage reaction at the Asp-Pro sequence in acid conditions and by deamidation at the Asn-Pro sequence at neutral conditions [24]. Another method to avoid protein chemical degradation is to modify the amino acids of the native proteins [24,42]. As an example, glycosylated Interferon-β-1a (INF- β-1a) was a more stable protein molecule without affecting its biological activity than the deglycosylated form of INF- β-1a [24]. Diverse analytical techniques are available to investigate degradation products (e.g. size-exclusion chromatography (SEC), polyacrylamide

gel electrophoresis (PAGE), reverse phase chromatography (RP-HPLC) and mass spectroscopy (MS)). However, the combination of analytical techniques like RP-HPLC and MS or capillary electrophoresis and MS are used to separate and identify aggregates where MS may give information about molecular weight and sites of reaction [24,39]. As an example, RP-HPLC and MS has been used to detect hydrolyzed bFGF protein [24].

1.6.1.2. Protein physical stability

Physical degradation of proteins is often the result of changes in the environmental conditions (e.g. temperature, pH, pressure and presence of excipients). Evidence of physical degradation of proteins is the presence of partially unfolded, unfolded and aggregated proteins (**Figure 1.3**) [39]. Aggregated proteins have different sizes and shapes and can be classified as soluble or insoluble, reversible or irreversible and covalent or non-covalent. The shape and size of aggregates may be affected by the amino acid sequence, distribution of hydrophobic groups, sample preparation method, temperature, pH and protein concentration [39]. The size of protein aggregates changes from submicron to visible particles on aggregation. As an example, thermally denatured BSA has been shown to form aggregates of 6.3 nm in radius [39,45] whereas amyloidogenic lysozyme formed fibers of 8–10 nm of diameter [39,46]. Commonly, the secondary structure of proteins aggregates is composed of a high proportion of β-sheet structure as has been reported for insulin [39,47], lysozyme [39,46] and BSA [35,48]. The presence of aggregates in protein solution could be controlled by knowing the causes of protein degradation for each formulation as well as having diverse analytical techniques to characterize them [39]. **Table 1.2** shown a list of analytical techniques used to investigate protein conformation and aggregation. Commonly, a combination of analytical techniques is needed to confirm the structure of proteins [49]. As an example, secondary structure elements of human calcitonin were investigated using the combination of FTIR and circular dichroism (CD) spectroscopy. In that study, FTIR spectroscopy was used to investigate the presence of β-sheet whereas CD spectroscopy detected the presence of α-helix structure in fibrillated human calcitonin [50]. In this thesis, physical stability of proteins is studied using FTIR and fluorescence spectroscopy and SEC methods. The theory and biological applications of these techniques will be presented in the next paragraphs.

Table 1.2 Analytical techniques used to investigate protein conformation and aggregation [7,23,24,39,51-53]

Principle	Technique name	Provided information
Separation methods	Size exclusion chromatography	Provide information about size of proteins and detect indirectly insoluble aggregates. Quantification of proteins.
	Reverse phase chromatography	Detect and quantify isoforms of aggregated proteins
	Capillary electrophoresis	Characterization of protein structure and detect protein aggregates. Separate ionic species by charge and size.
	Analytical ultracentrifugation	Provide information about size (i.e. molecular weight and size distribution) and shape of aggregated and unfolded proteins
Spectroscopic methods	Circular dichroism	Characterization of protein structure. Far UV: secondary structure and near UV: tertiary structure and ligand binding.
	Fourier transform infrared spectroscopy	Characterization of protein secondary structure in any physical state and complex systems, protein identification by comparison with database.
	Raman spectroscopy	Detect secondary structure, protein identification by comparison with database.
	Intrinsic fluorescence	Characterization of protein structure (shape, size, state of folding or ligand binding) and dynamic properties (protein flexibility).
	Extrinsic fluorescence	Detect conformational changes with limited capacity to identify aggregates.
	Nuclear magnetic resonance spectroscopy	Characterization of tertiary structure of proteins in solution by atomic resolution. Study protein-ligand interactions atom by atom.
	Mass spectroscopy	Detailed structural information about protein structure (primary, secondary, tertiary and quaternary structure), protein complexes and their interaction with enzymes, substrates and ligands.
	X-ray spectroscopy	Characterization of tertiary structure of proteins. Identification of atomic composition.
	Ultraviolet absorption spectroscopy	Study protein conformation and stability. Give information of tertiary structure. Turbidity assays and enzymatic activity studies.
Light scattering methods	Dynamic light scattering	Detect monomeric protein, protein monomer in the presence of oligomers (i.e. dimmers and trimers) and proteins monomer with aggregates.
Microscopic methods	Atomic force microscopy	Investigate function and dynamic properties of proteins in their physiological environment. Provide information about forces involved in folded/unfolded structure.
	Electron microscopy	Detailed information on surface morphology.
Calorimetric techniques	Differential scanning calorimetry	Characterization of proteins and their interaction with other macromolecules measuring the energy of those reactions. Investigate thermal stability of proteins i.e. unfolded and aggregated proteins (heat capacity as function of temperature).
	Isothermal titration calorimetry	Characterization of proteins and their interaction with other macromolecules by measuring the energy of those reactions. Provide thermodynamic information of binding reactions (heat effect of binding as function of composition).
Other	X-Ray crystallography	Study tertiary structure by atomic resolution.
	Surface plasmon resonance	Provide information on kinetics and binding affinities of proteins.

1.6.2. Protein stability: analytical techniques

1.6.2.1. FTIR spectroscopy: theory

In infrared spectroscopy, a source of light (beam or energy) is passed through the sample exciting the electrons within an atom which results in vibrational and rotational movements of atoms producing energy. The adsorbed energy is detected by the spectrophotometer giving a characteristic spectrum for a molecule where each bond type corresponds with a specific signal (i.e. intensity and position) [54,55]. Infrared radiation is divided in three regions near-IR (10000-4000 cm^{-1}), mid-IR (4000-400 cm^{-1}) and far-IR (400-100 cm^{-1}) [56]. In the near-IR region, C-H, N-H and O-H stretching are observed. In general, the analysis of bands in this region is complicated because bands are significantly overlapped giving weaker signals than in the mid-IR region [57,58]. The mid-IR region is divided in four regions: the stretching region (4000-2500 cm^{-1}), the triple bond region (2500-2000 cm^{-1}), the double bond region (2000-1500 cm^{-1}) and the fingerprint region (1500-600 cm-$^{-1}$) [58]. Functional groups appear in the fingerprint region where small molecular modifications can be detected [59]. In the far-IR region vibrations produced by heavy atoms, molecular skeleton vibrations, molecular torsions and crystal lattice vibrations are seen [58]. In the case of protein analysis, protein secondary structure has been investigated using absorbance in the mid-IR region (4000-400 cm^{-1}) where nine amide bands can be identified and these are shown in **Table 1.3** [60,61].

FTIR spectroscopy has been available for more than 50 years over which time diverse biological materials have been analyzed including proteins, biomembranes, nucleic acids and animal tissues [60,62-64]. FTIR spectroscopy is widely used to investigate protein physical stability because FTIR allows the analysis of samples in diverse physical states such as solids, liquids, pastes, films and powders. Samples in any of these states can be studied by FTIR spectroscopy since different methods and accessories are currently available which are suited to different sample states. As an example, attenuated total reflectance spectroscopy (ATR) is useful for the analysis of solid and hydrated samples using different accessories like germanium (Ge), zinc selenide (ZnSe) or diamond crystals and diffuse reflectance spectroscopy (DRIFT) is useful for the analysis of powders [60]. In this thesis, protein physical stability in aqueous solutions was investigated by transmission FTIR using CaF_2 windows with a constant path length (Biocell®). In this method, the protein solution is placed between the two crystals and the IR beam passed through the samples by one point (**Figure 1.4**). Used in this way, FTIR spectrosocopy is non-destructive [60], it can analyze proteins of

different hydrodynamic size and the spectrum is obtained in few minutes [65]. However, FTIR spectroscopy has limited sensitivity which is the main disadvantage of this method for protein analysis as a solution concentration of 5 mg/mL is needed [60].

Table 1.3 List of amide bands detected by FTIR spectroscopy with their corresponding wavenumber (cm^{-1}), functional groups and type of vibration [54,60,65-67]

Amide Band	Wavenumber (cm^{-1})	Vibration	Comments
Amide A	3300	N-H stretching	
Amide B	3100	N-H stretching	
Amide I	1600-1700	C=O stretching out of phase C-N stretching	Significant interference with water band (1700 - 1600 cm^{-1}) and amino acid side chains (1800 - 1400 cm^{-1})
Amide II	1500-1600	N-H bending C-N stretching	
Amide III	1220-1330	C-N stretching N-H in plane bending Weak C-C stretching and C=O in plane bending	Very weak absorbance and overlapped with C-H vibration of amino acid side chain
Amide IV	625-767	O-C-N bending	
Amide V	640-800	N-H bending out of plane	
Amide VI	537-606	C=O bending out of plane	
Amide VII	200	Skeletal torsion	

In the analysis of protein structure the amide I band (1600 – 1700 cm^{-1}) is the most relevant band because it contains information of secondary structures (i.e. α-helix, 3_{10}-helix, β-sheet, turn and random signals) (**Table 1.4**). Shift in the position of these secondary structures are attributed to protein instability [54,68]. The principal disadvantage of FTIR to investigate protein structure in solution is that the water absorption greatly overlaps the amide I band [65]. Researchers have used water subtraction methods to deconvolute the protein spectrum [60,65]. (Subtraction and pre-processing methods used in spectroscopy are described in Chapter 2).

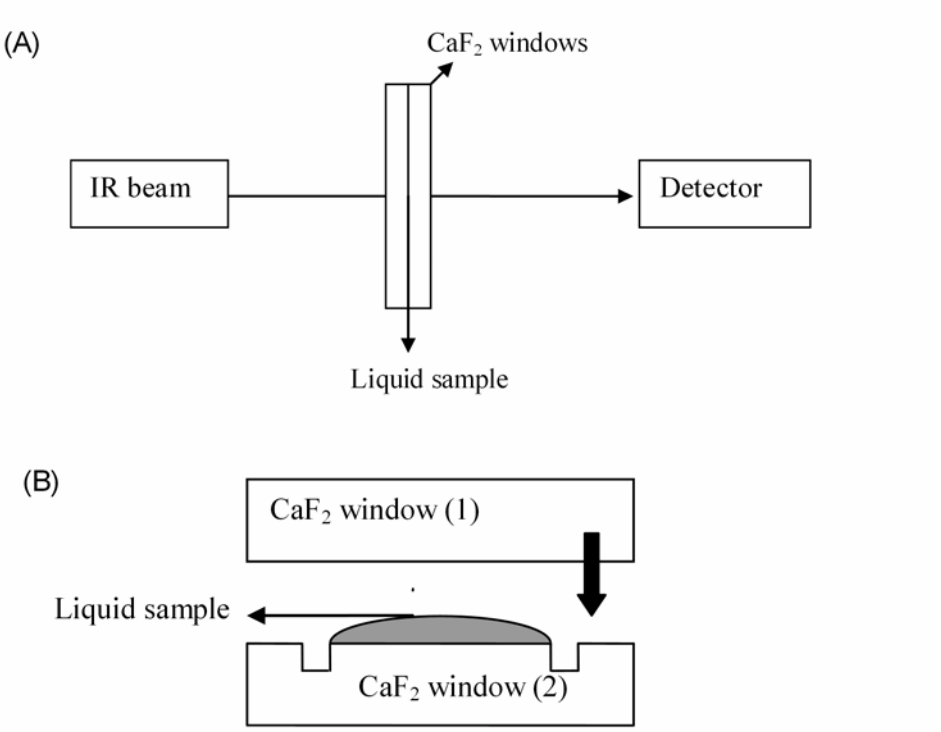

Figure 1.4 (A) Schematic representation of FTIR spectroscopy. A liquid sample (i.e. protein solution) is located between the two CaF_2 windows (BioCell™, (Jupiter, Florida, USA)). The IR beam passes through the sample in one point giving a characteristic signal that is detected as spectrum [55]. (B) The two CaF_2 windows are represented in further detail. Both windows are placed together (as indicated by the black arrow) and the liquid sample forms a film between these windows (0.1 μm path lengh), controlling the thickness of the sample.

Table 1.4 Secondary structures present in the amide I band with their corresponding wavenumber (cm^{-1}). Values in parenthesis represent the fluctuation in the position of each secondary structures detected by FTIR [54,56,65].

Secondary structures amide I	**Wavenumber (cm^{-1}) (range)***
A-helix	1654 (1648-1657)
Intramolecular β-sheet	1633 and 1684 (1630-1640/1680-1690)
Turn helix	1672 (1659-1666)
Disordered	1654 (1640-1645)
Intermolecular β-sheet	1610-1620 and 1680-1690** (1610-1625/1670-1695)

*Values in parenthesis depends on solvent interactions [56]
**Narrowed bands represent aggregation of proteins in denatured state [65].

1.6.2.2. Fluorescence spectroscopy: theory

In fluorescence spectroscopy, electrons within an atom are excited using light or radiation which transfers electrons from a basal to an excited energy state [69-71]. Following this, excited electrons return to the basal state via two steps: firstly, electrons can release part of the adsorbed energy moving from the excited state to a lower level of energy and then, the remaining energy is released by electrons by mechanisms of competitive emission of a photon (fluorescence), radiation-less loss, phosphorescence, photo-oxidation or energy transfer [70-72]. The fluorescence spectrophotometer detects the released energy from electrons returning from the excited state as transference of charge and reduction of fluorophore groups [70]. Molecules are fluorescence-active if they contain fluorophore groups which can absorb and emit fluorescence energy. Fluorophore groups produce fluorescence with specific intensity, wavelength and life time. Fluorescence can be divided in: intrinsic fluorescence where the fluorophore group is a small part of the molecule (i.e., aromatic amino acids like tryptophan (Trp), tyrosine (Tyr) and phenylalanine (Phe)) (**Table 1.4**) [8,70,72,73] and extrinsic fluorescence where the fluorophore groups are peptides and proteins linked to the molecule [70]. Fluorescence spectroscopy usually requires low concentration of proteins [32] (e.g. 20 mg/mL of BSA in 10 mM of sodium phosphate buffer; pH 7.4 [73] and 0.1 mg/mL of TP40 (Cys-replaced mutant of TGF-α-PE40); pH 7.2 [24]), it is not destructive, and the sample can be recovered after the measurement [72].

Table 1.5 Amino acid residues that produce fluorescence classified according to the maximum emission at each excitation wavelength (nm) in aqueous solution pH 7 [70].

Amino acid residues	Excitation (nm) in H_2O(pH 7)	Emission max (nm) in H_2O (pH7)
Trp	280	348
Tyr	274	303
Phe	257	282

The structure of proteins can be studied using intrinsic fluorescence spectroscopy since proteins can contain aromatic amino acids responsible for fluorescence emission: Trp, Tyr and Phe [69,74]. The intensity and position of the maximum emission depends on how exposed the fluorescent amino acids are to an aqueous environment which is subsequently interpreted as depending on how the amino acid chains are folded in the tertiary structure [8,24,69,73,75]. Excitation of a protein solution at 295 nm allows the study of principally the Trp residue [24,69,75]. The position of the maximum emission depends on the polar characteristics of the solvent [24], environment properties and changes associated with differences on dielectric constant (i.e. polarity) of the solvent. In protein solutions containing the three amino acids (Trp, Tyr and Phe), the maximum emission will be dominated by Trp. This is because Trp contains stronger fluorescence emission than Tyr and Phe and part of the energy released from Phe and Tyr is transferred to Trp [72]. In denatured protein solutions, Trp is exposed to a less polar environment which can cause a blue shift of the Trp maximum emission and decrease in the intensity of the maximum emission [69].

1.6.2.3. Size exclusion chromatography (SEC): theory

Liquid chromatography has been widely used to separate, identify and purify molecules within a mixture. The equipment is composed on a solid stationary phase (separation column), a detector UV/Vis or photodiode array (PDA) and the liquid mobile phase containing the solvent and the sample. Currently, there is a variety of chromatography methods which are defined by the characteristics of the stationary phase like reverse phase chromatography (separation based on hydrophobicity), size exclusion chromatography (separation based on size), and hydrophobic interaction chromatography (separation based on charge). In the case of SEC, the stationary phase is a column packed with well defined porous particles. The specific pore dimension used to separate molecules based on their size, shape and molecular weight. SEC detects the presence of different sized components within a mixture processing this information into a chromatogram showing characteristic peaks attributed to the relation between the absorbance or intensity (Y-axis) and time (X-axis) [76].

SEC is a useful analytical technique that gives qualitative and quantitative information about components within a mixture [77] i.e. folded and aggregated proteins within liquid protein formulations [78]. In the case of protein analysis, SEC can be used to identify and separate proteins that have different hydrodynamic size (i.e. native and aggregated proteins) [77,78].

Molecules with large hydrodynamic size eluted faster from the column than molecules with smaller hydrodynamic size [76,79]. Native BSA (globular conformation) has a smaller hydrodynamic size than the soluble aggregated proteins (extended conformations) [80] so that, aggregated protein is eluted earlier than native BSA [76]. SEC can be quantitative since the size of the peak (typically area or height) is proportional to the concentration of the protein. So that, it is possible to build a calibration curve between concentration and peak area or peak height and then, linear regression is used to estimate the concentration of the unknown sample [77].

1.7. Multivariate analysis (MVA)

Spectroscopy data are commonly pre-processed by diverse algorithms to achieve a strong relationship between the used X-data (i.e. spectra) and the predicted Y-data (i.e. protein concentration) [66]. Pre-processing methods use mathematical functions which are applied to the raw spectra before the development of statistical analysis to increase the quality of the information obtained for quantitative models [81]. A proper choice of pre-processing methods is crucial to obtain an accurate prediction model. However, during pre-processing care must be taken to avoid an artificial correlation between variables of the data set (i.e. wavenumber and concentration) [66]. Examples of mathematical functions commonly used for spectral data are: baseline correction (BC), area normalization (AN), derivatization (1^{st}D or 2^{nd}D), standard normal variate (SNV) and multiplicative scatter correction (MSC). All these mathematical functions and its application in protein analysis are used and will be explained in Chapter 2 of this thesis.

In protein formulation, spectral data may contain complex information that corresponds to components within a mixture, intrinsic characteristics of each component and interactions within them [82]. The analysis of those spectra could include the use of chemometrics, which is a discipline used to obtain information from chemical data using mathematics and statistics [82]. Spectral data could be analysed using univariate calibration which predicts a variable Y in function of a single variable X [82,83]. To achieve an accurate relation between variables X and Y, two principles must be achieved: selectivity and linearity. Selectivity implies that variable Y is not influenced by another variable and linearity means that a linear relationship is obtained between variables X (i.e. absorbance at one wavenumber) and Y (i.e. concentration) [83]. Additionally, the analysis of protein spectra may be investigated using MVA which can

investigate several variables at the same time. This means that the whole spectrum could be used to predict the concentration of unknown samples. So that, MVA should give more accurate regression models than univariate calibration [84]. MVA may predict concentration of unknown samples using regression models that relate multiple variables in the X-axis (i.e. spectra) with the Y-axis (i.e. sample concentration) [85,86]. Regression models like partial least square (PLS) is one of the most popular and well known methods used to characterize qualitative and quantitative information of protein structure [87,88]. Other regression methods used in MVA are principal component analysis, factor analysis and singular value decomposition [60].

In MVA, the spectra data set is arranged in a Table where every row represents the measurements of one sample and columns represent each variable [83] and the whole data set is divided in calibration and validation sets. A calibration set is composed of spectra (X) at different concentrations obtained from reference samples of known concentration. Then, a validation set is used to estimate how well the model can predict the concentration of unknown samples [84,86]. Statistical analysis for spectroscopy studies using PLS regressions are presented in Chapter 3.

1.8. Protein stability to possible role of protein adsorption to interfaces

Protein physical stability may be affected by adsorption of protein molecules to interfaces (i.e. solid-liquid, liquid-liquid and air-liquid) [89,90]. Protein molecules adsorb to solid-liquid interfaces: lysozyme [91] and BSA [92], liquid-liquid interfaces: BSA [93-95], insulin [93], β-casein, ovalbumin [95] and lysozyme [72,74,75], and air-liquid interfaces: soy protein isolate [96] and natural silk fibroin [97]. Literature suggests that following adsorption at an oil-water interface the protein may adopt unfolded conformations, change the oil-water interfacial properties, and/or interact with the surrounding protein molecules to form a network [98]. Since there is considerable opportunity for pharmaceutical proteins to encounter interfaces during production and storage conditions then it may be important to investigate this phenonmeon in greater detail [99]. The study of protein adsorption to the oil-water interface is presented in Chapters 4 and 5 of this thesis.

1.8.1. Mechanism of protein adsorption to the oil-water interfaces

The adsorption of proteins to interfaces involves different steps [100]. Protein adsorption is reported to start with diffusion of protein molecules from the bulk solution to the interface [90,92]. If the interaction between protein and interface is favorable, globular and flexible protein molecules (i.e. human serum albumin (HSA), α-chymotrypsin [90], BSA [90,92,93], lysozyme [90,93,101] and β-casein [95,102]) at the interface can undergo attachment, molecular relaxation and conformational rearrangement so that much of its structure aligns along the plane of the interface [90,92]. This spread of protein molecules is affected by the space available in the interface and the speed at which protein molecules are adsorbed in the available space. At equilibrium, the interface will be covered by a mix of protein conformations [103] and it has been suggested that these finally evolve into a multilayer structure [98] (**Figure 1.5**).

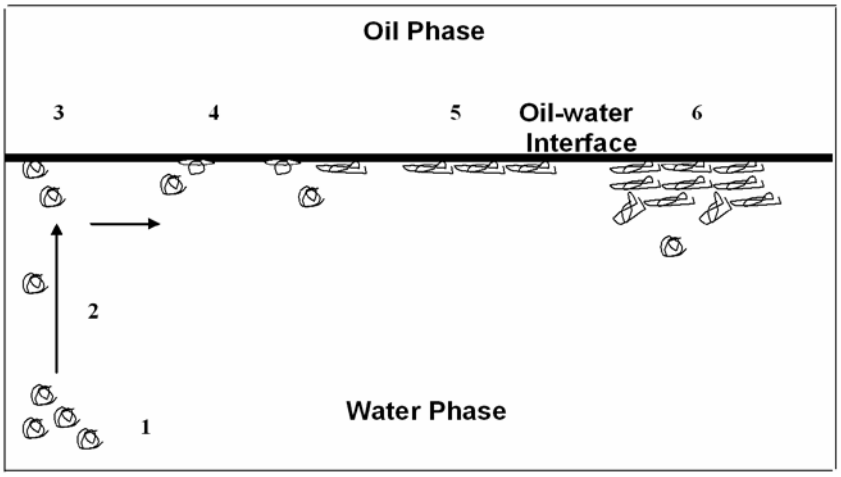

Figure 1.5 Scheme of protein adsorption to the oil-water interface. 1) Native protein dissolved in the water phase, 2) diffusion of native protein from the bulk solution to the oil-water interface, 3) adsorption of native protein (attachment) to the oil-water interface, 4) relaxation, spread and reorientation of hydrophobic groups of adsorbed protein to the oil-water interface, 5) monolayer formation and 6) multilayer formation.

1.8.2. Methods used to investigate adsorption of proteins at interfaces

The adsorption of proteins to interfaces has been previously investigated for some systems using rheology and interfacial tension (IFT) measurements [93,102,104], reflectometry [105], total internal reflection fluorescence (TIRF) [78-80], surface plamon resonance (SPR) [106] and isothermal titration calorimetry (ITC) [107]. In this thesis, protein adsorption to interfaces was investigated using a rheometer and a pendant drop tensiometer. The theory and biological application of rheometer and a pendant drop tensiometer will be introduced in the next paragraphs.

1.8.2.1. Interfacial rheology: theory

Interfacial rheology can be studied using dilatational and shear rheology measurements [104,108]. Dilatation rheology examines the viscoelastic properties of the interface and gives information about short-term stability of interfacial structures [108]. This form of rheology uses a constant shape but variable interfacial area (i.e. expansion and compression) [82,84]. In comparison, shear rheology investigates the strength of interfacial structures that result from intermolecular interactions at the interface. Shear rheology gives information about long-term stability and it is studied at constant area but variable shape [81,83,84]. Shear rheology is more sensitive than dilatational rheology in detecting inter-molecular interactions between adjacently adsorbed molecules and can also be used to recognize the adsorption of small amount of excipients to the interface [108]. As an example, oscillatory shear rheology was used to investigate lysozyme adsorption to the oil-water interface in the presence of excipients like sorbitan monooleate 80 (S80). Results showed tha the interfacial adsorption of lysozyme depend on the concentration of excipients showing a delay in its adsorption to the interface in the presence of increased concentrations of S80 [101].

Liquid-liquid interfaces are studied by shear rheology using an oscillatory accessory that applies torsional stress to the interface [109]. Shear rheology measurements have been used to study the kinetic of protein adsorption to liquid-liquid interfaces over time where the formation of a gel or protein film at the interface (i.e. multilayer) [75,87] has been described for globular (e.g. BSA [93,95] and lysozyme [93,95,102]) and flexible (e.g. β-casein [95,102]) proteins. In this thesis, a rheometer with double-wall ring (DWR) geometry was used to investigate protein adsorption to interfaces giving information about time-sweep, frequency-sweep and strain amplitude-sweep steps which are explained in **Chapter 4 section 4.2.3**.

1.8.2.2. Pendant drop tensiometer: theory

The pendant drop tensiometer has been widely used to investigate mechanical properties of materials adsorbed to gas-liquid and liquid-liquid interfaces [110]. This method investigates the IFT of a drop in terms of pressure per unit of area [109,110] where the molecular interaction of a drop with its interface (i.e. liquid or gas) results in a decrease in the IFT values [111]. This is explained due to changes in the shape of the drop as consequence of surface tension force (e.g. espheric form) and gravitational force (e.g. elongate form) [110]. IFT measurements are mainly used to identify protein diffusion from bulk solution to interfaces [93,112] giving information about the initial stages of protein adsorption to interfaces prior to monolayer formation [95]. Typically in surface tension experiments an initial rapid decrease in IFT occurs as the monolayer is formed. Following this the rate of decrease of IFT slows and a plateau may be reached when a multilayer structure is formed [101]. IFT measurements have been used to investigate the kinetic of protein adsorption (i.e. lysozyme, insulin [93] and soy protein isolate [96]) to the oil-water interface where a good correlation between IFT and rheology results have been reported for lysozyme and insulin [93]. Pendant drop tensiometer is an easy to use method which utilize small amount of sample [110,113] however, its principal limitation is that both phases must have different density [110]. IFT measurements are explained by Laplace-Young equation which is shown in **Chapter 4 section 4.2.4**.

1.9. Protein stability: Influence of excipients to modify protein adsorption to interfaces

Excipients used in the preparation of biotherapeutics have received attention to increase the knowledge of how excipients affect protein stability and how these interactions may be useful for rational development of controlled release delivery systems for therapeutic proteins [114]. Excipients are commonly used in protein drug formulations to stabilized liquid formulations and prevent degradation products of chemical instability. The effect of excipients in protein formulations is concentration dependent and protein dependent which can be classified in sugars and polyols, amino acids, amines, salts, polymers and surfactants [24,112]. Excipients used to prevent protein adsorption must contain higher surface activity than proteins [114]. The interaction of excipients with protein solutions is influenced by the presence of water molecules where a different interaction must be expected between excipients and dried proteins [112]. Excipients interact with proteins using different mechanism which are summarized in **Table 1.6**.

Table 1.6 Classification of common excipients used in protein formulation [24,112,114,115]

Excipients	Formulation effect and mechanism	Examples	Protein type used
Surfactant	Anti adsorption effect due to competitive adsorption.	Polysorbate 20 and 80	
Antioxidants	Oxidation protection effect due to competitive adsorption.	Acid ascorbic and vitamin E	
Sugar and polyols	Stabiliser effect due to preferential exclusion.	Glucose and A-lactoglobulin	BSA and Ribonuclease-A
Salt	Stabiliser effect due to preferential binding and interaction with protein bound water. Control tonicity effect due to preferential binding. Reduce electrostatic interaction due to changes in the ionic strength of the solvent.	Potassium phosphate and sodium sulphate NaCl	Apoflavodoxin Lactoglobulin
Amino acids	Stabiliser effect due to preferential exclusion, preferential hydration and decrease protein-protein interactions.	Alanine and glycine	BSA and lysozyme
Polymers	Stabiliser effect due to competitive adsorption, preferential exclusion, preferential hydration and steric exclusion.	Cyclodextrin and PEG	BSA and insulin
Buffer salts and antiacids	pH regulator effect.	Phosphate and $Mg(OH)_2$	

1.10. BSA: General properties

BSA is a globular protein [116] of 66 KDa [117] which contains 582-585 amino acid residues and 17 disulphide bonds [116] (**Appendix A**). The native structure of BSA is mainly composed of α-helix structure (i.e. 55% to 65%) [73,118] and two Trp residues (i.e. Trp-134 and Trp-212) [73,90]. It's conformation has been investigated using a variety of analytical techniques like differential scanning calorimetry, FTIR, fluorescence and circular dichroism spectroscopy [24,118]. Reports have shown that BSA is denatured at temperatures lower than its melting temperature (T_m) (<56.8°C) forming partially unfolded structures whereas BSA may form hydrophobic aggregates due to irreversibly denaturation at temperatures higher than its T_m [24]. Denatured BSA may lose its globular and compact native conformation forming an extended protein structure [48,65] with different properties than native BSA. Moreover, BSA contains 60% of hydrophobic amino acids [93] which confer surface activity to BSA [116]. BSA is classified as soft protein which means that BSA modifies its native and globular structure after adsorption to interfaces [92]. Those characteristics made BSA an interesting protein to investigate an alternative method of protein quantification using MVA as well as to investigate the kinetic of protein adsorption to interfaces in the presence of heat-denatured BSA or excipients as shown in the following chapters.

1.11. Thesis aims

This thesis addresses the following two hypotheses:

1. Spectroscopy and MVA could be used to develop methods of protein characterization and quantification, able to detect small amount of unfolded proteins in the bulk solution.

2. The adsorption of native protein to liquid-liquid interfaces is affected by the presence of unfolded proteins and excipients in the bulk solution.

The specific aims of this thesis were:

i) To investigate a variety of pre-processing methods for FTIR and fluorescence spectra to identify changes in the secondary and tertiary structure of proteins as well as to develop a standard protocol of pre-processing methods to maximize the information obtained from those spectra about physical stability of protein structure in solution.

ii) To investigate the use of PLS regression in combination with FTIR and fluorescence spectroscopy as an alternative method to quantify the loss of native protein structure.
   a. To compare the native protein concentration predicted by PLS models with traditional methods of protein spectroscopy analysis like area overlap (FTIR), and the linear regression between fluorescence intensity at the maximum emission wavelength vs. concentration of native protein.
   b. To investigate how well PLS models can predict the loss of native protein in solutions heated at 40°C, 50°C and 60°C and compare these results with protein concentration obtained experimentally using SEC.

iii) To characterize the oil-water interfacial adsorption of native and thermally denatured protein, and to examine how introduction of a small amount of denatured protein in the bulk solution affects the adsorption of a native protein to the oil-water interface using a rheometer with a DWR attached and the pendant drop tensiometer.

iv) To use interfacial rheology and IFT measurements to detect changes in the kinetic and mechanism of surface adsorption of native protein to the oil-water interface in the presence of excipients (i.e. phospholipids, NaCl and polymers). Additionally, physical stability of protein in the presence of these excipients is confirmed by FTIR spectroscopy.

Chapter 2: Investigation of spectral pre-processing methods

2.1. Introduction

The spectral data obtained from FTIR, ATR, Raman fluorescence and Near-IR [119-122] spectroscopy are pre-processed or transformed to reduce the noise [81,123-127], eliminate unwanted variables in the data (i.e. different magnitudes), increase the relationship between X- and Y-data [66] and decrease the effect of light scattering to improve the linearity between spectral signals and concentrations [128-130]. Scattering is caused by the presence of insoluble particles, bubbles, cells and fibres in liquid samples [119,128-130]. Rayleigh and Lorentz-Mie are two sources of scattering described by Rinnan *et al.* (2009). Rayleigh scattering is influenced by wavelength while Lorentz-Mie scattering is affected by particle shape [129]. Particles with smaller diameter than the wavelength of the light are affected by the source of Rayleigh scattering whereas for particles with larger diameter the scattering effect is dominated by Lorentz-Mei [129].

A diverse range of pre-processing methods is available which has been assessed in this Chapter to improve the quality of the spectral data [81,128]. Before the application of pre-processing techniques, the raw spectrum needs to be plotted to study the source of spectral noise. This step is relevant to discriminate if spectral variations are attributed to scattering effects or spectral noise as consequence of differences in the chemical composition of the sample (i.e. absorbance) [119]. As an example, light scattering is often causing systematic variations in solid samples, which can be observed as shift in the baseline [129]. Pre-processing techniques are classified as reference dependent and reference independent methods [130]. Reference dependent methods require the use of a reference value (e.g. optimized scaling and net analyte pre-processing techniques) whereas reference independent methods do not depend on the use of a reference value (e.g. BC [131], AN [132], derivatives (1^{st}D or 2^{nd}D), SNV and MSC [128,132,133]) [130]. Pre-processing methods are commonly performed on spectral data before the development of statistical analysis (e.g. MVA and classification model) [129] to obtain appropriate chemical information and increase the goodness of fit of the regression models [57,81]. Pre-processing methods can be performed in just one step (i.e. MSC and SNV) or using a stepwise approach where a corrected spectrum is obtained at each step and is then subjected to further step(s) (i.e. BC and AN) [134]. The selection of one or more than one of these pre-processing methods shown to improve the qualitative and quantitative information obtained

from predicted models [128]. However, pre-processing methods must be used carefully to avoid artificial corrections between X- and Y-data [57,66]. Rinnan *et al.* (2009) proposed that the criteria to select the best pre-processing method or combination of methods could be based on the most linear model obtained from regression analysis [129]. Nevertheless, the corrected spectrum will be different depending on the pre-processing method that is being applied; so that the effect obtained using each pre-processing method must be well understood and carefully chosen to be able to make a proper interpretation of MVA results [135,136].

A general description of each pre-processing method used in this thesis is introduced in the following paragraphs.

2.1.1. Background subtraction of FTIR and fluorescence spectra

Background subtraction was conducted by point to point subtraction between absorbance of the original protein spectrum and the solvent spectrum [58] for FTIR (1350 to 4000 cm^{-1}) and fluorescence (250 to 500 nm) spectroscopy [55,125]. For the BSA solutions studied by FTIR spectroscopy the amide I band of protein (1600-1700 cm^{-1}) is overlapped by a strongly absorbing water band from 1600 to 1700 cm^{-1} [55,134]. Bulk water and water vapour spectra were subtracted from the BSA solution spectrum in two independent steps to give a flat base line between 2300-1750 cm^{-1} [60,61,73,137,138]. Bulk water and water vapour subtraction were performed in two successive steps (Equations 2.1 and 2.2) to allow off-line spectral processing.

$$Wss = Ops - Ws * f \quad (2.1)$$

where Wss is the water subtracted spectrum, Ops is the original protein spectrum, Ws is the water spectrum and f is the subtraction factor.

$$Vwss = Wss - VWs * f \quad (2.2)$$

where $Vwss$ is the water vapour subtracted spectrum, Wss is the water subtracted spectrum and VWs is the water vapour spectrum.

Subtraction factors used in Equations 2.1 and 2.2 were specific for each spectrum analysed and allowed for the differences in path length between the background spectra and the sample spectra and, for the different level of water vapour in the sample compartments. Subtraction factors used in each spectrum were selected by visual inspection to obtain a flat base line

between 2300-1750 cm^{-1} [60,73,137,138]. The water vapour spectrum is characterised by several sharp bands between 4000 – 3500 cm^{-1} and 2000 - 1300 cm^{-1} which are attributed to rotational motions. The presence of these sharp bands in the protein spectrum may cause incorrect amide I band assignments [60]. In Equation 2.1, three water bands were subtracted which appear at 3400 cm^{-1} (O-H stretching), 2125 cm^{-1} (water association) and 1645 cm^{-1} (H-O-H bending) [139] whereas the water vapour bands being subtracted in Equation 2.2 appeared at around 2200 cm^{-1} [60]. Samples were kept inside the FTIR spectrophotometer for five minutes before the measurement to minimise the water vapour contribution to the original native BSA spectrum. For fluorescence spectroscopy, the characteristic Trp maximum emission appears between 300-400 nm [140]. The subtraction factor used in each spectrum was selected by visual inspection to obtain a flat base line before 300-400 nm using Equation 2.1. The water subtracted spectrum of native BSA was further used to perform additional pre-processing methods through this Chapter.

2.1.2. Baseline correction of FTIR and fluorescence spectra

BC reduces spectral noise attributed to low frequency which is not related to chemical information [81]. In this Chapter, BC was used to compare different spectra in the same Y-axis. This method was useful to correct spectra were some of the data were located in the positive Y-axis and the rest of the data were in the negative Y-axis (e.g. 2^{nd}D of amide I band). A linear BC was fitted at Y=0 [141]. Data points that were above or over this value were fitted in the baseline giving a BC spectrum [142]. The corrected spectrum was obtained using the minimum number of points (i.e. two to five points) required to produce a straight baseline therefore causing the least alteration in the spectrum shape [55]. The BC method could be applied to the whole spectrum or specific regions as shown in this Chapter (i.e. amide I band (1600-1700 cm^{-1}) and Trp emission (300-400 nm)). Each spectrum was BC individually rather than correcting all spectra at the same time [143] to minimise possible errors in the corrected spectrum.

2.1.3. Normalization processes for FTIR and fluorescence spectra

Spectra pre-processing using normalization methods was used to study different spectra in the same scale [81]. This technique allows identification of regions of each spectrum which are modified due to the presence of denatured proteins [81]. In this thesis, normalization was pre-

processed using the AN method which gives all spectra in the same scale. It was calculated using two steps: firstly the integral of each spectrum was calculated giving an area under the curve for each spectrum. Then, each absorbance measured was divided by the total spectral area by simple arithmetic. As a result all the spectra were converted to an area of 1.00 [81].

The AN method is described by Equation 2.3.

$$Y' = \frac{Y}{a} \tag{2.3}$$

where Y' is the absorbance for the area normalized spectrum, Y is the absorbance value in the original spectrum and a is the total area under curve of the spectrum.

2.1.4. Smoothing methods

FTIR spectra were smoothed using the Savitzky-Golay polynomial method second order. The fitted values at each absorbance (X-values) were calculated using a second degree polynomial function over five to 13 points. The X-value was located at the centre and for five points smoothing there were two points above and below the central X-value. Smoothing methods were calculated using Equation 2.4 [66,144]. A smoothed spectrum corresponds to a spectrum taken at low resolution [58].

$$X_j^* = \frac{1}{N}\sum_{h=-k}^{k} C_h X_{j+h} \tag{2.4}$$

where X_j^* is the smoothed spectra, N is the normalizing constant, k is the number of values at each side of j and, C_h are the coefficients that depend on the polynomial degree [66,144]. The spectral range was extended to outside range of amide I (i.e. 1705 to 1595 cm^{-1}) to account for the loss of end points due to smoothing. The Savitzky-Golay method was used to smooth FTIR spectra over this range and to calculate the differentiation methods described in the next paragraphs.

2.1.5. Differentiation methods

The 2ndD of amide I of proteins (i.e. FTIR spectroscopy) was used to investigate protein physical stability. In this work, 1stD and 2ndD were obtained using a Savitzky-Golay method which estimates a polynomial regression to transform each absorbance row to a new and

smoothed row [143]. The 1stD corresponds to the slope at each point in the original data set [58]. Each peak in the original spectrum is equal to zero in the 1stD spectrum whereas each peak of the 1stD spectra corresponds to regions with the maximum slope value in the original spectrum [143,145]. The 2ndD method studies the curvature at each point in the original spectrum [58,143,145]. The 2ndD spectrum gives a minimum at the center of the original peak whereas positive peaks in the original spectra result in negative peaks in the 2ndD spectrum [143]. The 2ndD method is useful to obtain information on peaks in close proximity and represents changes in the curvature of the original spectrum [143,145] (i.e. changes in the direction of the curve and presence of hidden bands). The position of negative peaks can be used to identify hidden overlapping peaks in the original spectra.

The derivative function of smoothed spectra using the Savitzky-Golay method is described in Equation 2.5.

$$f(x) = a_n x^n + a_{n-1} x^{n-1} + a_{n-2} x^{n-2} + ... a_0 \quad (2.5)$$

where a_0 and a_n are the derivative values at each wavenumber (x) and n is the number of data points. a_1 is the 1stD, a_2 is the 2ndD [146].

Then, the derivative of $f(x)$ is defined in Equation 2.6.

$$f'(x) = n a_n x^{n-1} + (n-1) a_{n-1} x^{n-2} + ... a_1 \quad (2.6)$$

2.1.6. Multiplicative scatter correction (MSC)

MSC was used to remove the light scattering effect in the raw spectrum. This method calculates an average spectrum from the whole data set (i.e. native BSA, 50% native BSA and thermally denatured BSA protein) giving two coefficients: the offset or additive effect (a) and the slope or multiplicative effect (b) of the regression line. These coefficients are then used to estimate a regression of each individual spectrum (i.e. native BSA, 50% native BSA and thermally denatured BSA protein) on the average data [129,145]. The corrected MSC spectrum is similar to the average spectrum [66,147] containing approximately the same degree of light scattering [66].

The MSC effect for spectrum (i) is defined by Equation 2.7.

$$x_i^T = a_i + b_i \bar{x}^T + e_i^T \quad (2.7)$$

where x_i^T is the row vector of the absorbance measurements, $\bar{x}^T$ is the mean spectrum, a_i is the additive effect and bias, b_i is the multiplicative effect and slope and, e_i^T is the residual vector which contains the chemical variance. e_i^T corresponds to the difference between the mean spectrum and the residual vector [129,130,147].

Then, coefficients a_i and b_i are replaced in Equation 2.8 to calculate the MSC spectra ($X_{ij}(MSC)$).

$$X_{ij}(MSC) = \frac{X_{ij} - a_i}{b_i} \quad (2.8)$$

where X_{ij} is the absorbance at the jth point in spectrum (i) [66,129,148,149].

2.1.7. Standard normal variate (SNV)

SNV and MSC are related methods which correct for multiple scattering effects however, spectra pre-processed using SNV are scaled independently (without calculation of a mean spectrum like in MSC). Each spectrum is centred about its own mean intensity and scaled by its own standard deviation [66,122]. SNV corrects the original spectrum by centring the row of each spectrum at zero and scaling the absorbance of each spectrum from -2 to +2 using Equations 2.9 and 2.10:

$$X_{ij}(SNV) = \frac{X_{ij} - Mean(x)}{SDev(x)} \quad (2.9)$$

$$SDev(x) = \sqrt{\sum_{j=1}^{m} \frac{\left(X_{ij} - Mean(x)\right)^2}{m}} \quad (2.10)$$

where X_{ij} is the absorbance in spectrum (i), $Mean(x)$ and $SDev(x)$ are mean and standard deviation of X-axis and m is the number of columns [66,122,133,145].

Several reports have described the use of these pre-processing techniques to quantify the spectral data obtained from FTIR, ATR, Near-IR, fluorescence and Raman spectroscopy [119-122]. However, few authors have described in detail the advantages and/or disadvantages of applying these techniques alone or in combination for studying protein conformation data. The overall aim of this Chapter was to evaluate changes in the FTIR and fluorescence spectra when different pre-processing methods were applied to the original spectrum. FTIR spectroscopy was used to investigate changes in the amide I band of BSA (1700-1600 cm^{-1}) which contain more relevant information about the secondary structure of protein (i.e. α-helix, β-sheet, turns and disorder elements) than amide II or amide III [24,48,54,65,75]. In the case of fluorescence spectra, the Trp maximum emission (300-400 nm) was used to investigate changes in the tertiary structure [24,75] of native BSA, 50% native and heat-denatured BSA. These pre-processing methods are further used to develop a standard protocol for pre-processing FTIR and fluorescence spectra, which is expected to maximise information relevant to protein secondary and tertiary structure.

2.2. Materials and Methods

2.2.1. Materials

BSA was obtained from Sigma-Aldrich, USA (B4287, 95%).

2.2.2. Preparation of native BSA, heat-denatured BSA and binary mixtures of BSA (1% and 5%)

BSA was dissolved in distilled water to give protein solutions at 1% and 5% w/w. Samples were heated at 90°C for 30 minutes to give heat-denatured BSA while the unheated initial solution represented native BSA. Binary mixtures of 50% w/w native: 50% denatured BSA were prepared by weighing each solution in an analytical balance followed by gentle mixing.

2.2.3. Infrared spectroscopy (FTIR)

FTIR spectra were acquired using a Varian 3100 FTIR Excalibur series spectrometer with Varian resolutions Pro software (version 5.0, Agilent Technologies, Mulgrade, Victoria, Australia). Binary mixtures (50% w/w native: 50% denatured BSA solutions) of 12 µL were analysed using a CaF_2 transmission window from BioCell™ (Jupiter, Florida, USA) with a six µm path length and five cm diameter. A total of 16 scans were collected with a resolution of 4 cm^{-1}. The sample chamber was constantly purged with dry air (purge gas generators, PG28L, PEAK Scientific Instruments, Belmont, Victoria, Australia).

The amide I band of protein spectra (1600-1700 cm^{-1}) was pre-processed by BC, AN and smoothing (Savitzky-Golay with five to 13 points smoothing), 1stD and 2ndD calculation (Savitzky-Golay with five to 13 points smoothing) [73,131,137,150], SNV, MSC [150] and the combination of derivative, BC and AN methods. Pre-processing was conducted using The Unscrambler®X (Smoothing, 1stD and 2ndD, SNV and MSC, CAMO Software Oslo, Norway, Version 10.1) and Origin®Pro (BC and AN, Origin Lab Corp. Version 8.5). Water and water vapour were subtracted to give a flat base line between 2300-1750 cm^{-1} using Microsoft Excel (2003) [60,73,137,138].

2.2.4. Fluorescence spectroscopy

Fluorescence spectra were recorded using a Hitachi F-7000 fluorescence spectrophotometer and Fl solutions software (version 2.1, Hitachi High-Technology Corporation, Tokyo, Japan). The sample cell (10 mm path length) was obtained from Bio-Tools, Inc. (NSW, Australia). Samples were excited at 295 nm and the emission was recorded between 250-500 nm. The scan speed was 240 nm min^{-1}, excitation and emission slit widths were 5 nm and voltage of the photomultiplier detector (PMT) was set at 400 V. Water was subtracted [69,73] and the emission band between 300-400 nm was pre-processed using BC, AN, SNV, MSC [150] and a combination of BC and AN methods. Pre-processing was conducted with The Unscrambler®X software.

2.3. Results

2.3.1. Background subtraction

FTIR spectra of water, native BSA (5% w/w) in water and the water vapour are shown in **Figure 2.1(A)**. The water spectrum showed bands for FTIR spectroscopy at 3400 cm^{-1} and 1645 cm^{-1} whereas the water vapour spectrum showed sharp bands around 4000-3500 cm^{-1} and 2000-1250 cm^{-1} and a band around 2300 cm^{-1}. The spectrum of native BSA in water was overlapped with water between 1700 and 1600 cm^{-1}. The spectrum of native BSA in water was water and water vapour subtracted to give a flat baseline between 2300-1750 cm^{-1} as was shown in **Figure 2.1(B)**. The subtracted spectra showed bands at 1700-1600 cm^{-1}, 1480-1575 cm^{-1} and 1229-1301 cm^{-1} (**Figure 2.1(C)**).

In the case of fluorescence spectroscopy, the maximum emission of native BSA in water appears around 350 nm and the water band appears at 290 nm (**Figure 2.2**). Water was subtracted from the raw data to reduce the solvent influence in the maximum intensity values of Trp residue (300-400 nm).

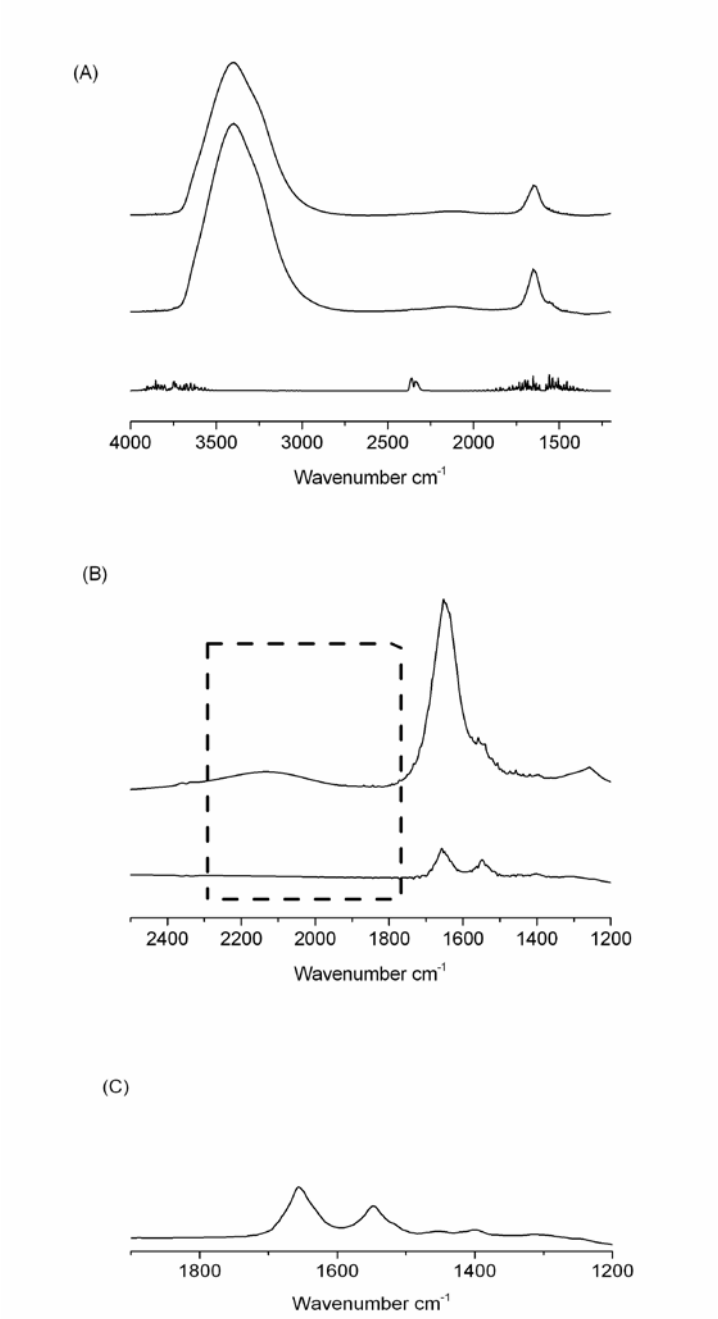

Figure 2.1 Typical example of FTIR spectra showing native BSA (5% w/w) before and after water and water vapour subtraction (from top to bottom): (A) The original spectra of water, native BSA in water and water vapour (before subtraction) and (B) spectra of native BSA in water and native BSA after water subtraction and (C) spectra of native BSA after water and water vapour subtraction. The square in Figure 2.1(B) illustrates the flat baseline region after water and water vapour subtraction (2300-1750 cm^{-1}).

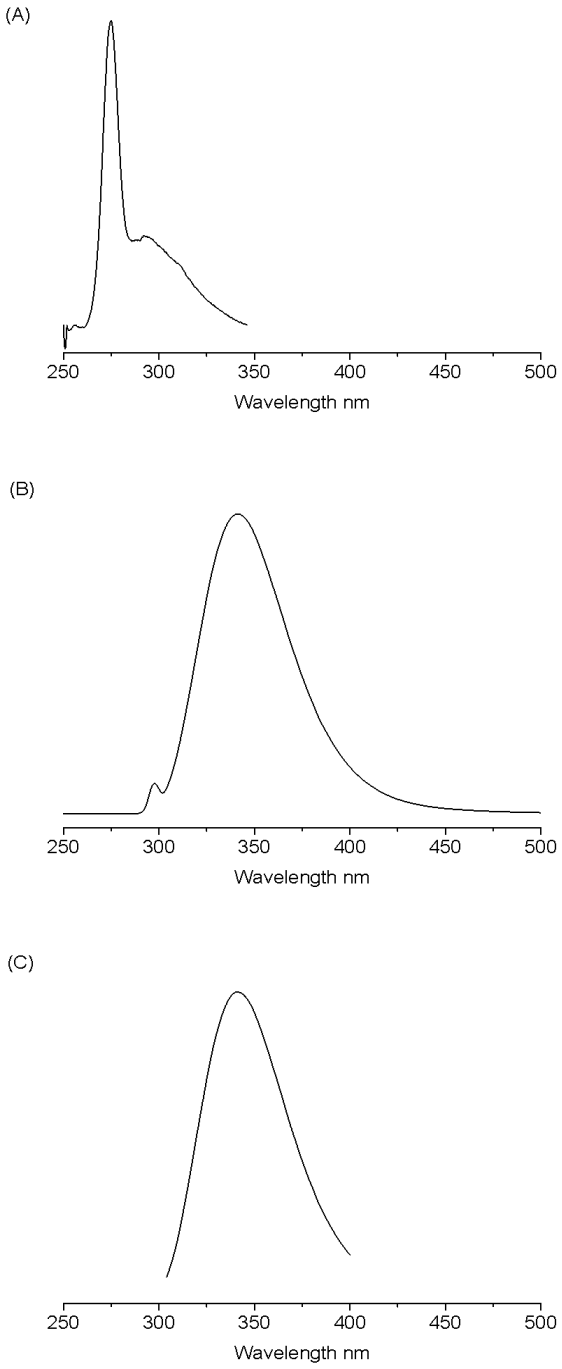

Figure 2.2 Typical example of fluorescence spectra showing native BSA (1% w/w) before and after water subtraction (from top to bottom): (A) the original spectrum of water, (B) the original spectrum of native BSA in water and (C) the native BSA spectrum after water subtraction. (Spectra of water (A) and protein in water (B) are in different scales).

2.3.2. Baseline correction

The amide I band of native BSA (5% w/w) was BC as shown in **Figure 2.3**. The linear BC spectrum showed a decrease in absorbance intensity at the end points of amide I band (1700 and 1600 cm^{-1}) which was represented using arrows. The end points of the amide I band were fitted to Y=0. The maximum absorbance (1654.9 ± 0.0 cm^{-1}) remained at the same wavenumber following the linear BC. The absorbance at 1600 cm^{-1} (ΔA: 0.009 ± 0.002) was reduced more than at 1700 cm^{-1} (ΔA: 0.006 ± 0.003) (mean ± s.d., n=3). This increased the slope of the spectra over the range 1600 to 1654 cm^{-1} more than in the region from 1654 to 1700 cm^{-1}.

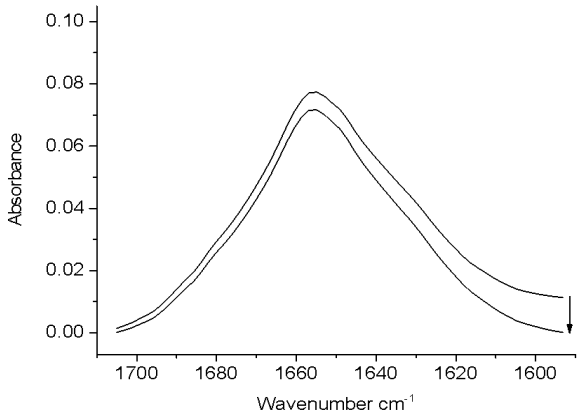

Figure 2.3 Typical example of FTIR spectra showing a comparison between the amide I band of native BSA (5% w/w) before and after linear BC (i.e. Y=0). Arrow indicates the decrease in the absorbance intensity in the original spectra to perform the linear BC method.

Spectra of native BSA, 50% native BSA and heat-denatured BSA were BC to compare changes in the secondary structure of proteins (**Figure 2.4**). The heat-denatured BSA (5% w/w) (dashed line) showed a characteristic shoulder at 1610-1630 cm^{-1} and a decrease in the band at 1654 cm^{-1}. The spectrum of amide I band for 50% native BSA had a similar shape than for amide I of native BSA but showing higher absorbance intensity. Arrows indicates the shift in the absorbance intensity of the original spectra that were necessary to perform the linear BC. However, native BSA, 50% native BSA and heat-denatured BSA spectra were in different scales and it was necessary to perform an additional pre-processing method (i.e. normalization) to better investigate the differences in the secondary structure of these protein solutions.

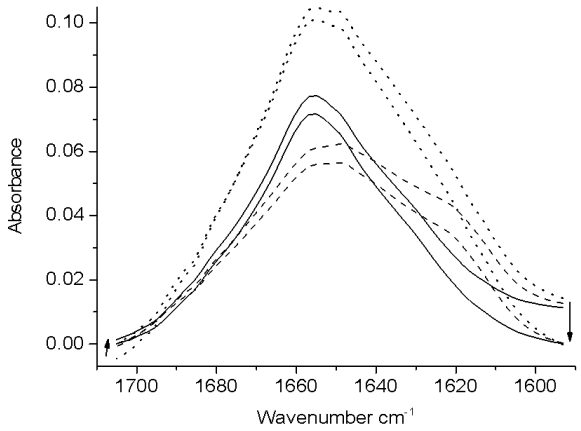

Figure 2.4 Typical example of FTIR spectra showing a comparison between the amide I band (5% w/w) before and after linear BC (i.e. Y=0). Native BSA (straight line), 50% native BSA (dotted line) and heat-denatured BSA (dashed line). Arrows indicates the increase or decrease in the absorbance intensity in the original spectra to perform the BC method.

In the case of fluorescence spectroscopy, the intensity of the Trp band (300-400 nm) was shifted giving a linear BC spectrum with constant value (Y=0) (**Figure 2.5**). The shift in the intensity of native BSA is indicated using arrows. The maximum emission of Trp band for native BSA alone was shifted from 341.6 ± 0.5 to 340.6 ± 0.0 which was obtained by visual inspection of the point of maximum absorbance between 300-400 nm (mean ± s.d., n=3).

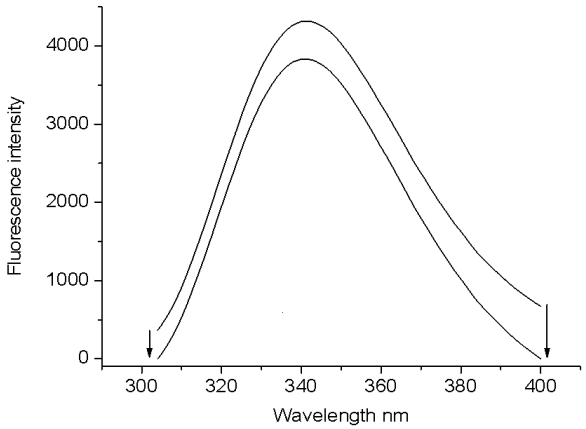

Figure 2.5 Typical examples of fluorescence spectra of BSA protein showing the Trp maximum intensity for 100% native BSA (300-400 nm) before and after linear BC. Arrows indicates the shift in the fluorescence intensity after BC.

Fluorescence spectra of native BSA, 50% native and heat-denatured BSA were used to study changes in tertiary structure of proteins using linear BC (**Figure 2.6**). After BC, the maximum fluorescence intensity (300-400 nm) for native BSA, 50% native BSA and thermally denatured BSA were shifted from (341.6 ± 0.5 nm, 338.7 ± 0.2 nm and 334.6 ± 0.2 nm respectively) to (340.6 ± 0.0 nm, 338.5 ± 0.3 nm and 334.7 ± 0.1 nm respectively). Arrows indicate the shift in the fluorescence intensity after linear BC.

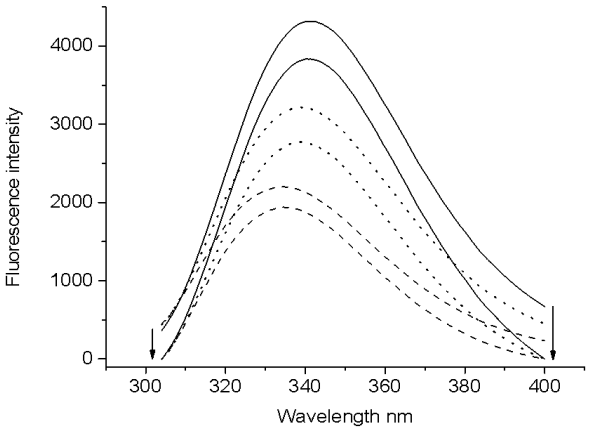

.

Figure 2.6 Typical example of fluorescence spectra of BSA protein showing the Trp maximum intensity (300-400 nm) before and after linear BC for native BSA (straight line), 50% native BSA (dotted line) and heat-denatured BSA (dashed line). Arrows indicate the decrease in the fluorescence intensity after BC.

2.3.3. Area normalization

The FTIR spectra of native BSA were pre-processed using AN to compare different spectra in the same scale to gain additional information about protein conformation. The amide I band of native BSA was area normalized as shown in **Figure 2.7**. The position of the maximum intensity at 1654.9 cm^{-1} was not shifted after AN of the original spectrum.

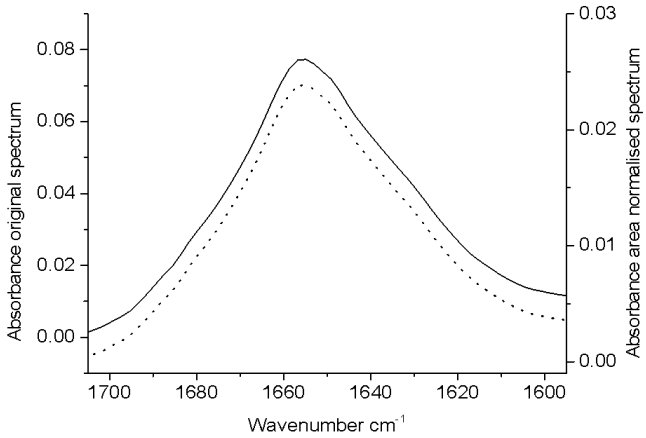

Figure 2.7 Typical example of FTIR spectra of amide I pre-processed using AN for native BSA of the original spectrum (straight line) and after AN (dotted line).

The position of the maximum intensity for native BSA and 50% native BSA pre-processed using AN was 1654.9 ± 0.0 cm^{-1} whereas for heat-denatured BSA spectra this band was shifted to 1649.1 ± 0.0 cm^{-1} (**Figure 2.8**). Additionally, a second band was obtained for solutions of heat-denatured BSA around 1620 cm^{-1}. Spectra of amide I pre-processed using the AN gives all the spectra in the same scale which allowed a better comparison between changes in the secondary structure of proteins attributed to α-helix (1654.9 cm^{-1}) and intermolecular β-sheet elements (1610-1630 cm^{-1}) among original spectra of native BSA, 50% native BSA and heat-denatured BSA. The intensity of the α-helix band at 1654.9 cm^{-1} was reduced from the native BSA to the heat-denatured BSA.

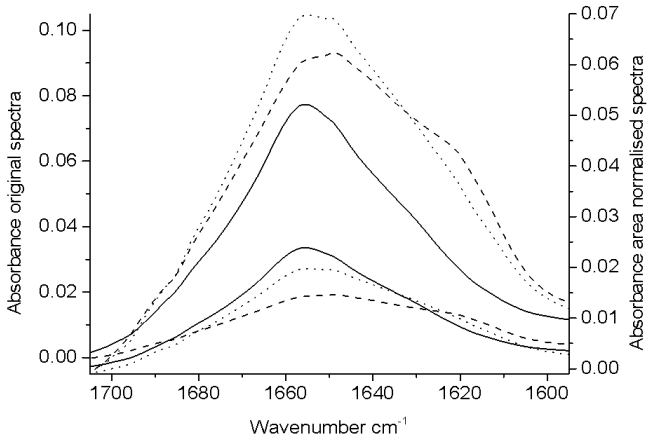

Figure 2.8 Typical example of FTIR spectra of amide I pre-processed using AN for native BSA (straight line), 50% native (dotted line) and heat-denatured BSA (dashed line) (Top lines: before pre-processing. Bottom lines: after pre-processing).

The amide I band was pre-processed using a combination of methods (i.e. BC and AN) to investigate if the association of those methods gave additional information about protein structure (**Figure 2.9**). The position of the maximum absorbance for the amide I band pre-processed using BC and AN for native BSA was 1652.99 ± 0.0 cm^{-1} which was consistent with the information obtained from spectra pre-processed using AN alone (**Figure 2.8**).

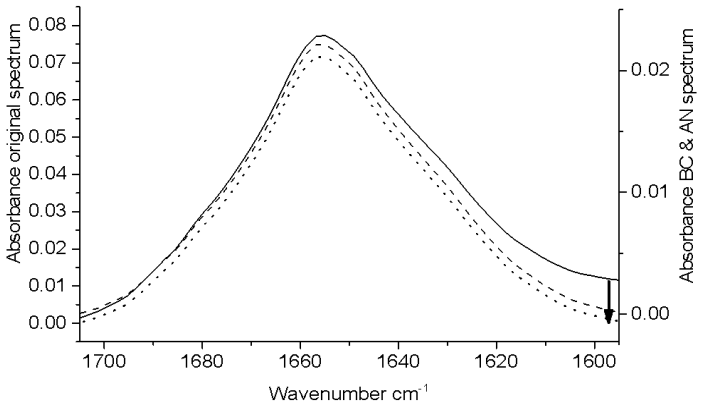

Figure 2.9 Typical example of FTIR spectra of amide I band pre-processed using BC and AN: the original spectrum before pre-processing (straight line), the BC spectrum (dotted line) and the spectrum after BC and AN (dashed line).

Native BSA, 50% native and heat-denatured BSA spectra were used to investigate changes in protein physical stability after linear BC and AN of the amide I band (**Figure 2.10**). The combination of these pre-processed methods gave spectra at the same scales and similar starting and ending values of absorbance (i.e. Y=0). The position of the maximum absorbance for native BSA and 50% native BSA was 1652.99 ± 0.0 cm^{-1} and for heat-denatured was 1649.13 ± 0.0 cm^{-1}.

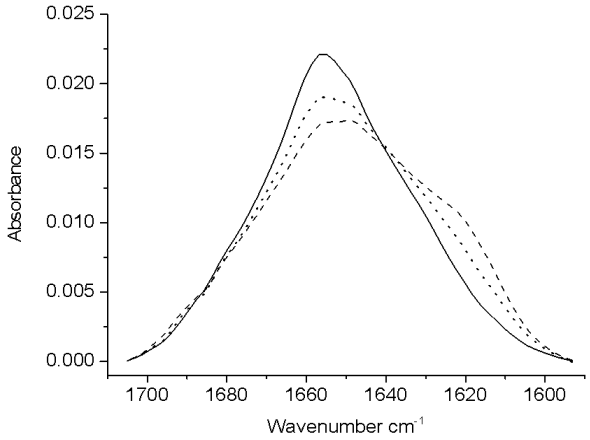

Figure 2.10 Typical example of FTIR spectra of amide I band (1700-1600 cm^{-1}) pre-processed using linear BC and AN: native BSA (straight line), 50% native (dotted line) and heat-denatured BSA (dashed line).

Fluorescence spectra of native, 50% native and heat-denatured BSA pre-processed using AN were used to investigate changes in the tertiary structure of proteins comparing all these spectra in the same area (**Figure 2.11**). In comparison with original spectra shown in **Figure 2.6,** the area normalized spectrum of Trp (300-400 nm) showed a blue shift in the maximum emission from native BSA (341.3 ± 0.3 nm) compared to heat-denatured BSA (334.4 ± 0.1 nm). The peak of maximum fluorescence intensity increased from native to heat-denatured spectra. However, those spectra had a different baseline.

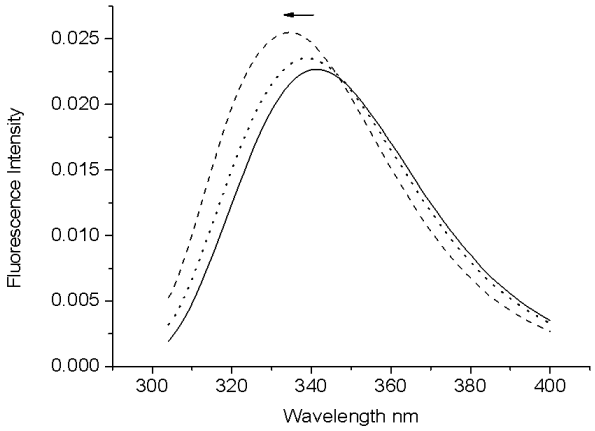

Figure 2.11 Typical example of fluorescence spectra of Trp emission (300-400 nm) pre-processed using AN: native BSA (straight line), 50% native (dotted line) and heat-denatured BSA (dashed line). Arrow indicates the blue shift from native BSA (341.3 ± 0.3 nm) to heat–denatured BSA (334.4 ± 0.1 nm).

Fluorescence spectra of native BSA, 50% native and heat-denatured BSA were pre-processed using BC in combination with AN as shown in **Figure 2.12**. Spectra pre-processed using BC and then, AN show smaller differences in the magnitude of fluorescence intensity of Trp maximum emission between native BSA and heat-denatured BSA than spectra pre-processed using AN alone (**Figure 2.11**). The maximum Trp emission of spectra for native BSA, 50% native BSA and heat-denatured BSA were 340.8 ± 0.3 nm, 338.4 ± 0.2 nm and 334.8 ± 0.0 nm respectively (**Figure 2.12**).

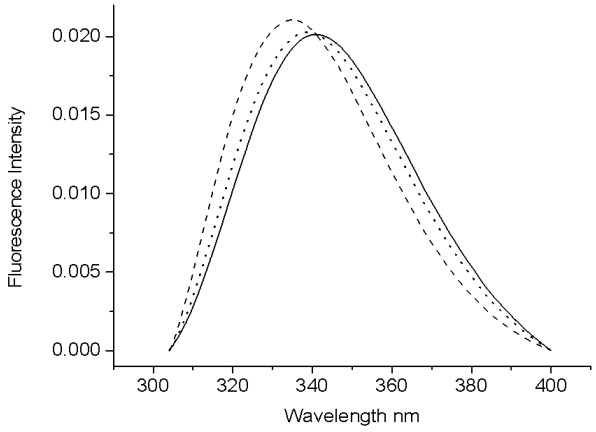

Figure 2.12 Typical example of fluorescence spectra of Trp emission (300-400 nm) pre-processed using BC and AN: native BSA (straight line), 50% native (dotted line) and heat-denatured BSA (dashed line).

2.3.4. Smoothing methods

The spectrum of native BSA (amide I band) was smoothed in 5, 9 and 13 points using the Savitzky-Golay method to investigate the decrease in the spectral noise and the loss of relevant information in the smoothed spectra (**Figure 2.13**). The original amide I band did not show a considerable amount of noise to be reduced, due to the bulk water and water vapour subtraction steps. When smoothed in 13 points the shape of the original amide I band changed considerably and this was considered an example of excessive smoothing. The original spectrum of the amide I band for native BSA alone showed a narrow peak at 1654.9 cm^{-1} whereas spectra smoothed in 13 points showed a wide peak which shifted to 1652.9 cm^{-1} (**Table 2.1**). Additionally, the loss of peak information with excessive smoothing was investigated for native BSA, 50% native BSA and heat-denatured BSA (**Table 2.1**). Smoothed spectra shifted the peak position of amide I with the increase in smoothing points from zero to 13 points.

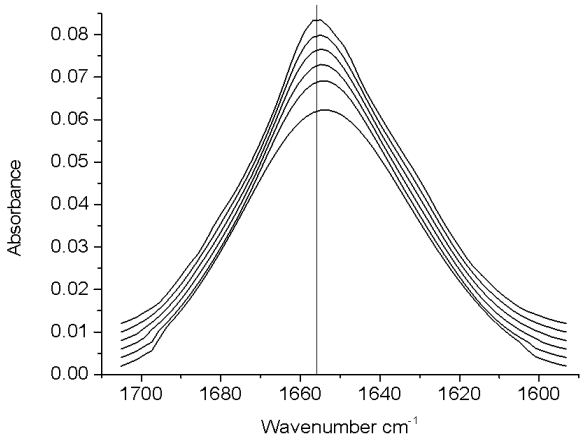

Figure 2.13 Typical example of FTIR spectra of amide I band pre-processed using smoothing (Savitzky-Golay) and BC (from top to bottom): spectra smoothed in 0, 5, 7, 9, 11 and 13 points. The vertical line (1654 cm^{-1}) shows the shift in the maximum absorbance of native BSA with the increased in smoothing points from 0 to 13 points. (Spectra were off set for clarity).

Table 2.1 Peak positions for the original and smoothed spectra for native BSA, 50% native BSA and heat-denatured BSA. (mean ± s.d.).

Pre-processing method	**Native BSA alone (wavenumber cm^{-1})**	**50% Native BSA (wavenumber cm^{-1})**	**Heat-denatured BSA (wavenumber cm^{-1})**
Original spectra	1654.9 ± 0.0	1654.3 ± 1.1	1649.1 ± 0.0
Smoothed in 5 points	1654.9 ± 0.0	1652.9 ± 0.0	1649.1 ± 1.9
Smoothed in 7 points	1654.9 ± 0.0	1652.9 ± 0.0	1649.8 ± 2.2
Smoothed in 9 points	1653.6 ± 1.1	1652.3 ± 1.1	1649.1 ± 1.9
Smoothed in 11 points	1652.9 ± 0.0	1651.7 ± 1.1	1648.4 ± 1.1
Smoothed in 13 points	1652.9 ± 0.0	1651.1 ± 0.0	1648.4 ± 1.1

2.3.5. Differentiation methods

Derivative methods using five to 13 smoothing points were used to investigate the relationship between smoothing effect and the loss of relevant information about protein secondary structure. The 1stD spectrum (**Figure 2.14**) showed two turning points around 1650 cm^{-1} and 1665 cm^{-1} which represent changes in the curvature of the original spectrum of amide I as shown in **Figure 2.3**. 1stD spectra crossed the X-axis at 1654 cm^{-1} which corresponds with the maximum absorbance in the amide I band (e.g. α-helix band) (**Figure 2.14**). This value did not change with the increase of smoothing points which was assessed by visual inspection. However, the increase in the number of smoothing points from five to 13 reduced the spectral noise around 1680-1700 cm^{-1} and 1610-1630 cm^{-1} which was assessed by visual inspection. Additionally, smoothing the 1stD in 13 points reduced information of amide I band giving a wide curve around 1680-1700 cm^{-1} and 1610-1630 cm^{-1}. Spectra pre-processing using the 1stD smoothed in 11 points showed a shift in the cross-over point at zero which corresponds to the maximum absorbance of native BSA (1654.9 ± 0.0 cm^{-1}), 50% native BSA (1652.9 ± 0.0 cm^{-1}) and thermally denatured BSA (1649.1 ± 1.9 cm^{-1}).

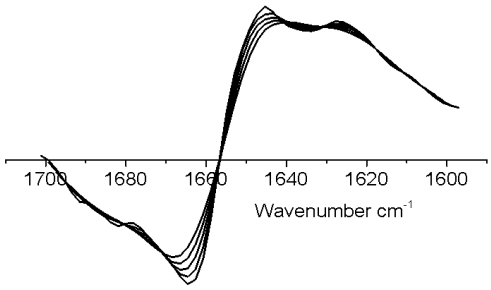

Figure 2.14 Typical example of FTIR spectra of amide I band pre-processed using 1stD smoothed with 13, 11, 9, 7 and 5 points showing the two turning points (around 1650 and 1660 cm^{-1}). The horizontal line shows the intersection with zero which represents the maximum absorbance at 1654.9 cm^{-1} for the original spectra.

FTIR spectra of the amide I band pre-processed using the 2ndD are shown in **Figure 2.15**. The positive peak in the original spectrum of BSA at 1654.9 cm^{-1} resulted in a negative peak in the 2ndD spectrum which appears at the same position (i.e. 1654.9 cm^{-1}). Spectra were pre-processed using the Savitzky-Golay method with 5, 7, 9, 11 and 13 points smoothing to investigate the decrease in spectral noise and the loss of relevant information. The 2ndD of amide I smoothed in 5 points contained large amount of sharp bands around 1700-1680 cm^{-1}, 1654 cm^{-1}, 1650 cm^{-1} and 1600-1630 cm^{-1}. In contrast, the spectrum smoothed in 13 points shown a wide band at 1654 cm^{-1} without bands around 1700-1680 cm^{-1}, 1650 cm^{-1} and 1600-1630 cm^{-1}. The 2ndD spectra smoothed from 7 to 11 points reduced the sharpness of these bands giving smoothed spectra. A large decrease in the absorbance intensity was observed for spectra smoothed in 13 points in comparison with spectra smoothed in five points.

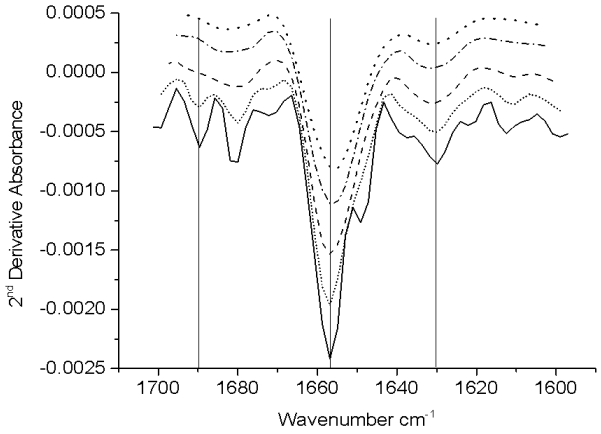

Figure 2.15 Typical example of FTIR spectra of amide I band pre-processed using 2ndD (Savitzky-Golay) smoothed in (from top to bottom): 13 points (dotted line), 11 points (dash dotted line), 9 points (dashed line), 7 points (short dotted line) and 5 points (straight line). Vertical lines show loss of peaks with increasing smoothing. (Spectra were off set for clarity).

The spectrum of the amide I band was pre-processed using the 2ndD of the amide I band smoothed in 11 points and then, the 2ndD spectrum was BC giving the whole data set in the same Y-axis. Arrows indicate the shift down in absorbance intensity after linear BC (**Figure 2.16(A)**). After that, AN was applied to the 2ndD and the BC spectrum of the amide I band (**Figure 2.16(B)**). The corrected spectrum of native BSA using the 2ndD smoothed in 11 points, BC and AN showed the α-helix band at 1654 cm^{-1} without bands at 1610-1630 cm^{-1}. Additionally, the corrected spectrum did not show evidence of spectral noise.

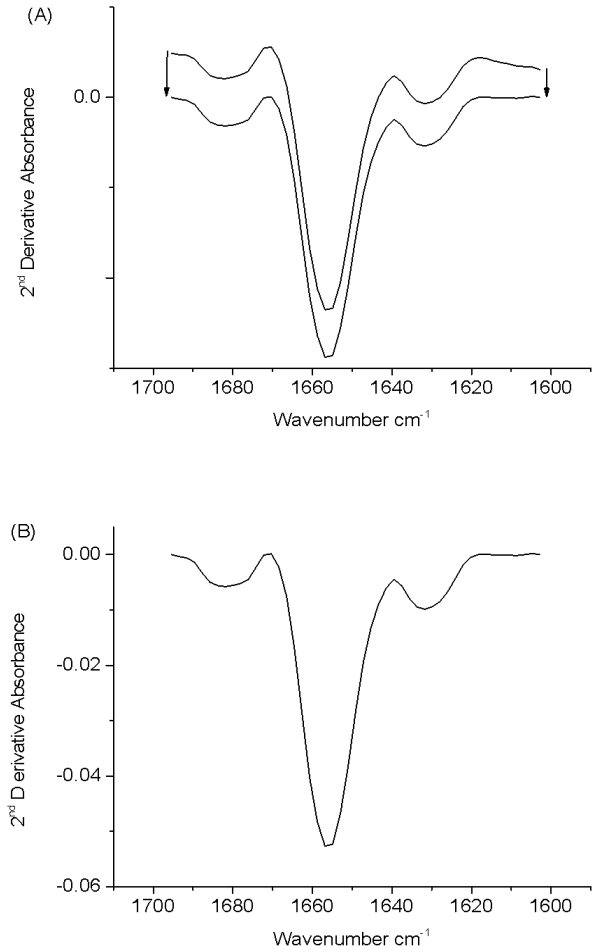

Figure 2.16 Typical example of 2ndD of amide I band smoothed in 11 points (Savitzky-Golay) pre-processed using (A) BC and (B) BC and AN. Arrows indicates the shift in absorbance after linear BC method.

FTIR spectra of the amide I band pre-processed using a combination of techniques (2nd D (11), BC, AN) were used to compare the secondary structure of native BSA, 50% native BSA and heat-denatured BSA (**Figure 2.17**). In comparison with the amide I of native BSA, spectra of heat-denatured BSA and 50% native BSA showed appearance of bands at 1610 - 1630 cm^{-1} and 1654.9 cm^{-1}.

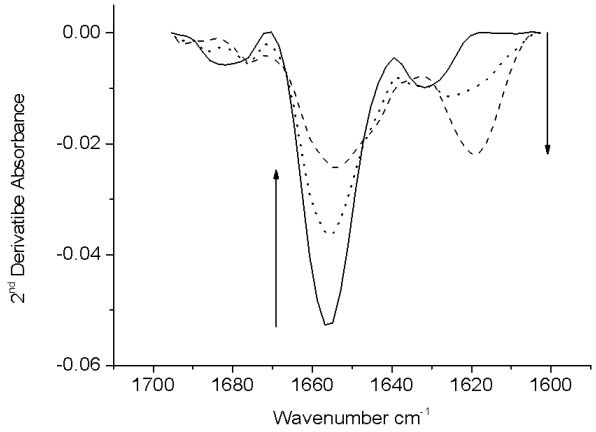

Figure 2.17 Typical example of FTIR spectra of amide I band pre-processed using 2ndD smoothed in 11 points, BC and AN: native BSA (straight line), 50% native BSA (dotted line) and heat-denatured BSA (dashed line). Arrows indicate the decrease in α-helix content (1654 cm^{-1}) and increase of intermolecular β-sheet (1610-1630 cm^{-1}).

2.3.6. Multiplicative scatter correction

Multiplicative scatter correction spectra showed the main differences attributed to α-helix (1654 cm^{-1}) and β-sheet bands (1610-1630 cm^{-1}) of native BSA, 50% native and heat-denatured BSA (**Figure 2.18**). Spectra of native BSA, 50% native and heat-denatured BSA were used to calculate an average spectrum using the MSC method. In comparison with original spectra of native BSA, 50% native BSA and heat-denatured BSA (**Figure 2.4**), amide I spectra pre-processed using MSC decreased the absorbance intensity from native BSA alone to heat-denatured BSA in the band at 1654 cm^{-1}. The characteristic band attributed to aggregates was shown for heat-denatured BSA and also for the 50% native BSA to be around 1610-1630 cm^{-1}.

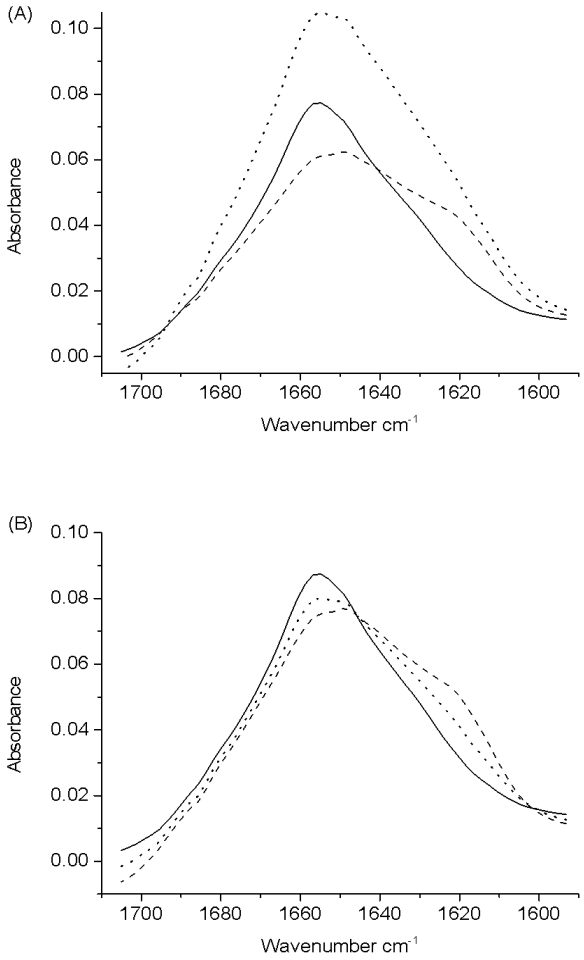

Figure 2.18 Typical example of FTIR spectra of amide I band of native BSA (straight line), 50% native (dotted line) and heat-denatured BSA (dashed line): (A) original spectra and (B) spectra pre-processed using MSC method.

Fluorescence spectra of native BSA, 50% native BSA and heat-denatured BSA were pre-processed using MSC as shown in **Figure 2.19**. This pre-processing method showed the shift in the maximum emission of Trp from 342 nm (for native BSA) to 334 nm (for heat-denatured BSA). Additionally, this method reduced the differences in fluorescence intensity that were found in the original spectra of Trp maximum emission of native BSA, 50% native BSA and heat-denatured BSA (**Figure 2.6**).

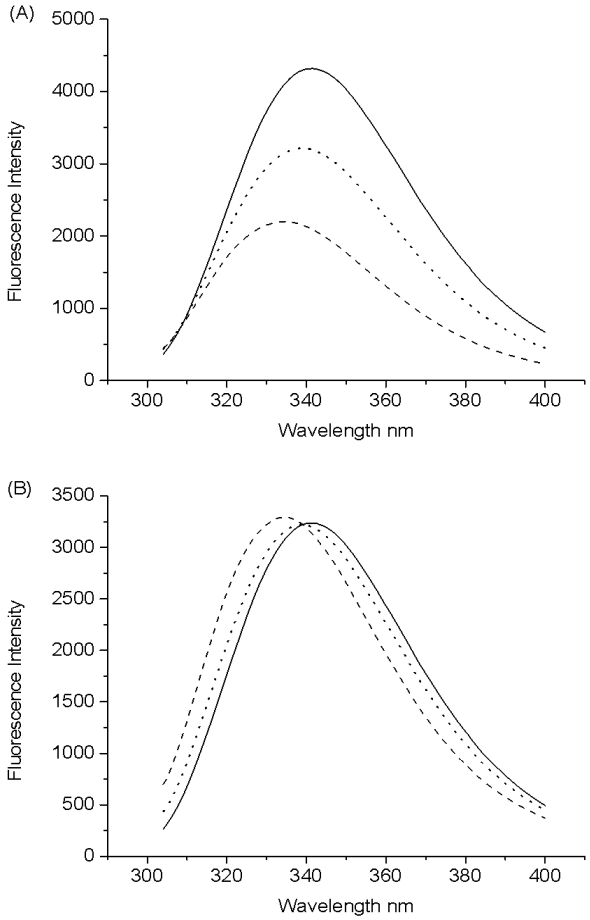

Figure 2.19 Typical example of fluorescence spectra of Trp emission of native BSA (straight line), 50% native BSA (dotted line) and heat-denatured BSA (dashed line): (A) original spectra and (B) spectra pre-processed using MSC method.

2.3.7. Standard normal variate

FTIR spectra were pre-processed using the SNV method showing the principal differences in of the amide I band for native BSA, 50% native BSA and heat-denatured BSA at 1654 cm^{-1} and 1610-1630 cm^{-1} (**Figure 2.20**). The differences in the absorbance intensity obtained in original spectra (**Figure 2.4**) were reduced using SNV method.

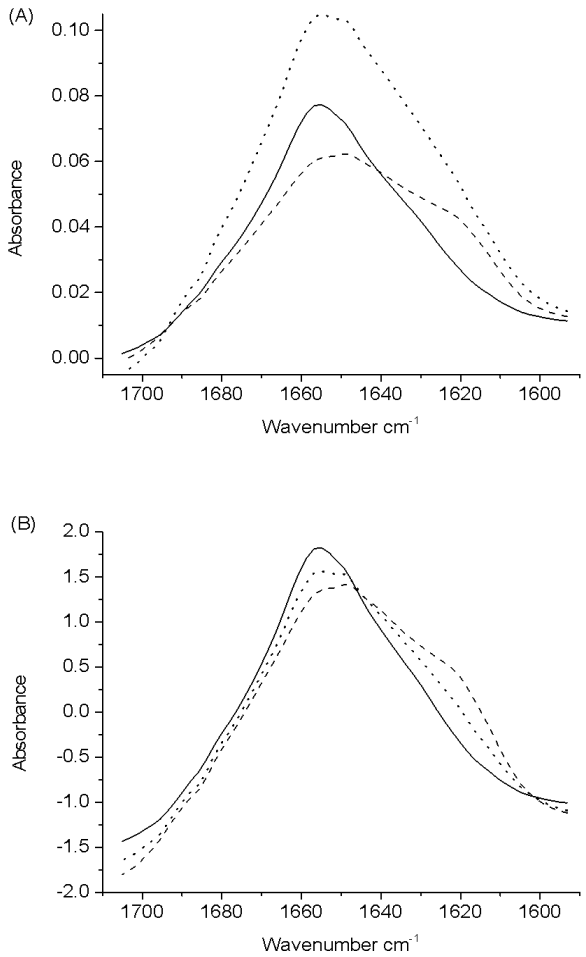

Figure 2.20 Typical example of FTIR spectra of amide I band of native BSA (straight line), 50% native (dotted line) and heat-denatured BSA (dashed line): (A) original spectra and (B) spectra pre-processed using the SNV method.

Fluorescence spectra pre-processed using the SNV method was shown in **Figure 2.21**. In comparison with original spectra (native BSA, spectra of 50% native BSA and heat-denatured BSA) (**Figure 2.6**), the SNV method showed a shift in the maximum emission of Trp from 342 nm for native BSA to 334 nm for heat-denatured BSA reducing the differences in the fluorescence intensity.

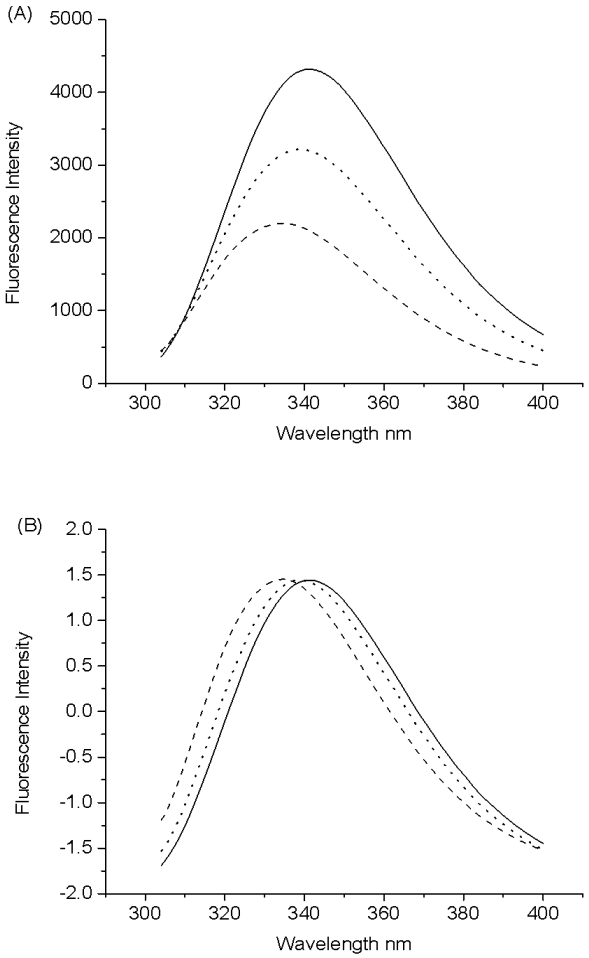

Figure 2.21 Typical example of fluorescence spectra of native BSA (straight line), 50% native BSA (dotted line) and heat-denatured BSA (dashed line): (A) original spectra and (B) spectra pre-processed using SNV method.

2.4. Discussion

In this Chapter, pre-processing methods were used alone (i.e BC, AN, derivatives, SNV and MSC) or in combination with other methods (i.e. 2nd D, BC, AN (FTIR spectra) and BC, AN (fluorescence spectra)) to obtain additional information that explains changes in the secondary (FTIR spectroscopy) and tertiary (fluorescence spectroscopy) structure of proteins. Pre-processing methods were applied to the original spectra of native BSA, 50% native BSA and thermally denatured BSA to demonstrate that the use of pre-processing methods is necessary in the study of protein structure and it needs to be carefully performed with attention given to the changes that occur with each step.

Typical bands of proteins in solution were found using FTIR spectroscopy. The water spectrum showed the characteristic bands for FTIR spectroscopy at 3400 cm^{-1} (O-H stretching) and 1645 cm^{-1} (H-O-H bending) [139] whereas the water vapour spectrum showed characteristic sharp bands around 4000-3500 cm^{-1} and 2000-1250 cm^{-1} and a band around 2300 cm^{-1} attributed to rotational motions [60]. The spectrum of native BSA in water showed the characteristic amide I band (1645 cm^{-1}) overlapped with water between 1700-1600 cm^{-1} (C=O stretching) [60,73,137-139]. The spectrum of native BSA in water was water and water vapour subtracted to give a flat baseline between 2300 and 1750 cm^{-1} which was consistent with previous reports [60,73,137,138]. The subtracted spectra showed characteristics amide I, II and III bands at 1700-1600 cm^{-1} (C=O stretching), 1480-1575 cm^{-1} (N-H bending and C-N stretching) and 1229-1301 cm^{-1} (N-H bending and C-N stretching) respectively [139].

The water band (H-O-H) absorbs strongly around the amide I band of proteins (1700-1600 cm^{-1}). However, the strong absorption of water can be avoided using CaF_2 windows with a short pathlength (6-8 μm) and protein solutions at concentrations higher than 10 mg/mL [151]. In this thesis, both recommendations were considered to control the strong adsorption of water in the amide I band region. The Varian resolution Pro software has the rapid-scan option giving a spectrum in a few milliseconds. Commonly, protein spectra are collected using 16 to 100 scans and the resolution is fixed in four or eight cm^{-1} [151-154] In this thesis, FTIR spectra were collected using 16 scans with a resolution of four cm^{-1} giving a good relationship between the scan rate and the data acquisition.

Background subtraction is considered a critical step within spectral pre-processing methods [55] to obtain an appropriate protein spectrum which gives qualitative and quantitative information about the structure of proteins [68]. In the case of FTIR spectroscopy, background subtraction is a necessary pre-processing method because the amide I band (1600-1700 cm^{-1}) overlaps with water bands. Additionally, amide I of BSA is affected by the presence of water vapour bands which contribute to increase in spectral noise in the amide I band affecting the quality of this band (**Figure 2.1(B and C)**) [60]. An alternative method to minimize water vapour contribution is to allow a longer incubation time inside the measurement chamber of the spectrophotometer giving extra time to purge the remaining air. Protein solutions were equilibrated in the sample chamber of the spectrophotometer for five and ten minutes where spectral noise attributed to water vapour was clearly decreased (data no shown). This alternative method to reduce water vapour contribution may be useful when a small number of samples are being analysed. In this work, FTIR spectroscopy was used to measure several protein samples to investigate protein physical stability in native protein, 50% native and heat-denatured BSA solutions. Thus, protein solutions needed to be measured as soon as possible to avoid protein degradation, so that protein samples could not remain inside the spectrophotometer during a long period of time.

In the case of fluorescence spectroscopy, the water band did not interfere directly with the Trp band (300-400 nm) [69] because the water band appears before the Trp emission. The maximum emission of native BSA in water appears around 350 nm [73] and the water band appears at 290 nm [140]. The water vapour signals did not show to affect the quality of Trp band or increase the noise of Trp band (**Figure 2.2**). Background subtraction results for FTIR and fluorescence spectra were in agreement with previous reports showing that this pre-processing method is a crucial first step in protein analysis using spectroscopy [60,69,151].

The subtraction method used in this Chapter has been extensively reported and applied in several publications [55,60,69,73,125,137,138]. Background subtracted spectra were obtained straight forward since unwanted peaks (i.e. water and water vapour signals) were removed by visual inspection from the original spectrum. However, the main consideration of background subtraction is to avoid over-subtraction of the original spectrum which may produce a loss of important spectral information [137,138]. In the case of FTIR, background subtraction was performed using Microsoft Excel. However, the mathematical principle used for Excel Microsoft and Varian resolution Pro software is the same and the subtracted spectrum

obtained from any of these methods should be similar. In the case of fluorescence spectra, the background subtraction was performed using the Fl solutions software, nevertheless a similar subtracted spectrum must be obtained using Microsoft Excel.

Spectra pre-processed using BC did not improve the quality of the information obtained about protein physical stability in comparison with original spectra. Indeed, this method did not give new information to explain protein conformation in comparison with the raw spectra and similar spectra were obtained before and after the application of this method. This may be explained because linear BC modified the magnitude of the Y-axis (i.e. FTIR absorbance and fluorescence intensity) but the shape of the curves were kept intact. This may be explained because the light scattering effect produced a slope in the raw spectrum [130]. In the case of liquid samples, the BC FTIR and fluorescence spectra did not modify the curves and slopes of the raw spectra. Moreover, linear BC did not affect the position of the principal amide I bands for FTIR spectroscopy (i.e. 1654 cm^{-1}) (**Figure 2.4**) and the Trp band for fluorescence spectroscopy (i.e. 342 nm) (**Figure 2.6**). This result was in agreement with the work reported by Rinnan *et al.* (2009), where Near-IR spectra of proteins in a sugar mixture pre-processed using the BC method did not improve the spectral data [130]. Baseline offset is another method used to perform a BC which corrects the spectral data set to the minimum point within the spectra [130,148]. Spectra pre-processed using the baseline offset method may change the Y-axis of the original spectra [130]. Yet, the baseline offset method should not give new information about the shift in the position of amide I band or Trp emission or show the presence of new bands. This means that similar information about protein physical stability must be obtained after BC using the baseline linear or the baseline offset correction methods.

Normalization removes spectral variations dividing each spectrum by a number (i.e. a constant, mean, minimum, maximum etc). The common goal of normalization is to convert all spectra in the same scale [141,148]. Diverse normalization methods are possible where the principal difference between them is that the original spectrum is divided by an area, peak height, mean, or maximum Y-value [141]. The AN method is useful to improve the correlation of spectroscopy signals which increases the precision of quantitative analysis. Commonly, normalized area is preceded by BC [141]. In the analysis of protein stability, the most common method of normalization used to investigate protein secondary structure is the AN [52,73,131]. Jorgensen *et al*. (2004) reported the use of AN in combination with 2^{nd}D of amide I to calculate the area overlap of BSA and HAS in different water oil emulsions [73].

In this Chapter, spectra were pre-processed using AN. This method transforms all the spectra in the same area (total AUC = 1) which allows investigating changes in the spectrum to be attributed to loss of secondary and tertiary structure of proteins. Moreover, normalization has been used to investigate the relationship between shift in the maximum emission of the fluorophores (i.e. 2-acetylanthracene and 2-anilinonaphthalene) and the effect of solvents of different polarity (i.e. water, methanol, octanol, hexane, dioxane and cyclohexane) using fluorescence spectroscopy studies [155]. AN was applied to circular dichroism spectra of native proteins to quantify protein content using PLS models [141]. In this thesis, FTIR spectra pre-processed using AN (**Figure 2.8**) showed differences and similarities between native BSA, 50% native BSA and heat-denatured BSA spectra more clearly than for spectra pre-processed using linear BC (**Figure 2.4**). The principal differences between native BSA, 50% native BSA and heat-denatured BSA spectra were characterised by a decrease in the absorbance intensity at 1654 cm^{-1} as a result of decreased α-helix content and the presence of bands at 1610-1630 cm^{-1} attributed to aggregates or intermolecular β-sheets structures. The principal similarity between those spectra was in the absorbance intensity of 50% native and heat-denatured BSA at 1654 cm^{-1} (**Figure 2.8**) which is an indication of the loss of secondary structure in the 50% native BSA solution [48,65].

In the case of fluorescence spectroscopy, changes in the Trp band (e.g. blue shift and reduced fluorescence intensity) were attributed to loss of tertiary structure in the heat-denatured BSA [155-157]. The maximum fluorescence intensity (300-400 nm) for native BSA, 50% native BSA and thermally denatured BSA were shifted from (341.6 ± 0.5 nm, 338.7 ± 0.2 nm and 334.6 ± 0.2 nm respectively) to (340.6 ± 0.0 nm, 338.5 ± 0.3 nm and 334.7 ± 0.1 nm respectively). This may indicate that Trp is more exposed to the polar environment as a result of the loss of tertiary structure [69,150]. The advantage of using area normalization over BC methods was to visualise better the shift in the position of the Trp maximum emission (**Figure 2.11**). However, fluorescence spectra pre-processed using the AN method were not BC. This may explain the different magnitude of the Trp maximum emission between native BSA, 50% native and heat-denatured BSA spectra. Thus, these spectra may be BC to verify that change in fluorescence intensity can be explained due to loss of tertiary structure of BSA [69,155-158]. The combination of BC and AN methods was useful to investigate the blue-shift from native BSA (342 nm) to heat-denatured BSA (334 nm) as well as the differences in the fluorescence

maximum intensity of native BSA, 50% native BSA and heat-denatured BSA that may be attributed to loss of tertiary structure of proteins (**Figure 2.12**).

Spectra contain random noise plus characteristic signals for each sample. The level of noise for each sample will depend on the experimental conditions used to obtain each spectrum [127]. Smoothing is a pre-processing technique where the spectral noise is reduced [81]. However, smoothing may remove sample signals that could be interesting to include in the analysis [55,57,81]. The smoothed spectrum is similar to the original spectrum with lower resolution [57,58,81]. For spectra being pre-processed using a combination of techniques, smoothing must be performed at the end. This may avoid the loss of relevant information that could be resolved by other techniques. Moreover, spectral smoothing is an integral part of derivative calculation so it was an important aspect to study.

The amide I band was used to investigate the effect of increasing smoothing points (0, 5, 7, 9, 11 and 13 points, **Figure 2.13**) to reduce the spectral noise. The original spectrum of the amide I band did not contain a large amount of spectral noise which was investigated by visual inspection. However, this method was used to investigate the loss of relevant information as a result of over-smoothing which was characterised by a loss in the shape of the amide I band at 1654 cm^{-1}. An over-smoothed spectrum is obtained when an excessive number of smoothed points are chosen which may affect the quality of spectral data [55] since relevant information could be lost [144]. An over-smoothed spectrum was obtained for the amide I band smoothed in 13 points (**Figure 2.13**) giving a broad band which has lost the shape and curvature of the original spectrum. Moreover, an uncorrected smoothed spectrum is obtained when a too small number of smoothing points is selected and spectral noise remains in the smoothed spectrum. Spectra smoothed in five points kept the shape of the original amide I spectrum. This suggests that smoothing the amide I band spectrum in five points could be suitable to reduce spectral noise and keep the shape of amide I band. This is in agreement with results shown in **Table 2.1**. In comparison with original spectra, the position of the maximum peak of native BSA alone at 1654 cm^{-1} was stable until spectra smoothed in seven points. Then, the position of the maximum peak of native BSA alone showed a shift to lower wavenumbers which could means that amide I band smoothing in 9 or more points are less stable. The raw fluorescence spectrum of native, 50% native and heat denatured BSA did not show evidence of spectral noise and for that reason, raw Trp bands were not smoothed.

Differentiation is an objective method [61] to study protein physical stability which gives information about changes in band intensity and shift positions of protein bands. The 1stD and 2ndD were calculated [58,61] to investigate protein structure. The principal advantage of 2ndD methods is that near or overlapped bands in the original spectrum can be identified to study each band as separated signals [143]. In this Chapter, 1stD and 2ndD were calculated for FTIR spectra to identify the presence of overlapping bands in the amide I region (i.e. α-helix at 1654 cm^{-1} and intermolecular β-sheets at 1610-1630 cm^{-1}). Additionally, the 2ndD method could identify other protein bands that cannot be easily studied by other pre-processing methods, including intermolecular β-sheet (1680-1690 cm^{-1}) and turn helix elements (1672 cm^{-1}). Fluorescence spectra were not pre-processed using the 2ndD because Trp emission does not contain bands in close proximity that need to be separated by this method. However, 1stD may be useful to investigate the shift of Trp maximum emission (300-400 nm) as result of loss of tertiary structure of proteins.

Differentiation methods can introduce noise into the spectrum [57,61,66] which may reduce the accuracy of the spectral analysis [57]. However, the Savitzky-Golay algorithm allows simultaneous smoothing and derivatisation of the spectrum [56,66,81]. This method requires defining a number of smoothing points prior to the calculation. In this thesis, the derivative spectra (1stD and 2ndD) were smoothed from five to 13 points using the Savitzky-Golay method. If the spectrum is pre-processed using a low number of smoothed points (i.e. five points), the derivative obtained by Savitzky-Golay is not better that the original spectrum. In contrast, if the spectrum is pre-processed using a high number of smoothed points (i.e. 13 points), the derivative obtained by Savitzky-Golay may loose relevant information from the original spectrum [143]. This was in agreement with the results obtained in this thesis where the 2ndD spectrum, smoothed in 13 points, showed to decrease the absorbance intensity at 1654 cm^{-1} and loss the shape of the original spectrum of amide I band (**Figure 2.15**). These results indicate that this spectrum was over-smoothed. In contrast, spectral noise was reduced for spectra smoothed in five points which indicates that additional smoothing points may be necessary to reduce the remaining spectral noise. From these results, the 2ndD spectrum smoothed in 9 or 11 points could be the best alternative because the corrected spectrum kept the relevant information of the original spectrum whilst giving smoothed bands. This was in agreements with Rinnan *et al*. (2009) whom reported than spectra pre-processed using 2ndD may be smoothed using 7 to 11 points to obtain more linear regressions models than using

higher or lower smoothing points [130].Similar results were found for 1stD spectrum smoothed using the Savitzky-Golay method. Spectra smoothed in 13 points were over-smoothed and spectra smoothed in five points showed residual spectral noise (**Figure 2.14**). From these results, it seems that using a 1stD (Savitzky-Golay with 9 or 11 points smoothing) should give a better signal. Near-IR spectra pre-processed by 2ndD (Savitzky-Golay with seven to 15 points smoothing) reduced the spectral noise more for protein spectra smoothed using a high number of smoothing points [130].

Spectra pre-processed using the 1stD of amide I band cannot be used to separate hidden bands which made this method less useful than 2nd D to investigate the secondary elements (i.e. α-helix and β-sheet structures). However, using the 1st D spectrum was useful to identify the peak position of the amide I band which crossed the X-axis at zero. The peak position for native BSA (1654.9 ± 0.0), 50% native BSA (1652.9 ± 0.0) and heat-denatured BSA (1649.1 ± 1.93) were not shifted when the 1stD smoothed in 11 points was applied to those spectra. This means that using the 1stD is a good method to investigate the peak position of the amide I band.

In previous reports, the 2ndD method has been used in combination with BC and AN to obtain information about the secondary structure of proteins. The combination of those techniques (i.e. 2nd D, BC and AN) improved the comparison of the principal peaks used to investigate protein physical stability by FTIR spectroscopy (i.e. α-helix and β-sheet structures) [131]. This was in agreement with results shown in **Figure 2.16**. However, the combination of 2nd D, BC and AN methods involves extra pre-processing steps which could be time consuming and may increase the possibility of error as a result of manipulation of the data set. Spectra of native BSA, 50% native BSA and heat-denatured BSA were investigated using 2nd D, BC and AN of the amide I band (**Figure 2.17**). The combination of those methods (i.e. 2nd D, BC and AN) showed clearly a decrease in the intensity in the α-helix band (i.e. 1654 cm^{-1}) and the presence of intermolecular β-sheets (i.e. 1610-1630 cm^{-1}) [47,64] attributed to the loss of secondary structure. Other derivative techniques are gap derivative and gap segment. These techniques calculate the difference between nearby points which may increase the noise in the corrected spectrum [143]. The derivative spectra obtained using the Savitzky-Golay method must contain less noise than derivative spectra pre-processed using gap derivative or gap segments methods. However, peak position of the principal bands must be similar for derivative spectra obtained using Savitzky-Golay or gap derivative and gap segment methods.

MSC and SNV are mathematically connected methods which transform the original spectrum giving apparently similar spectra [66,145,149]. This was in agreement with our results were pre-processed spectra using MSC and SNV looked similar as shown **Figures 2.18(B)** (MSC) vs. **2.20(B)** (SNV) for FTIR spectra and, **Figures 2.19(B)** (MSC) vs. **2.21(B)** (SNV) for fluorescence spectra. However, the principal difference between MSC and SNV is that the SNV method scaled each individual spectrum from (-) 2 to (+) 2, the data set is centred at zero and the calculation of the mean spectrum is not required [66].

MSC method can correct the spectrum for additive effects (i.e. amplification and light scattering [66,150]) and multiplicative effects (i.e. offset shifts and chemical effects [81]) and changes in the path lengths [147,150]. The success of using MSC as pre-processing method depends on how well the calculated mean spectrum represents the true mean spectrum. Additionally, the accuracy of the mean spectrum may affect the assessment of (a) and (b) coefficients [159]. In this Chapter, MSC was used for native BSA, 50% native BSA and thermally denatured BSA. These samples show spectral differences which may affect the accuracy of the mean spectrum used to estimate (a) and (b) coefficients. This must be more relevant when the MSC method is used to quantify protein structure. Reports have shown that MSC and SNV are suitable pre-processing methods to quantify protein structure using PLS regressions in combination with spectroscopy data [122,133].

Spectra pre-processed using MSC and SNV methods were useful to identify the presence of the α-helix band (i.e. 1654 cm^{-1}) and intermolecular β-sheets (i.e. 1610-1630 cm^{-1}) attributed to loss of secondary structure of heat denatured BSA and the shift in the Trp maximum emission from 342 to 334 nm as loss of tertiary structure. However, spectra pre-processed using MSC and SNV methods were not BC thus, the differences in the absorbance intensity cannot be considered to explain the changes in the secondary or tertiary structure of native, 50% native and heat-denatured BSA. Moreover, MSC keeps intact the shape of the curve [66] so that, the MSC pre-processed spectra has similar appearance to the original spectra [81].

Spectra of native, 50% native and heat-denatured protein pre-processed using the MSC and SNV methods (**Figures 2.18(B)** and **2.20(B)** respectively) gave similar information than their AN spectra (**Figures 2.8)**. A similar tendency was observed for fluorescence spectra pre-processed using MSC and SNV methods (**Figures 2.19(B)** and **2.21(B)**) where MSC and

SNV spectra of native, 50% native and heat-denatured protein showed a blue shift from native BSA at 342 nm to heat-denatured BSA at 334 nm. These results were similar than for the area normalized spectra of Trp using fluorescence spectroscopy (**Figure 2.11**). The differences in the fluorescence intensity for native, 50% native and heat-denatured protein were minimised showing all these spectra at similar intensity. Helland *et al*. (1995) reported than the selection of SNV or MSC as pre-processing methods to reduce light scattering and improve linearity did not give considerable differences in the development of linear quantification models if SNV or SNV are applied [149]. This is in agreement with the results obtained in this thesis where similar R^2, RMSE values and number of factors explaining the PLS regression were obtained for PLS models using FTIR and fluorescence spectroscopy (**Chapter 3 section 3.3.1**).

The pre-processing of FTIR spectra was more complex than for fluorescence spectra. This is explained because FTIR spectra required additional subtraction steps (i.e. water and water vapour subtraction) than for fluorescence spectra. Moreover, the amide I band of FTIR contains hidden bands (i.e. α-helix, β-sheets, turns and disorder structures) that require a suitable pre-processing method(s) able to find that hidden bands. According to Militello, et al. (2003) it was not possible to distinguish between α-helix and disordered structures at 1650 cm^{-1} and spectral modifications in that region are mainly attributed to decrease in α-helix structures [160].

Fluorescence spectroscopy of BSA protein was studied at 295 nm to minimise the influence of other amino acids (i.e. Tyr and Phe) which make the analysis of changes in the tertiary structure of proteins more difficult [24,75,161]. Data analysis of fluorescence spectroscopy has been reported to be more difficult than for other techniques like Near-IR and FTIR spectroscopy due to the Rayleigh scattering effect [136]. In this thesis, however, fluorescence spectra were shown to have less spectral noise than spectra obtained using FTIR spectroscopy so that less pre-processing methods were needed.

This Chapter has covered different pre-processing methods applied to spectroscopy to show the information that can be obtained from each of these pre-processing methods to study protein structure. As an example, this Chapter demonstrated the influence of different smoothing points or derivative methods in the pre-processed spectra and the advantage of using different methods to the same spectrum (i.e. 2^{nd} D, BC and AN) to investigate protein

structure. The application of these pre-processing methods will be further used to quantify protein physical stability using MVA of proteins (Chapter 3). Results obtained in this Chapter could be used as a guide for future researchers to identify the most suitable pre-processing methods for their spectroscopic analysis. However, different proteins contain different amino acid residues and secondary structures. Thus, the information obtained from BSA analysis of this Chapter should be adapted for different proteins.

Several authors have described the use of pre-processing methods to improve the qualitative and quantitative spectral data analysis obtained using FTIR, Near-IR and Raman spectroscopy [119-121,126]. However, pre-processing methods are also published for the analysis of other analytical techniques like Raman spectroscopy and gas chromatography-mass spectrometry [126,136,143]. Rinnan *et al*. (2009) have reported the use of Near-IR spectroscopy to investigate protein content in a sugar mixture. Spectra were pre-processed using similar pre-processing methods than in this thesis (i.e. BC, 1^{st}D and 2^{nd}D, MSC and SNV) and then, pre-processed spectra were used to quantify protein concentration in the sugar mixture using PLS regression. The major differences with this work are that pre-processing techniques were applied alone without combination of techniques giving PLS models that need a high number of PLS factors to explain the variability of each model (i.e. five to nine factors) [130]. Recently, Devos *et al.* (2014) reported that linearity of predicted models improved when pre-processing techniques were used in combination (i.e. SNV and normalization and 1^{st} D, SNV and normalization) and a proper order of pre-processing methods was used [128] which is in agreement with this work.

2.5. Conclusions

FTIR and fluorescence spectra need to be pre-processed to gain information about protein structure. However, pre-processing methods must be performed carefully paying attention to the changes that occur at each step. The amide I band of proteins, studied using FTIR spectroscopy, contains hidden bands in close proximity which make its pre-processing more complex than for fluorescence spectra. For FTIR spectroscopy, the most crucial method is the background subtraction because water and water vapour signals overlap with the amide I band of protein (1700-1600 cm^{-1}). Thus, this pre-processing method is critical to obtain the proper protein signal and decreasing the spectral noise. Moreover, the 2^{nd}D of amide I band was useful to separate and identify the presence of hidden bands (i.e. α-helix and β-sheet). However, spectra of different protein forms (i.e. native BSA, 50% native BSA and thermally denatured BSA) were more clearly compared when a combination of pre-processing methods was used (i.e. 2^{nd} D, BC and AN). The optimal number of points for smoothing of FTIR spectra of amide I band pre-processed using 2^{nd} D was between 9 and 11 points. Using those points of smoothing, the spectral noise was decreased but keeping the peak information in the smoothed spectra. The principal information found in the fluorescence spectra using these pre-processing methods was the shift in the Trp maximum emission from 342 nm for native BSA to 338 nm for thermally denatured BSA which can be studied by 1^{st}D, MSC, SNV and the combination of BC and AN methods.

Chapter 3: Multivariate analysis for the quantitation of changes in native protein concentration in solution using FTIR and fluorescence spectroscopy

3.1. Introduction

Analysis of protein drug physical stability in formulations is an increasingly important area in the pharmaceutical sciences [9,13]. However, a significant problem when developing new biotherapeutics is the poor physical stability of the incorporated protein [114]. To achieve a product that is stable, biologically effective and safe, incorporated proteins need to maintain their conformation (secondary, tertiary and sometimes also quaternary structures) during processing, storage and use [9,24,32].

Analytical techniques used to investigate protein structure should ideally be able to detect changes from native to partially folded and unfolded structures. Binding assays are used to investigate the affinity of proteins to interact with other molecules (i.e. proteins, dyes or ligands) giving information about small changes in protein structure as consequence of molecular interactions. In these methods, the signal measured is directly proportional to concentration [162]. Nuclear magnetic resonance and X-ray crystallography have shown to be sensitive to investigate the structure of the complex formed between protein and ligands [163,164]. In stability testing, emphasis is placed on the identification and quantification of small amounts of non-native protein in the formulation. There are many review articles that describe the advantages and limitations of current analytical methods with the general consensus that an array of analytical methods is needed to adequately quantify protein physical stability in pharmaceutical dosage forms [24,29,49,65,73,75,165]. From these reviews, FTIR and fluorescence spectroscopy are recognised for their usefulness in determining changes in protein secondary and tertiary structure respectively [49,54,165-167].

Traditionally, the amide I band of proteins (determined by FTIR) has been used to study the secondary structure using Fourier self deconvolution, spectral derivation, curve fitting [48,60,65,168-170] and area overlap methods [60,73,167,171]. Fourier self deconvolution resolves overlapping bands using two parameters, the full width at half-height of the band and the resolution enhancement factor K [60,168,170]. The main disadvantage of this method is that both parameters must be established manually and that it is possible to deconvolute the spectra in different ways. In addition, there is a risk that noise can be amplified during data processing

[60,170,172]. Calculation of spectral derivatives, e.g. 2ndD, can also introduce noise but use of the Savitzky-Golay algorithm minimises this by allowing calculation of derivatives and smoothing of the spectrum, simultaneously [60]. Curve fitting is a further method used to obtain the number, shapes, positions, widths and heights of several overlapping bands which are obtained using fitting of the bands to Gaussian or Lorentzian functions, or a combination of these functions. This technique allows calculation of the contributions from each secondary structure (e.g. α-helix, β-sheet, turns, random) to the overall amide I band [60,168,169]. It is suggested that results obtained by curve fitting should be compared with 2ndD and Fourier self deconvolution spectra to validate peak positions in the original spectra [60]. Finally, the area overlap method calculates the common area in the amide I 2ndD spectra between native and perturbed protein [60,73,131,167,173]. Quantitative change in secondary structure can be derived from the linear relationship between the area overlap and concentration of native protein in standard solutions.

Protein tertiary structure can be studied using intrinsic fluorescence spectroscopy since many proteins contain aromatic amino acids responsible for fluorescence emission: Trp, Tyr and Phe [8,69]. The intensity and position of the maximum emission depends on how exposed the fluorescent amino acids are to the aqueous environment which, in turn, is dependent on the protein tertiary structure [8,24,69,75]. Excitation of a protein solution at 295 nm allows the study of the Trp fluorescence contribution [8,24,75].

MVA has been increasingly used to investigate spectral changes in dosage forms containing small molecules [150,174,175] with applications more recently shifting to the study of protein structure [176-178]. One of the methods used in quantitative MVA is partial least squares regression (PLS). This method is used to estimate the best correlation between measured variables (e.g. spectra) and sample characteristics (e.g. concentration) [87,88] and to identify outliers, trends and grouping within an analytical data set [88]. From this information, quantitative models are constructed, and these can be used to analyse unknown future samples.

In this Chapter, the use of partial least squares models (PLS) with different spectral pre-processing approaches was investigated to quantify protein physical stability in solution from FTIR and fluorescence spectra. Additionally, PLS was compared with traditional methods of protein spectroscopy analysis like area overlap (FTIR) and linear regression between

fluorescence intensity at the maximum emission wavelength vs. concentration of native protein. PLS models were then used to predict native BSA concentrations in heat-denatured samples heated at 40°C, 50°C and 60°C.

3.2. Materials and methods

3.2.1. Materials

BSA and other chemicals were used as described in **Chapter 2 section 2.2.1**.

3.2.2. Preparation of native BSA, heat-denatured BSA and binary mixtures of BSA (50% w/w to 100% w/w)

Solutions of BSA 1% and 5% w/w in distilled water were prepared. Samples were heated at 90°C for 30 minutes to give heat-denatured BSA while the unheated initial solution represented native BSA. The heat-denatured BSA solutions remained clear and the loss of BSA monomer was confirmed by SEC (**Figure 3.1.**). Binary mixtures (w/w) of native and heat-denatured BSA solutions were prepared by weighting each solution in an analytical balance to obtain the desired (w/w) concentration. These solutions were prepared in triplicate over the range of 50% to 100% w/w native BSA.

3.2.3. Size exclusion chromatography (SEC)

A Shimadzu chromatographic system was used that comprised a LC-10 AT vp liquid chromatographic unit, a SIL-10AD vp auto injector unit and a SPD –M10A vp diode array detector. The column (BioSep-SEC-S2000, 300 x 7.80 mm) was from Phenonemex (Auckland, New Zealand), the chromatograms were recorded at 280 nm with CLASS-VP software (version 6.14, Shimadzu, Kyoto, Japan). The mobile phase comprised 50 mM phosphate buffer and 150 mM NaCl (pH 6.9) with a flow rate of 0.5 mL min^{-1} and an injection volume of 50 µL was used. Samples were prepared at a total concentration of 100 µg mL^{-1} BSA. The mobile phase was degassed by filtration under vacuum and all solutions were filtered through 0.45 micron filters (Phenex-RC, Phenomenex) prior to analysis.

A calibration curve for native BSA was prepared from stock solution of BSA 1% w/w in triplicate. From this solution, eight aliquots with a volume between 0.01-0.12 mL were

separately diluted in 10 mL of phosphate buffer pH 6.9, to obtain eight solutions of BSA, with concentrations between 10 and 120 µg mL^{-1}. Absorbance was measured at 280 nm.

3.2.4. Infrared spectroscopy (FTIR)

FTIR spectroscopy was used as described in **Chapter 2 section 2.2.2**.

The amide I band of protein spectra (1600-1700 cm^{-1}) was pre-processed by BC, AN, 1stD and 2ndD calculation (Savitzky-Golay with 7 and 11 points smoothing) [73,131,137,150], SNV and MSC [150] as described in **Chapter 2 section 2.1**. Additionally, the amide I band was analysed using the area overlap method over the range of 50% to 100% w/w native BSA. The area overlap calculates the common area between the amide I band of native protein and altered protein pre-processed by 2ndD (Savitzky-Golay), BC and AN [60,73,131,167]. The area overlap was calculated using the following steps: 1) 2ndD of the amide I band was calculated (**Chapter 2 section 2.1.5.**) 2) the 2ndD is BC between 1600 and 1700 cm^{-1} (**Chapter 2 section 2.1.2.**) and is integrated to calculate the area under curve, 3) each spectrum of amide I band pre-processed using the combination of 2ndD and BC methods was divided by its area under curve to normalize the area to 1.00, 4) the altered protein spectrum (understood as any spectrum different from native protein) was subtracted from the native protein spectrum and then, the area overlap between those spectra was calculated by integrating the absorbance data of each protein solutions [131,167]. Using this method similar spectra will have an area overlap close to 1 (or 100%) whereas different spectra will have values close to zero [60,167,171]. A linear model was fitted to the percentage area overlap versus concentration of native protein using Origin Lab Corp. Version 8.5.

3.2.5. Fluorescence spectroscopy

Fluorescence spectroscopy was used as described in **Chapter 2 section 2.2.3**. Additional to the PLS analysis, fluorescence spectra pre-processed by BC and AN were used to estimate a linear relationship between the maximum emission wavelength (300-400 nm) and concentration of native protein over the range of 50% to 100% w/w native BSA using Origin Lab Corp. Version 8.5.

3.2.6. Partial least squares (PLS) regression

The Unscrambler®X was used to build PLS models using the amide I region (1600 -1700 cm^{-1}) of the FTIR spectra for triplicate mixtures (50 to 100% w/w native BSA). The amide I spectra were pre-processed as described above and the triplicate spectra were divided into a calibration set (Replicates 1 and 2) and a prediction set (Replicate 3). PLS was then conducted using the test set validation method with the non-linear iterative partial least squares (NIPALS) algorithm. The X and Y weights were 1.00 and spectra were mean centred. The quality of the PLS models was assessed by comparing the number of PLS factors, correlation coefficient (R^2), root mean square error of calibration (RMSEC) and root mean square error of prediction (RMSEP) in the calibration and prediction sets respectively. PLS models were built using the lowest number of PLS factors which explained a large percentage (70% to 90%) of the total variation of the original data set [179]. R^2 gave information of the goodness of fit of the model where R^2 near to 1 or -1 indicates a more linear model [180]. RMSE is a fit index which calculates the average error between the predicted and measured data set [181]. Plots of measured versus predicted concentration with 95% confidence intervals were used to determine the predictive ability of the models.

3.2.7. Thermal stability of BSA in solution using PLS models

Three solutions of native BSA (1% and 5% w/w) were heated at 40°C, 50°C and 60°C. Aliquots were taken at defined time points and FTIR or fluorescence spectra were measured. For FTIR spectroscopy, aliquots were taken over 60 minutes at 10 minute intervals. For fluorescence spectroscopy, aliquots were taken over 10 minutes at one minute intervals. Additionally, SEC was used as a complementary analytical method. Aliquots (0.1 mL, 1%) were taken at 0, 10, 30 and 60 min and diluted in 10 mL phosphate buffer pH 6.9 giving a total protein concentration of 100 µg mL^{-1}. SEC chromatograms were measured. Native BSA remaining was estimated using a calibration curve of native BSA over the concentration range 10 and 120 µg mL^{-1} ($A_{220\ nm}$ = 806*[BSA] $_{\mu g\ mL^{-1}}$). The calibration curve was linear over this range (R^2= 0.993).

3.2.8. Statistical data analysis to asses protein concentration measurements using FTIR and fluorescence spectroscopy and, SEC methods

Protein concentration differences between FTIR and fluorescence spectroscopy and, SEC methods were statistically assessed using two different data sets. The first data set included protein concentration measurements from the three analysis methods (FTIR, and fluorescence spectroscopy, and SEC), at two measurements times (0 and10 min), whereas the second data set included results from FTIR spectroscopy, and SEC at reading times of 0, 10, 30, and 60 min, as described in section 3.2.2.5. For each data set, two nested beta regression models (full and reduced) [182] were used to assess whether the analysis method was a significant predictor of the protein concentration measurements. Beta regression model were chosen because they were specifically developed to deal with data naturally bound between zero and one like percentages [182] which is the case in the present data set. The full model explained protein concentration (as percentage of the native protein concentration) by *i*) the analysis method (FTIR, and fluorescence spectroscopy, and SEC), *ii*) time (0-10 min), and *iii*) temperature (40°C, 50°C and 60°C) whereas, the reduced model explained protein concentration by *i*) time (0, 10, 30 and 60 min) and *ii*) temperature (40°C, 50°C and 60°C). An overall P-value for the effect of the analysis method was obtained using a likelihood ratio test, comparing the full and reduced models. If the likelihood ratio test was not significant ($P > 0.05$), both models (full and reduced) have the same capacity to predict protein concentration. Therefore, the different analysis methods yield similar results. Finally, model over-dispersion was estimated using the ratio of Pearson residuals divided by residual degrees of freedom to evaluate the assumption that sample repetitions were independent. If the ratio was greater than 1.5, robust standard errors were calculated for the adjustment of standard errors using the so called 'sandwich estimator' to adjust for data correlation [183]. Visual inspection of residual plots was used to assess any obvious deviations from homoscedasticity.

3.3. Results

SEC confirmed the presence of soluble aggregates (retention time = 11 minutes) and absence of monomer BSA in the heat-denatured solutions. Native BSA solutions, in contrast, showed the elution of dimers and monomers of BSA at 13 and 14 minutes, respectively (**Figure 3.1**).

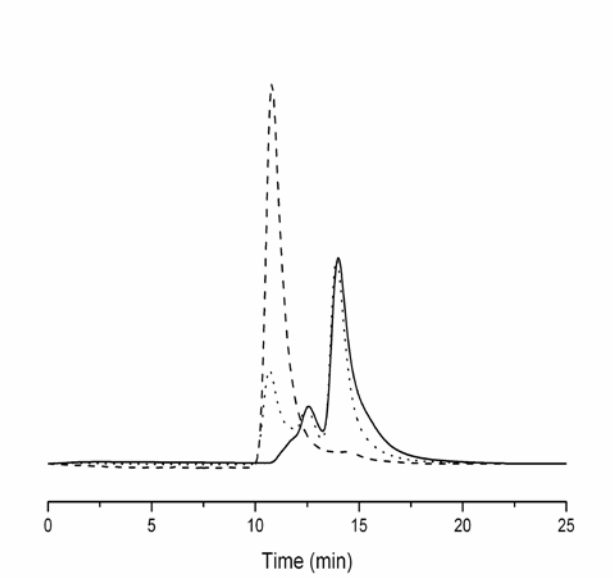

Figure 3.1 Typical example of SEC chromatogram showing the presence of soluble aggregates in heat-denatured solution and absence in the native BSA solution. Soluble aggregates eluted at 11 minutes while dimers and monomers of native protein solution eluted at 13 and 14 minutes respectively. 100% w/w native BSA solution (solid line), soluble aggregates of heat-denatured BSA solution (dashed line) and binary mixture of 50% w/w native: 50% w/w heat denatured BSA solution (dotted line). SEC chromatograms are area normalized.

The typical appearance of the FTIR amide I spectra of native, heat-denatured and 50:50 w/w binary mixtures of native:denatured BSA are shown in **Figure 3.2(A)**. First and second derivatives calculated using the Savitzky-Golay method with 7 and 11 points of smoothing are also shown in **Figures 3.2(B)-3.2(E)**. The 1^{st}D spectrum gives the slope of the curve of the amide I band (**Figures 3.2(B) and (C)**), while the 2^{nd}D represents the rate of change of slope and hence gives information of the curvature of the amide I band (**Figures 3.2(D) and (E)**). In the 2^{nd}D spectra, increased denatured BSA was characterised by the decreased intensity of the band at around 1656 cm^{-1}, and increased intensity of the band at 1600-1630 cm^{-1}.

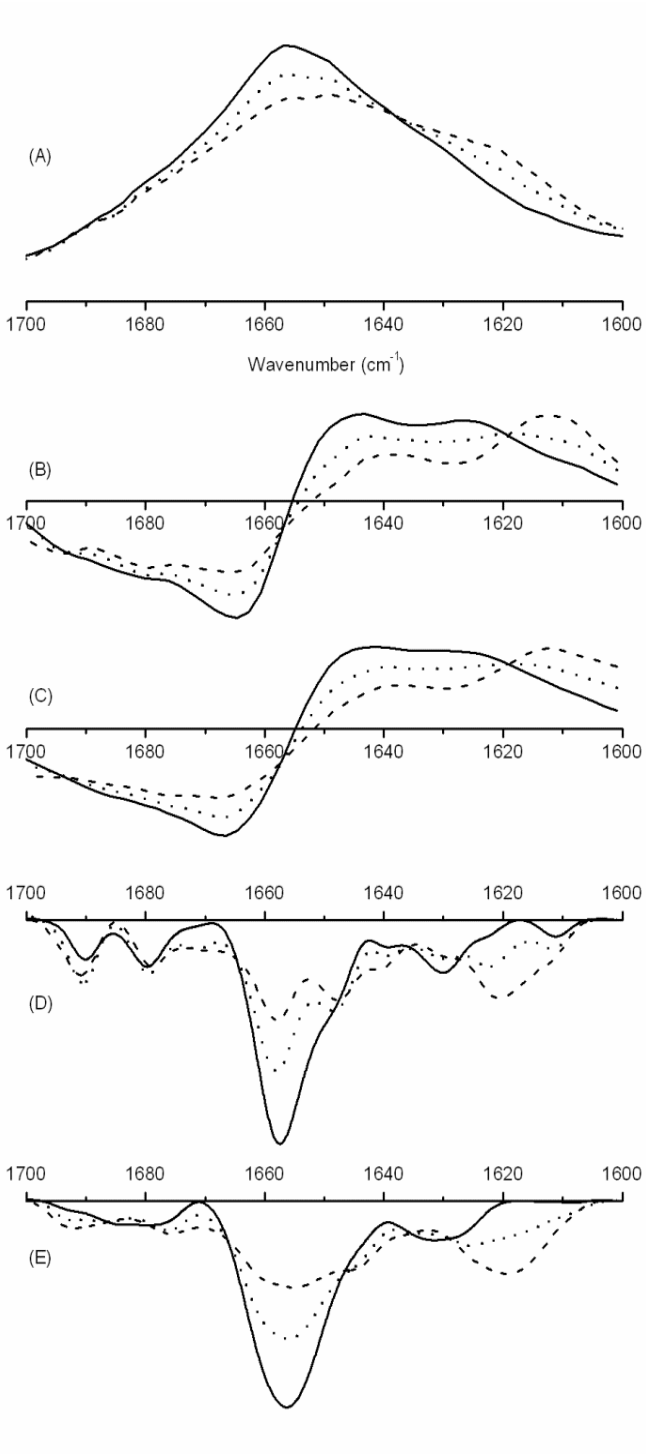

Figure 3.2 Typical example of FTIR spectra showing the amide I band for 100% w/w native BSA (solid line), heat-denatured BSA solution (dashed line) and 50% w/w native BSA in solution (dotted line). Amide I band pre-processed using: (A) BC, AN; (B) 1st D(7); (C) 1st D(11); (D) 2nd D(7), BC, AN; (E) 2nd D(11), BC, AN. The number in the parenthesis after the pre-processing method indicates the number of points of smoothing. Total protein concentration was 5% w/w.

Two main peaks between 1640 and 1670 cm^{-1} were identified in the 2^{nd}D curve when 7 points of smoothing were used, while only one broader peak was observed when 11 points of smoothing were used (**Figures 3.2(D) and (E)**). Stability of the binary mixtures during the analysis was confirmed by analysing the 100% native, and 50% w/w native BSA solutions following storage at room temperature (RT) for one and seven days (**Appendix B.1**).

Fluorescence spectra with two different pre-processing methods (BC and combined BC and AN) are given in **Figure 3.3(A) and (B)** and these show a maximum emission around 342 nm for native BSA in solution which blue-shifted towards 338 nm as the heat-denatured BSA content increased. The increased heat-denatured BSA content also resulted in a decreased in fluorescence intensity (**Figure 3.3(A)**).

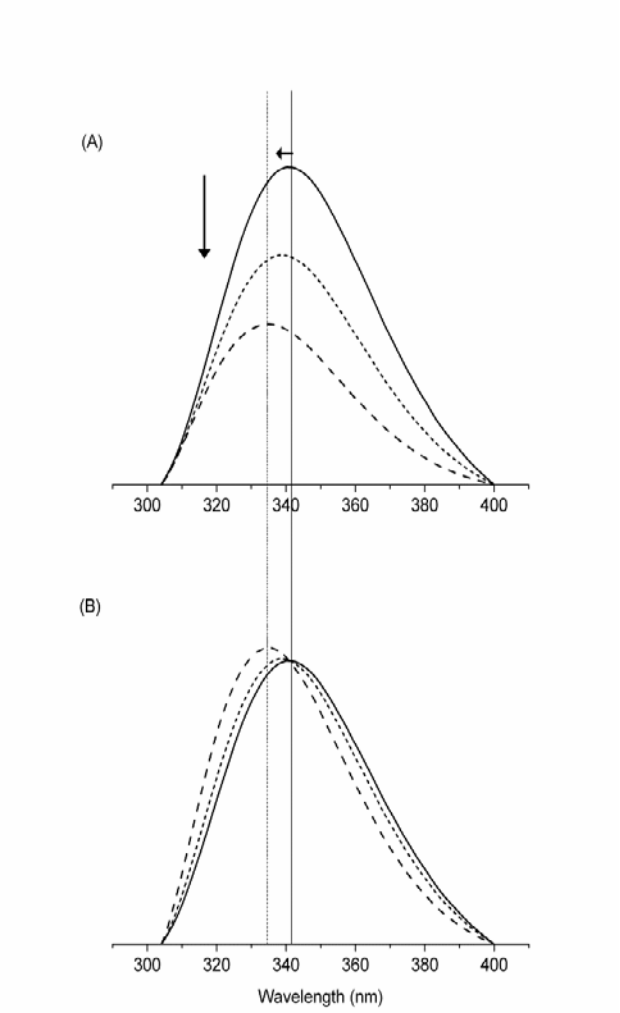

Figure 3.3 Typical example of fluorescence spectra showing Trp emission for 100% w/w native BSA (solid line), heat-denatured BSA solution (dashed line) and 50% w/w native BSA in solution (dotted line). Trp emission was pre-processed using: (A) BC and, (B) AN, BC. Arrows indicate the shift in the maximum emission of Trp. Total protein concentration was 1% w/w.

3.3.1. Partial least square analysis (PLS)

A summary of PLS regression models derived from FTIR and fluorescence spectra is shown in **Tables 3.1 and 3.2** respectively. These models were built using a combination of pre-processing techniques which aimed to reduce noise while preserving meaningful spectral variation, thereby maximising the quality of the regressions. The best model for each spectroscopic method was chosen on the basis of the number of PLS factors, percentage of error (RMSE %) and R^2 values and are described in the following sections.

Table 3.1 Partial least squares analysis of FTIR amide I spectra. Total BSA concentration was 5% w/w, percentage native BSA was 50% to 100% w/w. (n=3).

Pre-processing method	Factors	Calibration (12 spectra)		Prediction (6 spectra)	
		RMSE%	R^2	RMSE%	R^2
BC, AN	3	3.46	0.959	1.97	0.987
SNV	3	1.47	0.992	5.41	0.899
MSC	3	1.47	0.992	5.46	0.898
1^{st} D(7)	3	2.89	0.971	2.15	0.909
1^{st}D(11)	3	3.42	0.960	5.64	0.891
2^{nd}D(7), BC, AN	3	1.35	0.993	3.25	0.964
2^{nd}D(11), BC,AN	3	0.91	0.997	1.64	0.991

RMSE% = Root mean square error
R^2 = Correlation coefficient
BC, AN: Baseline correction and area normalization
SNV: Standard normal variate
MSC: Multiplicative scatter correction
1^{st} D (7): First derivative (smoothed 7 points)
1^{st} D (11): First derivative (smoothed 11 points)
2^{nd}D (7), BC, AN: Second derivative (smoothed 7 points)
2^{nd}D (11), BC, AN: Second derivative (smoothed 11 points)

Table 3.2 Partial least squares analysis of fluorescence emission spectra. Total BSA concentration was 1% w/w, percentage native BSA was 50% to 100% w/w. (n=3).

Pre-processing method	Factors	Calibration (12 spectra)		Prediction (6 spectra)	
		RMSE%	R^2	RMSE%	R^2
BC	2	1.00	0.997	0.87	0.997
BC, AN	1	1.38	0.993	1.32	0.994
SNV	1	1.42	0.993	1.05	0.996
MSC	1	1.42	0.993	1.06	0.996

RMSE% = Root mean square error
R^2 = Correlation coefficient
BC: Baseline correction
AN: Area normalization
SNV: Standard normal variate
MSC: Multiplicative scatter correction

3.3.2. FTIR spectra (amide I) model

A summary of the PLS models from FTIR spectra is given in **Table 3.1**. Both the SNV and MSC pre-processing resulted in improved models compared with BC, AN amide I spectra. SNV and MSC models explained the variability of the data set using similar number of PLS factors (i.e. three factors) but gave lower root mean square error (RMSE) and improved R^2 (i.e. nearer to one) in the calibration and prediction sets compared with BC, AN amide I spectra. The 1^{st}D spectra gave little or no improvement in the value of RMSE and R^2 values for calibration and prediction set over the AN amide I band while 2^{nd} D provided the best PLS model. The model constructed using 2^{nd} D with 7 points smoothing was similar in terms of PLS factors, R^2 and RMSEC and RMSEP to the models with SNV and MSC pre-processing, whereas the model constructed from 2^{nd} D with 11 points smoothing gave the greatest improvement with three PLS factors; RMSE= 0.91% and 1.64% and R^2= 0.997 and 0.991 for the calibration and prediction sets respectively. Scores and loadings plots for the model constructed from 2^{nd} D and 11 points smoothing are given in **Figures 3.4(A) and (B)**. The scores plot shows that samples increasing in native BSA content tend to be aligned along the factor 1 axis (**Figure 3.4(A)**). Loadings plots (**Figure 3.4(B)**) for factor 1 showed a negative peak at 1651-1662 cm^{-1} and a positive peak at 1612-1625 cm^{-1}. Factor 2 showed a positive peak at 1610-1624 cm^{-1}, and a negative peak at 1651-1660 cm^{-1}. Factor 3 (not shown) improved the quality of the model. **Figure 3.4(C)** shows the agreement between the standard concentration and predicted concentration with R^2 of 0.997 and 0.991 for the calibration and prediction sets respectively (**Table 3.1**).

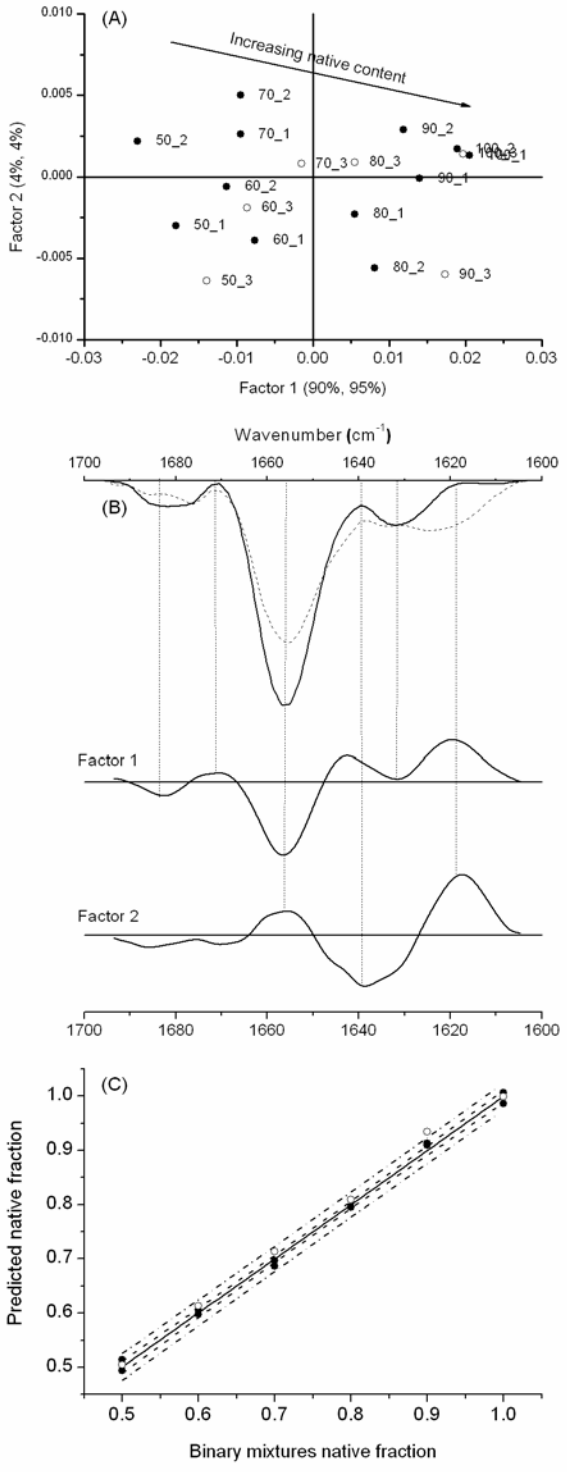

Figure 3.4 Typical example of FTIR spectra of amide I band pre-processed using 2nd D(11), BC, AN: (A) Scores plot, (B) Spectra of 100% w/w native BSA (solid line) and 50% w/w native BSA (dashed line) and loadings plots (Factors 1 and 2) and (C) Standard concentration (●) versus predicted (○) concentration. 95% confidence limits and prediction limits for the validation standards are shown as dashed and dash-dot-dash lines respectively.

Changes in the secondary structure of protein were also quantified using the area overlap method (**Figure 3.5**). These results showed that the area overlap decreased from 1.00 to 0.82 when the binary mixture concentration was changed from 100% native to 50% w/w native BSA (**Appendix B.2**). The percentage area overlap versus native concentration showed a linear fit which gave a slope of 0.368 ± 0.03 and intercept of 0.630 ± 0.02 (R^2 of 0.973) (**Appendix B.3**).

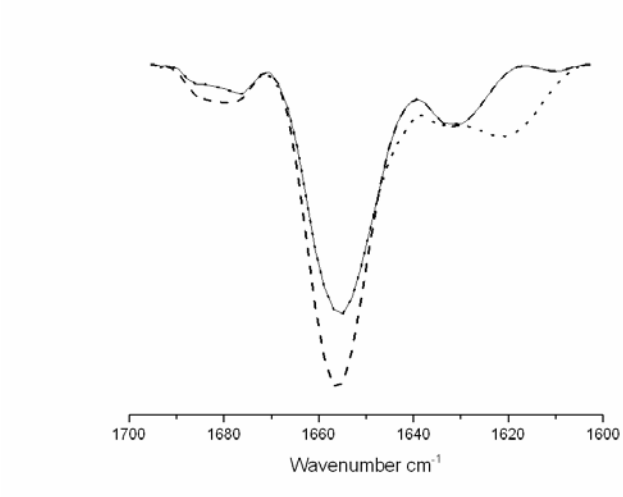

Figure 3.5 Typical example of amide I band showing the area overlap (straight line) between native BSA (dashed line) and 50% w/w native BSA (dotted line). Spectra were pre-processed using 2ndD (11), BC, AN.

3.3.3. Fluorescence spectra model

A summary of the PLS models for intrinsic Trp fluorescence is shown in **Table 3.2**. SNV, MSC, and the combined BC and AN, pre-processing gave an improved analysis compared with spectra using BC pre-processing alone. The model constructed from BC and AN spectra gave the greatest improvements with one PLS factor explaining the 99% of the spectra variability, RMSE% = 1.38% and 1.32% and R^2 of 0.993 and 0.994 for the calibration and prediction respectively. Scores and loadings plots are given for this model in **Figure 3.6(A) and (B)**. The scores plot shows that samples increasing in native content were aligned along the Factor 1 axis representing the shift in the maximum emission (**Figure 3.6(A)**). The loadings plot (**Figure 3.6(B)**) showed a negative region between 315 and 327. **Figure 3.6(C)** showed good agreement between the standard concentration and predicted concentration with R^2 of 0.993 and 0.994 for the calibration and prediction sets respectively.

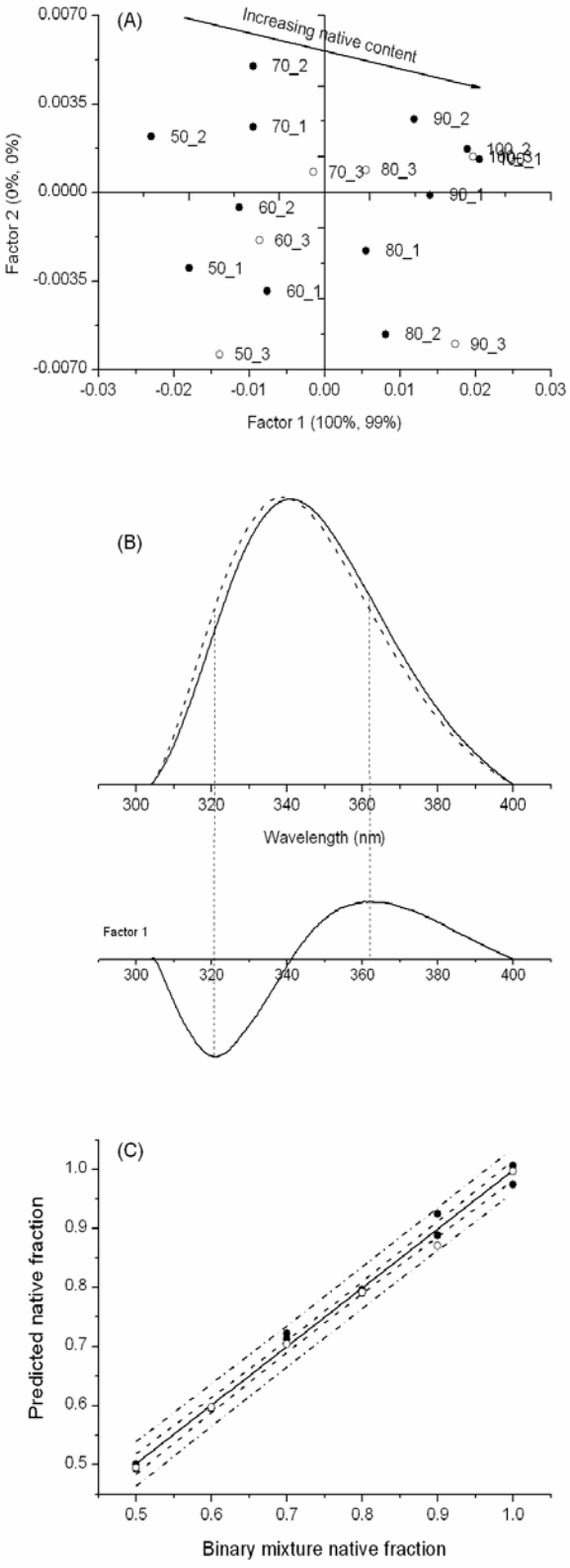

Figure 3.6 Typical example of fluorescence spectra of Trp emission pre-processed using BC and AN: (A) Scores plot, (B) Spectra of 100% w/w native BSA (solid line) and 50% w/w native BSA (dashed line) and loadings plots (Factor 1) and (C) Standard concentration (●) versus predicted (○) concentration. 95% confidence limits and prediction limits for the validation standards are shown as dashed and dash-dot-dash lines respectively.

Additional to the PLS analysis, changes in the tertiary structure of BSA were quantified using a linear relationship between fluorescence intensity at the maximum emission wavelength vs. concentration of native protein (100% native to 50% w/w native) which resulted in an R^2 value of 0.860, a slope of 91.7 (46.4 – 137.0) and an intercept of 69.7 (34.9 – 104.6) with 95% confidence limits (**Appendix B.4**).

3.3.4. Stability of BSA in solution using FTIR and fluorescence PLS models

In an independent experiment, the FTIR and fluorescence PLS models were used to predict the loss of native protein in solutions heated at 40°C, 50°C and 60°C. Spectra were pre-processed according to the best PLS models described above: 2^{nd}D (11 points smoothing), BC and AN (FTIR) (**Figure 3.7(A)**) and, BC and AN (fluorescence) (**Figure 3.7(B)**). In the case of FTIR spectroscopy, changes in the secondary structure of BSA were measured over 60 minutes. At 60 minutes, the PLS model predicted that the native structure of BSA was reduced to 92% ± 1.3% and 58% ± 4.1% in solutions heated at 40°C and 50°C respectively. Solutions heated at 60°C showed reduction in native BSA to less than 50% in 10 minutes. Using fluorescence spectroscopy, solutions heated at 40°C did not show considerable change in the native BSA concentration during the first 10 minutes whereas samples heated at 50°C and 60°C showed a reduction in the native concentration of protein to 84% ± 2.6% and 54% ± 5.0%, respectively within 10 minutes.

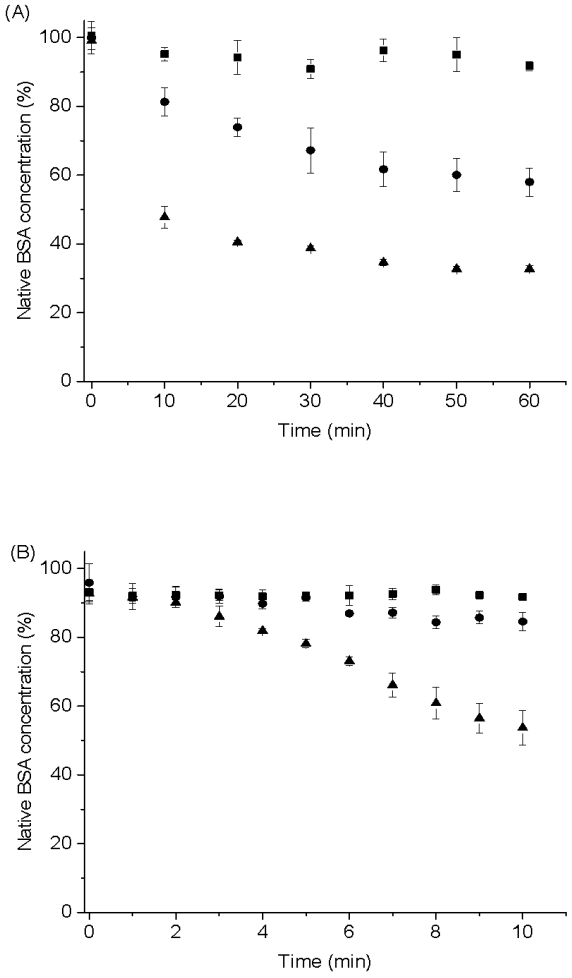

Figure 3.7 Prediction of loss of native concentration of BSA in solutions heated at 40°C (■), 50°C (●) and 60°C (▲). (A) Spectra were pre-processed using 2nd D(11), BC, AN (FTIR spectroscopy) and (B) BC, AN (fluorescence spectroscopy) (mean ± s.d.).

SEC confirmed the reduction of native BSA concentration in solutions heated at 40°C, 50°C and 60°C for one hour. Using SEC chromatography, solutions heated at 40°C did not show significant changes in the native BSA concentration during the first 10 minutes whereas samples heated at 50°C and 60°C showed a reduction in the native concentration of protein to 83% ± 0.7% (50°C) and 53% ± 2.0% (60°C), respectively within 10 minutes. At 60 minutes, SEC detected that native structure of BSA was reduced to 97% ± 2.3% (40°C), 71% ± 0.5% (50°C) and 25% ± 1.2% (60°C) in solutions held at 40°C, 50°C and 60°C respectively (**Figure 3.8**). A comparison of the native BSA concentration predicted using PLS models (FTIR and fluorescence) and SEC methods is shown in **Table 3.3**.

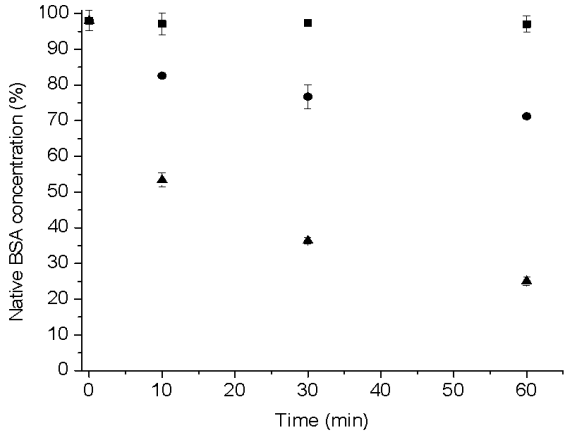

Figure 3.8 SEC chromatography results showing the prediction of loss of native concentration of BSA in solutions heated at 40°C (■), 50°C (●) and 60°C (▲). (mean ± s.d.).

Table 3.3 Comparison of native BSA concentration (%) in solutions heated at 40°C, 50°C and 60°C using PLS regression (FTIR and fluorescence spectroscopy) and SEC results. (n=3). (Mean ± S.D).

Time (min)	Temperature (°C)	Native BSA concentration (%)		
		PLS – FTIR	PLS – Fluorescence	SEC
0	40	100 ± 4.1%	93 ± 2.5%	98 ± 2.9%
	50	100 ± 1.7%	96 ± 5.5%	98 ± 2.9%
	60	99 ± 3.7%	93 ± 3.2%	98 ± 2.9%
10	40	95 ± 1.9%	92 ± 0.6%	97 ± 3.0%
	50	81 ± 4.2%	84 ± 2.6%	83 ± 0.7%
	60	48 ± 3.1%	54 ± 5.0%	53 ± 2.0%
30	40	91 ± 2.7%	-	97 ± 0.5%
	50	67 ± 6.6%	-	77 ± 3.4%
	60	39 ± 0.8%	-	36 ± 0.9%
60	40	92 ± 1.3%	-	97 ± 2.3%
	50	58 ± 4.1%	-	71 ± 0.5%
	60	33 ± 0.9%	-	25 ± 1.2%

3.3.5. Statistical analysis to compare protein concentration measurements using FTIR and fluorescence spectroscopy and, SEC methods

Results from the regression analysis for the first and second data sets are presented in **Table 3.4 and 3.5**, respectively. All fitted models were over-dispersed; therefore 'sandwich estimators' were used to correct biased standard errors (SE). The visual inspection of residual plots from final models did not reveal any obvious deviations from homoscedasticity (**Figures 3.9 and 3.10**). Non-significant differences were observed at the comparison of full and reduced models. In particular, the likelihood ratio test yielded P - values of 0.06 and 0.94 for the comparison of nested models in the first and the second data sets, respectively **(Tables 3.6 and 3.7**). These results indicate that the analysis method was not a significant factor explaining the observed differences in protein concentration. Therefore after controlling by the temperature effect, FTIR and fluorescence spectroscopy, and SEC methods were able to measure equivalent protein concentrations in the period between 0 and 10 minutes (data set 1 included protein concentration measurements from the three analysis methods (FTIR, and fluorescence spectroscopy, and SEC), at two measurements times (0 and 10 min)). Similarly, FTIR spectroscopy and SEC methods were able to measure equivalent protein concentrations in the period between 0 to 60 minutes (data set 2 included results from FTIR spectroscopy, and SEC at reading times of 0, 10, 30, and 60 min).

Table 3.4 Beta regression analysis table for the full and reduced model of the first dataset, representing protein concentration measurements from the three analysis methods (FTIR, and fluorescence spectroscopy, and SEC), at two measurements times (0 and10 min)

Full Model	**Estimate**	**SE**	**z**	**P-value**
(Intercept)	2.23563	0.33247	6.7244	1.76×10^{-11}
Protocol FTIR	0.09842	0.05802	1.6964	0.090
Protocol SEC	0.22068	0.12264	1.7994	0.072
Time	-0.0852	0.00888	-9.5894	2.2×10^{-16}
Temperature	-0.0226	0.00661	-3.4253	0.001
Reduced model				
(Intercept)	2.37124	0.32635	7.2659	3.71×10^{-13}
Time	-0.0866	0.00935	-9.2539	2.20×10^{-16}
Temperature	-0.022	0.00713	-3.0888	0.002

Table 3.5 Beta regression analysis table for the full and reduced model of the second dataset, representing protein concentration measurements from FTIR spectroscopy, and SEC, at reading times of 0, 10, 30, and 60 min

Full Model	**Estimate**	**SE**	**z**	**P-value**
(Intercept)	2.50537	0.43216	5.7973	6.74×10^{-09}
ProtocolSEC	-0.008	0.12303	-0.0653	0.948
Time	-0.0196	0.00327	-5.9899	2.10×10^{-09}
Temperature	-0.0308	0.01011	-3.0453	0.002
Reduced Model				
(Intercept)	2.50145	0.42897	5.8313	5.50×10^{-09}
Time	-0.0196	0.00327	-5.9944	2.04×10^{-09}
Temperature	-0.0308	0.01011	-3.0465	0.002

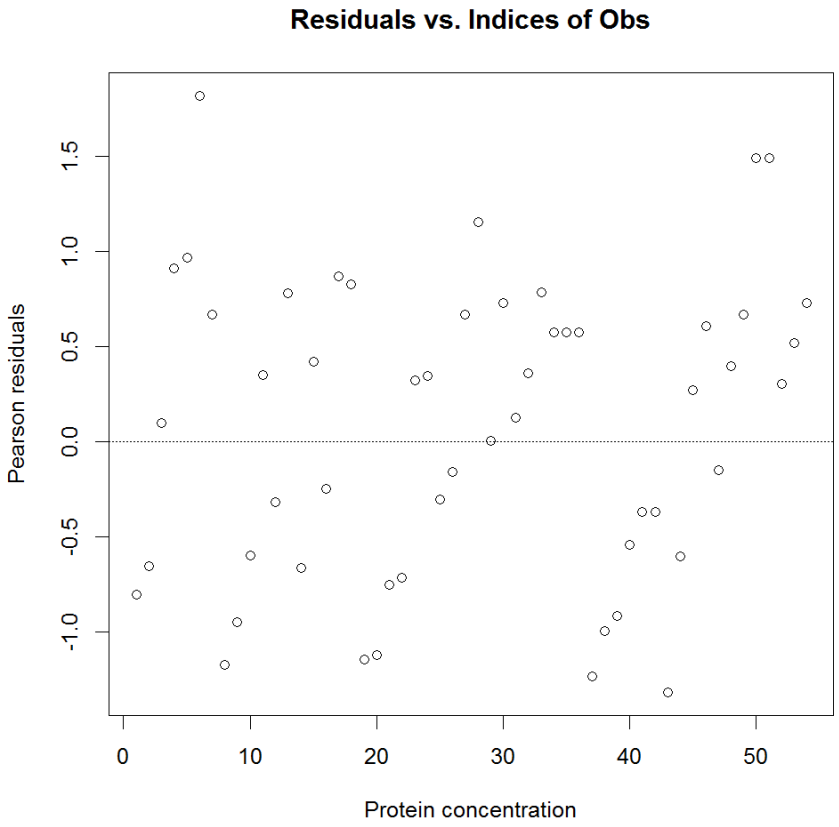

Figure 3.9 Residual plot full model beta regression analysis for the first data set, representing protein concentration measurements from the three analysis methods (FTIR, and fluorescence spectroscopy, and SEC), at two measurements times (0 and 10 min)

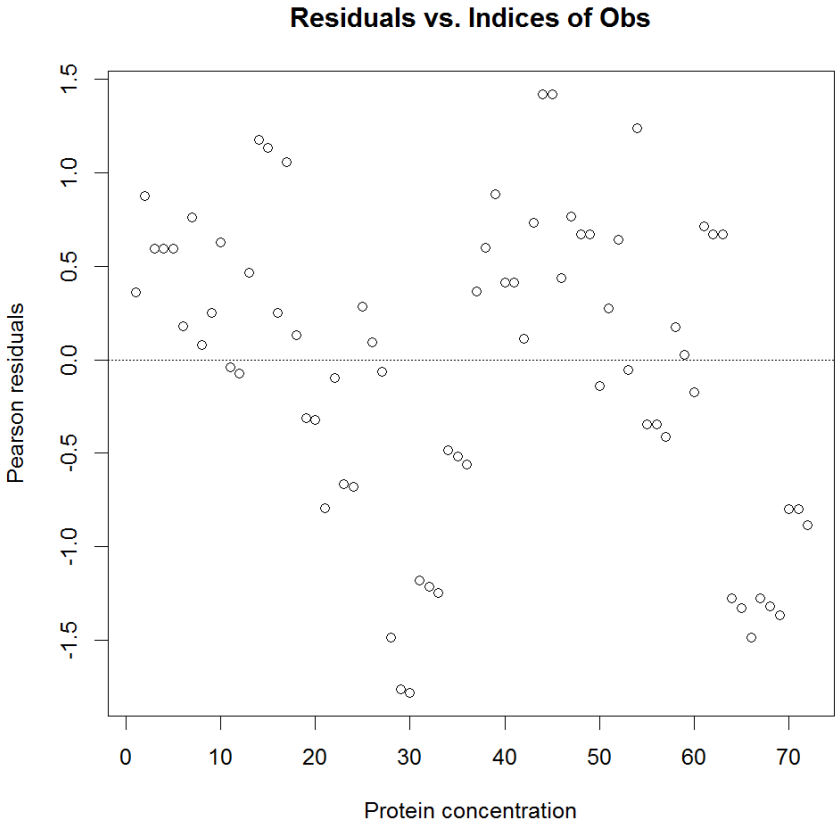

Figure 3.10 Residual plot full model beta regression analysis for the second data set, representing protein concentration measurements from FTIR spectroscopy, and SEC, at reading times of 0, 10, 30, and 60 min

Table 3.6 Likelihood ratio test results for the first data set assessing differences in the prediction of native protein concentration between two nested beta regression models (full vs. reduced)

Model	#Df	LogLik	Df	Chi^2	P-value
Full	6	145.64			
Reduced	4	142.84	-2	5.5918	0.06106

Full model: analytical method (SEC, FTIR and fluorescence spectroscopy), time (0-10 min) and temperature (40, 50 and 60°C). Reduced model: time (0 and 10 min) and temperature (40, 50 and 60°C). Df: degrees of freedom.

Table 3.7 Likelihood ratio test results of the second data set assessing differences in the prediction of native protein concentration between two nested beta regression models (full vs. reduced)

Model	#Df	LogLik	Df	Chi^2	P-value
Full	5	107.90			
Reduced	4	107.89	-1	0.006	0.938

Full model: Analytical method (FTIR spectroscopy and SEC), time (0, 10, 30, and 60 min) and temperature (40, 50 and 60°C). Reduced model: time (0, 10, 30, and 60 min) and temperature (40, 50 and 60°C). Df: degrees of freedom.

3.4. Discussion

PLS regression has a potential advantage over conventional univariate analytical techniques because the complete spectral region of interest can be included in the analysis. In this study the amide I band from FTIR spectroscopy and the emission spectra from fluorescence spectroscopy were used for the analysis. A decreased intensity of the α-helix band at around 1656 cm^{-1}, and increased intensity of the β-sheet band at 1600-1630 cm^{-1} may confirm the presence of unfolded or aggregated BSA in the binary mixtures [24,35,48,60]. Spectroscopy was used in combination with PLS since these methods are commonly used to investigate secondary and tertiary structure of proteins [49,54,165-167]. Literature also showed that spectroscopy was useful to estimate protein concentration using methods like curve fitting, area overlap and deconvolution (for FTIR spectroscopy) [48,60,65,73,168,170] and, linear regression between the maximum emission of fluorescence spectroscopy and protein concentration (for fluorescence spectroscopy) [69]. The models showed that PLS regression could be applied rapidly for the analysis of protein physical stability in pharmaceutical processing as there is no need for additional sample preparation.

The stability study of 100% native, and 50% w/w native BSA solutions using FTIR spectroscopy showed that binary mixtures of native and heat-denatured BSA had sufficient stability at room temperature to be used as analytical standards in this work and the thermal denaturation process (90ºC for 30 min) was not reversible after one week (**Appendix B.1**). The result of the stability study was in agreement with previous reports showing that protein aggregation caused by increased temperature is an irreversible process [32,184]. This study also confirm that the experimental conditions used in this work to obtain heat-denatured protein in solution are useful to investigate protein thermal stability in solution [168]. The stability study showed that the secondary structure of native BSA was stable for one week in BSA solutions stored at room temperature. This is in agreement with standard specifications for proteins in accelerated stability test where proteins must keep stable their native conformation in the desired formulation (i.e. liquid or freeze dried formulations) for protein samples stored at 40°C [32].

In addition to area overlap, protein thermal stability could be investigated using curve fitting and fourrier self deconvolution techniques which gave information about the contribution of each secondary elements (mainly α-helix and β-sheet) to the overlapping amide I band

[48,60,168]. The use of those methods in combination with spectroscopy have investigated the loss of native protein conformation which is associated to decrease in α-helix and increase in β-sheet content. The values of α-helix and β-sheet bands obtained using curve fitting and fourier self deconvolution techniques are reported to be in good agreement with reference values [43,63,178,185,186]. Based on those results, the physical stability of binary mixtures used in this Chapter (i.e. 100% w/w to 50% w/w native BSA) could be used to investigate whether PLS regression in combination with FTIR spectra pre-processed using curve fitting and fourier self deconvolution methods gave a more robust model than the PLS models obtained in this thesis (**Table 3.1**). In this thesis, PLS models were compared with univariate regressions obtained using traditional methods of protein spectroscopy analysis such as area overlap [60,73,131,167,171] (FTIR), and linear regression between fluorescence intensity at the maximum emission wavelength vs. concentration of native protein. It can be concluded that in contrast to PLS, the area overlap method showed poorer linear fit between area overlap and native protein concentration (R^2 = 0.973 compared with 0.997 for PLS). This may be explained because PLS includes the information of multiple variables (i.e. whole data set) to build the regression models whereas, univariate regressions (e.g. the value of area overlap (from one to zero) vs. concentration) only consider one variable. As more variables were taken to build the PLS models, the error was reduced giving a higher value of R^2 [187]. Similar conclusions were obtained when fluorescence spectra where analysed by linear regression between fluorescence intensity at the maximum emission (R^2 = 0.860 compared with 0.993 for PLS models). From these results, PLS appears to provide a good method for quantification of BSA physical stability in solution. PLS has shown utility in other applications involving quantitative analysis of spectral data [87,88]. Gabrielsson *et al*. (2002) reported the advantage of including the use of MVA in the development of pharmaceutical products where MVA may optimise the elaboration of pharmaceutical products from the experimental design to process control [87]. In this work, PLS regression was used in combination with FTIR and fluorescence spectroscopy to quantify protein concentration. These results showed that PLS could be used as an alternative method to assess protein concentration during protein drugs analysis. The best model describing BSA native conformation using FTIR spectra was obtained using a similar pre-processing sequence as the traditional area overlap method (i.e. 2^{nd}D, BC and AN of the amide I band). Hence, PLS using the 2^{nd}D spectra could be considered an extension of an already accepted analytical technique.

In this study, the 2ndD was calculated using the Savitzky–Golay algorithm with a second degree polynomial and seven or eleven points smoothing [145]. The number of smoothing points selected in this thesis to build the PLS regression models were in agreement with the number proposed by Rinnan *et al*. (2009) [130]. Using eleven points smoothing (i.e. five points either side of the smoothed point) reduced the spectra noise while still maintaining the key differences between native and denatured spectra. The resulting models produced the better quality of regression parameters when compared with spectra smoothed using seven points (e.g. higher R^2 and lower RMSE) (**Table 3.1**). Although use of fewer smoothing points is appropriate for detection specific secondary structures of amide I band (i.e. α-helix, turns, random and β-sheet) in traditional amide I band analysis this work has shown that simplifying the 2ndD spectra allowed the construction of the best PLS model.

Other MVA methods have been used to study the accuracy in secondary structure determination using different model proteins [176-178,188] where a variety of MVA methods have been investigated including multivariate curve resolution-alternating least squares (MCR-ALS) analysis [177], projection to latent structure discriminant analysis (PLS-DA) [176], and interval partial least squares (iPLS) methods [178]. Direct comparison with this work is difficult since in those studies, MVA was used to study the accuracy in the secondary structure determination whereas PLS was investigated as a possible method to quantify changes in native protein concentration in aqueous solutions. However, a general agreement with this work is the application of MVA methods to investigate protein secondary structure. In this Chapter, native protein concentration was calculated using PLS regression in combination with spectroscopy. Recently, diverse work has investigated the application of PLS regression to assess protein concentration using near infrared and FTIR spectroscopy. In these examples, PLS regressions have shown a good fit, which is explained by a high number of variables present in the model, allowing a more robust prediction [62,189-191]. MCR-ALS, PLS-DA or iPLS have shown their application to investigate secondary structure determination of proteins in solution. Therefore, those methods could be use to quantify native protein concentration as an alternative method to the PLS regression used in this work.

Loadings plots were used to identify spectra features within the amide I band that corresponded to each significant PLS factor. The first factor showed a negative peak at 1651-1662 cm^{-1} which probably reflected decreased α-helix content and a positive peak at 1612-1625 cm^{-1} corresponding to increased intermolecular β-sheet or aggregate content [48]. Factor 2

showed a positive peak at 1610-1624 cm^{-1}, and a negative peak at 1651-1660 cm^{-1} which may correspond to amide I regions where maximum differences exist between the native and denatured spectra. Factor 3 was difficult to attribute directly to any specific spectral modes. In the case of fluorescence spectra, the loadings plots (**Figure 3.6(B)**) showed a negative region between 315-327 nm that was interpreted as modifications in the tertiary structure of the protein as a consequence of Trp exposure to a less polar environment in aggregates.

A limitation of this study was that only one model protein (BSA) was investigated where small shifts in α-helix and β-sheet bands are an indication of protein unfolding. In order to avoid over-fitting the model to the data, the lowest number of PLS factors was chosen. Loadings plots were used to verify that each factor explained a specific structure of the protein (e.g. α-helix or β-sheet) and also to assess whether the PLS factor corresponded to noise. Using these critera the number of PLS factors was minimised to obtain the best model. Another criterion used to build the model was the identification and the study of each possible outlier. Outliers may adversely affect the models and thus should be removed if this is the case [192]. Detection of outliers and their influence on the models is relatively straightforward through inspection of, for example, the scores, residual and prediction plots. Outliers, however, were not found in the PLS models constructed in this work.

The developed models were used to predict the loss of native protein in samples heated at 40°C, 50°C and 60°C. The main consideration was that the models were built using protein concentrations between 100% native to 50% w/w native BSA; so the prediction of native protein concentration can only be made within this range. As an example, the change in native protein concentration at 60°C over 60 minutes was outside the concentration range of the models and PLS regression models can not be used to predict those protein concentrations. The concentration range (i.e. 100% native to 50% w/w native BSA) was chosen because it represents the early stage of protein degradation and hence could be applied to stability testing in protein pharmaceuticals where the loss of 5 to 10% protein native structure may represent the product shelf-life. Samples for fluorescence spectroscopy were taken over the first ten minutes to determine if the tertiary structure was altered, then the sample time for FTIR was extended to over 60 minutes. It was expected to see changes in the tertiary structure of protein earlier than for the secondary structure. For that reason, fluorescence studies were limited to 10 minutes only while FTIR spectroscopy was investigated for 60 minutes. The predicted concentration of native protein using the FTIR

model was lower than using the fluorescence model. This could be explained by FTIR spectroscopy detecting changes in the secondary structure of proteins which also involve the loss of tertiary structure whereas fluorescence spectroscopy detects only changes in the tertiary structure [60,69,150]. Small changes in secondary structure may occur which, at least at first, are not sufficiently large or at a sufficiently influential location, to make a change in tertiary structure energetically favourable. A further difference was that total protein concentrations were different in FTIR (5% w/w) and fluorescence (1% w/w) studies and this could also affect the rate of physical degradation [193]. However, protein concentration predicted using FTIR and fluorescence models (t=0 and 10 min) were not significantly different to protein concentration obtained using SEC as shown by the statistical analysis ($P > 0.05$). Similarly, the comparison of protein concentration measurements using FTIR spectroscopy or SEC methods did not render significant difference ($P > 0.05$), when further measurements times were considered (0, 10, 30, and 60 min).

Solutions incubated at 40°C and analyzed using fluorescence spectroscopy did not show changes during the first 10 minutes suggesting protein loss of BSA tertiary structure occurs slowly at this temperature. Longer incubation times could be used to investigate physical degradation at this temperature. In fact, samples heated at 40°C for 60 minutes showed only a small loss of BSA using FTIR spectroscopy with 92% ± 1.3% native structures remaining at 60 minutes (**Table 3.3**). SEC was used to experimentally verify the accuracy of the predicted native BSA concentrations in the heat-denatured solutions using PLS models. Moreover, SEC results were in agreement with previous reports where SEC has been used to identify and characterize soluble aggregates of BSA in solution [24,75,194,195]. SEC results showed a good match between the estimated concentrations given by each spectroscopy technique (i.e. FTIR and Fluorescence) at 40°C, 50°C and 60°C within the first 30 minutes (**Figure 3.7 and 3.8** and, **Table 3.3**). At 60 minutes, there were differences in the percentage of native BSA remaining at 50 and 60ºC between FTIR and SEC experiments. These differences may reflect the different physical properties being measured by each technique as FTIR showed changes in secondary structure whereas SEC showed aggregation to higher order aggregates. Additionally to FTIR and fluorescence spectroscopy, MVA has been used in combination to other analytical techniques like near infrared spectroscopy [196], circular dichroism spectroscopy [178], mass spectroscopy [196] and x-ray spectroscopy [197] to investigate the application of those analytical techniques and MVA in the quantification of protein concentration. In those reports, the combination of analytical techniques and MVA was

useful to quantify complexes data sets, to control confounding factors and to visualize the relationship between more than two variables at the same time.

In order to estimate PLS models for other proteins, it will be necessary to obtain protein specific FTIR or fluorescence spectra and to develop new models that explain physical stability for the protein in question. Once the model is established, the analysis of stability of the studied samples is relatively rapid since FTIR and fluorescence spectra can be measured without sample processing. For analysis of protein degradation by other stresses it may be necessary to select different conditions to produce the denatured standard as this sample should reflect the most likely pathway of protein physical degradation in the samples of interest. In this example, heat-denatured BSA was used so that the effect of heat on the stability of protein solutions could be investigated. A further development of this approach could be to investigate the effect of different stress conditions like exposure to solvents, changes in pH, shaking, homogenisation, pressure or other conditions to determine whether these stress conditions produce similar irreversible aggregates as those formed at high temperature (90ºC for 30 min) [32,194,195] or whether different conditions are needed to produce appropriate denatured standards.

Results from the beta regression analysis showed that the analysis method was not a significant factor explaining the observed differences in protein concentration. In particular, in the first data set the full model rendered non significant differences ($P > 0.05$) between the three analytical method under assessment. Additionally, the comparison of the full model with a reduced version, where analytic methods were excluded, render a similar ability of both model to predict protein concentration. Similar results were observed during the analysis of the second dataset. These results suggest that the three methods are able to measure similar protein concentration during the period time under analysis, therefore the use of any of them should generate similar results. Traditional statistical techniques such as ANOVA or liner regression were not used to investigate significant differences between native protein concentration predicted by analytical methods (i.e. FTIR and fluorescence spectroscopy and, SEC) because despite of the use to several methods for data normalization, the dependent variable (protein concentration) remained not-normally distributed, violating one of the basic assumptions of frequentist statistics. Beta regression models represent an alternative for the analysis of variable that are naturally bound between the zero and one interval, as concentration. In recent years, this approach has been recommended over traditional data-

normalization approaches because data involving proportions or percentages are naturally heteroskedastic and they are commonly asymmetric. Thus interval estimation and hypothesis testing tend to be inaccurate when the sample size is small [182].

3.5. Conclusions

PLS in conjunction with spectroscopy (FTIR and fluorescence) was suitable to quantify physical stability of BSA with potential application in protein drug formulation. However, FTIR and fluorescence spectra must be pre-processed to reduce noise in the spectra and improve PLS parameters. In the case of FTIR, the best model was obtained with 2^{nd}D, BC and AN of amide I (1600-1700 cm^{-1}) using three PLS factors, and resulted in 0.91% of error and an R^2 of 0.997. In the case of intrinsic Trp fluorescence, the best model was obtained after BC and AN of Trp emission (300-400 nm) using one PLS factor, and resulted in 1.38% of error and an R^2 of 0.993. PLS models appear suitable to quantify changes in native protein concentration in reasonably simple solution formulations while application to more complex formulations warrants future investigation.

Chapter 4: The effect of the presence of heat-denatured protein on protein interfacial stability

4.1. Introduction

Stability of protein structure is relevant in the pharmaceutical industry since protein drugs have to maintain their native structure to achieve products that are stable, biologically effective and non-immunogenic [99]. Protein physical stability is reported to be affected by adsorption to interfaces (i.e. solid-liquid, liquid-liquid and air-liquid interfaces) within pharmaceutical dosage forms [89,90] where intrinsic characteristics of the protein, interface and the solvent systems that comprise the dosage form may influence the rate and extent of loss of native protein. Proteins contain polar and non-polar regions which confer solubility, amphiphilic character and surface activity [90]. Surface activity appears to be an important determinant of a protein's susceptibility to aggregate at the interface and may be affected by intrinsic properties of the protein such as molecular weight [93], flexibility [89,116,198], size [101,116], concentration [101], charge [89,116], stability of the native structure [93,116], hydrophobicity [93,116] and isoelectric point (pI) [89,103]. Proteins of high MW (i.e. BSA), flexible or prepared at high concentrations may adsorbed faster to the oil-water interface than smaller proteins, less flexible or prepared at lower concentrations. Moreover, hydrophobic proteins may adsorb faster to interfaces than less hydrophobic proteins [199]. Environmental factors of the bulk solution such as polarity of solvent, pH and ionic strength are also considered important [89]. Hydrophobicity of proteins is increased for proteins prepared in solutions with high ionic strength which may affect proteins charge [199].

Upon adsorption to an oil-water interface protein molecules may adopt unfolded conformations, change the oil-water interfacial properties, and/or interact with the surrounding protein molecules to form a network [198]. Protein adsorption to interfaces has been explained using three stages (Regime I, II and III) [93,95,102], **Figure 4.1**. Regime I or induction, [95,102] is when protein diffusion occurs from the bulk solution to the interface. Regime I is typically characterized by a constant interfacial tension (IFT) over time and is mainly observed at low protein concentrations. Regime II or monolayer saturation [95,102] is when protein adsorption to the interface results in formation of a monolayer. In this regime, IFT is significantly reduced until a constant (or equilibrium) value is reached. Regime III or interfacial gelation [95,102] is reached when protein adsorption to the interface results in formation of a multilayer. During Regime III, IFT remains constant over time [95,101].

Rheology and IFT measurements are useful to study protein adsorption and interaction to the oil-water interface. These techniques should be used in combination to gain information about Regime I, II and III of protein adsorption to interfaces [93,95]. The advantage of rheological measurements is that information on regime III (or the multilayer formation) can be obtained [93] and once a stable interfacial structure is formed its physical properties including resistance to deformation can be assessed [200]. A plateau in elastic (G') and viscous (G'') moduli is reported to represent saturation of the oil-water interface by protein molecules and the end of protein attachment, relaxation and rearrangement [92]. The decrease in IFT over time, in terms of pressure per unit of area [109,110], corresponds to the intrinsic characteristics of proteins (conformation, molecular flexibility, size, charge and surface activity) to interact with the oil-water interface [200] showing regime I and II, which correspond to early stages of the monolayer formation [95].

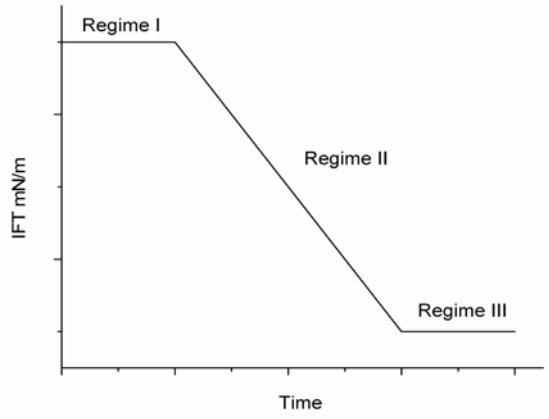

Figure 4.1 Schematic representation of Regime I, II and III of protein adsorption to interfaces using the pendant drop instruments (Adapted from Berverung *et al.* (1999)) [95]. (IFT over time, in terms of pressure per unit of area mN/m) [109,110]

The aim of this Chapter was to investigate protein adsorption at the oil-water interface by the combination of IFT measurements and interfacial rheology using the double-wall ring (DWR) geometry. The effects of introduction of heat-denatured protein to the aqueous phase on the rate and extent of protein adsorption were also investigated to help understand basic factors (stability of the native structure, hydrophobicity, flexibility, size, concentration, charge) that modify the protein's adsorption characteristics and to determine whether interfacial rheology measurements are sensitive to changes in protein conformation in the bulk solution phase [89].

4.2. Materials and methods

4.2.1. Materials

BSA (A-7906) was obtained from Sigma-Aldrich, USA. Phosphate buffer (pH 7, ionic strength 0.05M) was used to prepared native BSA solutions at 0.15 mM, 0.4 mM and 0.8 mM. The oil phase was composed of coconut oil (medium chain triglycerol, donated by H. Lundbeck A/S, Denmark) and was used as received.

4.2.2. Preparation of native BSA, heat-denatured BSA and binary mixtures of BSA solutions

Aliquots of native BSA solutions (0.4 mM and 0.8 mM) were diluted in phosphate buffer pH 7 to obtain concentrations of 0.2 mM, 0.27 mM, 0.4 mM and 0.47 mM. Further, a solution of native BSA at 0.15 mM in phosphate buffer was prepared and heated at 90°C in water for 30 minutes to give heat-denatured BSA. Native BSA (0.8 mM and 0.4 mM) and heat-denatured BSA (0.15 mM) were mixed to obtain binary mixtures of native BSA (0.4 mM and 0.2 mM) and heat-denatured BSA solutions (0.07 mM). Total protein concentration in binary mixtures was 0.47 mM and 0.27 mM. These solutions were prepared in triplicate.

4.2.3. Interfacial rheology measurements

Rheology studies were conducted with a TA AR-G2 rheometer (TA-Instruments, Waters, New Castle, USA) with DWR geometry using a method previously described by Baldursdottir *et al*. (2011) [101]. The system consisted of a square-edge ring (platinum-iridium alloy) and a Delrin® trough (Teflon) with a circular channel (**Figure 4.2**). The gap was zeroed without the ring attached and then kept constant at 12,000 μm. 18.8 mL of the water phase were measured using a mechanical pipette and added to into the Delrin® trough, then the DWR was lowered onto the water phase surface. A meniscus was formed between the ring and the water phase which confirmed a physical contact between the ring and the water phase. This meniscus was determined by visual inspection. Thereafter, an equal volume of the oil phase was carefully poured on top. Oscillatory shear measurements were conducted over time at a constant frequency of 0.1 Hz, strain of 0.1% (within the linear viscoelastic region) and at a temperature of 25°C. The linear viscoelastic region was determined plotting G' and G" moduli vs. oscillation torque (or strain) in a stress (or strain) sweep. When G'

modulus starts to bend downwards measurements were in the non-linear viscoelastic region. All the time-sweep measurements were followed with frequency sweeps (0.1% strain) and strain sweeps (0.1 Hz) to investigate the properties of the film after two hours of protein adsorption to the oil-water interface. Rheology measurements were conducted in triplicate for each solution.

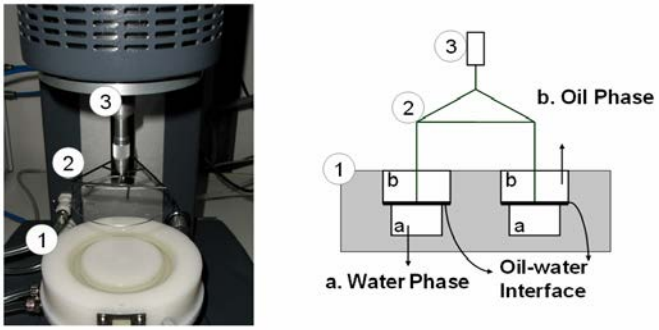

Figure 4.2 Photograph and schematic illustration of the TA AR-G2 rheometer with DWR geometry: 1) Delrin® trough with a circular channel, 2) DWR geometry (platinum/iridium alloy) and 3) geometry holder.

4.2.4. Data analysis for interfacial rheology

Time-sweep, frequency-sweep and strain amplitude-sweep steps were used to investigate and compare the time-course of interfacial layer formation, and frequency dependency and strength of the resultant viscoelastic multilayer. The time-sweep step was used to investigate the evolution of the BSA adsorption as a function of time giving the maximum value of G' and G" moduli (N/m) after two hours and the time to cross-over between G' and G" moduli (N/m). The time to cross-over is reported to represent the completion of monolayer formation and the beginning of multilayer formation [101,102,201]. The strain amplitude-sweep step was used to characterize resistance to breakage of the interfacial film after two hours. Plots of the logarithmic dynamic moduli (G' and G" in N/m) versus logarithmic oscillation torque (in mN/m) applied to the film were constructed [97]. Torque values at the first reduction of G' and G" were used as film breakage for G' and G" moduli, respectively. The frequency-sweep step was used to quantify elasticity or solid properties of the film after two hours of protein adsorption. Plots of the logarithmic complex viscosity (η^* in Ns/m) versus logarithmic frequency (ω in rad/sec) applied to the film were constructed and the slope obtained from the

linear relationship between η^* and ω indicates the solid-like behaviour of the interfacial film (see below).

The relationship between η^* and ω is explained by the following equations. Cox and Merz, (1958) postulated that the double logarithm of the steady flow viscosity (η) vs. the deformation as function of time, ($\dot{\gamma}$) (Equation 4.1) was equivalent to the double logarithm of absolute value of complex viscosity η^* vs. frequency (ω) [202,203] giving Equation 4.2. (The shear rate ($\dot{\gamma}$) is the velocity of changes (dv) over time (dt), ($\dot{\gamma} = \frac{dv}{dt}$)).

$$\eta = \frac{\sigma}{\dot{\gamma}} \qquad \text{(Newton's Law) (4.1)}$$

where, σ is the shear stress [202].

$$\eta^* = \frac{k}{\omega} \qquad (4.2)$$

where k is the consistency index. The double logarithm applied to Equation 4.2 gave a slope which represents the flow behaviour index (n) [203,204] also known as the power-law exponent ($0 < n < 1$) (Equation 4.3). Values of n close to one indicate that the film has more solid-like properties [97].

$$\log\left|\eta^*\right| = -n\log\omega + k \qquad (4.3)$$

Complex viscosity (η^*) is a measure of the overall resistance of the interfacial film to flow and combines both the deformation that is recoverable (elastic, η'') and non-recoverable (viscous, η') [205,206] where, $\eta^* = \eta' + \eta''$ [205]. The magnitude of the absolute value of complex viscosity $\left|\eta^*\right|$ is defined by Equations 4.4, 4.5 and 4.6. The absolute value of complex dynamic viscosity as a function of frequency ($\left|\eta^*(\omega)\right|$) is defined by Equation 4.7 [207].

$$\left|\eta^*\right| = \sqrt{\eta'^2 + \eta''^2} \qquad (4.4)$$

$$\eta' = \frac{G''}{\omega}; \eta'' = \frac{G'}{\omega} \qquad (4.5)$$

$$\left|\eta^*\right| = \sqrt{\eta'^2 + \eta''^2} = \left[\left(\frac{G''}{\omega}\right)^2 + \left(\frac{G'}{\omega}\right)^2\right]^{\frac{1}{2}} \quad (4.6)$$

$$\left|\eta^*(\omega)\right| = \sqrt{\frac{G'(\omega)^2 + G''(\omega)^2}{\omega}} \quad (4.7)$$

4.2.5. Interfacial tension measurements

IFT studies were performed using a pendant drop instrument (KRÜSS, Hamburg, Germany) as previously described by Baldursdottir *et al*. (2010) [93]. A drop of protein solution (aqueous phase) formed at the tip of a syringe (1.83 mm needle diameter) was lowered into a glass cuvette (4 x 2 x 1 cm) containing the oil phase (6.5 mL). The volume of the protein solution drop was held constant at 50 µL and experiments were performed at room temperature (**Figure 4.3**). To calculate the IFT, the drop profile was obtained from an image to which the Laplace-Young equation was fitted (Equation 4.8):

$$\Delta P = \gamma\left(\frac{1}{R_1} + \frac{1}{R_2}\right) \quad (4.8)$$

where ΔP is the pressure difference over the drop interface, γ is the interfacial tension (IFT), R_1 and R_2 are the radii of the maximum width and the length of the drop, respectively [111,208]. Drop Shape Analysis System (DSA100, version 1.90.0.22, KRÜSS, Germany) was used for the fitting. IFT measurements were performed in triplicate for each solution.

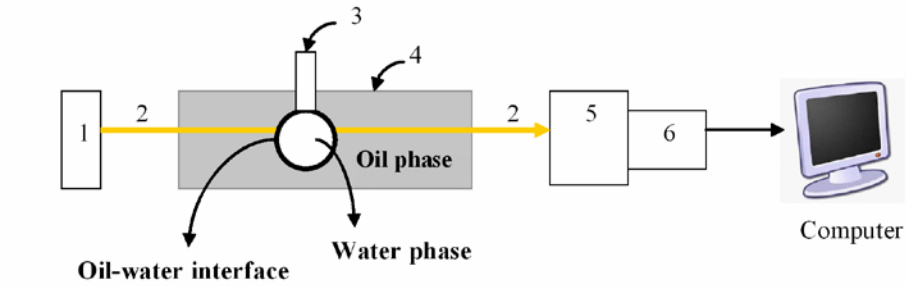

Figure 4.3 Schematic illustration of pendant drop tensiometer: 1) lamp, 2) light, 3) syringe (water phase), 4) cuvette (oil phase), 5) lenses and 6) camera.

4.2.6. Data analysis for interfacial tension measurements

The decrease in IFT was measured for each solution over one hour. The initial slope was calculated to compare the decay rates from zero to three minutes for each of the different BSA solutions. Additionally, the calculation of IFT after 30 minutes (IFT_{30}) was used to compare the decrease in IFT for each solution (i.e. native BSA alone (0.2 mM and 0.4 mM) and binary mixtures of native BSA (0.4 mM and 0.2 mM) and heat-denatured BSA solutions (0.07 mM). Total protein concentration in binary BSA mixtures was 0.47 mM and 0.27 mM.

4.2.7. Statistical analysis

Friedman's test was used to assess statistical differences between type of protein (native protein alone and binary mixtures of native BSA (0.4 mM and 0.2 mM) and heat-denatured BSA solutions (0.07 mM)) and BSA concentration (0.2 mM and 0.4 mM). Due to the low statistical power of non-parametric tests, a significant difference was accepted at a P - value $\leq$ 0.10. The Friedman's test was conducted with R software version 2.15.2 (R Foundation for Statistical Computing, Vienna, Austria).

4.3. Results

4.3.1. Interfacial rheology measurements using a double wall-ring (DWR) geometry

Increased elastic (G') and viscous (G") moduli were observed for the BSA solution at the oil-water interface with time. The increases in G' and G" moduli were observed from solutions of native BSA alone as well as from solutions of heat-denatured BSA (0.15 mM) (90°C for 30 min) (**Figure 4.4(A)**). The heat-denatured BSA slowed down the formation of a multilayer delaying the time to cross over between G' and G" moduli by approximately two hours compared to the native BSA (i.e. 96 min vs. 16 min respectively) (**Figure 4.4(B)**), with the final interfacial layer having lower G' and G" moduli (**Figure 4.4(A)**). The typical maximum G' and G" moduli for native BSA and heat-denatured BSA (0.15 mM) were 48 and 8 mN/m vs. 7 and 4 mN/m, respectively.

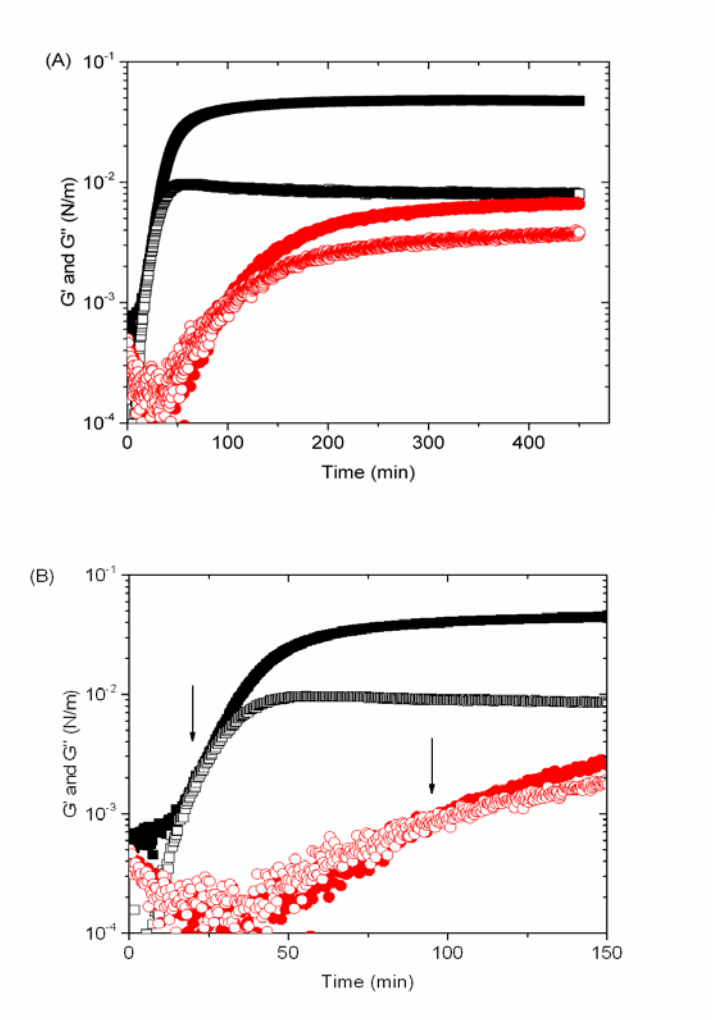

Figure 4.4 Typical example of elastic G' (solid symbols) and viscous G" (open symbols) moduli at the oil-water interface of native (■) and heat-denatured (●) BSA solutions (0.15 mM). (A) Protein adsorption over 400 min showing the differences in maximum G' and G" moduli and (B) time to cross over between G' and G" moduli highlighted using arrows (16 min for native BSA vs. 96 min for heat-denatured BSA). G' and G" moduli are in logarithmic scale.

Increases in G' and G" moduli were concentration dependent as the interfacial film formed more rapidly from the solution with a higher protein concentration (0.4 mM compared with 0.2 mM) (**Figure 4.5**). The addition of heat-denatured protein to a solution of native BSA delayed the time to cross-over between G' and G" moduli from 4 ± 1 min to 12 ± 3 min at 0.4 mM BSA and from 19 ± 3 min to 23 ± 1 min at 0.2 mM BSA (mean ± s.d., **Table 4.1**). The differences in time to cross-over for BSA concentration and type of protein (i.e. native protein alone and binary mixtures of native BSA (0.4 mM and 0.2 mM) and heat-denatured

BSA solutions (0.07 mM)) were significant as determined by Friedman's test (P = 0.029). (**Appendix C**).

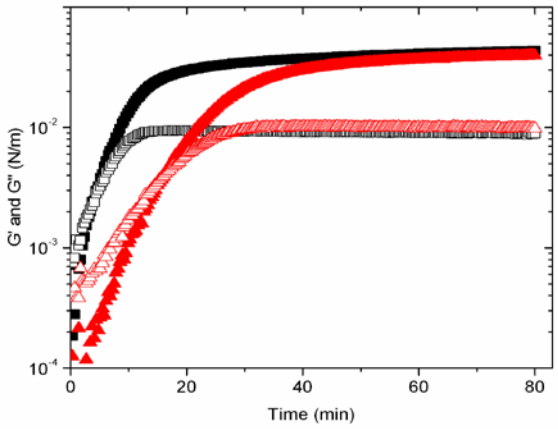

Figure 4.5 Typical example of elastic G' (solid symbols) and viscous G" (open symbols) moduli at the oil-water interface of native BSA alone at 0.4 mM (■) and 0.2 mM (▲). G' and G" moduli are in logarithmic scale.

The resulting maximum G' value was lower in the presence of heat-denatured protein than for the native protein alone (**Figure 4.6(A) and (B)**). After two hours, an equilibrium was reached where maximum values of G' (47 ± 5 mN/m) and G" (9 ± 1 mN/m) were observed for 0.4 mM native BSA. Addition of heat-denatured BSA (0.07 mM) to the aqueous phase decreased the maximum elastic modulus reached at equilibrium (G' 42 ± 6 mN/m) but giving similar G" (9 ± 1 mN/m) compared to native BSA alone (**Table 4.1**). Similar effects were observed at the lower native BSA concentration (0.2 M), except lower equilibrium moduli were reached (G' were 40 ± 2 mN/m and 35 ± 1 mN/m in the absence and presence of 0.07 mM heat-denatured BSA, respectively). The difference of G' moduli for different BSA concentrations and type of protein was significant as determined by Friedman's test (P = 0.072). Additionally, the difference between BSA concentration and type of protein (i.e. native protein alone and binary mixtures of native BSA (0.4 mM and 0.2 mM) and heat-denatured BSA solutions (0.07 mM)) was only significant for binary mixture at 0.2 mM (**Appendix C**). The difference of G" moduli for different BSA concentrations and type of protein (i.e. native protein alone and binary mixtures of native BSA (0.4 mM and 0.2 mM) and heat-denatured BSA solutions (0.07 mM)) was no significant as determined by Friedman's test (P > 0.1).

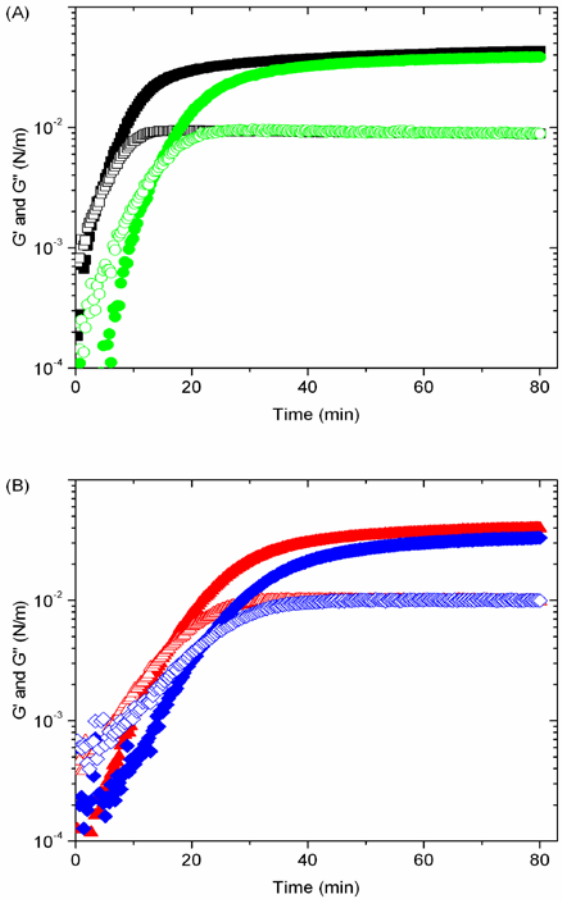

Figure 4.6 Typical example of elastic G' (solid symbols) and viscous G" (open symbols) moduli at the oil-water interface: (A) native BSA alone (0.4 mM) (■) and native BSA (0.4 mM) in the presence of heat-denatured protein (0.07 mM) (●) [total protein concentration was 0.47 mM], and (B) native BSA alone (0.2 mM) (▲) and binary mixture of native BSA (0.2 mM) in the presence of heat-denatured protein (0.07 mM) (◆) [total protein concentration was 0.27 mM]. G' and G" moduli are in logarithmic scale.

Table 4.1 Data analysis of rheology measurements. Time sweep step (time to cross-over and maximum elastic (G') and viscous (G") moduli) and frequency sweep step (power law exponent, n) data are shown (mean ± s.d., n=3).

BSA (mM)		Time to cross-over	Maximum (N/m) (x 1000)		Power law exponent*
Native	Heat-denatured	(min)	Elastic modulus (G')	Viscous modulus (G")	(n)
0.4	0	4 ± 1	47 ± 5	9 ± 1	-0.902 ± 0.004
0.4	0.07	12 ± 3	42 ± 6	9 ± 1	-0.871 ± 0.029
0.2	0	19 ± 3	40 ± 2	10 ± 0.4	-0.862 ± 0.009
0.2	0.07	23 ± 1	35 ± 1	10 ± 0.4	0.843 ± 0.006

(*) power law exponent (n) close to one means the final film has a more solid-like property.

Rheology studies were also used to compare the multilayer formation at the same total protein concentration for native BSA alone (0.47 and 0.27 mM) and, binary mixtures of native and heat-denatured BSA (0.47 mM and 0.27 mM) (**Figure 4.7(A) and (B)**). Again the multilayer was formed faster at higher native BSA concentration (0.47 and 0.27 mM) than for native protein at 0.4 mM and 0.2 mM respectively.

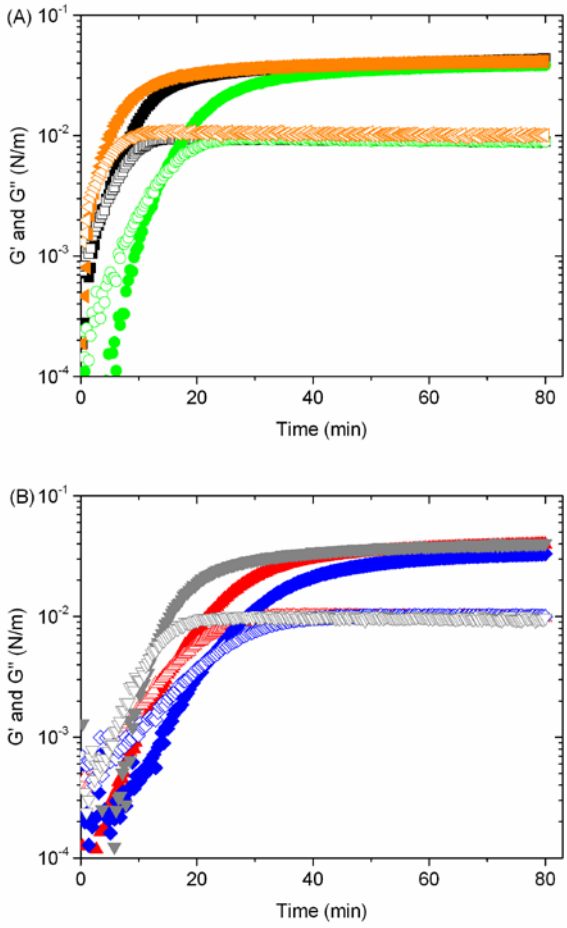

Figure 4.7 Typical example of elastic G' (solid symbols) and viscous G'' (open symbols) moduli at the oil-water interface at the same total protein concentration of native BSA alone or in the presence of heat-denatured BSA: (A) native BSA alone 0.47 mM (◀), 0.4 mM (■) and binary mixture 0.47 mM (●), and (B) native BSA alone 0.27 mM (▼), 0.2 mM (▲) and binary mixture 0.27 mM (◆). G' and G'' moduli are in logarithmic scale.

Strain amplitude-sweep experiments (**Figure 4.8**) showed that the oscillation torque at which the multilayer was disrupted was similar for films formed from different types of proteins like native alone (0.4 mM and 0.2 mM) and binary mixtures of native and heat-denatured BSA (0.47 mM and 0.27 mM). The oscillation torque that produced the first decrease in G' and G'' moduli for each solution were (mean ± s.d.): native BSA alone 0.2 mM (7 ± 1 mNm and 8 ±

1 mNm), binary mixtures at 0.27 mM (6 ± 0.1 mNm and 8 ± 0.1 mNm), native BSA alone at 0.4 mM (8 ± 1 mNm and 9 ± 1 mNm) and binary mixtures at 0.47 mM (9 ± 1 mNm and 9 ± 1 mNm). The difference in oscillation torque for G' modulus was not significant as determined by Friedman's test ($P > 0.1$). Statistical analysis showed significant differences in oscillation torque for G" modulus as determined by Friedman's test ($P = 0.042$). Additionally, the difference between BSA concentration and type of protein (i.e. native protein alone and binary mixtures of native BSA (0.4 mM and 0.2 mM) and heat-denatured BSA solutions (0.07 mM)) was only significant for binary mixture at 0.2 mM (**Appendix C**).

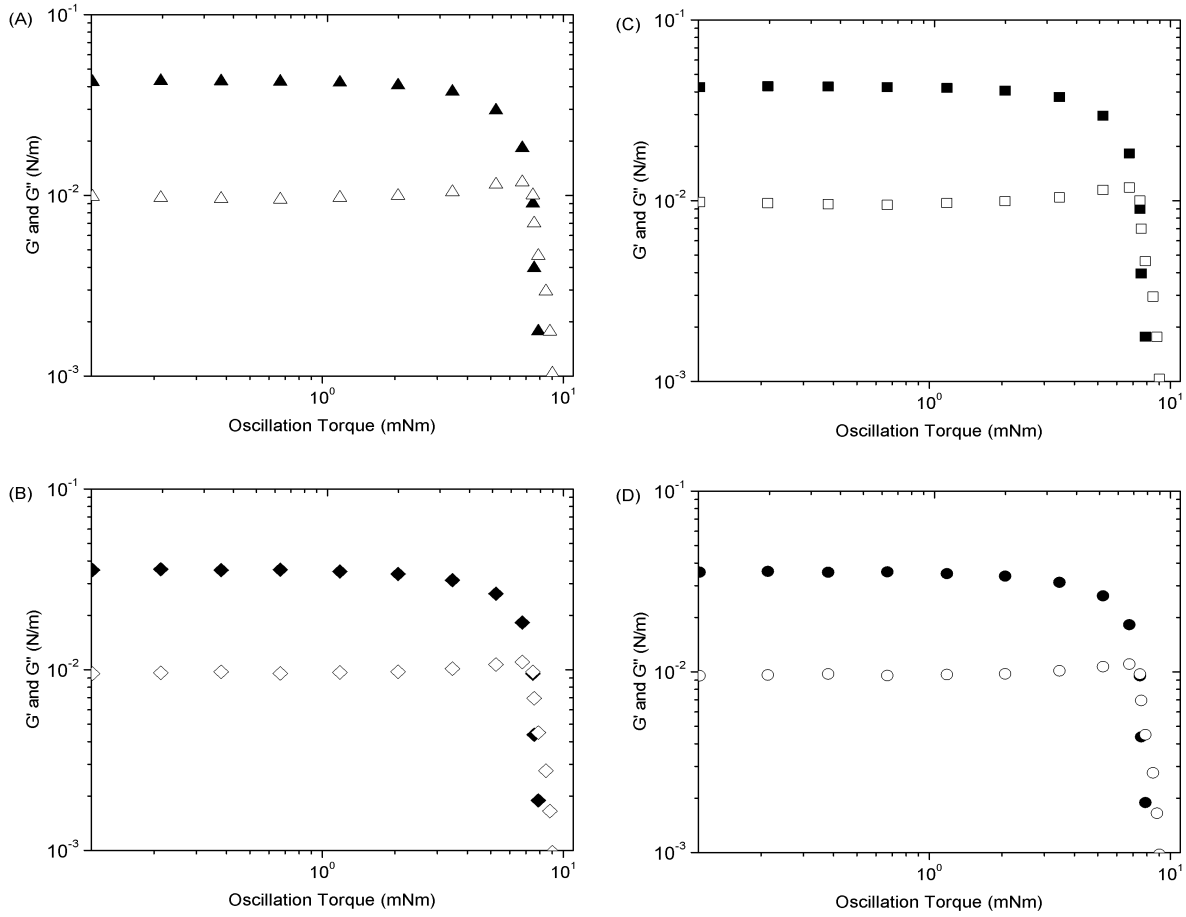

Figure 4.8 Typical example of elastic G' (solid symbols) and viscous G" (open symbols) moduli as a function of the oscillation torque (mNm) applied to the oil-water interface after two hours of adding protein. The reduction in G' and G" moduli indicates film breakage. (A) native BSA alone at 0.2 mM, (B) binary mixtures of native and heat-denatured BSA at 0.27 mM, (C) native BSA alone at 0.4 mM and (D) binary mixtures of native and heat-denatured BSA at 0.47 mM. G' and G" moduli and, oscillation torque are in logarithm scale.

Frequency-sweep measurements were used to determine the solid-like or liquid-like properties of the multilayer after two hours. The presence of heat-denatured protein in the bulk solution showed a tendency towards formation of a less solid-like film since the power law exponent (n) was lower in the presence of heat-denatured protein than for native protein alone (**Table 4.1**). The differences of power law exponent for different BSA concentrations and types of protein (i.e. native protein alone and binary mixtures) were significant as determined by Friedman's test (P = 0.086). Additionally, statistical analysis showed that this difference was only significant between BSA concentration and type of protein (i.e. native protein alone and binary mixtures of native BSA (0.4 mM and 0.2 mM) and heat-denatured BSA solutions (0.07 mM)) for native BSA at 0.2 mM (**Appendix C**).

4.3.2. Interfacial tension measurements using a pendant drop tensiometer

The reduction of the IFT was slower for the lower concentrations of the native BSA alone (0.2 mM) compared to the highest protein concentration (0.47 mM) (**Figure 4.9(A)**). In comparison, control experiments in the absence of BSA gave an IFT at t=20 minutes of 18.0 ± 1.3 (mN/m). The shape of the curves describing the decrease in the IFT values was also dependent on the addition of heat-denatured protein to the bulk solution. IFT appeared to decrease more slowly when heat-denatured BSA was added to native BSA at the lower concentration (0.2 mM), however, this was not noticeable at the higher concentration (0.4 mM). Furthermore, IFT measurements were used to compare the decrease of IFT at the same total protein concentration for native BSA alone (0.47 and 0.27 mM) (**Figure 4.9(B)**) and binary mixtures of native and heat-denatured BSA (0.47 mM and 0.27 mM) (**Figure 4.9(A)**) where native BSA alone decreased the IFT to similar values compared to binary mixtures.

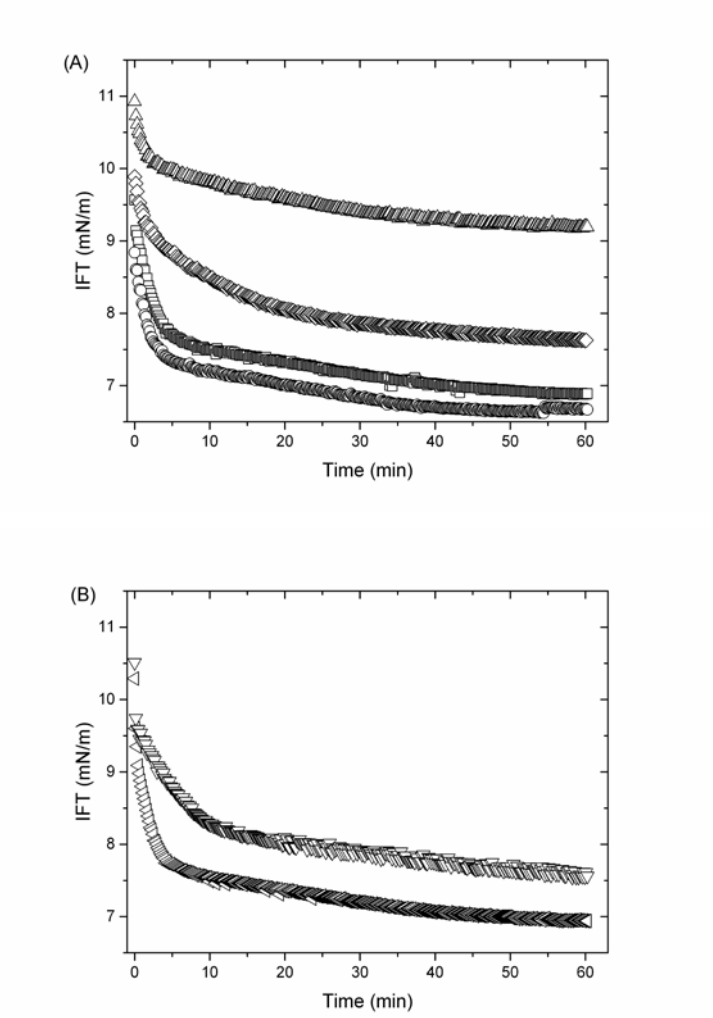

Figure 4.9 IFT measurements of BSA solutions: (A) native BSA alone at 0.4 mM (□) and 0.2 mM (△) and, binary mixtures of native and heat-denatured BSA, total protein concentration: 0.47 mM (○) and 0.27 mM (◇); (B) native BSA alone at 0.27 (▽) and 0.47 mM (◁). (n=3).

The decrease in the IFT was investigated by comparison of the IFT_{30} for solutions of native BSA alone (0.4 mM and 0.2 mM) and for binary mixtures of native and heat-denatured BSA. These results showed that the surface tension for the native protein alone (7.2 ± 0.3 mN/m (0.4 mM) and 9.4 ± 0.7 mN/m (0.2 mM) was higher than for the native protein in the presence of (0.07 mM) heat-denatured protein [6.8 ± 0.1 mN/m (0.4 mM) and 7.9 ± 0.2 mN/m (0.2 mM)] (**Table 4.2**). Statistical analysis shown significant differences in IFT_{30} for type of protein (i.e. native BSA alone and binary mixtures) and BSA concentration as determined by Friedman's test (P = 0.042) (**Appendix D**). Moreover, statistical analysis showed that this difference was only significant between BSA concentration and type of protein (i.e. native protein alone and binary mixtures of native BSA (0.4 mM and 0.2 mM) and heat-denatured BSA solutions (0.07 mM)) for native BSA at 0.2 mM. In the case of

native BSA at 0.4 mM, this statistical difference was only significant for BSA concentration (**Appendix C**)

Table 4.2 Data analysis of IFT measurements showing the initial decrease in slope (over the first three minutes) and IFT_{30} (mean ± s.d., n=3).

BSA (mM)		Initial slope (N/m/min) (t=3 min)	IFT_{30} (mN/m)
Native	Heat-denatured		
0.4	0	-0.441 ± 0.10	7.2 ± 0.3
0.4	0.07	-0.420 ± 0.14	6.8 ± 0.1
0.2	0	-0.238 ± 0.04	9.4 ± 0.7
0.2	0.07	-0.263 ± 0.04	7.9 ± 0.2

The rate of decrease of IFT over the first three minutes was also examined. This showed that the initial rate of decrease in the IFT was concentration dependent with a higher slope (over the first three minutes) for the native protein alone at 0.4 mM (-0.441 ± 0.10 N/m/min) than for 0.2 mM (-0.238 ± 0.04 N/m/min). The initial slope (over the first three minutes) was significant different as determined by Friedman's test (P = 0.060). Moreover, this difference was only significant for native BSA concentration (0.2 mM vs. 0.4 mM) (**Appendix D**). Moreover, binary mixtures of native and heat-denatured protein (0.47 mM and 0.27 mM) did not affect the initial rate of decrease of IFT showing similar initial slope (over the first three minutes) values than for native protein alone.

4.4. Discussion

Beverung *et al*. (1999) suggested that the increased elastic (G') and viscous (G") moduli with time may represent formation of a multilayer of protein molecules at the interface [95]. Previous studies have shown that the rate and extent of protein adsorption to an oil-water interface could be measured by interfacial rheology using a Du Nouy ring accessory [32,93,95,97,208]. Since this time a double wall-ring (DWR) accessory has become available which has been suggested to improve the sensitivity of the interfacial measurements [206]. This is due to differences in the radii between Du Nouy and DWR accesories which improves the contact between the ring and the sample. The DWR has a radii of 45 mm while the Du Nouy ring has a radii of 10 mm [101]. Baldursdottir *et al*. (2011) investigated the use of rheological measurements with the DWR geometry to study protein adsorption to the oil-water interface [101]. The study described here further examines the potential of this rheometer configuration to detect changes in protein adsorption due to the presence of heat-denatured protein.

Rheology studies were used to gain information about the time to cross-over between G' and G" moduli and the maximum magnitude of G' and G" moduli for native protein alone (0.2 mM and 0.4 mM) and binary mixtures of native and heat-denatured BSA. Total protein concentration in the binary mixtures was 0.27 mM and 0.47 mM. The time to cross-over between G' and G" moduli represent the beginning of a network gel or multilayer formation at the liquid-liquid interface [102,209]. In the current study, the time to cross-over gave relevant information about how the kinetics of protein adsorption to the oil-water interface was affected by the presence of heat-denatured BSA and protein concentration. Liu *et al*. (2013) reported that keratinocyte growth factor 2 (KGF-2) adsorbed to the air-water interface showing that the time to cross-over was faster for higher protein concentration. The time to crossover for KGF-2 at 0.5 mg/mL was a few seconds whereas the time to cross-over was two min for KGF-2 at 0.005 mg/mL [201]. This was in agreement with this work where the time to cross-over was faster for native BSA at 0.4 mM than for native BSA at 0.2 mM (4 ± 1 min and 19 ± 3 min respectively). The plateaus reached for G' and G" moduli represent the saturation of protein adsorption to the interface giving a maximum magnitude for G' and G" moduli [93]. G' and G" moduli reached a constant within two hours of protein adsorption, a plateau, which was used to investigate the stability of the network formed at the interface since a decrease in their magnitude is attributed to desorption of adsorbed protein from the interface [102,209].

Pendant drop tensiometer experiments were conducted as a complementary method to study protein adsorption. The interfacial tension obtained from the pendant drop experiments corresponds to the energy necessary to create a new surface [210]. This method was used to investigate regime II of protein adsorption to interfaces where IFT is reduced until a constant (or equilibrium) value is reached [95]. Typically pendant drop experiments report an initial rapid decrease in IFT as a monolayer is formed at the interface. Following this, the rate of decrease in IFT slows and a plateau is reached when no further change in IFT occurs [93,102]. Native BSA alone (0.15 mM, 0.2 mM, 0.27 mM, 0.4 mM and 0.47 mM) and heat-denatured BSA (30 min at 90°C; 0.15 mM) were used to characterize the oil-water interfacial adsorption of native and heat-denatured protein. The physical degradation of BSA solutions heated at 90°C for 30 min was confirmed using size exclusion chromatography as described in **Chapter 3 section 3.3**. Heat-denatured BSA eluted at 11 min while native BSA eluted at 14 min (**Figure 3.1**). Additionally, binary mixtures of native and heat-denatured BSA (0.27 mM and 0.47 mM) were used to examine how introduction of a small amount of heat-

denatured BSA in the bulk solution affected the adsorption of a native protein to the oil-water interface. These results suggest that the presence of heat-denatured BSA both delays the multilayer formation and modifies the molecular structure of the interfacial multilayer network. These results support the hypothesis that interfacial rheological studies have a potential role in describing and understanding the interfacial reactions that occur in pharmaceutical formulations. The explanations for the current results could be based on intrinsic characteristics of the protein itself (conformation, molecular flexibility, size, charge and pI).

BSA is a globular protein with 17 disulfide bonds [116] where 60% of its amino acids are considered hydrophobic [93]. It readily adsorbs to hydrophobic surfaces [89,103], making it a good model protein to study protein interfacial interactions. In the heat-denatured protein, the globular conformation is lost and the hydrophobic groups become more exposed to the aqueous phase compared to the native protein conformation [35,73,211]. Rheology results showed that heat-denatured protein (0.15 mM) formed a multilayer about two hours later than native BSA alone (**Figure 4.4(B)**) which may be explained by differences in protein flexibility and the kinetics of protein adsorption to the oil-water interface [95,212,213]. This may explain the decrease in G' and G" moduli for the heat-denatured protein (0.15 mM) at early time points. The presence of heat-denatured protein in the binary mixtures reduced the IFT more rapidly than native BSA alone (**Figure 4.9(A)**). This may suggest that the molar ratio of native to heat-denatured protein is important. At the concentrations used in this work the molar concentration ratio of heat-denatured to native BSA was 16% and 25% at native BSA concentrations of 0.4 mM and 0.2 mM BSA, respectively. The shape of the curves describing the decrease in the IFT values was also dependent on the addition of heat-denatured protein available in the bulk solution. These results may be attributed to the presence of protein with an extended conformation in the heat-denatured protein. This would result in an increased hydrophobic surface and perhaps an increased tendency for the heat-denatured form to associate with the hydrophobic oil surface. Being extended the heat-denatured molecules may also take up more space/molecule in the interface, at least initially. However, since the heat-denatured form represented a fraction (16% to 25%) of the total protein present in the system, there would still be opportunity for native protein to adsorb as well. The time to cross-over is consistent with transition from a monolayer to a multilayer formation at the interface [101,102,201]. The delay in formation of the multilayer at the interface may have been the result of steric hindrance from the competing small fraction of heat-denatured BSA. In the interface,

the adsorbed native protein itself is likely to go through conformational changes which depend on the surface coverage, time allowed for contact, and protein concentration. At a lower protein concentration, less surface coverage is obtained than at a higher concentration which means that adsorbed protein molecules have more time to rearrange and orientate their structure before a new protein molecule is attached to the interface [92]. This could explain the delay in the multilayer formation at lower protein concentration (0.2 mM) (**Figure 4.5**).

The adsorption of proteins to the oil-water interface is affected by protein charge. Adsorption of protein from solution at a pH close to the pI of the protein is increased due to decrease in electrostatic barriers, interfacial repulsion and solubility of protein in the bulk solution. Charge distribution is also relevant in protein adsorption because heterogeneous distribution of protein charge will produce sites in the protein surface susceptible to electrostatic interactions with the interface [116]. BSA absorbs at different pH values (4-9) and not only near its pI (4.5) [90]. However, at pH values lower than its pI, the protein is unfolded and thus adsorbs differently compared to folded protein to the oil-water interface [103]. According to Colac *et al*. (2013) molecules of proteins adsorbed less to the oil-water interface when the pH of an aqueous solutions of BSA (0.5 mM) was increased from 6.6 to 7.4 [94]. Moreover, the distribution of hydrophilic and hydrophobic groups in the surface of the protein also contributed to change in the protein charge and its adsorption behaviour [116]. Native BSA at pH 7 has a negative net charge (-18 mV) that is heterogeneously distributed throughout the protein and thereby contributes to increase the solubility of BSA in water [90]. Heat-denatured proteins (extended conformations) may have a different protein charge (i.e. distribution and density) [207,214] than native protein affecting the interaction of heat-denatured protein with the oil-water interface. The charge of denatured protein could be obtained from the pH-titration curve [215].

Protein size is another characteristic of proteins affecting its adsorption to interfaces. Protein size can determine the number of possible contact points between the protein and the interface. Larger proteins have more potential contact points to interact with the interface [116,216] and the adsorption of larger molecules will be less reversible than for small proteins because more energy is required to separate adsorbed large molecule from the interface [116]. In these experiments, the extended conformation of heat-denatured BSA presents a larger molecule than the globular conformation of native BSA [80] as loss of the secondary structure allows greater extension of the amino acid chains. Yohannes *et al*. (2010) investigated the

hydrodynamic size of BSA proteins heated at 80°C using asymmetrical flow field-flow fractionation method. Those results confirmed an increase in the hydrodynamic size from 7 nm for BSA at room temperature to values between 15 and 149 nm for heat-treated BSA solution [80]. In this thesis, SEC confirmed the presence of soluble aggregates in heat-denatured solution and absence in the native BSA solutions (**Figure 3.1**). In view of that, more potential contact points with the oil surface should be expected for heat-denatured BSA than for native BSA. This may help to explain the reduction in the IFT measurements where heat-denatured BSA has more contact points available (e.g. hydrophobic groups) allowing a faster interaction with the interface than for the native, globular, BSA alone (**Figure 4.9(A)**). Previously, rheology studies using a Du Nouy ring geometry were used to compare the multilayer formation between proteins with different molecular size and percentage of hydrophobic groups. That study showed that proteins like BSA at a concentration of 1.6 mM (66 KDa with 60% hydrophobic groups) adsorbed more amount of protein to the oil-water interface giving higher G' and G" moduli than small proteins like lysozyme (14.5 KDa with 52% hydrophobic groups) [93].

The addition of heat-denatured protein to a solution of native BSA delayed multilayer formation which could be explained by competition, diffusion and difference in protein flexibility. In the binary mixtures, native and heat-denatured protein molecules compete initially to reach the oil-water interface. However, the competition is affected by their relative affinity to reach the interface when different proteins are interacting in the bulk solution. The adsorbed layer should contain a higher proportion of those protein molecules that can access the interface first [217]. This could be investigated using IFT measurements since this technique gives information mainly about the monolayer formation [95]. In that case, heat-denatured proteins could be the first molecules to be adsorbed which may explain why the IFT is reduced faster in the binary mixtures than for native BSA alone (**Figure 4.9(A)**). However, interfacial rheology, which is used to investigate multilayer formation [93,102], showed that heat-denatured BSA (0.15 mM) delayed the multilayer formation by near two hours compared to native BSA (0.15 mM) (**Figure 4.4(B)**).

Diffusion of protein molecules to the interface could also explain the delay in multilayer formation due to changes in protein conformation (globular or extended). In this case, globular BSA (native) may be able to diffuse more rapidly than the more extended, or less compact heat-denatured or aggregated BSA [32,80]. In fact, it was reported than native BSA

heated at 63°C for one hour increased the hydrodynamic size from 7 nm for native BSA to 15-22 nm for unfolded BSA [80]. The presence of soluble aggregates would move as a larger species, therefore affecting diffusion rate too. In the binary mixtures, heat-denatured BSA (extended conformation) could be interacting with native and/or heat-denatured protein in the bulk solution forming different species that delay protein diffusion to the oil phase. Additionally, heat-denatured protein could simply act as a physical barrier hindering the native protein to freely attach to the interface. Another explanation for the delay in the multilayer formation is that heat-denatured protein may be less flexible than native protein [116,213]. For that reason, heat-denatured protein requires more time than native protein to orientate and adapt its hydrophobic groups towards the oil phase so that it is less likely to remain at the interface. During the multilayer formation, protein flexibility could affect the capacity of proteins to relax, spread and rearrange their molecular structure in the oil-water interface where the adsorbed proteins may orient their structure in more than one conformation [116].

Protein adsorption to the oil-water interface was investigated at the same total protein concentration for native BSA alone (0.47 and 0.27 mM) and binary mixtures of native and heat-denatured BSA (0.47 mM and 0.27 mM) (**Figure 4.7(A) and (B)**). Those experiments were conducted to confirm that the delay in multilayer formation in the presence of heat-denatured protein was not a consequence of the difference in total protein concentration. The binary mixtures containing denatured BSA suggested that the delay in multilayer formation was a consequence of heat-denatured BSA rather than the small increase in total protein concentration, which was shown to have an opposite effect (i.e. native BSA alone 0.47 and 0.27 mM showed a faster kinetic of protein adsorption to the oil-water interface than for binary mixtures of native and heat denatured BSA at the same total protein concentration (0.47 and 0.27 mM)). Rheology results showed that the method was sensitive to detect small increases in protein concentration (i.e. from 0.4 mM to 0.47 mM and 0.2 mM to 0.27 mM) as well as the presence of small amounts of heat-denatured BSA in the bulk solution (0.07 mM). In contrast, the drop in the IFT was more pronounced for proteins with higher protein concentration independently of the presence of heat-denatured protein in the binary mixtures (**Figure 4.9(A) and (B)**). This result was in agreement with previous reports of concentration dependencies [93,218] where an increase in protein concentration (i.e. BSA from 0.15 to 1.06 mM and lysozyme from 0.03 to 1.38 mM) resulted in an increase in the rate of protein adsorption to the oil-water interface [93,101,200]. Results obtained from the IFT measurements

could mean that the tensiometer is a less specific method than interfacial rheology to detect changes in protein concentration and the presence of heat-denatured protein on protein adsorption.

IFT measurements were started as soon as the drop between aqueous and oil phase was formed. The IFT of water and coconut oil (medium chain triglycerol)) was 18.0 ± 1.3 mN/m whereas the initial IFT for protein solutions in the oil-water interface was around 9-11 mN/m (**Figure 4.9(A))**. The difference in the initial values of IFT may be explained because regimen I or induction is too fast and can be only studied at very low concentration of proteins [95], so that there is some uncertainty around t=0 (IFT_0). Additionally, the difference in the initial IFT values must represent that protein is interacting with the oil at the interface so, this IFT value may not be caused by the presence of impurities in the oil phase which was used as received.

The strength and the solid-like properties of the multilayer interfacial film were investigated using strain amplitude-sweep and frequency-sweep measurements after two hours of protein adsorption. Strain amplitude-sweep experiments (**Figure 4.8**) suggest that the strength of the multilayer is an intrinsic characteristic of the protein itself which depends on protein concentration. The presence of heat-denatured protein in the bulk solution did not affect the strength of the multilayer because a similar oscillation torque was needed to disrupt the multilayer of all these solutions. From the frequency-sweep measurements it seems that the native, globular protein interacts with surrounded protein molecules and molecules of oil at the interface to produce an interfacial film where protein molecules are close to each other forming a tight film. This produces a film where the entire oil surface is densely covered giving a higher power law exponent (n) value. In contrast, the presence of heat-denatured protein could produce a softer, less densely packed film (**Table 4.1**).

In these experiments, the adsorption of BSA to the oil-water interface seems to result in an irreversible process where no desorption of the protein was observed under the experimental conditions. This is in agreement with Jeyachandran, *et al*. (2009) which found that BSA adsorbs to hydrophobic surfaces within 2 hours and that the adsorbed BSA remains at the interface for up to 12 hours. Desorption of BSA from the hydrophobic surface was only observed when this surface was washed with solutions of sodium dodecil sulfate 0.1 M or NaCl 1 M [219] The presence of heat-denatured protein in the binary mixtures did not induce

detachment of the adsorbed protein as indicated by constant magnitude of G' and G" moduli for two hours (**Figure 4.6(A) and (B)**) as well as constant values obtained from IFT measurements for one hour (**Figure 4.9(A)**). The presence of heat-denatured protein in the bulk solution had a significant effect on the first steps of protein adsorption to the oil-water interface as was determined by the rheology and interfacial tension methods. The presence of heat-denatured protein in the bulk solution significantly delayed the time to cross-over between G' and G" moduli ($P = 0.029$) but gave a similar magnitude of maximum G" moduli in comparison with native protein alone ($P > 0.1$). After two hours of protein adsorption, the film formed at the interface showed a more solid-like behaviour for native BSA alone than for native solutions in the presence of heat-denatured BSA ($P = 0.086$). The value of IFT_{30} was considerably reduced in the presence of heat-denatured protein in comparison with native BSA alone ($P = 0.042$). However, the influence of heat-denatured BSA in the value of the solid-like behaviour, oscillation torque for G" modulus and the value of IFT_{30} were more significant for BSA protein at the lowest concentration (i.e. 0.2 mM) (**Appendix C and D**).

In this thesis, the liquid-liquid interface was formed using oil and water because these two components have a different polarity which may form a stable interface in a short period of time. Additionally, oil-water was used to simulate an emulsion state that many proteins are exposed in some stage. Coconut oil was used by Baldursdottir *et al*. (2010) and Baldursdottir *et al*. (2011) to investigate the protein adsorption to the oil-water interface (i.e. BSA, insulin and lyzozyme). From those works, a stable interface was formed between the coconut oil and the water phase giving information of protein adsorption to the oil-water interface within two hours [93,101].

Statistical differences between type of protein and BSA concentration was assessed using the Friedman's test, which is the non-parametric equivalent of the repeated measures ANOVA. The Friedman's test was chosen because the low number of repetitions used in these experiments. Additionally, the response variables did not presented a normal distribution, violating one of the core assumptions of the ANOVA test. However, the use of a non-parametric test has the disadvantage of a reduced statistical power, in comparison to parametric tests. For this reason, a difference was declared as significant at a P - value ≤ 0.10. Moreover, post-hoc comparison analysis for the Friedman's test is characterized for an even lower statistical power [220]. Therefore, comparison between groups (combinations of type of

protein and BSA concentration) was conducted through visual inspection of box-plots (**Appendix C and D**).

Despite the low number of repetition used and the low power of the Friedman's test, significant differences were observed between BSA concentration and type of protein (i.e. native protein alone and binary mixtures of native BSA (0.4 mM and 0.2 mM) and heat-denatured BSA solutions (0.07 mM)) for the cross-over time, G' modulus, oscillation torque (G" modulus), the power law exponent (i.e. interfacial rheology measurements), IFT_{30} and initial slope (i.e. IFT measurements).

4.5. Conclusions

The combination of rheology and surface tension determination was shown to be sensitive for the characterization of protein adsorption at the oil-water interface. The information obtained from these methods (i.e. kinetics of protein diffusion, monolayer and multilayer formation) and the data analysis of these results (i.e. time to cross-over, G' and G" moduli, strength and solid-like properties of the viscoelastic film and drop in the IFT measurements) was useful to investigate the oil-water interfacial adsorption of native and heat-denatured protein and to examine how introduction of a small amount of heat-denatured protein affects the rate and extent of the adsorption of a native protein to the oil-water interface. The combination of protein characteristics affecting protein adsorption (i.e. stability of the native structure, hydrophobicity, flexibility, size, concentration and charge) contributed to understand the molecular interaction between native and heat-denatured proteins in the bulk solution and to explain the initial mechanism influencing their adsorption to the oil-water interface. These results showed that the presence of heat-denatured protein in the bulk solution affected the first steps of protein adsorption which was characterized by a delay in the multilayer formation at the different protein concentrations used in this work.

Chapter 5: Investigation of effects of selected excipient types (salt, phospholipid and polymer) on BSA interfacial adsorption

5.1. Introduction

In protein formulations, the most important groups of excipients are those that can impart improved stability to the protein native structure and/or reduce protein surface adsorption [221,222]. Sodium chloride is commonly used in protein drug formulations because it does not induce chemical degradation of proteins [24] and it is useful to reduce electrostatic interaction by changing the ionic strength of the solvent [39,112,223]. Phospholipids and polymers are useful as stabilizers of protein emulsions reducing the adsorption of proteins to interfaces [94,224,225].

Protein interfacial adsorption as a multilayer is often considered an irreversible process [226,227]. This is the case of BSA protein [226,227] and β-casein which shown an irreversible adsorption to liquid interfaces [227]. Fainerman *et al*. (2006) suggested that protein adsorption to interfaces is thermodynamically a reversible process but the reversibility of high molecular weight protein adsorption (i.e. BSA) is very slow, often taking many days [227]. Therefore, protein adsorption to interfaces could be considered as a practically irreversible process which is reported to be influenced by time, protein properties and protein concentration [92,102]. However, the presence of excipients (i.e. salts, polymers and surfactants) may affect protein adsorption within dosage forms [222,228] through mechanisms that affect protein adsorption or desorption from the interface [89,92].

The adsorption of proteins to interfaces in the presence of excipients is explained by the combination of two mechanisms: 1) the formation of a complex between protein molecules and excipients in the bulk solution and the competitive adsorption of these complexes and free molecules of excipients at the interface [228], 2) protein and excipient molecules adsorb sequentially or simultaneously to the oil-water interface forming a protein-excipient complex [115,229,230] which has a different surface activity than the protein alone [228]. In these two mechanisms, the complex is stabilised by ionic and/or hydrophobic forces [228,230] and conformational changes may result in the protein [229,230]. Excipients and proteins interacting through ionic forces form hydrophobic complexes which are more surface active than protein alone. In contrast, excipients and proteins interacting by hydrophobic forces form hydrophilic

complexes which are less surface active than protein alone [228]. Excipients and proteins that adsorb simultaneously to the interface may form the complex in the bulk solution or near the interface whereas excipients and proteins that adsorb sequentially to the interface form the complex at the interface [229,230]. If the protein and excipient form a complex in the bulk phase then adsorption to the interface may be changed through mechanisms of decreased free concentration or reduced adsorption potential of the complex formed. Complex formation could also occur at the interface, as protein and excipient molecules are forced closer together. Additionally, free excipient molecules remaining near the interface may compete with proteins to reach the interface [108]. This competition is influenced by native protein conformation, type of surfactant (i.e. ionic, non-ionic, oil- or water-soluble), nature of the interface (i.e. oil-water or air-water), concentration of proteins and excipients in the bulk solution, characteristics of the bulk phase (i.e. pH and ionic strength) [230], surface activity and the nature of the interaction between protein and excipients [39].

Desorption of proteins from interfaces depends on the mechanism used by proteins and excipients to form the complex at the interface [229]. Mechanisms such as the orogenic displacement, complexation and competitive adsorption are thought to be responsible for desorption of proteins from the interface [108,228,229]. Orogenic displacement is an alternative mechanism to the sequential adsorption of proteins [229]. In the orogenic displacement the adsorbed protein is displaced from the interface over time by a more surface active excipient such as a surfactant [108]. Surfactant adsorbs to the protein network and the number of adsorbed excipient molecules grows which compresses the already adsorbed protein molecules, increasing the surface pressure. After that, the protein network is broken and proteins are detached from the interface making sites in the interface available for adsorption of excipients [228,231-233]. As a consequence of that, protein is removed from the interface to the bulk solution [108,229,231-233]. Norde and Giaconelli (2000) have reported that desorption of protein from an interface results in appearance of protein aggregates in the bulk solution [92]. For simultaneous adsorption, complexes and free excipient molecules adsorb to the interface by competitive adsorption so that orogenic displacement does not apply [229].

Interfacial shear rheology has been used to investigate competitive adsorption between proteins and excipients giving information about structure of the interfacial film [108,228]. However, oscillation shear rheology does not give quantitative information of protein adsorption to interfaces [228,234]. Rheology measurements have shown that the adsorption of

protein in the presence of excipients is initially characterized by an increased in the magnitude of elasticity and viscosity in comparison with protein molecules alone [108,235]. Then, excipients that are adsorbed sequentially reach the interface to replace the adsorbed protein which is characterized by decreased G' and G" moduli [108] in several orders of magnitude [236].

The pendant drop technique has also been applied to measure the interfacial tension to investigate protein adsorption and desorption from interfaces. The kinetics of protein desorption from interfaces using IFT measurements was characterized by an increase in the value of the IFT after washing off the bulk solution [227,228]. Fainerman *et al*. (2006) reported an increase in the value of IFT of around 10 mN/m for protein desorption [227].

The combination of interfacial rheology and interfacial tension methods appear suitable to investigate protein adsorption to the oil-water interface in simple formulations. These techniques may have a potential application to investigate protein adsorption to interfaces in more complex proteins formulations. The aim of this Chapter was to assess the use of these techniques to examine how introduction of three groups of excipients (NaCl, phospholipids and polymers) affects the kinetics and/or mechanism of adsorption of native protein to the oil-water interface. Additionally, FTIR spectroscopy was used to investigate protein physical stability of the protein in the bulk solution at the equilibrium, as a consequence of the presence of these excipients in the oil-water interface.

5.2. Materials and methods

5.2.1. Materials

BSA was obtained from Sigma-Aldrich, USA (A-7906, 98%). Phosphate buffer (pH 7.4, ionic strength 0.05 M) was prepared by mixing 11.2 ml of KH_2PO_4 (1 M) and 38.8 ml K_2HPO_4 (1 M) and diluting to one liter with distilled water. The oil phase was composed of coconut oil (medium chain triglycerol donated by H. Lundbeck A/S, Denmark) and was used as received. Sodium chloride (NaCl) was obtained from Sigma-Aldrich, USA (7647-14-5). Dipalmitoylphosphatidylcholine (DPPC), distearoylphosphatidylcholine (DSPC) and 1,2-distearoyl-sn-glycero-3-phosphoglycerol, sodium salt (DSPG-Na) phospholipids were obtained from Lipoid GmbH, Germany. Poly(N,N-dimethylaminoethyl methacrylate)

(PDMAEMA) and PDMAEMA-PBuA$_{38700}$-PDMAEMA$_{33000}$ (PBuA) polymers were provided by the Laboratory of Polymer Chemistry, University of Helsinki, Finland and used as received.

5.2.2. Preparation of native BSA solutions (0.5 mM)

BSA was dissolved in phosphate buffer (pH 7.4, ionic strength 0.05 M) to give solutions of native BSA at 0.5 mM (aqueous phase). All solutions were prepared in triplicate.

5.2.3. Preparation of native BSA solutions (0.5 mM) in the presence of NaCl (0.1 M, 0.5 M and 1 M)

NaCl was dissolved in phosphate buffer (pH 7.4, ionic strength 0.05 M) at 0.1, 0.5 and 1 M. These solutions were used to dissolve native BSA (0.5 mM) in order to study the adsorption of native BSA to the oil-water interface in the presence of NaCl at different concentrations. All solutions were prepared in triplicate.

5.2.4. Preparation of native BSA solutions (0.5 mM) (aqueous phase) and phospholipids (DPPC, DSPC and DSPG-Na) (oil phase)

Phospholipids (i.e. DPPC, DSPC and DSPG-Na) were dissolved in the oil phase to prepare 10 mL of each phospholipid at 0.01% w/v (stock solution). The oil phase was composed of coconut oil (medium chain triglyceride) and was used as received. Aliquots of stock solutions were taken to prepare 25 mL of the oil phase containing DPPC ($1x10^{-4}$ % w/v DPPC/coconut oil, $5x10^{-4}$ % w/v DPPC/coconut oil and $1x10^{-3}$ % w/v DPPC/coconut oil), DSPC ($1x10^{-2}$ % w/v DSPC/coconut oil and $1x10^{-3}$ % w/v DSPC/coconut oil) and DSPG-Na ($5x10^{-3}$ % w/v DSPG-Na/coconut oil and $1x10^{-3}$ % w/v DSPG-Na/coconut oil). Then, these solutions were used to study the adsorption of native BSA to the oil-water interface in the presence of phospholipids. The aqueous phase was composed of native BSA (0.5 mM) dissolved in phosphate buffer (pH 7.4, ionic strength 0.05 M). All solutions were prepared in triplicate. The structure of DPPC, DSPC and DSPG-Na phospholipids are shown in **Figure 5.1**.

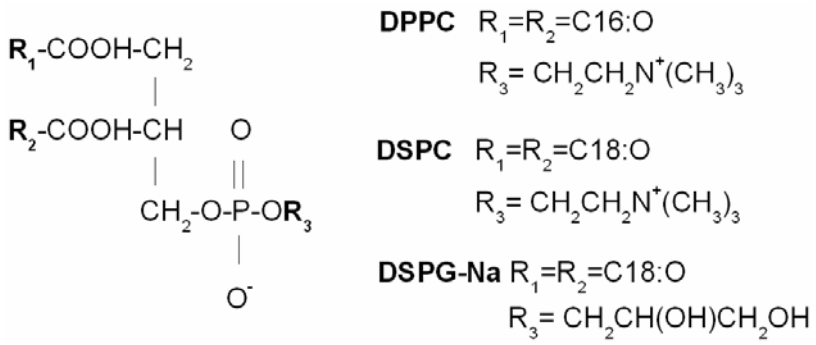

Figure 5.1 Chemical structure of phospholipids: DPPC, DSPC and DSPG-Na.

5.2.5. Preparation of native BSA solutions (0.5 mM) in the presence of PDMAEMA and PBuA polymers (aqueous phase)

PDMAEMA and PBuA polymers were used to investigate their influence in protein adsorption to interfaces (**Figure 5.2(A) and (B)**). PDMAEMA is a linear homo polymer with a molecular weight (Mn) of 93400 (g/mol), polydispersity index (PDI) of 1.5, water soluble and positively charged due the protonation of the amine groups [237]. PBuA is a linear block polymer composed on PDMAEMA groups at each side of the chain plus a poly butyl acetate group at the center which increases the hydrophobicity of this polymer. PBuA has a molecular weight (Mn) of 107300 (g/mol) and PDI of 1.28 [238].

PDMAEMA and PBuA polymers were dissolved or suspended in the aqueous phase at 8.75×10^{-3} % w/v. PDMAEMA was dissolved completely in the aqueous phase whereas PBuA, which is practically insoluble in water, was suspended in the aqueous phase. Native BSA (0.5 mM) was dissolved in each polymeric sample prior to the measurements. The oil phase was composed of coconut oil (medium chain triglyceride) and was used as received. All samples were prepared in triplicate.

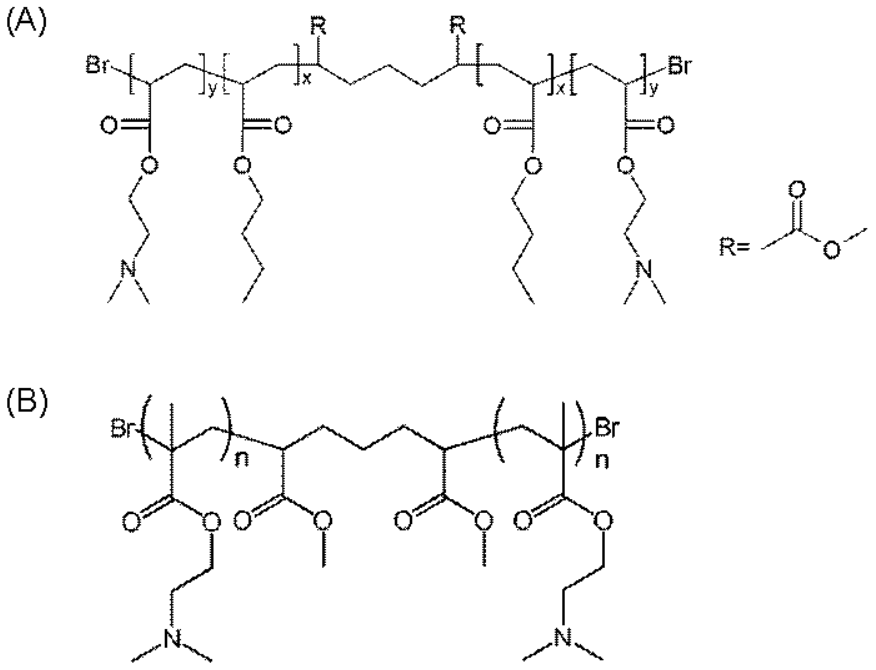

Figure 5.2 Chemical structure of polymers: (A) PBuA and (B) PDMAEMA.

5.2.6. Interfacial rheology measurements using a double wall-ring (DWR) geometry

Rheology studies were conducted using a TA AR-G2 rheometer (TA-Instruments, Waters, New Castle, USA) with DWR geometry using a method previously described by Baldursdottir *et al*. (2011) [101]. The equipment and method was previously described in **Chapter 4 (Section 4.2.2.)**. Rheology experiments were conducted in triplicate for each sample.

Time-sweep, frequency-sweep and strain amplitude-sweep steps were used to investigate and compare the kinetics of protein adsorption, frequency dependency and strength of the resultant viscoelastic multilayer as was measured as described in **Chapter 4 (Section 4.2.3.)**. Additionally, complex viscosity (η^* in Ns/m) over time was used to investigate viscosity properties of the interfacial film in the presence of excipients. The value of complex viscosity at two hours was used to compare the different samples.

5.2.7. Interfacial tension measurements using a pendant drop tensiometer

Interfacial tension (IFT) measurements were performed using a pendant drop instrument (KRÜSS, Hamburg, Germany) as previously described by Baldursdottir *et al*. (2010) [93]. The method and equipment were described in **Chapter 4 (Section 4.2.4.)**. IFT measurements were conducted in triplicate for each sample. The decrease in the IFT was studied to compare the kinetic of protein adsorption to the oil-water interface of native BSA alone and native BSA in the presence of NaCl, phospholipids and polymers for one hour and then, the initial slope (over the first three minutes) and IFT_{30} were calculated as was described in **Chapter 4 (Section 4.2.5)**.

5.2.8. Statistical analysis

One-way ANOVA was used to assess statistical differences between native protein alone and native protein in the presence of excipients: salt (NaCl (0.1 M, 0.5 M and 1 M)), phospholipids (DPPC ($1x10^{-3}$ % w/v), DSPC ($1x10^{-2}$ % w/v) and DSPG-Na ($5x10^{-3}$ % w/v)), and polymers (PDMAEMA and PBuA ($8.75x10^{-3}$ % w/v). Post-hoc Tukey's test analysis for multiple comparisons of means were calculated for protein solutions showing significant differences ($P < 0.05$). The parameters analysed were G' and G" moduli, time to cross-over, complex viscosity, the power law exponent for rheology studies, initial slope (over the first three minutes), and the decrease in the IFT_{30} for IFT measurements. Statistical analysis was conducted using R software version 2.15.2 (R Foundation for Statistical Computing, Vienna, Austria).

5.2.9. FTIR spectroscopy

FTIR spectroscopy was used to investigate secondary structure of proteins in the bulk solution after two hours of protein adsorption to the oil-water interface. FTIR spectra were acquired using a Bomen IR-spectrometer (Bomen, Canada). Samples of 12 µL were measured using a CaF_2 transmission windows from BioCell™ (Jupiter, Florida, USA) with six µm path length and five cm diameter. A total of 16 scans were collected with a resolution of 4 cm^{-1}. The sample chamber was constantly purged with dry air (pure gas generator from Whatman). Samples for spectroscopy analysis were aliquots of the aqueous phase (100 µL) taken from the bulk solution of the rheometer (Delrin® trough) at t = 0 and after two hours of protein adsorption to the oil-water interface.

Water (3500 and about 1640 cm^{-1}), and remaining water vapor (2200 cm^{-1}) signals were subtracted from the original spectra to obtain a flat line between 2000 and 1850 cm^{-1} [137,138]. Spectra were pre-processed by using the 2ndD (Savitzky-Golay with 11 points smoothing), BC and AN study physical stability of proteins in the aqueous phase [73,137]. The principal bands used to investigate protein physical stability are α-helix around 1654 cm^{-1} and intermolecular β-sheet around 1610-1620 cm^{-1} [48,65]. Pre-processing was conducted using a combination of software including The Unscrambler®X (2ndD, CAMO Software, Oslo Norway Version 10.1) and Origin®Pro (BC and AN, Origin Lab Corp. Version 8.5).

5.3. Results

5.3.1. Rheometer studies: Investigating the interfacial rheology of proteins in the presence of excipients

5.3.1.1. Rheology studies of native BSA alone (0.5 mM)

Native BSA alone (0.5 mM) formed a viscoelastic film at the oil-water interface showing the time to cross-over at 4 ± 2 min and constant G' (27 ± 2 mN/m) and G" (10 ± 1 mN/m) moduli at two hours (**Figure 5.3(A)**). The power law exponent of protein adsorption for native BSA alone was -0.812 ± 0.010 (**Appendix E**) and the complex viscosity increased until a maximum within the first hour and remained stable from one to two hours of protein adsorption. The value of complex viscosity at two hours was 45 ± 3 mNs/m (**Figure 5.3(B)**). Strain amplitude-sweep experiments (**Figure 5.3(C)**) show the oscillation torque at which the multilayer was disrupted. In the case of native BSA alone (0.5 mM) the oscillation torque mean values for G' and G" were 6 ± 1 mNm and 7 ± 1 mNm, respectively. After one hour, the magnitude of G' and G" moduli and complex viscosity for solutions containing phosphate buffer (without protein) (pH 7.4) and oil phase (without excipients) was less than $1x10^{-4}$ N/m.

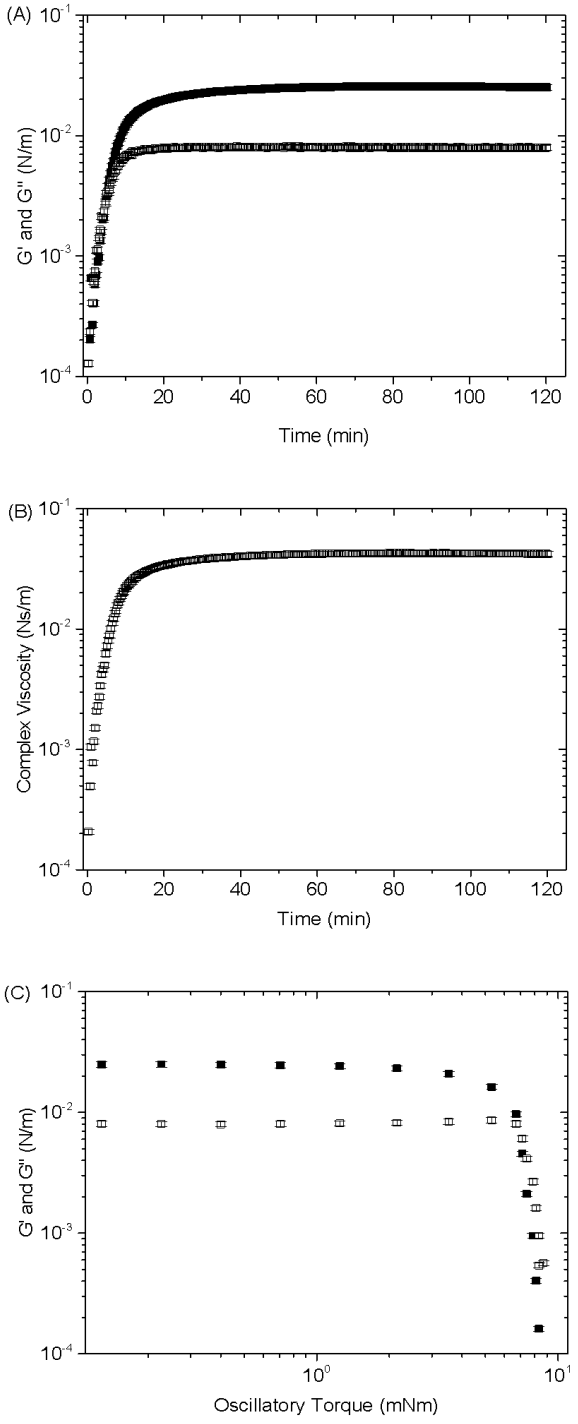

Figure 5.3 Native BSA alone (0.5 mM) (square) at the oil-water interface. (A) Elastic G' (CV = 31.1 %) (solid symbols,■) and viscous G" (CV = 26.8 %) (open symbols,□) moduli and (B) complex viscosity (open symbols,□) (CV = 27.4 %) as a function of time. (C) Elastic G' (solid symbols,■) and viscous G" (open symbols,□) moduli as a function of the oscillation torque applied to the oil-water interface after two hours of adding protein (CV (G') = 12.1% and (G") = 10.6 %). The sharp reduction in the modulus indicates film breakage. G' and G" moduli are in logarithmic scale.

5.3.1.2. Effect of NaCl (0.1 M, 0.5 M and 1 M) on the oil-water interfacial rheology measurements of native BSA (0.5 mM)

Native BSA (0.5 mM) dissolved in the presence of NaCl (0.1 M, 0.5 M and 1 M) adsorbed to the oil-water interface forming a stable interfacial film with constant G' and G" moduli within two hours. However, the effect of NaCl on protein adsorption was concentration dependent. NaCl at concentrations of 0.1 M and 0.5 M increased BSA adsorption to the oil-water interface giving values of G' and G" moduli of 35 ± 20 mN/m and 90 ± 2 mN/m (0.1 M) and 25 ± 6 mN/m and 10 ± 0.2 mN/m (0.5 M) respectively. Native BSA in the presence of NaCl (1 M) showed reduced protein adsorption to the oil-water interface giving a lower value of G' (10 ± 1 mN/m) and G" (7 ± 0.5 mN/m) moduli than for native BSA alone (27 ± 2 mN/m) and 10 ± 1 mN/m respectively) (**Figure 5.4 and Table 5.1**). Statistical analysis showed that the changes in the G' and G" moduli for native BSA in the presence of NaCl (0.1 M, 0.5 M and 1 M) were significant as determined by one-way ANOVA ($P < 0.05$). However, the increase in G' and G" moduli for native BSA alone and native BSA in the presence of NaCl (0.1 M) were only significantly different for the G' modulus as shown by the Tukey's post-hoc test ($P < 0.01$). The maximum values of G' and G" moduli between native BSA alone and native BSA in the presence of NaCl (0.5 M) were not significantly different as shown the Tukey's test analysis ($P > 0.05$). The reduction in G' and G" moduli between native BSA alone and native BSA in the presence of NaCl (1 M) were significantly different as shown by the Tukey's post-hoc test ($P < 0.01$) (**Table 5.2**).

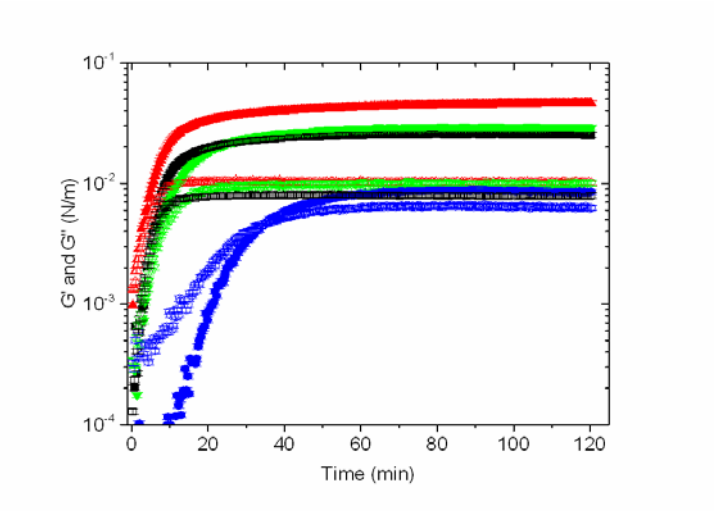

Figure 5.4 Elastic G' (solid symbols) and viscous G" (open symbols) moduli as a function of time. Native BSA alone (0.5 mM) (■) vs. native BSA (0.5 mM) dissolved in the presence of NaCl at 0.1 M (▲) (CV (G') = 45.7 % and (G") 19.5 %), 0.5 M (▼) (CV (G') = 32.7 % and (G") 22.2 %) and 1 M (●) (CV (G') = 53.1 % and (G") 42.3 %). G' and G" moduli are in logarithmic scale.

Table 5.1 Data analysis of rheology measurements for native BSA in the presence of NaCl (0.1 M, 0.5 M and 1 M). Rheology measurements correspond to data analysis of time sweep measurements (time to cross-over, elastic (G') and viscous (G") moduli and complex viscosity) and frequency sweep measurements (power law exponent, n). (mean ± s.d., n=3).

Native BSA (0.5 mM) + Excipients	Time to cross-over (min)	Maximum (N/m) (x1000) Elastic modulus (G')	Maximum (N/m) (x1000) Viscous modulus (G")	Complex dynamic viscosity (Ns/m) (x1000)	Power law exponent* (n)
Native BSA alone	4 ± 2	27 ± 2	10 ± 1	45 ± 3	-0.812 ± 0.010
Native BSA + NaCl (0.1 M)	3 ± 2	35 ± 20	90 ± 2	58 ± 32	-0.813 ± 0.120
Native BSA + NaCl (0.5 M)	6 ± 1	25 ± 6	1 ± 0.2	16 ± 4	-0.718 ± 0.100
Native BSA + NaCl (1.0 M)	29 ± 6	10 ± 1	7 ± 0.5	19 ± 2	-0.620 ± 0.020

(*) power law exponent (n) close to one means the final film has a more solid-like property.

Table 5.2 Tukey's test analysis for native BSA alone (0.5 mM) vs. native BSA (0.5 mM) in the presence of NaCl at 0.1 M, 0.5 M and 1 M. Tukey's test analysis was performed for solutions showing significant differences in the one-way ANOVA test ($P < 0.05$).

	Native BSA alone vs. Native BSA + NaCl (0.1 M)	Native BSA alone vs. Native BSA + NaCl (0.5 M)	Native BSA alone vs. Native BSA + NaCl (1 M)	Native BSA + NaCl (0.1 M) vs. Native BSA + NaCl (0.5 M)	Native BSA + NaCl (0.1 M) vs. Native BSA + NaCl (1 M)	Native BSA + NaCl (0.5 M) vs. Native BSA + NaCl (1 M)
Time to cross-over (min)	P>0.05	P>0.05	P<0.001	P>0.05	P<0.001	P<0.001
Elastic modulus G' (N/m)	P<0.001	P>0.05	P<0.001	P<0.001	P<0.001	P<0.01
Viscous modulus G" (N/m)	P>0.05	P>0.05	P<0.01	P>0.05	P<0.01	P<0.05
Power law exponent	P>0.05	P>0.05	P>0.05	P>0.05	P>0.05	P>0.05
Oscillation torque (mNm)	P<0.005 (G') P<0.05 (G")	P>0.05 (G') P>0.05 (G")	P<0.005 (G') P<0.005 (G")	P<0.005 (G') P<0.05 (G")	P<0.001 (G') P<0.001 (G")	P<0.005 (G') P<0.005 (G")

The time to cross-over between G' and G" moduli was shorter for native BSA in the presence of NaCl (0.1 M) than for native BSA alone giving values of 3 ± 2 min and 4 ± 2 min respectively. In the presence of NaCl (0.5 M and 1 M) the time to cross-over were 6 ± 1 min and 29 ± 6 min, respectively (**Table 5.1**). Statistical analysis showed that the time to cross-over for native BSA alone and native BSA in the presence of NaCl (0.1 M, 0.5 M and 1 M) was significant differently as determined by one-way ANOVA ($P < 0.05$). However, the increase in the time of cross-over between native BSA alone and native BSA in the presence of NaCl (0.1 M and 0.5 M) were not significantly different as shown the Tukey's post-hoc test ($P > 0.05$). The increase in time of cross-over between native BSA alone and native BSA in the presence of NaCl (1 M) was significantly different as shown by the Tukey's post-hoc test ($P < 0.001$) (**Table 5.2**).

The complex viscosity for native BSA in the presence of NaCl (0.1 M) reached a maximum value of 58 ± 30 mNs/m which was achieved faster than for native BSA alone (**Figure 5.5**

and Table 5.1). The complex viscosity of native BSA in the presence of NaCl (0.5 M and 1 M) were 16 ± 4 mNs/m and 19 ± 2 mNs/m respectively (**Figure 5.5 and Table 5.1**). Statistical analysis showed that the magnitude of complex viscosity between native BSA alone and native BSA in the presence of NaCl (0.1 M, 0.5 M and 1 M) were not significantly different as determined by one-way ANOVA ($P > 0.05$).

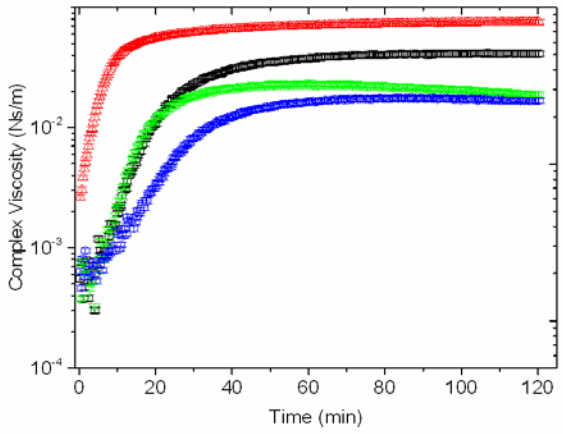

Figure 5.5 Complex viscosity as a function of time. Native BSA alone (0.5 mM) (□) vs. native BSA (0.5 mM) dissolved in the presence of NaCl at 0.1 M (△) (CV = 88.8 %), 0.5 M (▽) (CV = 40.3 %) and 1 M (○) (CV = 48.4 %). Complex viscosity is in logarithmic scale.

The interfacial film formed between the oil phase and the native BSA in the presence of NaCl (0.1 M) showed a similar power law exponent (- 0.813 ± 0.120) than for native BSA alone (- 0.812 ± 0.010). The values of the power law exponent were decreased in the presence of NaCl (0.5 M and 1 M) to - 0.718 ± 0.100 and - 0.620 ± 0.020, respectively (**Table 5.1**). Post-hoc comparisons (pair by pair), using Tukey's test, did not render any significant power law exponent differences ($P > 0.05$) between pairs of native BSA alone and native BSA in the presence of NaCl (0.1 M, 0.5 M or 1 M) (**Table 5.2**).

Strain amplitude-sweep experiments (**Figure 5.6**) showed the oscillation torque at which the interfacial film was disrupted for native BSA in the presence of NaCl at 0.1 M, 0.5 M and 1 M were G' (10 ± 0.3 mNm) and G" (10 ± 0.4 mNm) (0.1 M), G' (7 ± 1 mNm) and G" (7 ± 1 mNm) (0.5 M) and G' (3 ± 0.4 mNm) and G" (4 ± 0.4 mNm) (1 M). Statistical analysis showed that the strain amplitude-sweep experiments for native BSA alone and native BSA in the presence of NaCl (0.1 M, 0.5 M and 1 M) was significantly different as determined by

one-way ANOVA test ($P < 0.001$). The oscillatory torque at which the film was disrupted was significantly different for G' and G" moduli for all the protein solutions with the exception of native BSA alone vs. native BSA in the presence of NaCl (0.5 M) ($P > 0.05$) as shown by Tukey's test analysis for G' and G" moduli (**Table 5.2**).

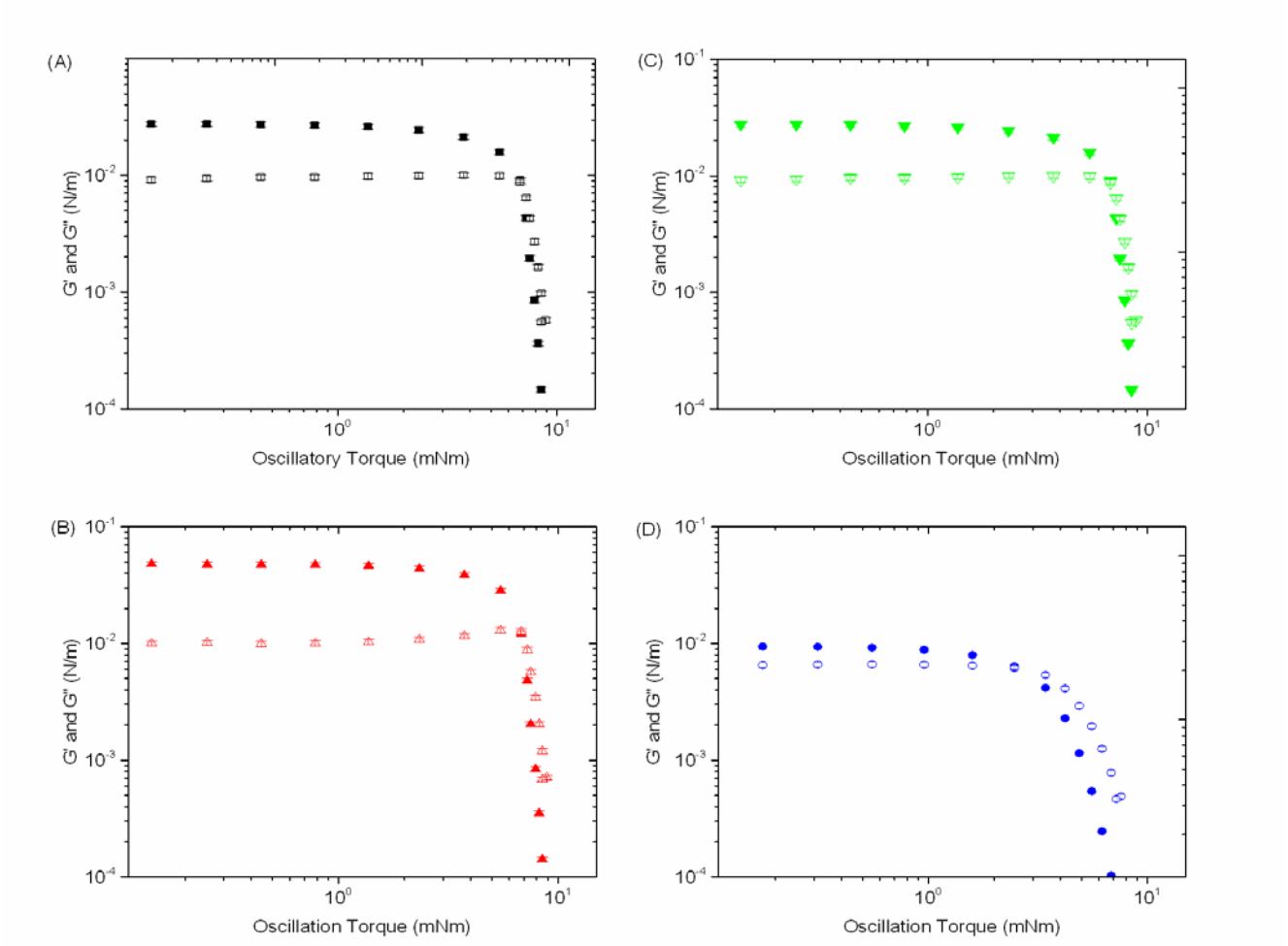

Figure 5.6 Elastic G' (solid symbols) and viscous G" (open symbols) moduli as a function of the oscillation torque applied to the oil-water interface after two hours of adding protein. The reduction in G' and G" moduli indicates film breakage. (A) Native BSA alone (0.5 mM) (■) vs. native BSA (0.5 mM) dissolved in the presence of NaCl at (B) 0.1 M (▲) (CV (G') = 3.6 % and (G") 4.7 %), (C) 0.5 M (▼) (CV (G') = 12.1 % and (G") 10.6 %) and (D) 1 M (●) (CV (G') = 10.4 % and (G") 8.9 %). G' and G" moduli and oscillation torque are in logarithmic scale.

5.3.1.3. Effect of phospholipids on the oil-water interfacial rheology measurements of native BSA (0.5 mM)

The interfacial adsorption of native BSA (0.5 mM) in the presence of DPPC initially showed an increase in G' and G" moduli until a maximum value was reached which was similar to that of native BSA alone (**Figure 5.7**). The initial increase in the G' and G" moduli was followed by a progressive decrease in G' and G" moduli from 1 x10^{-2} N/m to 1 x10^{-4} N/m for the highest concentration of DPPC. The final magnitude of G' and G" moduli did not increase again within the two hours.

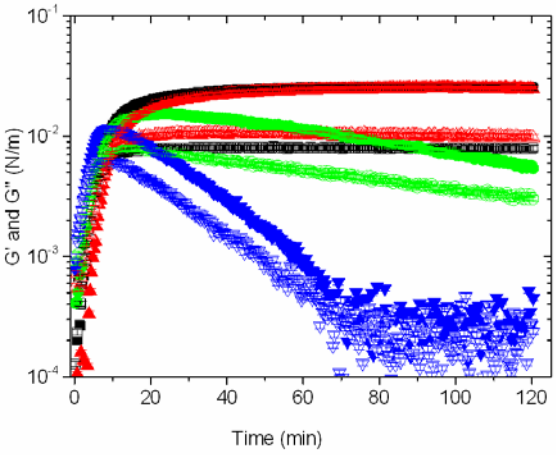

Figure 5.7 Elastic G' (solid symbols) and viscous G" (open symbols) moduli for native BSA alone (0.5 mM) (■) vs. native BSA (0.5 mM) in the presence of DPPC at different concentrations at the oil-water interface: 1x10^{-4} % w/v (▲) (CV (G') = 49.8 % and (G") 31.2 %), 5x10^{-4} % w/v (●) (CV (G') = 175 % and (G") 172 %) and 1x10^{-3} % w/v (▼) (CV (G') = 145 % and (G") 131 %). G' and G" moduli are in logarithmic scale.

The decrease in the G' and G" moduli for native BSA in the presence of DPPC was concentration dependent with a faster decrease observed for native BSA in the presence of higher concentrations of DPPC (5x10^{-4} % w/v and 1x10^{-3} % w/v) than for native BSA in the presence of DPPC at 1x10^{-4} % w/v (**Figure 5.7**). There was no evidence of protein desorption from the interface at the lowest concentration of DPPC (1x10^{-4} % w/v) and the magnitude of G' (20 ± 10 mN/m) and G" (8 ± 2 mN/m) moduli (**Table 5.3**) remained constant for two hours showing a similar behavior to that of native BSA alone (**Figures 5.7**). Statistical analysis showed that the G' moduli for native BSA alone and native BSA in the presence of DPPC (1x10^{-4} % w/v) were not significantly different as described by one-way ANOVA ($P > 0.05$). The value of G" modulus for native BSA alone and native BSA in the presence of DPPC

($1x10^{-4}$ % w/v) was significantly different as determined by one-way ANOVA test ($P < 0.05$). However, the G" modulus was not significantly different for native BSA alone and native BSA in the presence of DPPC at $1x10^{-4}$ % w/v as shown by Tukey's post-hoc test ($P > 0.05$) (**Table 5.4**). Statistical analysis also showed that the G' moduli for native BSA alone and native BSA in the presence of DPPC at $5x10^{-4}$ % w/v were not significantly different as described by one-way ANOVA ($P > 0.05$). In contrast, the decrease in the G" modulus for native BSA alone and for native BSA in the presence of DPPC at $5x10^{-4}$ % w/v was significantly different as shown by Tukey's test analysis ($P < 0.05$) (**Table 5.4**). The magnitude of the G" modulus for native BSA in the presence of DPPC ($1x10^{-4}$ % w/v) and native BSA in the presence of DPPC ($5x10^{-4}$ % w/v) were not significantly as shown by the Tukey's post-hoc test ($P > 0.05$) (**Table 5.4**).

Table 5.3. Data analysis of rheology measurements for native BSA in the presence of phospholipids (DPPC ($1x10^{-4}$ % w/w, $5x10^{-4}$ % w/w and $1x10^{-3}$ % w/w), DSPC ($1x10^{-2}$ % w/w) and DSPG-Na ($5x10^{-3}$ % w/w)). Rheology measurements correspond to data analysis of time sweep measurements (time to cross-over, elastic (G') and viscous (G") moduli and complex viscosity) and frequency sweep measurements (power law exponent, n). (mean ± s.d., n=3).

Native BSA (0.5 mM) + Excipients	Time to cross-over (min)	Maximum (N/m) (x1000) Elastic modulus (G')	Viscous modulus (G")	Complex dynamic viscosity (Ns/m) (x1000)	Power law exponent* (n)
Native BSA alone	4 ± 2	27 ± 2	10 ± 1	45 ± 3	-0.812 ± 0.010
Native BSA + DPPC ($1x10^{-4}$ % w/w)	6 ± 4	20 ± 10	8 ± 2	34 ± 16	-0.738 ± 0.080
Native BSA + DPPC ($5x10^{-4}$ % w/w)	6 ± 1	10 ± 5	4 ± 2	18 ± 9	-0.740 ± 0.040
Native BSA + DPPC ($1x10^{-3}$ % w/w)	3 ± 1	< 1	< 1	< 1	n/a
Native BSA + DSPG-Na ($5x10^{-3}$ % w/w)	6 ± 2	< 1	< 1	< 1	n/a
Native BSA + DSPC ($1x10^{-2}$ % w/w)	3 ± 1	< 1	< 1	< 1	n/a

n/a: not applicable. (*) power law exponent (n) close to one means the final film has a more solid-like property).

Table 5.4 Tukey's test analysis for native BSA alone (0.5 mM) vs. native BSA (0.5 mM) in the presence of phospholipids (DPPC ($1x10^{-4}$ % w/w, $5x10^{-4}$ % w/w and $1x10^{-3}$ % w/w), DSPC ($1x10^{-2}$ % w/w) and DSPG-DSPG-Na ($5x10^{-3}$ % w/w)). Tukey's test analysis was performed for solutions showing significant differences in the one-way ANOVA test ($P < 0.05$).

	Native BSA alone vs. Native BSA + DPPC ($1x10^{-4}$ % w/w)	Native BSA alone vs. Native BSA + DPPC ($5x10^{-4}$ % w/w)	Native BSA alone vs. Native BSA + DPPC ($1x10^{-3}$ % w/w)	Native BSA + DPPC ($1x10^{-4}$ % w/w) vs. Native BSA + DPPC ($5x10^{-4}$ % w/w)	Native BSA + DPPC ($1x10^{-4}$ % w/w) vs. Native BSA + DPPC ($1x10^{-3}$ % w/w)	Native BSA + DPPC ($5x10^{-4}$ % w/w) vs. Native BSA + DPPC ($1x10^{-3}$ % w/w)
Viscous modulus (G") (N/m)	P>0.05	P<0.05	n/a	P>0.05	n/a	n/a
Complex viscosity (Ns/m)	P>0.05	P<0.05	n/a	P>0.05	n/a	n/a
Oscillation torque (mNm)	P>0.05 (G') P>0.05 (G")	P<0.05 (G') P<0.05 (G")	n/a	P>0.05 (G') P>0.05 (G")	n/a	n/a

G': elastic and G": viscous moduli. n/a: not applicable.

The maximum value of complex viscosity was achieved faster for native BSA in the presence of DPPC than for native BSA alone (**Figure 5.8**). After two hours, the complex viscosity for native BSA in the presence of DPPC at $5x10^{-4}$ % w/v (18 ± 9 mNs/m) and DPPC at $1x10^{-3}$ % w/v (1 ± 0.2 mNs/m) were lower than for native BSA alone (45 ± 3 mNs/m) (**Figure 5.8 and Table 5.3**). The decrease in the magnitude of the G' and G" moduli and the complex viscosity could represent desorption of protein from the oil-water interface and the loss of the multilayer film. Statistical analysis showed that the difference in the magnitude of complex viscosity between native protein alone and native protein in the presence of DPPC ($5x10^{-4}$ % w/v and $1x10^{-3}$ % w/v) was significant as determined by one-way ANOVA ($P < 0.05$). However, a post-hoc Tukey's test showed that the magnitude of complex viscosity was only significantly different between native protein alone and native protein in the presence of DPPC ($5x10^{-4}$ % w/v) ($P<0.05$) (**Table 5.3**). The magnitude of complex viscosity between native BSA in the presence of DPPC ($1x10^{-4}$ % w/v) and native BSA in the presence of DPPC ($5x10^{-4}$ % w/v) were not significantly different as shown by the Tukey's test ($P > 0.05$) (**Table 5.4**).

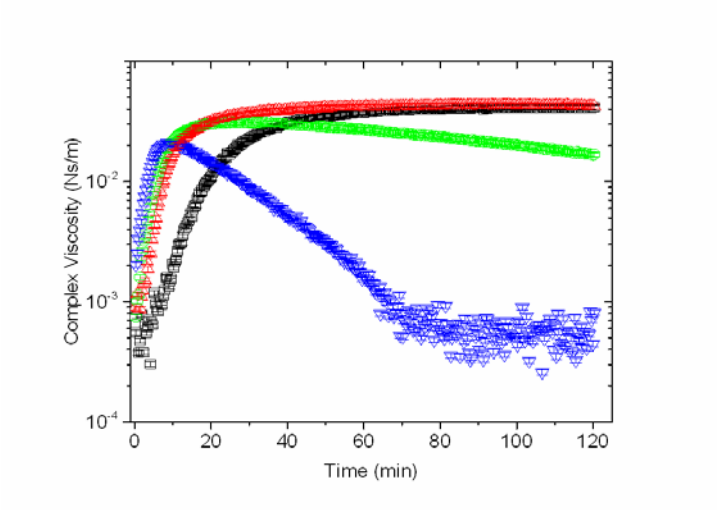

Figure 5.8 Complex viscosity (open symbols) as a function of time for native BSA alone (0.5 mM) (■) vs. native BSA (0.5 mM) in the presence of DPPC at different concentrations at the oil-water interface: $1x10^{-4}$ % w/v (▲) (CV = 46.1 %), $5x10^{-4}$ % w/v (●) (CV = 34.8 %) and $1x10^{-3}$ % w/v (▼) (CV = 130 %). Complex viscosity is in logarithmic scale.

The time to cross-over for native BSA in the presence of DPPC were 6 ± 4 min ($1x10^{-4}$ % w/v), 6 ± 1 min ($5x10^{-4}$ % w/v) and 3 ± 1 min ($1x10^{-3}$ % w/v) (**Table 5.3**). Statistical analysis showed that differences in time to cross-over between native protein alone and native protein in the presence of DPPC ($1x10^{-4}$ % w/v, $5x10^{-4}$ % w/v and $1x10^{-3}$ % w/v) were not significant as determined by one-way ANOVA ($P > 0.05$).

The frequency sweep measurements showed that the power law exponents for native BSA in the presence of DPPC at $1x10^{-4}$ % w/v and $5x10^{-4}$ % w/v were 0.738 ± 0.080 and 0.740 ± 0.040 respectively (**Table 5.3**). Statistical analysis showed that the differences in the power law exponent between native protein alone and native protein in the presence of DPPC ($1x10^{-4}$ % w/v and $5x10^{-4}$ % w/v) were not significant as determined by one-way ANOVA ($P > 0.05$). Native BSA in the presence of DPPC at $1x10^{-3}$ % w/v showed no evidence of interfacial film formation, indicated by the low values of G' and G" moduli, after two hours of protein adsorption so that the frequency sweep measurements were not performed for this solution.

Strain amplitude-sweep experiments (**Figure 5.9**) showed the oscillation torque at which the multilayer was disrupted for native BSA in the presence of DPPC of $1x10^{-4}$ % w/v 4 ± 2 mNm, and of $5x10^{-4}$ % w/v 2 ± 1 mNm. Statistical analysis showed that the differences in the

oscillation torque applied to the film between native protein alone and native protein in the presence of DPPC ($1x10^{-4}$ % w/v and $5x10^{-4}$ % w/v) were significant as determined by one-way ANOVA ($P < 0.05$). However, Tukey's test analysis showed that the oscillation torque at which the multilayer was disrupted for native BSA in the presence of DPPC was only significantly different between native protein alone and native protein in the presence of DPPC ($5x10^{-4}$ % w/v) ($P < 0.05$) (**Table 5.4**). Native BSA in the presence of DPPC at $1x10^{-3}$ % w/v showed no evidence of interfacial film formation, indicated by the low values of G' and G" moduli, after two hours of protein adsorption so that, the strain amplitude-sweep measurements were not performed for this solution.

The adsorption of native BSA to the oil-water interface was also investigated using phospholipids with different head groups and length chain. Native BSA in the presence of DSPC ($1x10^{-2}$ % w/v) and DSPG-Na ($5x10^{-3}$ % w/v) showed a similar tendency to that of native BSA in the presence of DPPC ($5x10^{-4}$ % w/v and $1x10^{-3}$ % w/v) reducing the magnitude of G' and G" moduli and complex viscosity from 10^{-2} to 10^{-3}-10^{-4} (N/m) (approximate values) within two hours of protein adsorption (**Figures 5.10(A and B)**).

The time to cross-over for native protein in the presence of DPPC ($1x10^{-3}$ % w/v), DSPC ($1x10^{-2}$ % w/v) and DSPG-Na ($5x10^{-3}$ % w/v) were 3 ± 1 min, 3 ± 1 min and 6 ± 2 min, respectively (**Table 5.3**). The differences in time to cross-over between native protein alone and native protein in the presence of any of these phospholipids (DPPC ($1x10^{-3}$ % w/v), DSPC ($1x10^{-2}$ % w/v) and DSPG-Na ($5x10^{-3}$ % w/v)) were not significant as determined by one-way ANOVA ($P > 0.05$).

There was no evidence of interfacial film formation at the interface after two hours of protein adsorption in the presence of phospholipids (i.e. DPPC ($1x10^{-3}$ % w/v), DSPC ($1x10^{-2}$ % w/v) and DSPG-Na ($5x10^{-3}$ % w/v)). For that reason, frequency-sweep (e.g. power law exponent) and strain amplitude-sweep (e.g. resistant to breakage) measurements were not performed on these solutions.

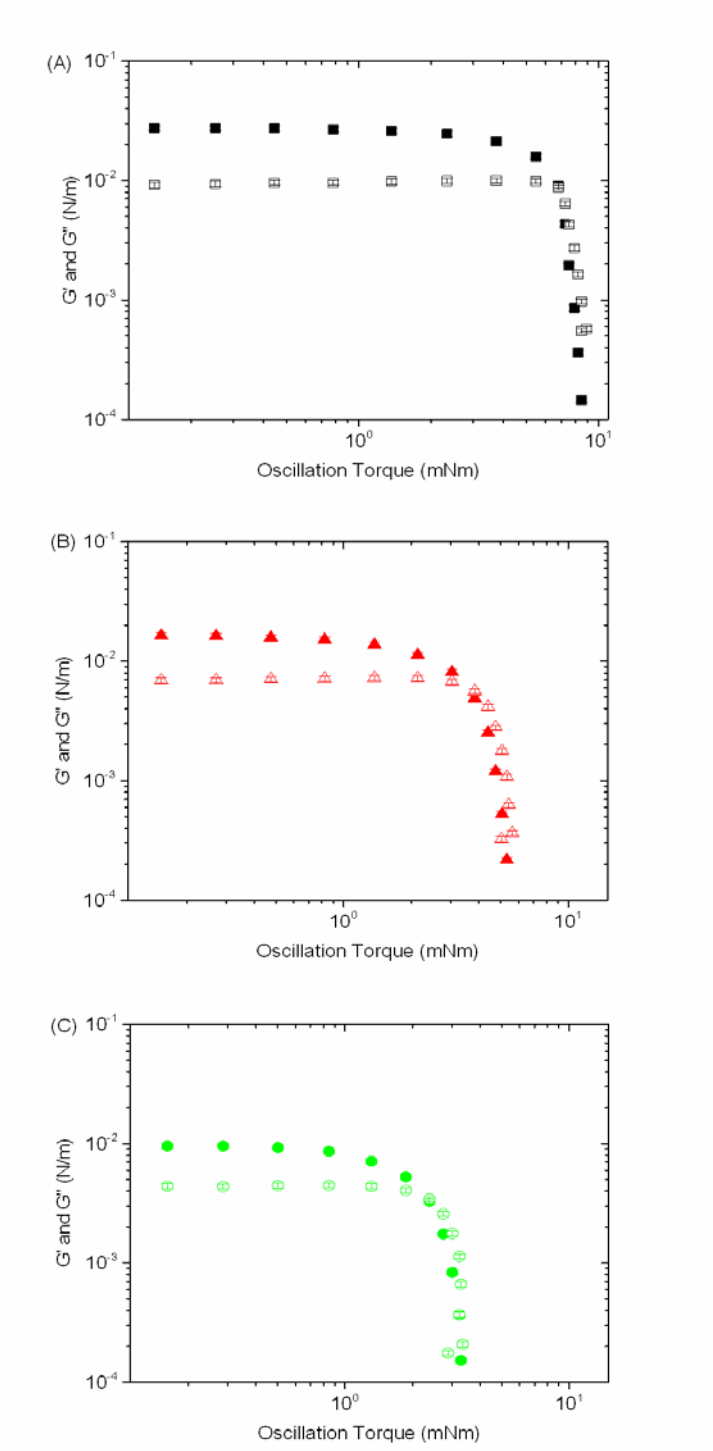

Figure 5.9 Elastic G' (solid symbols) modulus as a function of the oscillation torque applied to the oil-water interface after two hours of adding protein. (A) Native BSA alone (0.5 mM) (■) and native BSA (0.5 mM) in the presence of DPPC at (B) $1x10^{-4}$ % w/v (▲) (CV (G') = 57.9 % and (G") 53.2 %) and (C) $5x10^{-4}$ % w/v (●) (CV (G') = 34.2 % and (G") 32.3 %). G' and G" moduli and oscillation torque are in logarithmic scale.

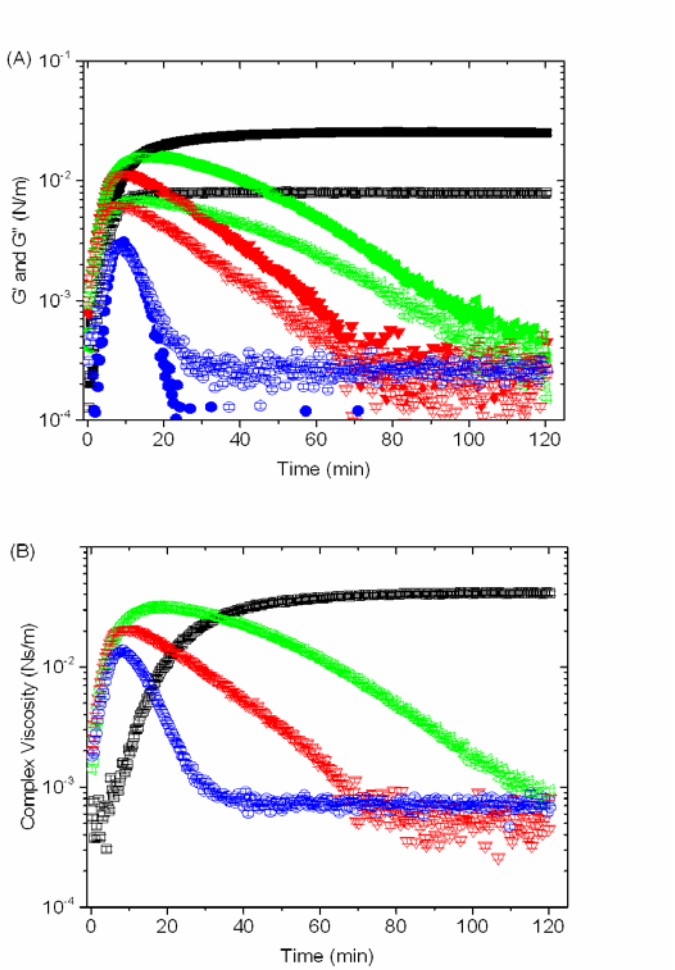

Figure 5.10 Native BSA alone (0.5 mM) (■) vs. native BSA (0.5 mM) dissolved in the presence of different phospholipids at the oil-water interface: DPPC $1x10^{-3}$ % w/v (▼) (CV (G') = 175 % and (G") 172 %), DSPC $1x10^{-2}$ % w/v (◀) (CV (G') = 85.0 % and (G") 73.1 %) and DSPG-Na $5x10^{-3}$ % w/v (●) (CV (G') = 329 % and (G") 174 %): (A) Elastic G' (solid symbols) and viscous G" (open symbols) moduli and (B) complex viscosity (open symbols) as a function of time. Complex viscosity is in logarithmic scale.

5.3.1.4. Effect of polymers on the oil-water interfacial rheology measurements of native BSA (0.5 mM)

The adsorption of proteins to the oil-water interface was investigated in the presence of two polymers added to the aqueous phase which have different solubility properties (i.e. PDMAEMA is a water soluble polymer while PBuA due to a polybutylacetate group decreased its water solubility, is practically insoluble).

The addition of PDMAEMA and PBuA polymers ($8.75x10^{-3}$ % w/v) to the protein solution reduced the magnitude of G' and G" moduli from 27 ± 2 mN/m and 10 ± 1 mN/m,

respectively, for native BSA alone to 8 ± 3 mN/m (G' modulus) and 4 ± 1 mN/m (G" modulus) for native BSA in the presence of PDMAEMA and 7 ± 10 mN/m (G' modulus) and 3 ± 4 mN/m (G" modulus) for native BSA in the presence of PBuA (**Figure 5.11 and Table 5.5**). The differences of G' and G" moduli between native protein alone and native protein in the presence of any of these polymers (PDMAEMA and PBuA $8.75x10^{-3}$ % w/v) groups were significant as determined by one-way ANOVA ($P < 0.05$). A post-hoc Tukey's test showed that the G' moduli for solutions of native BSA alone and native BSA in the presence of polymers were significantly different from each other ($P < 0.05$) whereas the G" moduli were only significantly different for native BSA alone and native BSA in the presence of PBuA ($P < 0.05$) (**Table 5.6**). Additionally, the Tukey's test showed that the magnitude of G' and G" moduli between native BSA in the presence of PBuA and native BSA in the presence of PDMAEMA were not significantly different from each other ($P > 0.05$) (**Table 5.6**).

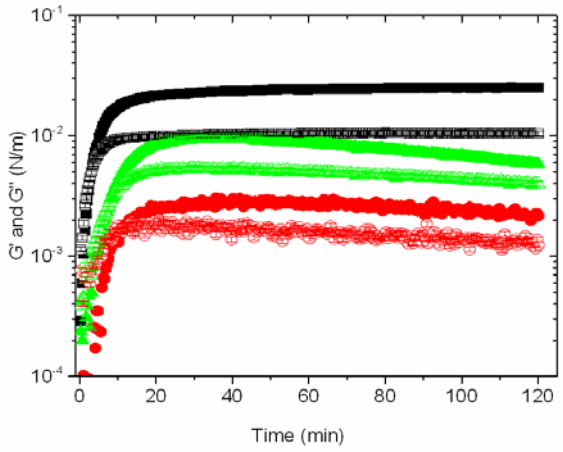

Figure 5.11 Elastic G' (solid symbols) and viscous G" (open symbols) moduli as a function of time. Native BSA alone (0.5 mM) (■) vs. native BSA (0.5 mM) in the presence of polymers of different water solubility pH 7.4: PDMAEMA at $8.75x10^{-3}$ % w/v (▲) (CV (G') = 40.5 % and (G") 24.1 %) and PBuA at $8.75x10^{-3}$ % w/v (●) (CV (G') = 85.6 % and (G") 69.4 %). G' and G" moduli are in logarithmic scale.

The time to cross-over for native BSA in the presence of PBuA and PDMAEMA ($8.75x10^{-3}$ % w/v) were 9 ± 0.3 min and 7 ± 2 min, respectively (**Table 5.5**). However, the difference of time to cross-over between native protein alone and native protein in the presence of these polymers (PDMAEMA and PBuA $8.75x10^{-3}$ % w/v) were not significantly different as determined by one-way ANOVA ($P > 0.05$).

Table 5.5 Data analysis of rheology measurements for native BSA in the presence of polymers (PDMAEMA ($8.75x10^{-3}$ % w/v) and PBuA ($8.75x10^{-3}$ % w/v)). Rheology measurements correspond to data analysis of time sweep measurements (time to cross-over, elastic (G') and viscous (G") moduli and complex viscosity) and frequency sweep measurements (power law exponent, n). (mean ± s.d.) (n=3).

Native BSA (0.5 mM) + Excipients	Time to cross-over (min)	Maximum (N/m) (x1000) Elastic modulus (G')	Viscous modulus (G")	Complex dynamic viscosity (Ns/m) (x1000)	Power law exponent* (n)
Native BSA alone	4 ± 2	27 ± 2	10 ± 1	45 ± 3	-0.812 ± 0.010
Native BSA + PDMAEMA ($8.75x10^{-3}$ % w/v)	7 ± 2	8 ± 3	4 ± 1	15 ± 5	(-)
Native BSA + PBuA ($8.75x10^{-3}$ % w/v)	9 ± 0.3	7 ± 10	3 ± 4	12 ± 17	(-)

(-) value not calculated. (*) power law exponent (n) close to one means the final film has a more solid-like property).

The complex viscosity for native BSA in the presence of PDMAEMA and PBuA ($8.75x10^{-3}$ % w/v) (15 ± 5 mNs/m and 12 ± 17 mNs/m respectively) were lower than for native BSA alone (45 ± 3 mNs/m) (**Figure 5.12 and Table 5.5**). The differences in complex viscosity between native protein alone and native protein in the presence of any of these polymers (PDMAEMA and PBuA $8.75x10^{-3}$ % w/v) were significant as determined by one-way ANOVA ($P < 0.05$). Tukey's post-hoc test showed that the magnitude of complex viscosity for native BSA alone and native BSA in the presence of any of these polymers were significantly different from each other ($P < 0.05$) (**Table 5.6**). However, the magnitude of complex viscosity between native BSA in the presence of PBuA and native BSA in the presence of PDMAEMA were not significantly different ($P > 0.05$) (**Table 5.6**).

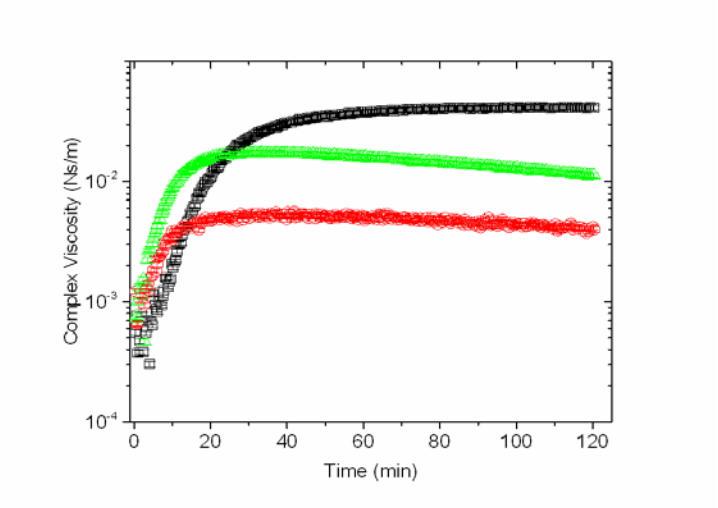

Figure 5.12 Complex viscosity as a function of time. Native BSA alone (0.5 mM) (□) vs. native BSA (0.5 mM) in the presence of polymers of different water solubility pH 7.4: PDMAEMA at $8.75x10^{-3}$ % w/v (△) (CV = 36.9 %) and PBuA at $8.75x10^{-3}$ % w/v (○) (CV = 119 %) at the oil-water interface. Complex viscosity is in logarithmic scale.

Table 5.6 Tukey's test analysis for native BSA alone (0.5 mM) vs. native BSA (0.5 mM) in the presence of polymers (PDMAEMA ($8.75x10^{-3}$ % w/v) and PBuA ($8.75x10^{-3}$ % w/v)). Tukey's test analysis was performed for solutions showing significant differences in the one-way ANOVA test ($P < 0.05$).

	Native BSA alone vs. Native BSA + PBuA ($8.75x10^{-3}$ % w/v)	Native BSA alone vs. Native BSA + PDMAEMA ($8.75x10^{-3}$ % w/v)	Native BSA + PBuA ($8.75x10^{-3}$ % w/v) vs. Native BSA + PDMAEMA ($8.75x10^{-3}$ % w/v)
Elastic modulus (G') (N/m)	P<0.05	P<0.05	P>0.05
Viscous modulus (G") (N/m)	P<0.05	P>0.05	P>0.05
Complex viscosity (Ns/m)	P<0.05	P<0.05	P>0.05

5.3.2. Pendant drop tensiometer studies: Investigating the interfacial tension of proteins in the presence of excipients

5.3.2.1. Interfacial tension measurements of native BSA alone (0.5 mM)

The value of IFT for native BSA protein (0.5 mM) was studied for one hour as shown in **Figure 5.13**. The value of IFT_{30} and the initial slope (over the first three minutes) (mean ± s.d., n=3) were used to investigate the effect of native BSA protein in the oil-water interface. The IFT_{30} for native BSA alone was 7.6 ± 0.2 mN/m showing an initial slope (over the first three minutes) of -0.468 ± 0.080 N/m/min. In comparison, control experiments in the absence of proteins gave an IFT at t=20 minutes of 18.0 ± 1.3 mN/m.

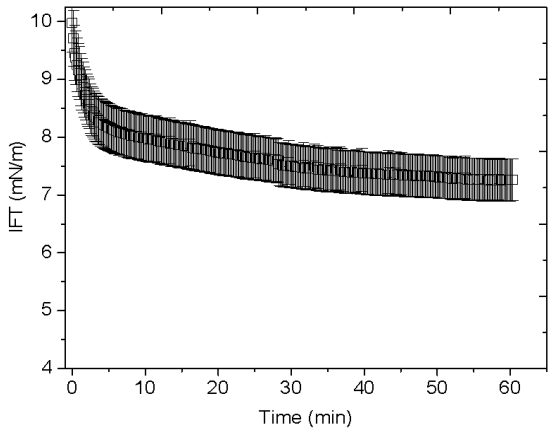

Figure 5.13 IFT (mN/m) as a function of time for native BSA alone (0.5 mM) (CV = 6.2 %) (n=3).

5.3.2.2. Effect of NaCl on the oil-water interfacial tension measurements of native BSA (0.5 mM)

Native BSA in the presence of NaCl (0.1 M, 0.5 M and 1 M) showed a lower IFT than native BSA alone (**Figure 5.14**). The decrease in the IFT was NaCl concentration dependent. The IFT_{30} decreased significantly more for solutions containing NaCl (6.8 ± 0.1 mN/m (NaCl 0.1 M), 5.6 ± 0.1 mN/m (NaCl 0.5 M) and 4.7 ± 0.01 mN/m (NaCl 1 M)) than for native BSA alone (7.6 ± 0.2 mN/m) (**Table 5.7**). The differences of IFT_{30} for native protein alone and native protein in the presence of NaCl (0.1 M, 0.5 M and 1 M) were significant as determined by one-way ANOVA ($P < 0.05$). Moreover, Tukey's post-hoc test confirmed that the

decrease in the IFT_{30} for all these solutions were significantly different from each other ($P < 0.001$) (**Table 5.8**).

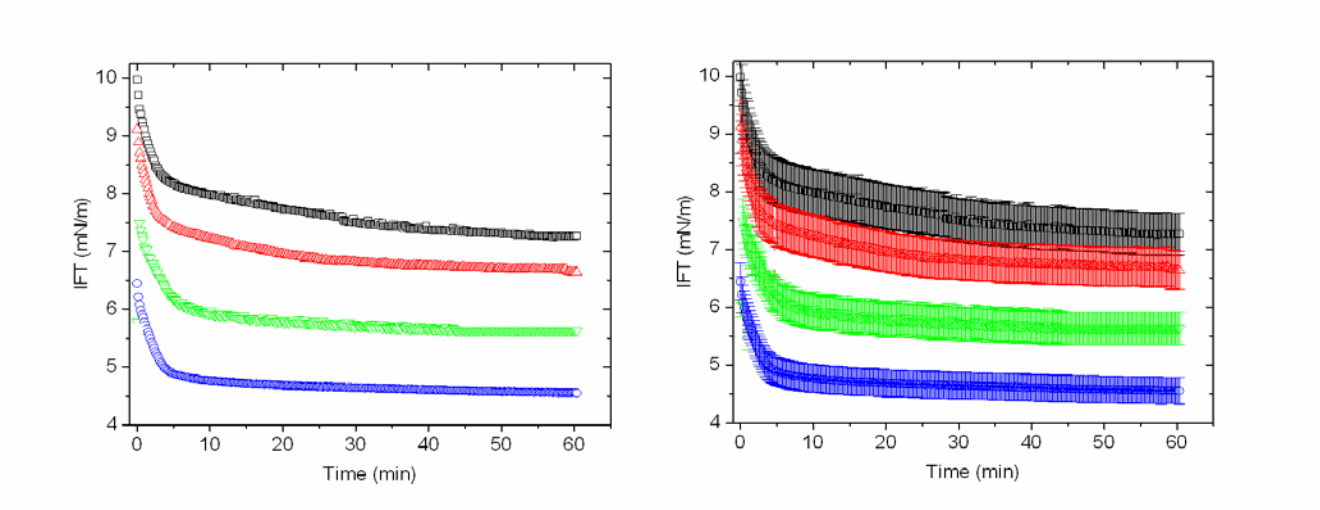

Figure 5.14 IFT mN/m as a function of time with (right) and without (left) error bars. Native BSA alone (0.5 mM) (□) vs. native BSA (0.5 mM) dissolved in the presence of NaCl at 0.1 M (△) (CV = 5.4 %), 0.5 M (▽) (CV = 4.6%) and 1 M (○) (CV = 6.2 %). (n=3).

Table 5.7 Data analysis of interfacial tension measurements for native BSA in the presence of NaCl (0.1 M, 0.5 M and 1 M). IFT measurements illustrate the initial slope (over the first three minutes) and the IFT_{30} values (mean ± s.d.) (n=3).

Native BSA (0.5 Mm) + Excipients	Initial slope (N/m/min) (t=3 min)	IFT_{30} (mN/m)
Native BSA alone	- 0.468 ± 0.080	7.6 ± 0.2
Native BSA + NaCl (0.1 M)	-0.464 ± 0.070	6.8 ± 0.1
Native BSA + NaCl (0.5 M)	-0.493 ± 0.010	5.6 ± 0.1
Native BSA + NaCl (1.0 M)	-0.387 ± 0.020	4.7 ± 0.01

Table 5.8 Tukey's test analysis results for native BSA alone (0.5 mM) vs. native BSA (0.5 mM) in the presence of NaCl at 0.1 M, 0.5 M and 1 M. Tukey's test analysis was performed for solutions showing significant differences in the one-way ANOVA test ($P < 0.05$).

	Native BSA alone vs. Native BSA + NaCl (0.1 M)	Native BSA alone vs. Native BSA + NaCl (0.5 M)	Native BSA alone vs. Native BSA + NaCl (1 M)	Native BSA + NaCl (0.1 M) vs. Native BSA + NaCl (0.5 M)	Native BSA + NaCl (0.1 M) vs. Native BSA + NaCl (1 M)	Native BSA + NaCl (0.5 M) vs. Native BSA+ NaCl (1 M)
IFT_{30}	P<0.001	P<0.001	P<0.001	P<0.001	P<0.001	P<0.001

The initial slope (over the first three minutes) describing the decrease in the IFT between zero and three minutes showed similar values for native BSA alone (-0.468 ± 0.070 N/m/min) and BSA in the presence of NaCl at 0.1 M (-0.464 ± 0.070 N/m/min). The values of the initial slope for native BSA in the presence of NaCl at 0.5 M and 1 M were -0.493 ± 0.010 N/m/min and -0.387 ± 0.020 N/m/min respectively. Statistical analysis showed that the differences of initial slope between native protein alone and native protein in the presence of NaCl (0.1 M, 0.5 M and 1 M) were not significant as determined by one-way ANOVA ($P > 0.05$).

5.3.2.3. Effect of phospholipids on the oil-water interfacial tension measurements of native BSA (0.5 mM)

Native BSA (0.5 mM) in the presence of DPPC decreased the IFT_{30} more than native BSA alone (**Figure 5.15**). The decrease in the IFT_{30} for native BSA in the presence of DPPC was: 7.2 ± 0.04 mN/m ($1x10^{-4}$ % w/v), 7.4 ± 0.04 mN/m ($5x10^{-4}$ % w/v) and 7.3 ± 0.04 mN/m ($1x10^{-3}$ % w/v) (**Table 5.9**). Statistical analysis showed that the differences in IFT_{30} between native protein alone and native protein in the presence of DPPC ($1x10^{-4}$ % w/v, $5x10^{-4}$ % w/v and $1x10^{-3}$ % w/v) were significant as determined by one-way ANOVA ($P < 0.05$). A Tukey's post-hoc test showed that the differences in the IFT_{30} between native BSA alone and native BSA in the presence of DPPC ($1x10^{-4}$ % w/v and $1x10^{-3}$ % w/v) were significant ($P < 0.01$ and $P < 0.05$ respectively) whereas the decrease in the IFT_{30} between native BSA alone and native BSA in the presence of DPPC ($5x10^{-4}$ % w/v) were not significantly different ($P > 0.05$) (**Table 5.10**). The post-hoc Tukey's test also showed that the decrease in the IFT_{30} for native BSA in the presence of DPPC at any concentration ($1x10^{-4}$ % w/v, $5x10^{-4}$ % w/v and $1x10^{-3}$ %) were not significantly different from each other ($P > 0.05$) (**Table 5.10**).

The initial slope in the IFT (over the first three minutes) for native BSA in the presence of DPPC was: -0.507 ± 0.020 N/m/min ($1x10^{-4}$ % w/v), -0.579 ± 0.050 N/m/min ($5x10^{-3}$ % w/v) and -0.557 ± 0.070 N/m/min ($1x10^{-3}$% w/v) (**Table 5.9**). Statistical analysis showed that the differences of the initial slope in the IFT (over the first three minutes) between native protein alone and native protein in the presence of DPPC ($1x10^{-4}$ % w/v, $5x10^{-4}$ % w/v and $1x10^{-3}$ % w/v) were not significant as determined by one-way ANOVA ($P > 0.05$).

Table 5.9 Data analysis of interfacial tension measurements for native BSA in the presence of phospholipids (DPPC ($1x10^{-4}$ % w/w, $5x10^{-4}$ % w/w and $1x10^{-3}$ % w/w), DSPC ($1x10^{-2}$ % w/w) and DSPG-Na ($5x10^{-3}$ % w/w)). IFT measurements illustrate the initial slope (over the first three minutes) and the IFT_{30} values (mean ± s.d) (n=3).

Native BSA (0.5 mM) + Excipients	Initial slope (N/m/min) (t=3 min)	IFT_{30} (mN/m)
Native BSA alone	- 0.468 ± 0.080	7.6 ± 0.2
Native BSA + DPPC ($1x10^{-4}$ % w/w)	-0.507 ± 0.020	7.2 ± 0.04
Native BSA + DPPC ($5x10^{-4}$ % w/w)	-0.579 ± 0.050	7.4 ± 0.04
Native BSA + DPPC ($1x10^{-3}$ % w/w)	-0.557 ± 0.070	7.3 ± 0.04
Native BSA + DSPG-Na ($5x10^{-3}$ % w/w)	-0.469 ± 0.050	7.0 ± 0.03
Native BSA + DSPC ($1x10^{-2}$ % w/w)	-0.401 ± 0.060	6.7 ± 0.1

Table 5.10 Tukey's test analysis for native BSA alone (0.5 mM) vs. native BSA (0.5 mM) in the presence of phospholipids (DPPC ($1x10^{-4}$ % w/w, $5x10^{-4}$ % w/w and $1x10^{-3}$ % w/w), DSPC ($1x10^{-2}$ % w/w) and DSPG-Na ($5x10^{-3}$ % w/w)). Tukey's test analysis was performed for solutions showing significant differences in the one-way ANOVA test ($P < 0.05$).

	Native BSA alone vs. Native BSA + DPPC ($1x10^{-4}$ % w/w)	Native BSA alone vs. Native BSA + DPPC ($5x10^{-4}$ % w/w)	Native BSA alone vs. Native BSA + DPPC ($1x10^{-3}$ % w/w)	Native BSA + DPPC ($1*10^{-4}$ % w/w) vs. Native BSA + DPPC ($5x10^{-4}$ % w/w)	Native BSA + DPPC ($1*10^{-4}$ % w/w) vs. Native BSA + DPPC ($1x10^{-3}$ % w/w)	Native BSA + DPPC ($5*10^{-4}$ % w/w) vs. Native BSA + DPPC ($1x10^{-3}$ % w/w)
IFT_{30}	P<0.01	P>0.05	P<0.05	P>0.05	P>0.05	P>0.05

	Native BSA alone vs. Native BSA + DSPG-Na ($5x10^{-3}$ % w/w)	Native BSA alone vs. Native BSA + DSPC ($1x10^{-2}$ % w/w)	Native BSA alone vs. Native BSA + DPPC ($1x10^{-3}$ % w/w)	Native BSA + DSPC ($1*10^{-2}$ % w/w) vs. Native BSA + DSPG-Na ($5x10^{-3}$ % w/w)	Native BSA + DPPC ($1*10^{-3}$ % w/w) vs. Native BSA + DSPG-Na ($5x10^{-3}$ % w/w)	Native BSA + DSPC ($1*10^{-2}$ % w/w) vs. Native BSA + DPPC ($1x10^{-3}$ % w/w)
IFT_{30}	P<0.001	P<0.001	P<0.05	P>0.05	P<0.01	P<0.001

The decrease in the IFT_{30} for native BSA in the presence of DPPC ($1x10^{-3}$ % w/v), DSPC ($1x10^{-2}$ % w/v) and DSPG-Na ($5x10^{-3}$ % w/v) were 7.3 ± 0.04 mN/m, 6.7 ± 0.1 mN/m) and 7.0 ± 0.03 mN/m respectively (**Figure 5.15 and Table 5.9**). Statistical analysis showed that the decrease in the IFT_{30} for native BSA in the presence of phospholipids with different head groups and chain lengths (DPPC ($1x10^{-3}$ % w/v), DSPC ($1x10^{-2}$ % w/v) and DSPG-Na ($5x10^{-3}$ % w/v)) were significantly different as determined by one-way ANOVA ($P < 0.05$). Additionally, a Tukey's post-hoc test showed that the decrease of IFT_{30} for protein solutions was significantly different for all protein solutions with the exception of native BSA in the presence of DSPC ($1x10^{-2}$ % w/v) vs. native BSA in the presence of DSPG-Na ($5x10^{-3}$ % w/v) ($P > 0.05$) (**Table 5.10**).

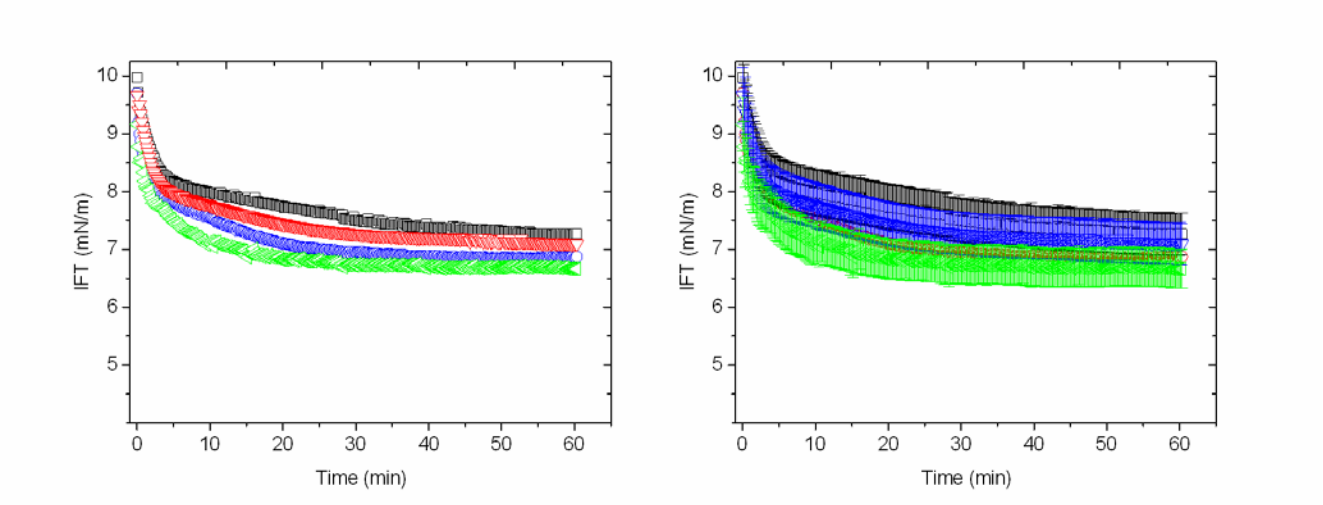

Figure 5.15 IFT (mN/m) as a function of time (with (right) and without (left) error bars). Native BSA (0.5 mM) (□) vs. native BSA in the presence of phospholipids: DPPC $1x10^{-3}$ % w/v (▽) (CV = 5.6 %), DSPC $1x10^{-2}$ % w/v (◁) (CV = 5.5 %) and DSPG-Na $5x10^{-3}$ % w/v (○) (CV = 6.1 %) (n=3).

The initial slope describing the drop in the IFT (over the first three minutes) for native BSA in the presence of DPPC ($1x10^{-3}$ % w/v), DSPC ($1x10^{-2}$ % w/v) and DSPG-Na ($5x10^{-3}$ % w/v) was: -0.557 ± 0.070 N/m/min, -0.401 ± 0.060 N/m/min and -0.469 ± 0.050 N/m/min respectively (**Table 5.9**). Statistical analysis showed that the differences in initial slope (over the first three minutes) between native protein alone and native protein in the presence of phospholipids with different head groups and chain lengths (DPPC ($1x10^{-3}$ % w/v), DSPC ($1x10^{-2}$ % w/v) and DSPG-Na ($5x10^{-3}$ % w/v) were not significant as determined by one-way ANOVA ($P > 0.05$).

5.3.2.4. Effect of polymers on the oil-water interfacial tension measurements of native BSA (0.5 mM)

The decrease in the IFT for native BSA (0.5 mM) in the presence of the polymers PDMAEMA and PBuA is shown in **Figure 5.16**. The value of IFT_{30} for native BSA in the presence of PDMAEMA and PBuA ($8.75x10^{-3}$ % w/v) was 7.0 ± 0.3 mN/m and 7.2 ± 0.1 mN/m, respectively (**Table 5.11**). Statistical analysis showed that the values of IFT_{30} for native BSA in the presence of these polymers were not significantly different as described by one-way ANOVA ($P > 0.05$).

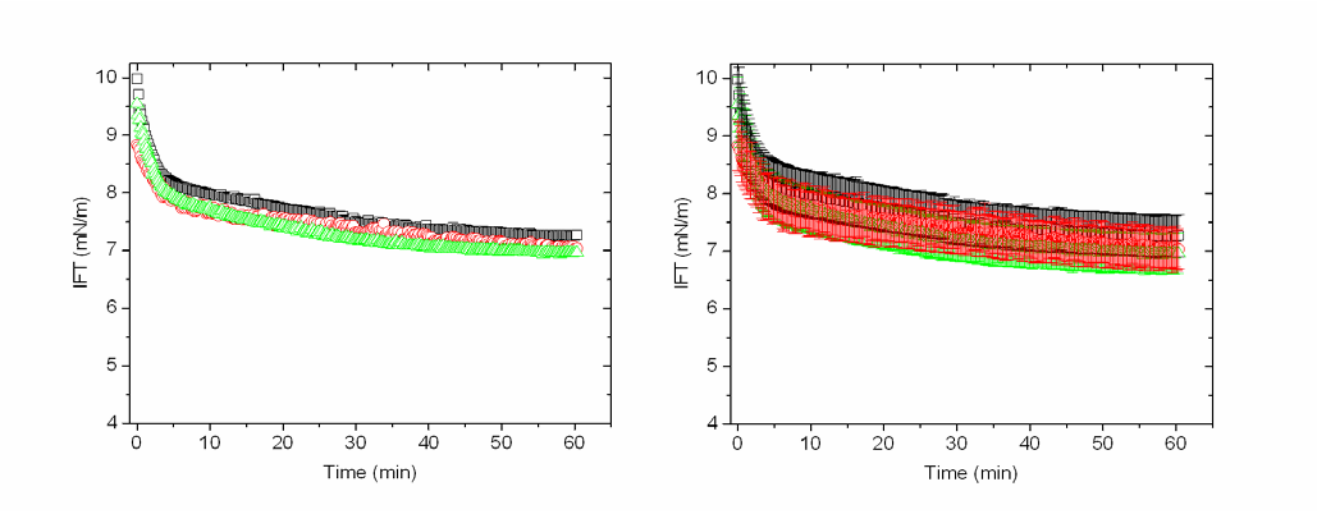

Figure 5.16 IFT (mN/m) as a function of time. Native BSA alone (0.5 mM) (□) vs. native BSA (0.5 mM) in the presence of polymers of different water solubility: PDMAEMA at $8.75x10^{-3}$ % w/v (△) (CV = 6.2 %) and PBuA at $8.75x10^{-3}$ % w/v (○) (CV = 4.6 %) (n=3).

Table 5.11 Data analysis of IFT measurements for native BSA in the presence of polymers (PDMAEMA ($8.75x10^{-3}$ % w/v) and PBuA ($8.75x10^{-3}$ % w/v)). IFT measurements illustrate the initial slope (over the first three minutes) and the IFT_{30} values (mean ± s.d.) (n=3).

Native BSA (0.5 Mm) + Excipients	Initial slope (N/m/min) (t=3 min)	IFT_{30} (mN/m)
Native BSA alone	- 0.468 ± 0.080	7.6 ± 0.2
Native BSA + PDMAEMA ($8.75x10^{-3}$ % w/v)	-0.334 ± 0.090	7.0 ± 0.3
Native BSA + PBuA ($8.75x10^{-3}$ % w/v)	-0.237 ± 0.030	7.2 ± 0.1

The initial slope (over the first three minutes) describing the decrease in the IFT was higher for native BSA alone (-0.468 ± 0.070 N/m/min) than for native BSA in the presence of PDMAEMA (-0.334 ± 0.090 N/m/min) and for native BSA in the presence of PBuA (-0.237 ± 0.030 N/m/min). Statistical analysis showed that the difference of initial slope (over the first three minutes) between native protein alone and native protein in the presence of these polymers (PDMAEMA and PBuA) were significant as determined by one-way ANOVA ($P < 0.05$). However, a post-hoc Tukey's test showed that the initial slope (over the first three minutes) for protein solutions was only significantly different between native BSA alone and native BSA in the presence of PBuA ($P < 0.05$) (**Table 5.12**).

Table 5.12 Tukey's test analysis for native BSA alone (0.5 mM) vs. native BSA (0.5 mM) in the presence of polymers (PDMAEMA ($8.75x10^{-3}$ % w/v) and PBuA ($8.75x10^{-3}$ % w/v)). Tukey's test analysis was performed for solutions showing significant differences in the one-way ANOVA test ($P < 0.05$).

	Native BSA alone vs. Native BSA + PBuA ($8.75x10^{-3}$ % w/v)	Native BSA alone vs. Native BSA + PDMAEMA ($8.75x10^{-3}$ % w/v)	Native BSA + PBuA ($8.75x10^{-3}$ % w/v) vs. Native BSA + PDMAEMA ($8.75x10^{-3}$ % w/v)
Initial slope (t=3 min)	P<0.05	P>0.05	P>0.05

5.3.3. FTIR spectroscopy studies: Investigating the secondary structure of proteins in the bulk solution after two hours of adsorption to the oil-water interface

FTIR spectroscopy was performed for the set of experiments showing detachment of native BSA from the oil-water interface due to the molecular interaction between BSA and excipients as shown from the interfacial rheology studies. This analysis was specifically performed for native BSA in the presence of phospholipids (DPPC $1x10^{-3}$ % w/v, DSPC $1x10^{-2}$ % w/v and DSPG-Na $5x10^{-3}$ % w/v) and polymers (PDMAEMA and PBuA ($8.75x10^{-3}$ % w/v)) (**Figures 5.10(A) and 5.11**).

FTIR spectroscopy was used to investigate the secondary structure of native BSA alone at t = 0 and after two hours of protein adsorption. The amide I band (1700 – 1600 cm^{-1}) was pre-processed using the 2ndD (Savitzky-Golay with 11 points smoothing), BC and AN to unit area (**Chapter 2 sections 2.2.4.2, 2.2.4.3 and 2.2.4.5**). This analysis was conducted to investigate

whether there was a change in secondary structure in BSA in the bulk solution. [48,65]. FTIR spectroscopy of the amide I band showed no evidence of physical denaturation of proteins or intermolecular β-sheet structures during the time scale of these experiments. Amide I spectra were similar for aliquots taken at t = 0 and after two hours of protein adsorption to the oil-water interface (**Figure 5.17**).

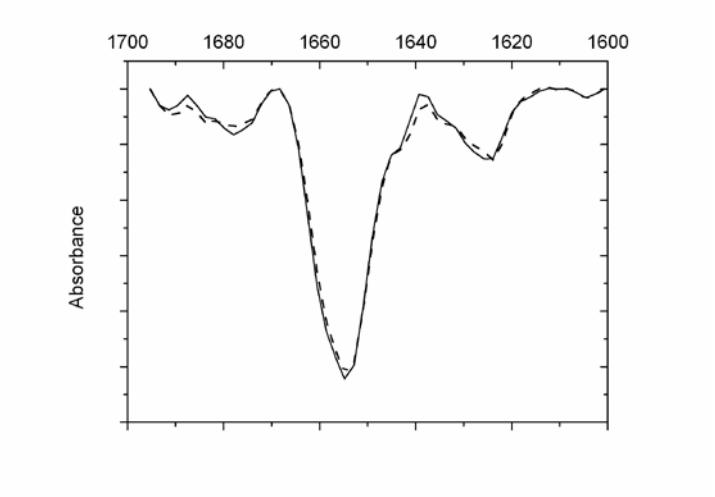

Figure 5.17 FTIR spectra showing the typical amide I band of native BSA (0.5 mM) after two hours of protein adsorption to the oil-water interface. Spectra correspond to BSA aliquots taken from the bulk solution of the rheometer (Delrin® trough). Native BSA alone t=0 (straight line) and t=2 h (dashed line). Original spectra were pre-processed using 2ndD, BC and AN.

FTIR spectroscopy was used to investigate the secondary structure of proteins at the bulk solution after two hours of protein adsorption to the oil-water interface in the presence of phospholipids (DPPC ($1x10^{-3}$ % w/v), DSPC ($1x10^{-2}$ % w/v) and DSPG-Na ($5x10^{-3}$ % w/v)). FTIR spectra showed that desorbed BSA from the oil-water interface kept its secondary structure giving similar spectra than for native BSA alone (**Figure 5.18**). Moreover, FTIR spectra showed the α-helix band at around 1656 cm^{-1} without bands at around 1600-1630 cm^{-1} attributed to appearance of intermolecular β-sheet structures or aggregate content [48,65].

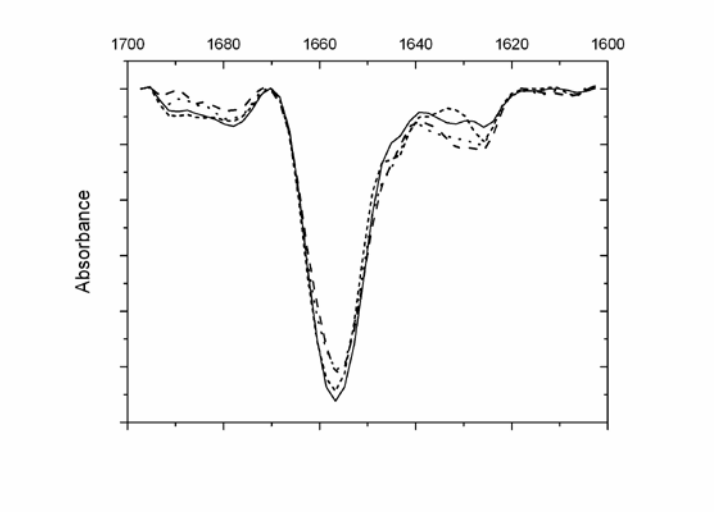

Figure 5.18 FTIR spectra showing the typical amide I band of native BSA (0.5 mM) after two hours of protein adsorption to the oil-water interface. Spectra correspond to BSA aliquots taken from the bulk solution of the rheometer (Delrin® trough). Native BSA alone t=0 (straight line) vs. native BSA in the presence of phospholipids t= 2 h: DPPC $1x10^{-3}$ % w/v (short dashed line), DSPC $1x10^{-2}$ % w/v (dotted line), DSPG-Na $5x10^{-3}$ % w/v (dashed line). Original spectra were pre-processed using 2^{nd}D, BC and AN.

FTIR spectra of native BSA in the presence of PDMAEMA ($8.75x10^{-3}$ % w/v) showed a similar amide I spectra than for native BSA alone without evidence of aggregated proteins (**Figure 5.19**). However, the spectra of native BSA in the presence of PBuA ($8.75x10^{-3}$ % w/v) showed to decrease α-helix intensity (around 1656 cm^{-1}) after two hours of protein adsorption which may be attributed to change in native protein conformation (e.g. partially unfolded BSA). However, bands at around 1600-1630 cm^{-1} attributed to appearance of intermolecular β-sheet structures and loss of secondary structure were not observed [48,65] (**Figure 5.19**).

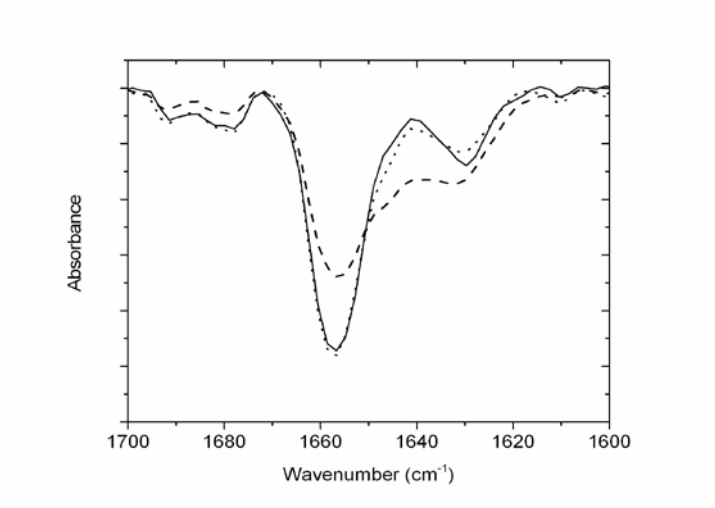

Figure 5.19 FTIR spectra showing the typical amide I band of native BSA (0.5 mM) after two hours of protein adsorption to the oil-water interface. Spectra correspond to BSA aliquots taken from the bulk solution of the rheometer (Delrin® trough). Native BSA alone t=0 (straight line) vs. native BSA (0.5 mM) in the presence of polymers of different water solubility: PDMAEMA at $8.75x10^{-3}$ % w/v (dotted line) and PBuA at $8.75x10^{-3}$ % w/v (dashed line). Original spectra were pre-processed using 2^{nd}D, BC and AN.

5.4. Discussion

In Chapter 4 interfacial rheology (DWR) and IFT measurements were used to detect changes in protein adsorption in the presence of small amounts of heat-denatured protein. The work described in this Chapter examines the use of these techniques to detect changes in protein adsorption caused by excipients commonly present in protein formulations like NaCl, phospholipids and polymers. As discussed in Chapter 4, protein molecules, upon adsorption to an oil-water interface may adopt unfolded conformations, change the oil-water interfacial properties, and/or interact with the surrounding protein molecules to form a network [98]. The stages in protein adsorption to interfaces are described as induction (regime I), monolayer saturation (regime II) and interfacial gelation (regime III) [93,95,102]. Proteins may spontaneously diffuse from the bulk solution to the interface giving a monolayer which may further evolve to a multilayer. The spontaneous diffusion of proteins from the bulk solution to the interface is a consequence of the free energy since the energy in the bulk solution is higher than at the interface [212,227]. Adsorbed proteins may change its secondary structure to adopt a more energetically favorable conformation of their hydrophobic and hydrophilic groups [221].

After gelation, protein adsorption to interfaces is often considered an irreversible process [92,102]. This was in agreement with results obtained in this Chapter where solutions of native proteins alone formed an irreversible multilayer at the oil-water interface in the time scale of these experiments (**Figure 5.3(A) and 5.13**). The irreversibility of the multilayer has been reported by dilution of the bulk phase without evidence of protein desorption from the interface [102,228]. The adsorption of proteins to interfaces is affected by excipients interacting with proteins and the interface [217,222]. The interaction between proteins and excipients may be initially explained if excipients and protein molecules compete to reach the oil-water interface [217]. The presence of excipients may affect the adsorption of proteins because excipients can remove or desorb the adsorbed protein [108]. Proteins adsorbed to the oil-water interface forming a viscoelastic film whereas excipients used here (i.e. NaCl, phospholipids and polymer) are not able to form the viscoelastic film by themselves giving low values in the magnitude of G' and G" moduli (data no shown). Therefore, this measurement may correspond to noise [93] and modification in the protein adsorption behavoiur to the oil-water interface in the presence of these excipients could be attributed to interactions between molecules of proteins and excipients. In this Chapter, protein adsorption to interfaces in the presence of excipients was investigated using sequential adsorption (for phospholipids) and

simultaneous adsorption (for NaCl and polymers) [228] of proteins and excipients to the oil-water interface.

Desorption of protein from liquid or solid interfaces in the presence of excipients has been explained by two competitive mechanisms: solubilisation and replacement [236]. In solubilisation, a water soluble excipient present in the bulk solution increases the solubility of the adsorbed protein forming a protein-excipient complex that removes the adsorbed protein from the interface. The interaction between excipient and adsorbed protein is higher than for excipient and surface. In contrast, replacement occurs when the excipient has more affinity for the surface than for the adsorbed protein and the excipient removes the adsorbed protein from the interface due to competitive displacement [236]. Commonly, these two mechanisms are combined and excipients interact with adsorbed protein by hydrophobic interactions forming a protein-excipient complex at the interface and then, the remaining free molecules of excipient near the interface produce a competition between molecules of the protein-excipient complex attached to the interface and free molecules of excipient near the interface. This competition may finally remove the adsorbed protein. However, adsorbed proteins are removed from the interface only if a high amount of proteins form a protein-excipient complex and desorbed proteins are changed by free excipients molecules [228].

In this Chapter, a rheometer with DWR geometry and a pendant drop tensiometer methods were used as complementary techniques to investigate the mechanism and kinetics of protein adsorption to the oil-water interface in the presence of excipients like salts, phospholipids and polymers. The results suggested that the presence of these excipients may affect the interfacial film preventing the formation of the interfacial film or modifying the molecular structure of the interfacial network. The explanations for these results could be based on intrinsic characteristics of the protein itself (conformation, molecular flexibility, size, charge and surface activity), the interaction between excipients and proteins as well as the hydrophobicity of the oil-water interface.

The decrease in the IFT was studied for native BSA in the presence or absence of excipients during one hour (**Figures 5.13 - 5.16**). Differences in the IFT equilibrium time were observed between solutions. Therefore, the decrease in the IFT was studied after 30 minutes of protein adsorption to the oil-water interface. The value of IFT_{30} was useful to compare the decrease in the IFT for all these solutions at the same time.

5.4.1. Effect of excipients on protein adsorption to interfaces

Protein formulations should minimize the presence of unfolded and aggregated proteins. Excipients are used in protein formulations to reduce aggregated proteins using internal and external mechanisms. The internal mechanism changes the structure of proteins using chemical reactions whereas external mechanism modifies the surrounding environment of proteins using excipients [39].

5.4.1.1. Native BSA in the presence of salt

The presence of salts in protein formulations may affect the physical stability of the protein which depends on the protein type and concentration, ionic interactions and charged groups of proteins [24,222]. Neutral salts show a different behavior when they are added to protein solutions at low or high concentration. At low concentration (i.e. 0.1-0.15 M), salts interact with charged groups of proteins affecting the electrostatic interaction between proteins [112,115]. At high concentrations, salts in the presence of proteins have an osmotic effect which may change the thermodynamic properties of water [90]. The electrostatic effect of salts can be divided in salt hydration or non-specific electrostatic shielding (at high salt concentration) and specific ion binding to protein (at low salt concentration) [21,24]. Depending on the presence of repulsive or attractive forces affecting protein stability, the shielding effect may stabilize or destabilize proteins due to salt bridges [24].

Modification in the electrostatic forces attaches proteins strongly to the interface [89] which may affect the physical stability of proteins [222]. This could explain the increase in the magnitude of the G' modulus for native BSA in the presence of NaCl 0.1 M in comparison with native BSA alone ((**Figures 5.4 and 5.5)** and **Table 5.1**). This result could be attributed to an increase in protein adsorption to the oil-water interface and surface activity of native BSA due to electrostatic interaction between proteins and NaCl [234].

NaCl was used to investigate the effect of the ionic strength in the competition of protein molecules to the interface [115]. Zhang *et al.* (2004) reported that proteins (i.e. skim milk power and whey protein isolate) in the presence of low concentration of NaCl (i.e. 0 - 0.4 M) did not affect the competition between protein molecules to reach the interface [115]. This is partially in agreement with rheology results presented in this Chapter where the time to cross-over, G" modulus and the power law exponent between native BSA alone and native BSA in the

presence of NaCl (0.1 M) did not show significant differences. However, the amount of protein adsorbed to the interface may be related to the saturation of the multilayer (or magnitude of G' modulus) which was considerably higher for native BSA in the presence of NaCl (0.1 M) than for native BSA alone ($P < 0.001$). Rheology results were in agreement with Tantipolphan *et al*. (2007) who found that the adsorption of BSA to hydrophobic surface was increased in the presence of NaCl (0.1 M) [239].

Protein adsorption to the oil-water interface in the presence of NaCl (0.1 M) could be also explained by small amounts of ionic excipients (e.g. NaCl) contributing to attach proteins to interfaces stronger than for protein alone. In fact, proteins in the presence of ionic excipients at low concentration ($5x10^{-7}$ - 10^{-6} M) have showed to increase the shear viscosity due to increase in protein adsorption to interfaces [228]. However, there were no significant differences in the magnitude of complex viscosity between native BSA alone and native BSA in the presence of NaCl at the lowest concentration (0.1 M).

Zhang *et al*. (2004) reported that neutral salts added at high concentration (0.8 M) reduced the solubility of proteins due to the salting out effect [115]. The salting out effect is used as method of protein separation. This method consists on the precipitation of proteins in aqueous solution by increasing the ionic strength of the solution using high concentration of salts like NaCl [240]. This may explain rheology results showing that native BSA in the presence of NaCl (1 M) significantly decreased the maximum magnitude of G' and G" moduli showing a delayed in the time to cross-over in comparison with native BSA alone ((**Figures 5.4 and 5.5)** and **Table 5.1**)). This result was also in agreement with Tantipolphan *et al*. (2007) who found that BSA adsorbed more to solid interfaces in the presence of lower concentrations of NaCl (0.1 M) than in the presence of high NaCl concentrations (1 M) [239].

The low value of the G' and G" moduli could be interpreted as multilayer formation being saturated using less amount of protein molecules. This means that fewer molecules of free proteins are available in the bulk solution to be adsorbed to the interface in comparison with the amount of free NaCl (1 M). Additionally, the delay in the multilayer formation from 4 ± 2 min for the native BSA alone to 29 ± 6 min for native BSA in the presence of NaCl (1 M) (**Table 5.1**) could be caused by protein complexation [228]. This complex must be formed in the bulk solution between native BSA and NaCl molecules. The complex may delay the diffusion of free molecules of native BSA due to steric hindrance avoiding that native BSA reached the

oil-water interface. Moreover, the amount of free molecules of native BSA available after complexation must be considerable lower than for native BSA alone.

Protein solutions including NaCl (1 M) may increase hydrophobic interactions between adsorbed proteins and excipients forming a complex in the interface which is less surface active than native protein alone. This complex may be further desorbed from the interface due to competitive adsorption [234]. Initially, native BSA in the presence of NaCl (1 M) may be able to freely adsorb to the oil-water interface but the presence of NaCl (1 M) removes the adsorbed native BSA. Free molecules of native BSA present in the bulk solution are still able to be adsorbed to the interface replacing the desorbed protein. However, the amount of free native BSA that is able to adsorb in the presence of NaCl (1 M) is lower than for native BSA alone. This could explain the lower magnitude of G' and G" moduli and the delay in the time to cross-over for native BSA in the presence of NaCl (1 M) in comparison with native BSA alone. On the other hand, excipients interacting with the hydrophobic groups of proteins in the bulk solution may decrease the affinity of proteins for the interface [217]. This may also explain the decrease in the magnitude of G' and G" moduli and the delay in the time to cross-over in comparison with native BSA alone.

Protein solutions containing a high concentration of salt may increase protein-protein interaction which in turn may influence protein aggregation [239]. As there was no evidence of protein desorption from the oil-water interface in the presence of NaCl using rheology studies, FTIR spectroscopy was not used to investigate changes in the secondary structure of protein after two hours of protein adsorption to the oil-water interface. Additionally, Tantipolphan *et al*. (2007) reported that BSA in the presence of NaCl (1 M) showed similar fluorescence spectra and size exclusion chromatograms than native BSA alone after four hours [239]. This may support the fact that native BSA in the presence of NaCl (1 M) should not affect the secondary structure of the protein.

The power law exponent decreased with the increase of NaCl from 0.1 M to 1 M. This means that the viscoelastic film has a less solid-like behaviour after two hours of protein adsorption to the oil-water interface in the presence of NaCl than for native BSA alone. This result could be explained because NaCl at the highest concentration (1 M) reduces protein solubility due to the salting out effect [115]. Additionally, native BSA in the presence of NaCl (1 M) may decrease protein adsorption to interfaces giving a viscoelastic film which forms a less

compact structure than for native BSA alone. This may also be attributed to the fewer free molecules of native BSA available to be adsorbed in the oil-water interface than for native BSA alone as a consequence of protein complexation in the bulk solution.

The drop of IFT_{30} measurements for native BSA in the presence of NaCl was concentration dependent decreasing significantly more for native BSA at the highest concentration of NaCl (1 M) than for native BSA alone. It has been reported that small excipients (i.e. molecules of small size) reduce the IFT more at high concentrations giving a more densely packed layer [217]. This is partially in agreement with results presented in this Chapter. Native BSA in the presence of NaCl at the highest concentration (1 M) reduced the IFT_{30} significantly more than native BSA alone ($P < 0.001$) however, the value of the power law exponent which explains the density of the packed film between native BSA alone and the native BSA in the presence of NaCl showed no significant differences ($P > 0.05$) (**Table 5.2**).

5.4.1.2. Native BSA in the presence of phospholipids

Phospholipids are molecules widely found in biological membranes [224] which have an hydrophilic head and hydrophobic tail giving a partition between the aqueous and the oil phases of the interface [212]. This characteristic makes phospholipids an useful carrier for protein drugs since phospholipids can form a bilayer [241,242] that protect hydrophobic groups of proteins within their core. The oil-water system is a model environment in which interfacial rheological measurements can be made. Protein formulations tend to be nanoparticulate, but proteins will be exposed to hydrophobic surfaces. Proteins as drugs may be formulated as part of oil-water emulsions since emulsions keep protein stability and are a suitable form of route of administration [73,242,243]. In this Chapter the effect of phospholipids on the adsorption of native BSA to the oil-water interface was investigated increasing the concentration of phospholipids in the oil phase as well as comparing the effect of phospholipids of different head groups and chain lengths.

Protein adsorption to interfaces in the presence of phospholipids is commonly studied mixing proteins and phospholipids together in the bulk solution [224,234]. In this study, the adsorption of proteins and phospholipids were investigated using different phases (i.e. protein was dissolved in the aqueous phase while phospholipids were dissolved in the oil phase). Therefore, native BSA and phospholipids were simultaneously adsorbed to the oil-water

interface [224]. These experiments avoided the interaction between proteins and phospholipids in the bulk solution as well as the sequential adsorption of the complex formed by proteins and phospholipids in the bulk solution which may influence the mechanism of protein adsorption to interfaces [224,234].

The mechanism of protein adsorption to interfaces in the presence of phospholipids is described to be dependent on the component ratio (e.g. proteins or phospholipids) [224,234]. In this work, the protein concentration was kept constant at 0.5 mM while the concentration of each phospholipid was gradually increased to study protein desorption within two hours. The concentration of phospholipids used in this thesis was lower than for native BSA. In particular, the concentration of phospholipids was increased from $1x10^{-4}$ % w/v until the rheology studies showed a considerable decrease in the magnitude of G' and G" moduli and complex viscosity within two hours. The decrease in G' and G" moduli and complex viscosity were attributed to an entire desorption of protein from the interface giving a similar scatter in the data than for the oil-water interface alone (i.e. without protein) (**Appendix F)**. The scatter showed in **Appendix F** is in agreement with the scatter showed by Baldursdottir *et al*. (2010) for the air-water interface alone (without protein) [93]. Rheology studies of native BSA in the presence of DPPC ($1x10^{-4}$ % w/v, $5x10^{-4}$ % w/v and $1x10^{-3}$ % w/v) showed that desorption of protein from the oil-water interface was concentration dependent, that is faster for native BSA in the presence of DPPC at the highest concentration ($1x10^{-3}$ % w/v) (**Figure 5.7 and 5.8**). A similar tendency was obtained for native BSA in the presence of increased concentrations of DSPG-Na and DSPC (data not shown).

Protein desorption from the oil-water interface has been described as a sudden increase in the IFT values [227,228]. In this Chapter, IFT measurements did not show desorption of proteins from the interface as was shown using the rheometer with the DWR attached. This may suggest that the pendant drop tensiometer may be a less sensitive technique than the rheometer to detect protein desorption from interfaces at the time scale of the experiments of this Chapter. In fact, the decrease in the IFT for native BSA in the presence of phospholipids was concentration dependent and it was constant for at least one hour (**Figure 5.8(C)**). Statistical analysis shows that the decrease in the IFT_{30} for native BSA in the presence of DPPC ($1x10^{-4}$ % w/v, $5x10^{-4}$ % w/v and $1x10^{-3}$ % w/v) was significantly different in comparison to native BSA alone.

Phospholipids of different chain length and with different head groups were used to compare their influence on the protein adsorption to interfaces. Previous reports have described that the head groups of phospholipids have shown to influence more the protein adsorption to interfaces than its chain length groups [224,234]. In this work, DPPC and DSPC were used to compare protein adsorption to the oil-water interface in the presence of phospholipids of similar head groups (phosphatidylcholine group) and different chain length (16 vs. 18 atoms of carbon respectively). Whereas, DSPG-Na and DSPC were used to compare protein adsorption to the oil-water interface in the presence of phospholipids with different head groups (phosphatidylglycerol vs. phosphatidylcholine respectively) and similar chain length (18 atoms of carbons) [244,245]. The kinetics of protein adsorption to the oil-water interface in the presence of phospholipids was investigated using the same total concentration for DPPC, DSPC and DSPG-Na ($1x10^{-3}$ % w/v) (data not shown). Results suggest that DPPC was the most efficient phospholipids to avoid protein adsorption to the oil-water interface. Whereas, native BSA in the presence of DSPC or DSPG-Na ($1x10^{-3}$ % w/v) showed similar kinetics of adsorption than for native BSA alone, without evidence of protein desorption within two hours. These results also indicate that the head groups of phospholipids (phosphatidylcholine vs. phosphatidylglycerol) are more important in avoiding protein adsorption to interfaces than the increase in the chain length of phospholipids from 16 to 18 carbon atoms (DPPC vs. DSPC and DSPG-Na respectively).

The FTIR spectra indicated that the desorbed proteins from an oil-water interface in the presence of phospholipids (DPPC ($1x10^{-3}$ % w/v), DSPC ($1x10^{-2}$ % w/v) and DSPG-Na ($5x10^{-3}$ % w/v)) maintain their secondary structure stable (**Figure 5.18**). FTIR spectra of desorbed protein showed the typical bands of native proteins which are α-helix band around 1656 cm^{-1} and absence of intermolecular β-sheet aggregates around 1600-1630 cm^{-1} [48,65].

Desorption of proteins in the presence of phospholipids could be explained by a mechanism of replacement where phospholipids are more surface active than proteins [236]. In the mechanism of replacement, the most favorable interaction is between phospholipids and interfaces whereas interactions between proteins and phospholipids at the bulk solution to form a protein-phospholipids complex or, interactions between proteins and the oil-water interface are less favorable [236]. In this work, phospholipids were dissolved in the oil phase whereas proteins were dissolved in the aqueous phase. Initially, protein adsorbed to the oil-

water interfaces followed by a protein desorption from the oil-water interface at increased concentration of phospholipids. FTIR spectra of desorbed proteins in the presence of phospholipids did not show evidence of phospholipids interacting with native BSA in the bulk solution. This is because the typical band of phospholipids around 1765-1720 cm^{-1} attributted to C=O group was not found in the FTIR spectra taken from the bulk solution after two hours of protein adsorption to the oil-water interface [239,246]. If phospholipids and proteins were placed together in the aqueous phase, some of the molecules of phospholipids may interact with proteins forming a protein-phospholipids complex. The rest of the molecules of phospholipids must be freely dissolved in the bulk solution which could compete for the oil-water interface with free molecules of proteins and protein-phospholipids complex in the bulk solution. FTIR spectra should confirm the presence of phospholipids in the bulk solution giving phospholipids bands around 1765-1720 cm^{-1} attributted to C=O group.

Desorption of protein from the interface is concentration dependent [228]. This was in agreement with rheology results of native BSA protein in the presence of high concentration of phospholipids (DPPC ($1x10^{-3}$ % w/v), DSPC ($1x10^{-2}$ % w/v) and DSPG-Na ($5x10^{-3}$ % w/v)). In these experiments, the native protein was partially removed from the interface decreasing viscosity and elasticity to values near zero. The decrease in the magnitude of complex viscosity near to zero, at high phospholipid concentrations, could be explained because the interface only contains a low number of protein molecules which cannot interact with each other [228]. After desorption of proteins, the decrease in the magnitude of the G' and G" moduli and complex viscosity is similar to that of solutions only containing excipients [228,247]. This was in agreement with results presented in this Chapter for native BSA in the presence of phospholipids (DPPC ($1x10^{-3}$ % w/v), DSPC ($1x10^{-2}$ % w/v) and DSPG-Na ($5x10^{-3}$ % w/v)).

5.4.1.3. Native BSA in the presence of polymers

PDMAEMA and PBuA are flexible polymeric materials [237,248]. Polymers are developed and synthesized to have specific characteristic in their chemical composition, size, architecture and functionality which have increased the popularity of this material in the biomedical field [248]. In the pharmaceutical field, polymers are used as potential controlled release systems and targeting of proteins which are susceptible of instability [230,249]. PDMAEMA and PBuA ($8.75x10^{-3}$ % w/v) were used to investigate their effect on preventing protein adsorption to the

oil-water interface. PDMAEMA is a water soluble polymer while PBuA is practically insoluble in water [94,250]. In this Chapter, PDMAEMA was dissolved in the aqueous phase at pH 7.4 whereas PBuA was suspended in the aqueous phase at pH 7.4.

PBuA and PDMAEMA have similar molecular weights and the main difference in their chemical structure is the poly butyl acetate group present in the PBuA polymer. Native BSA is likely to interact with PDMAEMA and PBuA polymers due to electrostatic interactions forming a complex at the bulk phase that diffuses to the oil-water interface. Electrostatic interactions between protein and cationic polymers are affected by changes in the pH that may affect the charge of the protein [237]. Controlling the pH is possible to increase/decrease the interaction between proteins and polymers. Protein-polymer complexes could be less surface active than native BSA alone. This is in agreement with results presented in this Chapter because the magnitude of the G' moduli and complex viscosity were significantly lower for native BSA in the presence of PDMAEMA and PBuA polymers than for native BSA alone ($P < 0.05$) (**Table 5.2**). The presence of these complexes in the bulk phase could avoid the diffusion of free molecules of native BSA to the oil-water interface due to steric hindrance. However, the delay in the time to cross-over for native BSA alone and native BSA in the presence of these polymers was not significant as shown the one-way ANOVA ($P > 0.05$).

IFT measurements have shown that the adsorption of proteins in the presence of excipients is characterized by a faster decrease in the IFT than for protein alone [224,228]. IFT measurements did not show significant differences between native BSA alone and native BSA in the presence of any of these polymers. As was discussed earlier, this may confirm that the pendant drop tensiometer is a less sensitive technique than the rheometer with the DWR attached to detect desorbed protein into the bulk solution in the presence of excipients used in this Chapter. The initial slope of IFT (over the first three minutes) was used to quantify the earlier decrease in the IFT as a result of protein adsorption to the oil-water interface. The initial slope was calculated using the first three minutes to build a linear regression between decrease in the IFT and time. However, the initial slope was only significantly different for native BSA in the presence of PBuA polymer ($P < 0.05$). This could be attributed to the butyl acetate group in the PBuA which increase the interfacial activity of PBuA [94] reducing the IFT faster than for native BSA alone and native BSA in the presence of PDMAEMA.

FTIR spectroscopy was used to investigate the secondary structure of native protein in the presence of these two polymers after two hours of protein adsorption to the oil-water interface. Results showed that the secondary structure of native BSA was more affected by the presence of PBuA than for PDMAEMA. FTIR spectra of amide I in the presence of PBuA showed a decrease in the intensity of the α-helix band around (1656 cm^{-1}) without bands attributed to intermolecular β-sheet around (1600-1630 cm^{-1}) (**Figure 5.19**). This may be attributed to the formation of partially unfolded proteins. As was discussed earlier, the presence of the partially insoluble poly butyl acetate group in the PBuA increased the interfacial activity of this polymer [94] forming a complex with native BSA in the bulk solution. This complex may decrease protein adsorption to interfaces giving a lower magnitude for the G' and G" moduli and complex viscosity than for native BSA alone. Additionally, this complex may modify the secondary structure of the remaining BSA protein in the bulk solution.

5.4.2. Strength and solid-like properties of the multilayer film after two hour of protein adsorption in the presence of excipients

Strain amplitude sweep experiments showed that the strength of the multilayer was affected by the presence of the excipients in the aqueous and oil phases where the disruption of the interfacial film was concentration dependent. The oscillation torque needed to disrupt the interfacial film after two hours of protein adsorption in the presence of NaCl (0.1 M and 1 M) and DPPC ($5x10^{-4}$ % w/v) were significant lower than for native BSA alone. This could mean that native BSA in the presence of these excipients formed an interfacial film which is less densely cover by proteins than for films of native BSA alone. Additionally, it seems that the amount of adsorbed proteins in the interfacial film is critical to give strong properties to the interfacial films in comparison with the presence of excipients like NaCl or DPPC. This seems to be in agreement with the frequency sweep measurements. Native, globular protein interacts to produce a tight film where the entire interface is densely covered whereas the presence of excipients in the aqueous or oil phase could produce a softer, less densely packed film (**Table 5.1**). However, the value of the power law exponent (n) for native BSA alone and native BSA in the presence of NaCl and, phospholipids showed no significant differences ($P > 0.05$).

The coefficient of variation was calculated to know the variability associated with the various measurements. Interfacial rheology measurements had higher values of CV (%) than for IFT

measurements. This may be explained because IFT measurements required only one step to start the measurements (i.e. a drop of protein solution (aqueous phase) formed at the tip of a syringe was lowered into a glass cuvette containing the oil phase). Whereas, for rheology measurements more steps are involved (i.e. 18.8 mL of the water phase are added to into the Delrin® trough, the DWR was lowered onto the water phase surface, a meniscus was formed between the ring and the water phase which confirmed a physical contact between the ring and the water phase and, 18.8 ml of the oil phase was carefully poured on top). Moreover, native BSA in the presence of excipients (i.e. DPPC ($1x10^{-3}$ and $5x10^{-4}$) and PBuA ($8.75x10^{-3}$ % w/v) had the highest values of CV % for G' and G" moduli and complex viscosity. However, these values may be explained because native BSA in the presence of those excipients shown protein desorption from the oil-water interface affecting the variability of the measurement.

5.5. Conclusions

The combination of interfacial rheology and IFT measurements was useful to study the kinetics of protein adsorption to the oil-water interface in the presence of excipients (NaCl, phospholipids and polymers). However, interfacial rheology has been shown to be a more useful method than IFT measurements to investigate the kinetics of protein desorption from the oil-water interface for native proteins in the presence of these excipients at the concentrations and time scales used in this Chapter. The decrease in the IFT for native BSA in the presence of excipients is attributed to an increase in protein adsorption or excipient adsorption to interfaces [228] which was higher for native BSA in the presence of NaCl (0.5 M, 0.1 M and 1 M) than for BSA in the presence of phospholipids and polymers. Phospholipids were more useful to prevent protein adsorption to interfaces than polymers (PDMAEMA and PBuA) within the two hours of protein adsorption. The adsorbed protein to the oil-water interface was desorbed in the presence of phospholipids without affecting the physical stability of the secondary structure of BSA as shown by FTIR. Additionally, these results suggest that PDMAEMA could be a better polymer to avoid protein adsorption to interfaces than PBuA because PDMAEMA did not alter the secondary structure of BSA but a higher concentration would be needed.

Chapter 6: General discussion and future directions

Protein drugs may suffer physical and chemical degradation caused by molecular interactions between proteins and excipients in the formulation and environmental conditions during formulation and storage (e.g. temperature, pH, pressure and interfacial adsorption) [24,32,194]. The presence of degraded proteins is associated with a reduction in the therapeutic activity of the protein as well as increase of protein toxicity (i.e. immunogenic response) [32]. Protein degradation and the decrease in protein therapeutic effect make necessary to develop methods for easy detection and quantification of protein degradation and to investigate the intrinsic characteristics of proteins and interfaces that may avoid its adsorption to interfaces. In this thesis, the physical stability of proteins in solution was investigated by assessing protein conformation (i.e. secondary and tertiary structure) in the bulk phase as well as the kinetics of protein adsorption to oil-water interfaces.

Previous research indicates that the protein structure should be studied using a combination of different analytical techniques [49,73] (e.g. BSA and HSA were analyzed using differential scanning calorimetry, FTIR and fluorescence spectroscopy [73]). In this thesis, spectroscopy (FTIR and fluorescence) and SEC were used as analytical techniques to characterize and quantify different forms of proteins in solution (i.e. folded, unfolded and partially unfolded protein). FTIR and fluorescence spectroscopy gave information about secondary and tertiary structure of proteins, respectively [49,54,165-167]. SEC detected the presence/absence of soluble aggregates in BSA solutions [24,75,194,195] as consequence of heat-treatment. Analytical techniques like circular dichroism spectroscopy (i.e. far-UV CD and near-UV CD) and light scattering could also be used to investigate the physical stability of BSA in solution [163,251]. Results from those methods (i.e. circular dichroism spectroscopy and light scattering) could potentially be used to compare the information obtained from FTIR and fluorescence spectroscopy. Far-UV CD provides information about secondary structure of proteins whereas near-UV CD gives information about tertiary structure of proteins [163,194]. Light scattering investigate qualitative information about protein structure [29] which has been used to characterise protein aggregation, protein interactions and study the enzymatic activity of proteins [194,251]. In this research, the use of light scattering may detect the presence of BSA aggregates (i.e. traces) which may confirm SEC results obtained in this thesis. However, light scattering does not provide quantitative information [29] so that, light scattering can not be used to replace the quantitative information obtained using SEC.

FTIR and fluorescence spectra were pre-processed using several algorithms including AN [145], BC [58,131], 1st and 2nd D [58,145], MSC, SNV [66,145,147] to assess which pre-processing technique (or combination of techniques) gave the most complete and detailed information about protein structure in solution (i.e. folded, partially unfolded and unfolded protein) (**Chapter 2 section 2.3**). Then, pre-processing spectra were used to investigate which of those pre-processing methods could quantify native protein concentration using the best linear PLS regression model (**Chapter 3 section 3.3.1**).

In previous studies, data generated by the use of spectroscopy in combination with MVA, to investigate protein structure, has been analyzed through several methods, including MCR-ALS analysis [177], PLS-DA [176], iPLS methods [178] and PLS [62]. The present research shows a good agreement with those studies giving qualitative and quantitative information about protein content. In this thesis, results from the PLS analysis of spectroscopy data confirmed that the combination of those methods (i.e. PLS regression and spectroscopy (FTIR and fluorescence) could be used to quantify native protein content in solution. In particular, the best fitted model using FTIR spectra (i.e. 2nd D with 11 points smoothing, BC and AN spectra) was explained by three PLS factors; with RMSE= 0.91% and 1.64% and R^2= 0.997 and 0.991 for the calibration and prediction sets, respectively (**Chapter 3 sections 3.3.2**). Meanwhile, the best fitted model using fluorescence spectra (i.e. BC and AN spectra) was explained by one PLS factor, with RMSE% = 1.38% and 1.32% and R^2 of 0.993 and 0.994 for the calibration and prediction, respectively (**Chapter 3 sections 3.3.3**). To the best of this author's knowledge, there are no other published studies showing that native protein concentration has been quantified using the same combination of pre-processing techniques combined with a PLS model. One possible explanation is that current methods of protein quantification (i.e. curve fitting and deconvolution) in combination with PLS regression models have shown a good linearity so that, alternative methods of spectral quantification have not been investigated. Additionally, pre-processing methods used in this thesis require multiple steps, which could be considered as time consuming.

PLS regression modelling used in combination with spectroscopy has shown to be useful as an alternative to current methods for protein quantification (i.e. area overlap [60] and deconvolution methods for FTIR spectroscopy [58,60] and linear regression between maximum intensity vs. protein concentration using fluorescence spectroscopy [69]). In this thesis, the area

overlap method showed poorer linear fit between area overlap and native protein concentration (R^2 = 0.973) than for PLS model (R^2 = 0.997) (**Chapter 3 section 3.3.2**). This may be explained because the quantification of protein concentration using an univariate regression model (i.e. the area overlap vs. concentration) gave less robust models than for multivariate regression models (i.e. PLS). Likewise, the R^2 value for linear regression between fluorescence intensity at the maximum emission was 0.860 compared to 0.993 for PLS model (**Chapter 3 section 3.3.3**). The linearity obtained from those methods confirmed that the use of PLS to quantify protein concentration should be seriously considered to determinate protein content in future research. An extensive literature review did not find any previous studies reporting a similar comparison between the linearity obtained using those methods (i.e. area overlap and maximum fluorescence intensity vs. PLS regression models). Therefore, results showed in this thesis can not be compared to similar studies. The area overlap has been reported as a suitable method to compare modifications in the secondary structure of proteins attributed to loss of protein stability [60,73]. Jorgensen *et al*. (2004) reported the use of area overlap to investigate changes in the secondary structure of HSA and BSA proteins as result of exposition of these native proteins to different surrounding environment (i.e. water in oil emulsions) [73].

Beta regression models were used to assess differences in native protein concentration, quantified by spectroscopy and PLS regression, to native protein concentration quantified by SEC. Statistical analysis using beta regression models was chosen because this family of models allows a direct use of data bound between 0 – 1, such as proportions or percentages, avoiding the need of data transformation. The obtained results showed that FTIR spectroscopy, fluorescence spectroscopy, and SEC methods are able to measure equivalent protein concentrations, and no statistically significant difference between those methods was found (**Chapter 3 section 3.3.5**). The comparison of FTIR spectroscopy, fluorescence spectroscopy, and SEC methods for protein quantification, has not been studied before. Based on results presented in Chapters 2 and 3 of this thesis, this may be an important tool for researchers who want to evaluate which pre-processing technique provides the most relevant information about the physical stability of proteins in solution and also, which of these pre-processing techniques may be more appropriate to quantify native protein concentrations in liquid formulations.

Recent studies have described the use of a rheometer with a DWR geometry to study protein viscoelastic properties at the air-water and oil-water interfaces [97,101,104,206,252,253]. Some of these publications have described the application of this geometry to study the kinetics of protein adsorption to interfaces in the presence of excipients [94,101]. However, the kinetics of protein desorption from the oil-water interface in the presence of excipients has not received attention. In this thesis, the kinetics of protein adsorption/desorption to liquid-liquid interfaces was investigated for native proteins in the absence and presence of heat-denatured BSA (Chapter 4) and for native proteins in the presence of excipients (Chapter 5). Those analyses were performed using a rheometer with DWR geometry and interfacial tension measurements. The data analysis provided quantitative evidence of modifications in the interfacial film for native BSA alone and native BSA in the presence of thermally denatured BSA and/or excipients (i.e. NaCl, phospholipids and polymers). Results obtained from this thesis may be used to support the use of the DWR geometry in rheological studies of protein physical stability. Results obtained using this geometry confirmed the application of this method to investigate protein adsorption to interfaces, and its sensitivity to detect the formation of viscoelastic films at the oil-water interface, in the presence of different forms of proteins (i.e. folded, partially unfolded and unfolded) (Chapter 4). The method was also appropriate to investigate protein desorption from the oil-water interface in the presence of excipients (Chapter 5). This is a relevant information since protein adsorption to interfaces may affect protein physical stability in solution and the use of excipients may modify (i.e. delayed) the kinetic of protein adsorption to interfaces. Additionally, this approach could be used to investigate the effect of other factors involved in protein adsorption to interfaces, such as the influence of the interface itself (i.e. density of interface and protein solutions, hydrophobicity of proteins and interface and surface activity) as well as concentration of proteins and surface activity of proteins. The rheometer with DWR geometry attached is an indirect method which provide qualitative information on the kinetic of protein adsorption to interfaces.

Protein adsorption to interfaces is one of the relevant factors explaining protein physical stability in solution [24,35,104,194], representing the main research interest of this thesis. In future work, the application of interfacial rheology studies with the DWR geometry attached could be used to systematically investigate the kinetic of protein adsorption/desorption in the presence of other excipients of pharmaceutical interest such surfactants, sugars and antioxidants [24,112,114]. Moreover, the application of this equipment could investigate proteins

adsorption to interfaces in the presence of a mix of proteins, plus diverse excipients in the bulk phase. This work may be relevant since proteins are not formulated as pure ingredients and the interaction of different excipients with protein in solution must result in different kinetic of protein adsorption to interfaces. This method would provide information about earlier modifications in the kinetic of protein adsorption to liquid-liquid interfaces (i.e. oil-water emulsion) as consequence of protein interaction with excipients.

In pharmaceutical formulations, chemical modifications of proteins (i.e. acylation and PEGylation of proteins) are used to increase protein plasma half life in solutions decreasing proteins degradation. Those modifications also affect the kinetic of proteins adsorption to interfaces explained due to modifications in the hydrophobic/hydrophilic characteristics of proteins [42,107,254]. As examples, insulin was acylated to compare the interfacial adsorption of insulin and acylated insulin to hydrophobic interfaces (i.e. polystyrene beads) showing that both, insulin and acylated insulin, had a higher affinity by the hydrophobic interface than for the hydrophilic interface [254]. Moreover, PEGylation of glucagon reduced the interfacial adsorption of glucagon to hydrophobic interfaces (i.e. polystyrene beads, silicon wafers coated with polystyrene and quartz wafers coated with silane) [107].

The study of protein adsorption to liquid-liquid interfaces, using interfacial dilatational rheology measurements [104] is another avenue for future research. This measurement is used to gain information about structure of adsorbed protein to interfaces (i.e. monolayer and multilayer formation) [255]. Examples of methods used in dilatational interfacial measurements are: Langmuir [98,256] and the oscillation bubble methods [98]. The Langmuir trough apparatus can be used to study the monolayer formed due to adsorption of molecules (e.g. proteins and phospholipids) to interfaces by changing the area of the interface from a maximum to a minimum, i.e. by compression and expansion deformation [98,104,256,257]. In the Langmuir trough apparatus, the interfacial area is expanded and compressed moving the wall of the apparatus [98]. The use of a Langmuir trough apparatus was reported by Murray *et al.* (1997) to investigate bovine *β*-lactoglobulin protein adsorption to the oil-water and air-water interfaces in the presence of non-ionic surfactants [258]. The sensitivity shown by the Langmuir trough apparatus to detect differences in protein adsorption to the oil-water interface in the presence of excipients was in agreement with the sensitivity shown by shear rheology measurements reported in this thesis. Langmuir and shear rheology measurements can detect earlier changes in the kinetic of protein adsorption to the oil-water interface in the presence of small amount

of excipients. Therefore, measurements using the Langmuir trough apparatus could provide complementary information about the monolayer and multilayer formation at the oil-water interface to the oscillatory shear rheology results presented in this thesis. Moreover, Wang *et al.* (2012) reported the use of oscillation bubble measurements to investigate protein adsorption to liquid-liquid interfaces, where the area of the interface was changed by increasing and decreasing the size of the drop in ten percent from its initial size [255]. In this method, the size of the drop is automatically changed to specific values of amplitude and frequency [255,259]. The increase in surface pressure as a function of time was considered to be an indicator of protein adsorption to interfaces [98,255]. The oscillation bubble method was used to investigate the kinetics of protein adsorption of native and heat-denatured (at 90 and 120 °C) soy protein isolate to the oil-water interface [255]. Those results reported a faster interfacial pressure and dilatational modulus for the heat-denatured soy protein isolate than for its native form. These results were attributed to an increase in the protein flexibility and exhibition of hydrophobic groups to the oil-water interface as result of heat treatment of soy protein isolate. Similar results were described for other models of proteins like α-lactalbumin and β-lactoglobulin [255]. However, this is in disagreement with results shown in this thesis where the heat-denatured BSA protein shown a delayed in the kinetic of protein adsorption in comparison with native BSA alone (**Figure 4.4**). For that reason, the use of oscillation bubble measurements could give information about surface pressure and dilatational modulus, being a potential complementary technique to the interfacial tension method used in this thesis.

Ellipsometry is another method that could be used in future work. This technique has been used to investigate the thicknesses and refractive index of interfacial films [260,261]. However, while the application of this method has been widely reported to study solid-liquid and air-liquid interfaces [261,262], only a few reports applying this method to liquid-liquid interfaces can be found [263]. As an example, Kull *et al*. (1997) reported the use of ellipsometry to investigate the mechanism of protein adsorption to solid interfaces (i.e. sequential or competitive) using *β*-casein and *β*-lactoglobulin [261]. The study of protein adsorption to liquid-liquid interfaces using ellipsometry could give relevant information about differences in the thicknesses of interfacial films of native BSA vs. native BSA in the presence of denatured proteins or excipients, which may complement the results obtained in this thesis. However, it is important to consider and carefully investigate limitations and sensitivity of these complementary techniques.

The methodology used in this thesis (i.e. spectroscopy in combination with MVA as well as interfacial adsorption methods) was used to study physical stability of BSA could be extended to investigate physical degradation of other kinds of proteins in solution i.e. globular and non-globular proteins as well as therapeutic drugs like monoclonal antibodies, hormones and vaccine antigens. Additionally, this work could be extended to investigate the physical stability of proteins in pharmaceutical formulations (e.g. emulsions or reconstituted feezed dried products) using the methods described in this thesis (i.e. quantification of protein physical stability in the aqueous phase using PLS models and, characterization of the kinetic of protein adsorption to the oil-water interface using interfacial adsorption methods (i.e. DWR rheometer and interfacial tension measurements).

Conclusions

The physical stability of proteins in solution was investigated in this thesis and the principal conclusions are highlighted in the following sentences. FTIR and fluorescence spectroscopy in combination with PLS regression models were an efficient approach to develop a method of protein characterization and quantification. Those PLS models were able to detect small amounts of unfolded proteins in the bulk solution predicting native protein concentrations in solutions heated at 40, 50 and 60°C for ten minutes. This means that those quantification methods (i.e. PLS models) are helpful to determine product shelf-life in a short time frame (i.e. ten minutes). The linearity of the PLS models was improved when pre-processing techniques were applied to the raw spectral data. This thesis has shown that FTIR and fluorescence spectroscopy and PLS regression models are alternatives to current methods of protein quantification like curve fitting and deconvolution. Moreover, the adsorption of native protein to the oil-water interfaces was affected by the presence of unfolded proteins and excipients (i.e. NaCl and polymers) added in the bulk solution and in the oil phase (i.e. phospholipids). Using a rheometer with the DWR geometry attached, a sensitive method to detect changes in the kinetics of native protein adsorption to the interface in the presence of those components in the bulk solution was developed. This method was useful to get qualitative information explaining the first steps of protein adsorption to the oil-water interface (i.e. the time to cross-over and the maximum magnitude for G' and G") as well as to characterize the final properties of the interfacial film (i.e. solid-like properties). In summary, results obtained from this thesis contribute to the understanding of protein physical stability in solution by the evaluation of alternative quantification methods (i.e. PLS and spectroscopy) and techniques which detect earlier changes in the kinetics of protein adsorption to interfaces as consequence of protein degradation.

References

1. Walsh G 2006. Biopharmaceutical benchmarks 2006. Nat Biotechnol 24(7):769-776.
2. Leader B, Baca QJ, Golan DE 2008. Protein therapeutics: a summary and pharmacological classification. Nat Rev Drug Discov 7(1):21-39.
3. Malik NN 2008. Drug discovery: past, present and future. Drug Discov Today 13(21-22):909-912.
4. Dimitrov DS 2010. Therapeutic antibodies, vaccines and antibodyomes. MAbs 2(3):247-356.
5. Wendt MD. 2012. Protein-protein intercations as drug targets. Protein-protein intercations, ed., Berlin Springer-Verlag p1-55.
6. Knablein J. 2013. Twenty thousand years of biotech-from "traditional" to "modern biotechnology". Modern biopharmaceuticals Recent success stories, ed., Weinheim: Wiley-Blackwell. p 3-38.
7. Arakawa T, Philo JS. 2013. Biophysical and biochemical analysis of recombinant proteins. Pharmaceutical biotechnology: Fundamentals and applications, ed., New York: Springler. p 19-46.
8. Jorgensen L, Moeller EH, van de Weert M, Nielsen HM, Frokjaer S 2006. Preparing and evaluating delivery systems for proteins. Eur J Pharm Sci 29(3-4):174-182.
9. van de Weert M, Jorgensen L, Horn Moeller E, Frokjaer S 2005. Factors of importance for a successful delivery system for proteins. Expert Opin Drug Deliv 2(6):1029-1037.
10. Crommelin D. 2013. Formulation of biotech products, including biopharmaceutical considerations. Pharmaceutical biotechnology Fundamentals and applications, ed., New York: Springer. p 69-100.
11. Cleland JL, Daugherty A, Mrsny R 2001. Emerging protein delivery methods. Curr Opin Biotech 12(2):212-219.
12. Oosting RS. 2013. Molecular biotechnology: From DNA sequence to therapeutic protein. Pharmaceutical biotechnology Fundamentals and applications, ed., New York: Springler. p 1-18.
13. Walsh G 2010. Biopharmaceutical benchmarks 2010. Nat Biotechnol 28(9):917-924.
14. Walsh G 2012. New biopharmaceuticals. BioPharm International 25(6):34-38.
15. Walsh G 2013. Milestones and moderate progress in 2012 drug approvals. BioPharm International 26(4):54-56.
16. Ryan MP, Walsh G 2012. Veterinary-based biopharmaceuticals. Trends Biotechnol 30(12):615-620.
17. Campbell N, Reece J, Mitchell L. 1999. The structure and function of macromolecules. Biology, 5th ed.: Adisson Wesley Longman, Inc. p 65-77.
18. Maldonado AA, Ribeiro JM, Sillero A 2010. Isoelectric point, electric charge, and nomenclature of the acid–base residues of proteins. Biochem Mol Biol Edu 38(4):230-237.
19. Lesk A. 2004. Introduction to protein science: Architecture, function and genomics. ed.: New York Oxford University Press.
20. Mc Murry J. 1992. Aminoacids, peptids and proteins. Organic chemistry, ed., Mexico: Grupo editorial iberoamericana S.A. de C.V. p 1011-1054.
21. Chen T 1992. Formulation concerns of protein drugs. Drug Dev Ind Pharm 18(11-12):1311-1354.
22. Murphy R, Tsai A. 2006. Protein folding, misfolding, stability and aggregation. Misbehaving proteins: protein (mis)folding, aggregation and stability, ed., New York Springer Science and Business Media, LLC. p 3-13.

23. Ragoonanan V, Aksan A 2007. Protein Stabilization. Transfus Med Hemoth 34(4):246-252.
24. Wang W 1999. Instability, stabilization, and formulation of liquid protein pharmaceuticals. Int J Pharm 185(2):129-188.
25. Tompa P 2002. Intrinsically unstructured proteins. Trends Biochem Sci 27(10):527-533.
26. Linding R, Russell RB, Neduva V, GibsoN TJ 2003. GlobPlot: exploring protein sequences for globularity and disorder. Nucleic Acids Research 31(13):3701-3708.
27. Wright PE, Dyson JH 1999. Intrinsically unstructured proteins: re-assessing the protein structrure-function paradigm. J Mol Biol (293):321-331.
28. Wootton JC 1994. Non-globular domains in protein sequences: automated segmentation using complexity measures. Computers Chem 18(3):269-285.
29. Engelsman J, Garidel P, Smulders R, Koll H, Smith B, Bassarab S, Seidl A, Hainzl O, Jiskoot W 2011. Strategies for the Assessment of Protein Aggregates in Pharmaceutical Biotech Product Development. Pharm Res 28(4):920-933.
30. Rosenberg A 2006. Effects of protein aggregates: An immunologic perspective. AAPS J 8(3):E501-E507.
31. Baker M, Reynolds H, Lumicisi B, CJ. B 2010. Immunogenicity of protein therapeutics: The key causes, consequences and challenges. Self/Nonself (1):314-322.
32. Mahler H-C, Friess W, Grauschopf U, Kiese S 2009. Protein aggregation: Pathways, induction factors and analysis. J Pharm Sci 98(9):2909-2934.
33. Kendrich BS, Dong A, Allison D, Manning MC, Carpenter JF 1995. Quantifycation of the area of overlap between second derivative amide I infrared spectra to determine the structural similarity of a protein in different states. J Pharm Sci 2(85):155-158.
34. Chiti F, Dobson CM 2006. Protein Misfolding, Functional Amyloid, and Human Disease. Annu Rev Biochem 75(1):333-366.
35. Chi EY, Krishnan S, Randolph TW, Carpenter JF 2003. Physical stability of proteins in aqueous solution: Mechanism and driving forces in nonnative protein aggregation. Pharm Res 20(9):1325-1336.
36. Schon A, Velasquez-Campoy A. 2005. Calorimetry. In Jiskoot W, Crommelin D, editors. Methods for structural analysis of protein pharmaceuticals, ed., Arlington: AAPS. p 578-581.
37. Dill KA 1990. Dominant forces in protein folding Biochemistry 29 (31):7133-7155.
38. Murphy RM, Kendrick BS 2007. Protein misfolding and aggregation. Biotechnology Prog 23(3):548-552.
39. Wang W 2005. Protein aggregation and its inhibition in biopharmaceutics. Int J Pharm 289(1–2):1-30.
40. Foguel D, Silva JL 2004. New Insights into the Mechanisms of Protein Misfolding and Aggregation in Amyloidogenic Diseases Derived from Pressure Studies†. Biochemistry 43(36):11361-11370.
41. Khurana R, Gillespie JR, Talapatra A, Minert LJ, Ionescu-Zanetti C, Millett I, Fink AL 2001. Partially Folded Intermediates as Critical Precursors of Light Chain Amyloid Fibrils and Amorphous Aggregates†. Biochemistry 40(12):3525-3535.
42. Frokjaer S, Otzen DE 2005. Protein drug stability: a formulation challenge. Nat Rev Drug Discov 4(4):298-306.
43. Mauerer A, Lee G 2006. Changes in the amide I FT-IR bands of poly-l-lysine on spray-drying from α-helix, β-sheet or random coil conformations. Eur J Pharm Biopharm 62(2):131-142.
44. Rainer J 1991. Protein stability and molecular adaptation to extreme conditions Eur J Biochem 202(3):715-728.

45. Hagiwara T, Kumagai H, Nakamura K 1996. Fractal analysis of aggregates formed by heating dilute BSA solutions using light scattering methods. Biosci Biotech Bioch 60(11):1757-1763.
46. Booth DR, Sunde M, Bellotti V, Robinson CV, Hutchinson WL, Fraser PE, Hawkins PN, Dobson CM, Radford SE, Blake CCF, Pepys MB 1997. Instability, unfolding and aggregation of human lysozyme variants underlying amyloid fibrillogenesis. Nature 385(6619):787-793.
47. Nielsen L, Frokjaer S, Carpenter JF, Brange J 2001. Studies of the structure of insulin fibrils by Fourier transform infrared (FTIR) spectroscopy and electron microscopy. J Pharm Sci 90(1):29-37.
48. Jackson M, Mantsch HH 1995. The use and misuse of FTIR spectroscopy in the determination of protein structure. Crit Rev Biochem Mol 30(2):95-120.
49. Arvinte T. 2005. Concluding remarks: analytical methods for protein formulations. Methods for structural analysis of protein pharmaceuticals, 1st ed., Arlington: American Association of Pharmaceutical Scientists. p 661-666.
50. Arvinte T, Cudd A, Drake AF 1993. The structure and mechanism of formation of human calcitonin fibrils. J Biol Chem 268(9):6415-6422.
51. Zölls S, Tantipolphan R, Wiggenhorn M, Winter G, Jiskoot W, Friess W, Hawe A 2012. Particles in therapeutic protein formulations, Part 1: Overview of analytical methods. J Pharm Sci 101(3):914-935.
52. Jiskoot W, Crommelin D. 2005. Methods for structural analysis of protein pharmaceuticals. ed., Arlington: AAPS.
53. Carvalho A, Trincão J, Romão M. 2010. X-Ray Crystallography in Drug Discovery. Ligand-Macromolecular Interactions in Drug Discovery, ed.: Humana Press. p 31-56.
54. Barth A 2007. Infrared spectroscopy of proteins. Biochim Biophys Acta 1767(9):1073-1101.
55. Smith BC. 1996. Fundamentals of fourier transform infrared spectroscopy. ed., Boca Raton CRC Press, Inc.
56. Gunzler HG, Ulrich H. 2002. IR Spectroscopy: an introduction. ed., Weinheim, Cambridge Wiley-VCH Verlag GMBh.
57. Smith BC. 2002. Quantitative spectroscopy: theory and practice. ed., San Diego: Elsevier Science.
58. Stuart B. 2004. Spectral analysis. Infrared spectroscopy: fundamentals and applications, ed., West Sussex: John Willey and Sons, Inc. p 45-70.
59. Brown W. 1995. Organic Chemistry. ed., USA: Sounder collegue publisheing.
60. van de Weert M, Joachim A, Haris P. 2005. Fourier transform infrared spectroscopy. Methods for structural analysis of protein pharmaceuticals, 1st ed., Arlington: AAPS. p 131-157.
61. Dong A, Prestrelski SJ, Allison D, Carpenter JF 1994. Infrared spectrosocpy studies of lyophilization and temperature induced protein aggregation. J Pharm Sci 4(84):415-424.
62. Belanche A, Weisbjerg MR, Allison GG, Newbold CJ, Moorby JM 2013. Estimation of feed crude protein concentration and rumen degradability by Fourier-transform infrared spectroscopy. J Dairy Sci 96(12):7867-7880.
63. Calabrò E, Magazù S 2013. Non-Thermal Effects of Microwave Oven Heating on Ground Beef Meat Studied in the Mid-Infrared Region by Fourier Transform Infrared Spectroscopy. Spectrosc Lett 47(8):649-656.
64. Stuart B. 2004. Biological applications. Infrared spectrosocopy: fundamentals and applications, ed.: John Wiley and Sons Ltd. p 137-165.
65. Haris PI 1999. Characterization of protein structure and stability using fourier transform infrared spectroscopy. Pharm Pharmacol Comm 5(1):15-25.

66. Varmuza K, Filzmoser P. 2009. Preprocessing. Introduction to multivariate statistical analysis in chemometrics ed., Boca Raton: CRC Press Taylor and Francis Group.
67. Rahmelow K, Hübner W, Ackermann T 1998. Infrared Absorbances of Protein Side Chains. Anal Biochem 257(1):1-11.
68. Grob PC, Zeppezauer M 2010. Infrared spectroscopy for biopharmaceutical protein analysis. J Pharm Biomed Anal (53):29-36.
69. Jiskoot W, Viesser AJWG, Herron JN, Sutter M. 2005. Fluorescence spectroscopy. Methods for structural analysis of proteins pharmaceuticals, ed., Arlington: American Association Pharmaceutical Scientist Press. p 27-56.
70. Albani JR. 2007. Fluorescence spectroscopy principles. Principles and applications of fluorescence spectroscopy, ed., Oxford: Blackwell Publishing. p 101-105.
71. White NS, Errington R 2005. Fluorescence technqiues for drug delivery research: theory and practice. Adv Drug Deliv Rev 57(1):17-42.
72. Creighton TE. 1997 Protein structure a practical approach. ed., New York Oxford University Press.
73. Jorgensen L, Weert MVD, Vermehren C, Bjerregaard S, Frokjaer S 2004. Probing structural changes of proteins incorporated into water-in-oil emulsions. J Pharm Sci 93(7):1847-1859.
74. Walstra P, De Roos AL 1993. Proteins at air-water and oil-water interfaces: Static and dynamic aspects. Food Rev Int 9(4):503-525.
75. Tatford OC, Gomme PT, Bertolini J 2004. Analytical techniques for the evaluation of liquid protein therapeutics. Biotechnol Appl Biochem 40(1):67-81.
76. Snyder L, Kirkland J, Glajch J. 1997. Biochemical samples: Proteins, nucleic acids, carbohydrates and related components. Practical HPLC method development, ed., New York: John Wiley and Sons, Inc. p 521-536.
77. Snyder L, Kirkland J, Glajch J. 1997. Quantitation (Including trace analysis). Practical HPLC method development, ed., New York: Joh Willey and Sons, Inc. p 643-662.
78. Bischoff R, Barroso B. 2005. Liquid chromatography. Methods for structural analysis of protein pharmaceuticals, ed., Arlington: AAPS Press. p 277-329.
79. Varmuza K, Filzmoser P. 2009. Calibration. Introduction to multivariate statistical analysis in chemometrics, ed., Boca Raton: CRS Press Taylor and Francis Group.
80. Yohannes G, Wiedmer SK, Elomaa M, Jussila M, Aseyev V, Riekkola ML 2010. Thermal aggregation of bovine serum albumin studied by assymetrical flow fiel-flow fractionation. Anal Chim Acta 675(2):191-198.
81. Beebe KR, Pell RJ, Seasholtz MB. 1998. Pre-processing. Chemometrics: A practical guide, ed., New York: John Wiley and Sons, Inc. p 26-55.
82. Varmuza K, Flizmoser P. 2009. Introduction. Introduction to multivariate statistical analysis in chemometrics, ed., Boca Raton: CRS Press Taylor and Francis Group.
83. Bro R 2003. Multivariate calibration: What is in chemometrics for the analytical chemist? Anal Chim Acta 500(1–2):185-194.
84. Varmuza K, Filzmoser P. 2009. Multivariate data. Introduction to multivariate statistical analysis in chemometrics ed., Boca Raton: CRC Press Taylor and Francis Group.
85. Mia H. 2006. Robust Calibration. Practical Guide To Chemometrics, Second Edition, ed.: CRC Press. p 167-216.
86. Brereton RG. 2007. Calibration. Applied Chemometrics for Scientists, 1 ed., Chichester: John Wiley and Sons Ltd. p 193-220.
87. Gabrielsson J, Lindberg N-O, Lundstedt T 2002. Multivariate methods in pharmaceutical applications. J Chemom 16(3):141-160.
88. Wold S, Sjöström M, Eriksson L 2001. PLS-regression: a basic tool of chemometrics. Chemom Intell Lab Syst 58(2):109-130.

89. Pinholt C, Hartvig RA, Medlicott NJ, Jorgensen L 2011. The importance of interfaces in protein drug delivery – why is protein adsorption of interest in pharmaceutical formulations? Expert Opin Drug Deliv 8(7):949-964.
90. Yampolskaya G, Platikanov D 2006. Proteins at fluid interfaces: Adsorption layers and thin liquid films. Adv Colloid Interface Sci 128–130(0):159-183.
91. Koo J, Erlkamp M, Grobelny S, Steitz R, Czeslik C 2013. Pressure-Induced Protein Adsorption at Aqueous–Solid Interfaces. Langmuir 29(25):8025-8030.
92. Norde W, Giacomelli CE 2000. BSA structural changes during homomolecular exchange between the adsorbed and the dissolved states. J Biotechnol 79(3):259-268.
93. Baldursdottir SG, Fullerton MS, Nielsen SH, Jorgensen L 2010. Adsorption of proteins at the oil/water interface—Observation of protein adsorption by interfacial shear stress measurements. Colloids Surfaces B 79(1):41-46.
94. Colac S, Guzman P, Medlicott N, Tehnu H, Niskanen J, Alhoranta A, Jorgensen L, Baldursdottir S. Annual transactions of the nordic rheology society Copenhagen, Denmark, 2013.
95. Beverung CJ, Radke CJ, Blanch HW 1999. Protein adsorption at the oil/water interface: characterization of adsorption kinetics by dynamic interfacial tension measurements. Biophys Chem 81(1):59-80.
96. Santiago LG, Maldonado-Valderrama J, Martín-Molina A, Haro-Pérez C, García-Martínez J, Martín-Rodríguez A, Cabrerizo-Vílchez MA, Gálvez-Ruiz MJ 2008. Adsorption of soy protein isolate at air–water and oil–water interfaces. Colloids Surfaces A 323(1–3):155-162.
97. Wang L, Xie H, Qiao X, Goffin A, Hodgkinson T, Yuan X, Sun K, Fuller GG 2011. Interfacial Rheology of Natural Silk Fibroin at Air/Water and Oil/Water Interfaces. Langmuir 28(1):459-467.
98. Bos M, van Vliet T 2001. Interfacial rheological properties of adsorbed protein layers and surfactants: a review. Adv Colloid Interface Sci 91(3):437-471.
99. Vlieghe P, Lisowski V, Martinez J, Khrestchatisky M 2010. Synthetic therapeutic peptides: science and market. Drug Discov Today 15(1–2):40-56.
100. de Jongh HHJ, Kosters HA, Kudryashova E, Meinders MBJ, Trofimova D, Wierenga PA 2004. Protein adsorption at air–water interfaces: A combination of details. Biopolymers 74(1-2):131-135.
101. Baldursdottir SG, Jorgensen L 2011. The influence of size, structure and hydrophilicity of model surfactants on the adsorption of lysozyme to oil–water interface—Interfacial shear measurements. Colloids Surfaces B 87(1):96-102.
102. Freer EM, Yim KS, Fuller GG, Radke CJ 2004. Interfacial Rheology of Globular and Flexible Proteins at the Hexadecane/Water Interface: Comparison of Shear and Dilatation Deformation. J Phys Chem B 108(12):3835-3844.
103. Norde W 2008. My voyage of discovery to proteins in flatland …and beyond. Colloids Surfaces B 61(1):1-9.
104. Fuller GG, Vermant J 2012. Complex Fluid-Fluid Interfaces: Rheology and Structure. Annu Rev Chem Biom Eng 3(1):519-543.
105. Pinholt C, Kapp SJ, Bukrinsky JT, Hostrup S, Frokjaer S, Norde W, Jorgensen L 2013. Influence of acylation on the adsorption of GLP-2 to hydrophobic surfaces. Int J Pharm 440(1):63-71.
106. Pinholt C, Fanø M, Wiberg C, Hostrup S, Bukrinsky JT, Frokjaer S, Norde W, Jorgensen L 2010. Influence of glycosylation on the adsorption of Thermomyces lanuginosus lipase to hydrophobic and hydrophilic surfaces. Eur J Pharm Sci 40(4):273-281.

107. Pinholt C, Bukrinsky JT, Hostrup S, Frokjaer S, Norde W, Jorgensen L 2011. Influence of PEGylation with linear and branched PEG chains on the adsorption of glucagon to hydrophobic surfaces. Eur J Pharm Biopharm 77(1):139-147.
108. Maldonado-Valderrama J, Patino JMR 2010. Interfacial rheology of protein–surfactant mixtures. Curr Opin Colloid In 15(4):271-282.
109. Miller R, Ferri J, Javadi A, Krägel J, Mucic N, Wüstneck R 2010. Rheology of interfacial layers. Colloid Polym Sci 288(9):937-950.
110. Pelipenko J, Kristl J, Rošic R, Baumgartner S, Kocbek P 2012. Interfacial rheology: an overview of measuring techniques and its role in dispersions and electrospinning. Acta Pharm 6(2):123-140.
111. Kenji K. 2004. Contact Angle and Surface Tension Measurement. Surface and Interfacial Tension, ed.: CRC Press.
112. Ohtake S, Kita Y, Arakawa T 2011. Interactions of formulation excipients with proteins in solution and in the dried state. Adv Drug Deliv Rev 63(13):1053-1073.
113. Wu J, Li JB, Zhao J, Miller R 2000. Dynamic characterization of phospholipid/protein competitive adsorption at the aqueous solution/chloroform interface. Colloids Surfaces A 175(1–2):113-120.
114. Jorgensen L, Hostrup S, Moeller EH, Grohganz H 2009. Recent trends in stabilising peptides and proteins in pharmaceutical formulation – considerations in the choice of excipients. Expert Opin Drug Deliv 6(11):1219-1230.
115. Zhang Z, Dalgleish DG, Goff HD 2004. Effect of pH and ionic strength on competitive protein adsorption to air/water interfaces in aqueous foams made with mixed milk proteins. Colloids Surfaces B 34(2):113-121.
116. Magdassi S, Kamyshny A. 1996. Introduction: Surface activity and functional properties of proteins. In Magdassi S, editor Surface Activity of Proteins, ed.: CRC Press. p 1-38.
117. Peters T. 1995. The albumin molecule:Its structure and chemical properties. All About Albumin, ed., San Diego: Academic Press p9-75.
118. Estey T, Kang J, Schwendeman SP, Carpenter JF 2006. BSA degradation under acidic conditions: A model for protein instability during release from PLGA delivery systems. J Pharm Sci 95(7):1626-1639.
119. Rinnan A 2014. Pre-processing in vibrational spectroscopy - when, why and how. Anal Method 6(18):7124-7129.
120. Rinnan R, Rinnan Å 2007. Application of near infrared reflectance (NIR) and fluorescence spectroscopy to analysis of microbiological and chemical properties of arctic soil. Soil Biol Biochem 39(7):1664-1673.
121. Kher A, Udabage P, McKinnon I, McNaughton D, Augustin MA 2007. FTIR investigation of spray-dried milk protein concentrate powders. Vib Spectrosc 44(2):375-381.
122. Elshereef R, Budman H, Moresoli C, Legge RL 2006. Fluorescence spectrosocopy as a tool for monitoring solubility and aggregation behaviour of β-lactoglobulin after heat treatment. Biotechnol Bioeng 95(5):863-874.
123. Gemperline PJ. 2006. Future Trends in Chemometrics. Practical Guide To Chemometrics, 2nd ed.: CRC Press. p 509-520.
124. Steven DB. 2006. Signal Processing and Digital Filtering. Practical Guide To Chemometrics, 2nd ed.: CRC Press. p 379-416.
125. O'Haver T 2009. An introduction to signal processing in chemical analysis.
126. Chen D, Grant E 2012. Evaluating the validity of spectral calibration models for quantitative analysis following signal preprocessing. Anal Bioanal Chem (404):2317-2327.
127. Woodward AM, Alsberg BK, Kell DB 1998. The effect of heteroscedastic noise on the chemometric modelling of frequency domain data. Chemom Intell Lab Syst (40):101-107.

128. Devos O, Downey G, Duponchel L 2014. Simultaneous data pre-processing and SVM classification model selection based on a parallel genetic algorithm applied to spectroscopic data of olive oils. Food Chem 148(0):124-130.
129. Rinnan Å, Berg Fvd, Engelsen SB 2009. Review of the most common pre-processing techniques for near-infrared spectra. Trac-Trend Anal Chem 28(10):1201-1222.
130. Rinnan Å, Nørgaard L, van den Berg F, Thygesen J, Bro R, Engelsen SB. 2009. Data pre-processing. In Sun D-W, editor Infrared Spectroscopy for Food Quality Analysis and Control ed., San Diego: Academic Press. p 29-50.
131. Kendrick BS, Dong A, Allison SD, Manning MC, Carpenter JF 1996. Quantitation of the area of overlap between second-derivative amide I infrared spectra to determine the structural similarity of a protein in different states. J Pharm Sci 85(2):155-158.
132. Erickson L. 2006. Signal correction and compresion. Multi- and Megavariate data analysis: Part I, ed., Sweeden: Umetrics Academy. p 225.
133. Azzouz T, Puigdoménech A, Aragay M, Tauler R 2003. Comparison between different data pre-treatment methods in the analysis of forage samples using near-infrared diffuse reflectance spectroscopy and partial least-squares multivariate calibration method. Anal Chim Acta 484(1):121-134.
134. Powell JR, Wasacs FM, Jakobsen RJ 1986. An algorithm for the reproductible spectra subtraction of water form the FTIR spectra of proteins in dilute solutions and adsorbed monolayers. Appl Spectrosc 3(40):339-344.
135. Brereton RG. 2007. Pattern recognition. Applied chemometrics for scientists, ed., Chichester: John Wiley and Sons, Ltd. p 145-160.
136. Ni Y, Gu Y, Kokot S 2012. Interpreting analytical chemistry data: recent advancesin curve resolution with the aid of chemistry. Anal lett (45):933-948.
137. Dong A, Huang P, Caughey WS 1990. Protein secondary structures in water from second-derivative amide I infrared spectra. Biochemistry 29(13):3303-3308.
138. Dousseau F, Therrien M, Pézolet M 1989. On the spectral subtraction of water from the FT-IR spectra of aqueous solutions of proteins. Appl Spectrosc 43(3):538-542.
139. Kong J, Yu S 2007. Fourier Transform Infrared Spectroscopic Analysis of Protein Secondary Structures. Acta Biochimica et Biophysica Sinica 39(8):549-559.
140. Fadeev VV, Burikov SA, Volkov PA, Lapshin VB, Syroeshkin AV 2009. Raman scattering and fluorescence spectra of water from the sea surface microlayer. Oceanography 49(2):205-2010.
141. Oberg KA, Ruysschaert J-M, Goormaghtigh E 2004. The optimization of protein secondary structure determination with infrared and circular dichroism spectra Eur J Biochem (271):2937-2948.
142. Rinnan A, Norgaard L, van den Berg F, Thygesen J, Bro R, Engelsen SB. 2009. Data pre-processing. Infrared spectrosocopy for food and quality analysis and control, ed.: Elsevier Inc.
143. Brereton RG. 2007. Sequential methods Applied chemometrics for scientists, ed., West sussex: John Wiley and Sons, Ltd. p 116-120, 138-142.
144. Savitzky A, Golay MJE 1964. Smoothing and Differentiation of Data by Simplified Least Squares Procedures. Anal Chem 36(8):1627-1639.
145. Eriksson L, Johansson E, Kettaneh-Wold N, Trygg J, Wikstrom C, Wold S. 2006. Signal correction and compresion. Multi- and Megavariate Data Analysis: Part I ed., Umea: Umetrics Academy. p 224-225.
146. Owen T. 2000. Principles and applications of UV-visible spectroscopy. Fundamentals of modern UV-Visible spectrosoocpy, ed., Germany: Agilent Technologies. p 1-28.

147. Geladi P, MacDougall D, Martens H 1985. Linearization and Scatter-Correction for Near-Infrared Reflectance Spectra of Meat. Appl Spectrosc 39(3):491-500.
148. TheUnscramblerX®. 2014. The Unscrambler® appendices: method references In Team CSRD, editor, 10.2 ed., Oslo: CAMO Software AS. p multivariate data analysis and experimental design software solution, equipped with powerful methods including PCA, PLS, clustering and classification.
149. Helland IS, Næs T, Isaksson T 1995. Related versions of the multiplicative scatter correction method for preprocessing spectroscopic data. Chemom Intell Lab Syst 29(2):233-241.
150. Heinz A, Savolainen M, Rades T, Strachan CJ 2007. Quantifying ternary mixtures of different solid-state forms of indomethacin by Raman and near-infrared spectroscopy. Eur J Pharm Sci 32(3):182-192.
151. Fabian H, Naumann D. 2012. Millisecond-to-minute protein folding/misfolding events monitored by FTIR spectroscopy. Protein folding and misfolding Shining light by infrared spectroscopy, ed., Berlin: Springer. p 53-90.
152. Galvão MR, Costa SXS, Victorino KR, Ribeiro AA, Menezes FCH, Rastelli ANS, Bagnato VS, Andrade MF 2010. Influence of light guide tip used in the photo-activation on degree of conversion and hardness of one nanofilled dental composite. Laser Phys 20(12):2050-2055.
153. Rastelli ANS, Jacomassi DP, Bagnato VS 2008. Effect of power densities and irradiation times on the degree of conversion and temperature increase of a microhybrid dental composite resin. Laser Phys 18(9):1074-1079.
154. Ruckebusch C, Duponchel L, Huvenne J-P, Saurina J 2004. Multivariate curve resolution of step-scan FTIR spectral data. Vib Spectrosc 35(1–2):21-26.
155. Lakowicz JR. 2006. Solvent and environmental effects. Principles of fluorescence spectroscopy, ed., Baltimore: Springer US. p 205-235.
156. Keerati-u-rai M, Miriani M, Iametti S, Bonomi F, Corredig M 2012. Structural changes of soy proteins at the oil–water interface studied by fluorescence spectroscopy. Colloids Surfaces B 93(0):41-48.
157. Lakowicz JR. 2006. Time-resolved protein fluorescence. Principles of fluorescence spectroscopy, 3rd ed., Baltimore: Springer p577-606.
158. Vivian J, Callis PR 2001. Mechanisms of tryptophan fluorescence shifts in protein. Biophys J 80:2093-2109.
159. Fearn T, Riccioli C, Garrido-Varo A, Guerrero-Guinel JE 2009. On the geometry of SNV and MSC. Chemom Intell Lab Syst (96):22-26.
160. Militello V, Casarino C, Emanuele A, Giostra A, Pullara F, M. L 2004. Aggregation kinetics of bovine serum albumin studied by FTIR spectroscopy and light scattering. Biophys Chem 107(2):175-187.
161. Lakowicz JR. 2006. Flurophores. Principles of fluorescence spectroscopy, ed.: Springer. p 63-95.
162. Pollard TD 2010. A Guide to Simple and Informative Binding Assays. Mol Biol Cell 21(23):4061-4067.
163. Bloemendal M, Jiskoot W. 2005. Circular dichroism spectrosocopy. Methods for structural analysis of protein pharmaceuticals, ed., Arlington: AAPS. p 83-130.
164. Wishart D. 2005. Nuclear magnetic resonance spectrosocopy. Methods for structural analysis of protein pharmaceuticals, ed., Arlington: AAPS. p 199-244.
165. Staub A, Guillarme D, Schappler J, Veuthey J-L, Rudaz S 2011. Intact protein analysis in the biopharmaceutical field. J Pharmaceut Biomed Anal 55(4):810-822.

166. Reubsaet JLE, Beijnen JH, Bult A, van Maanen RJ, Marchal JAD, Underberg WJM 1998. Analytical techniques used to study the degradation of proteins and peptides: physical instability. J Pharmaceut Biomed Anal 17(6-7):979-984.
167. D'Antonio J, Murphy BM, Manning MC, Al-azzam WA 2012. Comparability of protein therapeutics: Quantitative comparison of second-derivative amide I infrared spectra. J Pharm Sci 101(6):2025-2033.
168. Cauchy M, D'Aoust S, Dawson B, Rode H, Hefford MA 2002 Thermal stability: A means to assure tertiary structure in therapeutic proteins. Biologicals 30:175–185.
169. Byler DM, Susi H 1986. Examination of the secondary structure of proteins by deconvolved FTIR spectra. Biopolymers 25(3):469-487.
170. Rahmelow K, Hübner W 1996. Fourier Self-Deconvolution: Parameter Determination and Analytical Band Shapes. Appl Spectrosc 50(6):795-804.
171. Teska BM, Li C, Winn BC, Arthur KK, Jiang Y, Gabrielson JP 2013. Comparison of quantitative spectral similarity analysis methods for protein higher-order structure confirmation. Anal Biochem 434(1):153-165.
172. Surewicz WK, Mantsch HH, Chapman D 1993. Determination of protein secondary structure by Fourier transform infrared spectroscopy: A critical assessment. Biochemistry 32(2):389-394.
173. Carpenter JF, Prestrelski SJ, Dong A 1998. Application of infrared spectroscopy to development of stable lyophilized protein formulations. Eur J Pharm Biopharm 45(3):231-238.
174. Strachan CJ, Pratiwi D, Gordon KC, Rades T 2004. Quantitative analysis of polymorphic mixtures of carbamazepine by Raman spectroscopy and principal components analysis. J Raman Spectros 35(5):347-352.
175. Zimper U 2010. Quantification of Process Induced Disorder in Milled Samples Using Different Analytical Techniques. Pharmaceutics 2(1):30-49.
176. Michaud F-T, Garnier A, Lemieux L, Duchesne C 2009. Multivariate analysis of single quadrupole LC-MS spectra for routine characterization and quantification of intact proteins. Proteomics 9(3):512-520.
177. Shariati-Rad M, Hasani M 2009. Application of multivariate curve resolution-alternating least squares (MCR-ALS) for secondary structure resolving of proteins. Biochimie 91(7):850-856.
178. Vonhoff S, Condliffe J, Schiffter H 2010. Implementation of an FTIR calibration curve for fast and objective determination of changes in protein secondary structure during formulation development. J Pharmaceut Biomed Anal 51(1):39-45.
179. Everitt B, Hothorn T. 2011. Principal component analysis. An introduction to applied multivariate analysis with R, ed., New York: Springer. p 61-103.
180. Everitt B, Hothorn T. 2011. Multivariate data and multivariate analysis. An introduction to applied multivariate analysis with R, ed., New York: Springer. p 1-24.
181. Everitt B, Hothorn T. 2011. Confirmatory factor analysis and structural equation models. An introduction to applied multivariate analysis with R, ed., New York: Springer. p 201-224.
182. Cribari-Neto F, Zeileis A 2010. Beta Regression in R. J Stat Softw 34(2):1-24.
183. Diggle PJ, Heagerty P, Liang K-Y, Zeger S. 2002. Time-dependent covariates. Analysis of longitudinal data, 2nd ed., Oxford University Press Oxford. p 277.
184. Manning MC, Chou DK, Murphy BM, Payne RW, Katayama DS 2010. Stability of protein pharmaceuticals: An update. Pharm Res 27(4):544-575.
185. Ngarize S, Herman H, Adams A, Howell N 2004. Comparison of Changes in the Secondary Structure of Unheated, Heated, and High-Pressure-Treated β-Lactoglobulin and

Ovalbumin Proteins Using Fourier Transform Raman Spectroscopy and Self-Deconvolution. J Agr Food Chem 52(21):6470-6477.
186. Maury M, Murphy K, Kumar S, Mauerer A, Lee G 2005. Spray-drying of proteins: effects of sorbitol and trehalose on aggregation and FT-IR amide I spectrum of an immunoglobulin G. Eur J Pharm Biopharm 59(2):251-261.
187. Martens H, Næs T 1984. Multivariate calibration. I. Concepts and distinctions. Trac-Trend Anal Chem 3(8):204-210.
188. Rahmelow K, Hübner W 1996. Secondary structure determination of proteins in aqueous solution by infrared spectroscopy: a comparison of multivariate data analysis methods. Anal Biochem 241(1):5-13.
189. Meng Y, Yao C, Xue S, Yang H 2014. Application of Fourier transform infrared (FT-IR) spectroscopy in determination of microalgal compositions. Bioresource Technol 151(0):347-354.
190. Cui C-J, Cai W-S, Shao X-G 2013. Near-infrared diffuse reflectance spectroscopy with sample spots and chemometrics for fast determination of bovine serum albumin in micro-volume samples. Chinese Chem Lett 24(1):67-69.
191. Garcia-Garcia JL, Perez-Guaita D, Ventura-Gayete J, Garrigues S, de la Guardia M 2014. Determination of biochemical parameters in human serum by near-infrared spectroscopy. Anal Method 6(12):3982-3989.
192. Adams MJ. 1995. Descriptive statistics. Chemometrics in analytical spectroscopy, 1st ed., Cambridge: The Royal Society of Chemistry. p 13-14.
193. Wright J. 2008. Overview of protein formulation and delivery. Protein Formulation and Delivery, 175 ed., New York: Informa Healtcare USA, Inc. p 3.
194. Hawe A, Wiggenhorn M, van de Weert M, Garbe JHO, Mahler H-c, Jiskoot W 2012. Forced degradation of therapeutic proteins. J Pharm Sci 101(3):895-913.
195. Demeule B, Lawrence MJ, Drake AF, Gurny R, Arvinte T 2007. Characterization of protein aggregation: The case of a therapeutic immunoglobulin. Biochim Biophys Acta 1774(1):146-153.
196. Gottlieb DM, Schultz J, Bruun SW, Jacobsen S, Søndergaard I 2004. Multivariate approaches in plant science. Phytochemistry 65(11):1531-1548.
197. Minh David DL, Makowski L 2013. Wide-Angle X-Ray Solution Scattering for Protein-Ligand Binding: Multivariate Curve Resolution with Bayesian Confidence Intervals. Biophys J 104(4):873-883.
198. A. Bos M, van Vliet T 2001. Interfacial rheological properties of adsorbed protein layers and surfactants: a review. Adv Colloid Interface Sci 91(3):437-471.
199. Pinholt C. 2011. Influence of PEGylation, acylation and glycosilation on the adsorption behaviour of pharmaceutical proteins at solid-liquid interfaces. Department of Pharmaceutics and Analytical Chemistry, Faculty of Pharmaceutical Science, ed., Denmark: University of Copenhagen. p 281.
200. Burgess DJ, Sahin NO 1997. Interfacial Rheological and Tension Properties of Protein Films. J Colloid Interface Sci 189(1):74-82.
201. Liu L, Qi W, Schwartz DK, Randolph TW, Carpenter JF 2013. The effects of excipients on protein aggregation during agitation: An interfacial shear rheology study. J Pharm Sci 102(8):2460–2470.
202. Cox WP, Merz EH 1958. Correlation of dynamic and steady flow viscosities. J Polym Sci, Part A: Polym Chem 28(118):619-622.
203. Kim C, Yoo B 2006. Rheological properties of rice starch–xanthan gum mixtures. J Food Eng 75(1):120-128.
204. Song K-W, Kuk H-Y, Chang G-S 2006. Rheology of concentrated xanthan gum solutions: Oscillatory shear flow behavior. Korea-Aust Rheol J 18(2):67-81.

205. Li S-P, Zhao G, Chen H-Y 2005. The Relationship between Steady Shear Viscosity and Complex Viscosity. J Dispersion Sci Technol 26(4):415-419.
206. Vandebril S, Franck A, Fuller G, Moldenaers P, Vermant J 2010. A double wall-ring geometry for interfacial shear rheometry. Rheol Acta 49(2):131-144.
207. Macosko CW. 1994. Linear viscoelasticity. Rheology: Principles, measurements and applications, ed., New York: VCH Publishers Inc. p 109-125.
208. Drelich J, Fang C, White CL. 2002. Measurement of interfacial tension in fluid-fluid systems. In Hubbard AT, editor Encyclopedia of Surface and Colloid Science, ed., New York: Marcel Dekker, Inc. p 3152-3166.
209. Freer EM, Yim KS, Fuller GG, Radke CJ 2004. Shear and Dilatational Relaxation Mechanisms of Globular and Flexible Proteins at the Hexadecane/Water Interface. Langmuir 20(23):10159-10167.
210. Small DM, Wang L, Mitsche MA 2009. The adsorption of biological peptides and proteins at the oil/water interface. A potentially important but largely unexplored field. J Lipid Res 50(Supplement):S329-S334.
211. Joubert MK, Luo Q, Nashed-Samuel Y, Wypych J, Narhi LO 2011. Classification and Characterization of Therapeutic Antibody Aggregates. J Biol Chem 286(28):25118-25133.
212. Damodaran S, Razumovsky L 2008. Role of surface area-to-volume ratio in protein adsorption at the air–water interface. Surf Sci 602(1):307-315.
213. Marsh JA 2013. Buried and Accessible Surface Area Control Intrinsic Protein Flexibility. J Mol Biol 425(17):3250-3263.
214. Pace CN, Alston RW, Shaw KL 2000. Charge-charge interactions influence the denatured state ensemble and contribute to protein stability. Protein Sci 9(7):1395-1398.
215. Winzor DJ 2004. Determination of the net charge (valence) of a protein: a fundamental but elusive parameter. Anal Biochem 325:1-20.
216. Wahlgren M, Arnebrant T 1991. Protein adsorption to solid surfaces. Trends Biotechnol 9(1):201-208.
217. Dickinson E 1999. Adsorbed protein layers at fluid interfaces: interactions, structure and surface rheology. Colloids Surfaces B 15(2):161-176.
218. Ramsden JJ 1995. Puzzles and paradoxes in protein adsorption. Chem Soc Rev 24(1):73-78.
219. Jeyachandran YL, Mielczarski BR, Mielczarski JA 2009. Quantitative and qualitative evaluation of adsorption/desorption of bovine serum albumin on hydrophilic and hydrophobic surfaces. Langmuir 25(19):11614-11620.
220. Conover WJ. 1999. Practical nonparametric statistics 3rd ed., New York: John Wiley & Sons.
221. Malzert-Fréon A, Benoît J-P, Boury F 2008. Interactions between poly(ethylene glycol) and protein in dichloromethane/water emulsions: A study of interfacial properties. Eur J Pharm Biopharm 69(3):835-843.
222. Kamerzell TJ, Esfandiary R, Joshi SB, Middaugh CR, Volkin DB 2011. Protein–excipient interactions: Mechanisms and biophysical characterization applied to protein formulation development. Adv Drug Deliv Rev 63(13):1118-1159.
223. Ludwig DB, Carpenter JF, Hamel J-B, Randolph TW 2010. Protein adsorption and excipient effects on kinetic stability of silicone oil emulsions. J Pharm Sci 99(4):1721-1733.
224. He Q, Zhang Y, Lu G, Miller R, Möhwald H, Li J 2008. Dynamic adsorption and characterization of phospholipid and mixed phospholipid/protein layers at liquid/liquid interfaces. Adv Colloid Interface Sci 140(2):67-76.
225. Mizuno NK, Smaby JM, Cunningham BA, Momsen MM, Brockman HL 2002. Phospholipid−Diacylglycerol complexes regulate colipase adsorption to monolayers. Langmuir 19(5):1802-1808.

226. Svitova TF, Wetherbee MJ, Radke CJ 2003. Dynamic of surfactant sorption at the air-water interface: continuos-flow tensiometry. J Colloid Interf Sci (261):170-179.
227. Fainerman VB, Miller R, Ferri JK, Watzke H, Leser ME, Michel M 2006. Reversibility and irreversibility of adsorption of surfactants and proteins at liquid interfaces. Adv Colloid Interface Sci 123–126(0):163-171.
228. Kotsmar C, Pradines V, Alahverdjieva VS, Aksenenko EV, Fainerman VB, Kovalchuk VI, Krägel J, Leser ME, Noskov BA, Miller R 2009. Thermodynamics, adsorption kinetics and rheology of mixed protein–surfactant interfacial layers. Adv Colloid Interface Sci 150(1):41-54.
229. Dan A, Kotsmar C, Ferri JK, Javadi A, Karbaschi M, Kragel J, Wustneck R, Miller R 2012. Mixed protein-surfactant adsorption layers formed in a sequential and simultaneous way at water-air and water-oil interfaces. Soft Matter 8(22):6057-6065.
230. Harada A, Kataoka K 2006. Supramolecular assemblies of block copolymers in aqueous media as nanocontainers relevant to biological applications. Prog Polym Sci 31(11):949-982.
231. Gunning PA, Mackie AR, Gunning AP, Wilde PJ, Woodward NC, Morris VJ 2004. The effect of surfactant type on protein displacement from the air–water interface. Food Hydrocolloid 18(3):509-515.
232. Mackie AR, Gunning AP, Wilde PJ, Morris VJ 1999. Orogenic Displacement of Protein from the Air/Water Interface by Competitive Adsorption. J Colloid Interf Sci 210(1):157-166.
233. Mackie AR, Gunning AP, Ridout MJ, Wilde PJ, Morris VJ 2001. Orogenic Displacement in Mixed β-Lactoglobulin/β-Casein Films at the Air/Water Interface. Langmuir 17(21):6593-6598.
234. Miller R, Fainerman VB, Makievski AV, Krägel J, Grigoriev DO, Kazakov VN, Sinyachenko OV 2000. Dynamics of protein and mixed protein/surfactant adsorption layers at the water/fluid interface. Adv Colloid Interface Sci 86(1–2):39-82.
235. Rippner Blomqvist B, Ridout MJ, Mackie AR, Wärnheim T, Claesson PM, Wilde P 2004. Disruption of Viscoelastic β-Lactoglobulin Surface Layers at the Air−Water Interface by Nonionic Polymeric Surfactants. Langmuir 20(23):10150-10158.
236. Dickinson E 1998. Proteins at interfaces and in emulsions Stability, rheology and interactions. J Chem Soc 94(12):1657-1669.
237. Alhoranta AM, Lehtinen JK, Urtti AO, Butcher SJ, Aseyev VO, Tenhu HJ 2011. Cationic Amphiphilic Star and Linear Block Copolymers: Synthesis, Self-Assembly, and in Vitro Gene Transfection. Biomacromolecules 12(9):3213-3222.
238. Lu DR, Lee SJ, Park K 1992. Calculation of solvation interaction energies for protein adsorption on polymer surfaces. J Biomat Sci-Polym E 3(2):127-147.
239. Tantipolphan R, Rades T, McQuillan AJ, Medlicott NJ 2007. Adsorption of bovine serum albumin (BSA) onto lecithin studied by attenuated total reflectance Fourier transform infrared (ATR-FTIR) spectroscopy. Int J Pharm 337(1-2):40-47.
240. Kadir F, Ives P, Luitjens A, van Corven E. 2013. Production and purification of recombinant proteins. Pharmaceutical biotechnology: fundamentals and applications, ed., New York: Springer. p 47-68.
241. Stenekes RJH, Loebis AE, Fernandes CM, Crommelin DJA, Hennink WE 2001. Degradable dextran microspheres for controlled release of liposomes. Int J Pharm:17-20.
242. Torchilin V 2005. Recent advances with liposomes as pharmaceutical carriers. Nat Rev Drug Discov 4:145-160.
243. Hirai M, Sato S, Kimura R, Hagiwara Y, Kawai-Hirai R, Ohta N, Igarashi N, Shimizu N 2015. Effect of protein encapsulation on thermal structural stability of liposome composed of glycosphingolipid/cholesterol/pospholipid. J Phys Chem B 119:3398-3406.

244. Walker RA, Conboy JC, Richmond GL 1997. Molecular Structure and Ordering of Phospholipids at a Liquid-Liquid Interface. Langmuir 13:3070-3073.
245. Pan J, Heberle FA, Tristram-Nagle S, Szymanski M, Koepfinger M, Katsaras J, Kučerka N 2012. Molecular structures of fluid phase phosphatidylglycerol bilayers as determined by small angle neutron and X-ray scattering. Biochim Biophys Acta 1818(9):2135-2148.
246. Nzai JM, Proctor A 1998. Determination of phospholipids in vegetable oil by fourier transform infrared spectroscopy. J Amer Oil Chem Soc 75(10):1281-1289.
247. Murray BS, Dickinson E 1996. Interfacial rheology and the dynamic properties of adsorbed films of food proteins and surfactants. Food Sci Technol Int 2(3):131-145.
248. Smart T, Lomas H, Massignani M, Flores-Merino MV, Perez LR, Battaglia G 2008. Block copolymer nanostructures. Nano Today 3(3–4):38-46.
249. Harada A, Kataoka K 2001. Pronounced activity of enzymes through the incorporation into the core of polyion complex micelles made from charged block copolymers. J Control Release 72(1–3):85-91.
250. Zhang C, Maric M 2011. Synthesis of Stimuli-responsive, Water-soluble Poly[2-(dimethylamino)ethyl methacrylate/styrene] Statistical Copolymers by Nitroxide Mediated Polymerization. Polymers 3:1398-1422.
251. Demeester J, De Smedt SS, Sanders NN, Haustraete J. 2005. Light scattering. Methods for structural analysis of protein pharmaceuticals ed., Arlington: AAPS. p 245-275.
252. Romero A, Verwijlen T, Guerrero A, Vermant J 2013. Interfacial behaviour of crayfish protein isolate. Food Hydrocolloid 30(1):470-476.
253. Barman S, Christopher GF 2014. Simultaneous Interfacial Rheology and Microstructure Measurement of Densely Aggregated Particle Laden Interfaces Using a Modified Double Wall Ring Interfacial Rheometer. Langmuir 30(32):9752-9760.
254. Pinholt C, Hostrup S, Bukrinsky JT, Frokjaer S, Jorgensen L 2011. Influence of acylation on the adsorption of insulin to hydrophobic surfaces. Pharm Res (28):1031-1040.
255. Wang J-M, Xia N, Yang X-Q, Yin S-W, Qi J-R, He X-T, Yuan D-B, Wang L-J 2012. Adsorption and Dilatational Rheology of Heat-Treated Soy Protein at the Oil–Water Interface: Relationship to Structural Properties. J Agr Food Chem 60(12):3302-3310.
256. Cámara CI, Yudi LM 2013. Potential-mediated interaction between dextran sulfate and negatively charged phospholipids films at air/water and liquid/liquid interfaces. Electrochim Acta 113(0):644-652.
257. Lucassen-Reynders EH, Benjamins J, Fainerman VB 2010. Dilational rheology of protein films adsorbed at fluid interfaces. Curr Opin Colloid In 15(4):264-270.
258. Murray BS, Ventura A, Lallemant C 1998. Dilatational rheology of protein+non-ionic surfactant films at air–water and oil–water interfaces. Colloids Surfaces A 143(2–3):211-219.
259. Liu L, Zhao Q, Liu T, Zhao M 2011. Dynamic surface pressure and dilatational viscoelasticity of sodium caseinate/xanthan gum mixtures at the oil–water interface. Food Hydrocolloid 25(5):921-927.
260. Mezzenga R, Fischer P 2013. The self-assembly, aggregation and phase transitions of food protein systems in one, two and three dimensions. Rep Prog Phys 76(4):43.
261. Kull T, Nylander T, Tiberg F, Wahlgren NM 1997. Effect of Surface Properties and Added Electrolyte on the Structure of β-Casein Layers Adsorbed at the Solid/Aqueous Interface. Langmuir 13(19):5141-5147.
262. Croguennec T, Renault A, Beaufils S, Dubois J-J, Pezennec S 2007. Interfacial properties of heat-treated ovalbumin. J Colloid Interf Sci 315(2):627-636.

263. Benjamins J-W, Jönsson B, Thuresson K, Nylander T 2002. New experimental setup to use ellipsometry to study liquid-liquid and liquid-solid interfaces. Langmuir 18(16):6437-6444.
264. Persaud DR, Barranco-Mendoza A 2004. Bovine serum albumin and insulin-dependent diabetes mellitus: is cow's milk still a possible toxicological causative agent of diabetes? Food Chem Toxicol 42(5):707-714.
265. Marconi E, Panfili G, Bruschi L, Vivanti V, Pizzoferrato L 1995. Comparative study on microwave and conventional methods for protein hydrolysis in food. Amino Acids 8(2):201-208.

APPENDIX A: The primary structure of BSA [264,265].

Arg-Thr-His-Lys-Ser-Glu-Ile-Ala-His-Arg-Phe-Lys-Asp-Leu-Gly-Glu-Glu-His-Phe-Lys[20]-
Gly-Leu-Val-Leu-Ile-Ala-Phe-Ser-Gln-Tyr-Leu-Gln-Gln-Cys-Pro-Phe-Asp-Glu-His-Val[40]-
Lys-Leu-Val-Asn-Glu-Leu-Thr-Glu-Phe-Ala-Lys-Thr-Cys-Val-Ala-Asp-Glu-Ser-His-Ala[60]-
Gly-Cys-Glu-Lys-Ser-Leu-His-Thr-Leu-Phe-Gly-Asp-Glu-Leu-Cys-Lys-Val-Ala-Ser-Leu[80]-
Arg-Glu-Thr-Tyr-Gly-Asp-Met-Ala-Asp-Cys-Cys-Glu-Lys-Glu-Gln-Pro-Glu-Arg-Asn-Glu[100]-
Cys-Phe-Leu-Ser-His-Lys-Asp-Asp-Ser-Pro-Asp-Leu-Pro-Lys-Leu-Lys-Pro-Asp-Pro-Asn[120]-
Thr-Leu-Cys-Asp-Glu-Phe-Lys-Ala-Asp-Glu-Lys-Lys-Phe-Trp-Gly-Lys-Try-Leu-Tyr-Glu[140]-
Ile-Ala-Arg-Arg-His-Pro-Tyr-Phe-Tyr-Ala-Pro-Glu-Leu-Leu-Tyr-Ala-Asn-Lys-Tyr-Asn[160]-
Gly-Val-Phe-Gln-Glu-Cys-Cys-Gln-Ala-Glu-Asp-Lys-Gly-Ala-Cys-Leu-Leu-Pro-Lys-Ile[180]-
Glu-Thr-Met-Arg-Glu-Lys-Val-Leu-Thr-Ser-Ser-Ala-Arg-Gln-Arg-Leu-Arg-Cys-Ala-Ser[200]-
Ile-Gln-Lys-Phe-Gly-Glu-Arg-Ala-Leu-Lys-Ala-Trp-Ser-Val-Ala-Arg-Leu-Ser-Gln-Lys[220]-
Phe-Pro-Lys-Ala-Glu-Phe-Val-Glu-Val-Thr-Lys-Leu-Val-Thr-Asp-Leu-Thr-Lys-Val-His[240]-
Lys-Glu-Cys-Cys-His-Gly-Asp-Leu-Leu-Glu-Cys-Ala-Asp-Asp-Arg-Ala-Asp-Leu-Ala-Lys[260]-
Try-Ile-Cys-Asx-Asx-Glx-Asx-Thr-Ile-Ser-Ser-Lys-Leu-Lys-Glu-Cys-Lys-Asp-Pro-Cys[280]-
Leu-Leu-Glu-Lys-Ser-His-Cys-Ile-Ala-Glu-Val-Glu-Lys-Asp-Ala-Ile-Pro-Glu-Asp-Leu[300]-
Pro-Pro-Leu-Thr-Ala-Asp-Phe-Ala-Glu-Asp-Lys-Asp-Val-Cys-Lys-Asn-Tyr-Gln-Glu-Ala[320]-
Lys-Asp-Ala-Phe-Leu-Gly-Ser-Phe-Leu-Tyr-Glu-Tyr-Ser-Arg-Arg-His-Pro-Glu-Tyr-Ala[340]-
Val-Ser-Val-Leu-Leu-Arg-Leu-Ala-Lys-Glu-Tyr-Glu-Ala-Thr-Leu-Glu-Glu-Cys-Cys-Ala[360]-
Lys-Asp-Asp-Pro-His-Ala-Cys-Tyr-Thr-SerVal-Phe-Asp-Lys-Leu-Lys-His-Leu-Val-Asp[380]-
Glu-Pro-Gln-Asn-Leu-Ile-Lys-Gln-Asn-Cys-Asp-Gln-Phe-Glu-Lys-Leu-Gly-Glu-Tyr-Gly[400]-
Phe-Gln-Asn-Ala-Leu-Ile-Val-Arg-Tyr-Thr-Arg-Lys-Val-Pro-Gln-Val-Ser-Thr-Pro-Thr[420]-
Leu-Val-Glu-Val-Ser-Arg-Ser-Leu-Gly-Lys-Val-Gly-Thr-Arg-Cys-Cys-Thr-Lys-Pro-Glu[440]-
Ser-Glu-Arg-Met-Pro-Cys-Thr-Glu-Asp-Tyr-Leu-Ser-Leu-Ile-Leu-Asn-Arg-Leu-Cys-Val[460]-
Leu-His-Glu-Lys-Thr-Pro-Val-Ser-Glu-Lys-Val-Thr-Lys-Cys-Cys-Thr-Glu-Ser-Leu-Val[480]-
Asn-Arg-Arg-Pro-Cys-Phe-Ser-Ala-Leu-Thr-Pro-Asp-Glu-Thr-Tyr-Val-Pro-Lys-Ala-Phe[500]-
Asp-Glu-Lys-Leu-Phe-Thr-Phe-His-Ala-Asp-Ile-Cys-Thr-Leu-Pro-Asp-Thr-Glu-Lys-Gln[520]-
Ile-Lys-Lys-Gln-Thr-Ala-Leu-Val-Glu-Leu-Leu-Lys-His-Lys-Pro-Lys-Ala-Thr-Glu-Glu-[540]-
Gln-Leu-Lys-Thr-Val-Met-Glu-Asn-Phe-Val-Ala-Phe-Val-Asp-Lys-Cys-Cys-Ala-Ala-Asp[560]-
Asp-Lys-Glu-Ala-Cys-Phe-Ala-Val-Glu-Gly-Pro-Lys-Leu-Val-Val-Ser-Thr-Gln-Thr-Ala[580]-
Leu-Ala[582]

APPENDIX B.1: Spectra of amide I band of BSA (5% w/w) showing the stability study (RT) of native BSA (A), 50% w/w native BSA (B) and heat-denatured BSA (C) at day one (straight line) and seven (dashed line). Spectra of amide I were pre-processed using BC and AN.

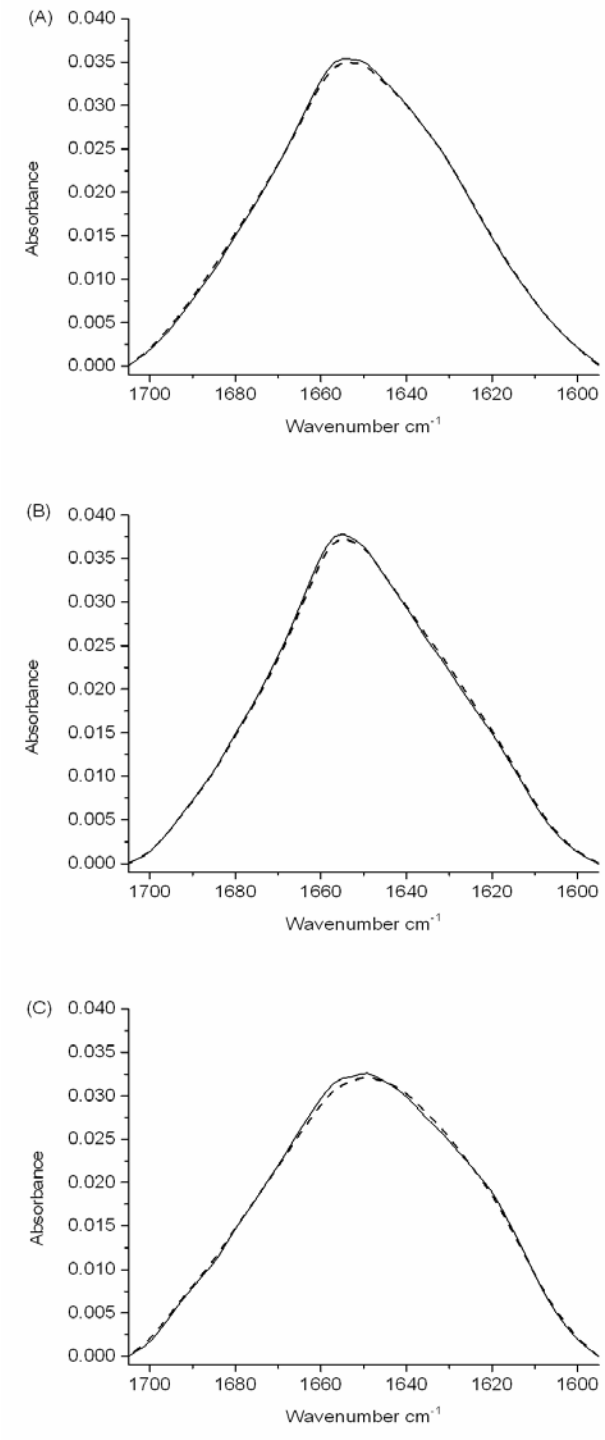

APPENDIX B.2: The table shows the value of area overlap between native BSA and binary mixtures of BSA (5% w/w) (mean ± s.d.) (n=3).

Native BSA concentration	R1	R2	R3	Mean	S.D.
50% w/w	0.816	0.800	0.839	0.818	0.020
60% w/w	0.860	0.856	0.864	0.860	0.004
70% w/w	0.857	0.860	0.889	0.869	0.020
80% w/w	0.920	0.927	0.919	0.922	0.004
90% w/w	0.963	0.970	0.977	0.969	0.007
100% w/w	1.000	1.000	1.000	1.000	6.1×10^{-5}

APPENDIX B.3: Figure represents the linear fit between the area overlap (%) and native BSA concentration of binary mixtures (5% w/w) (mean ± s.d.) (n=3).

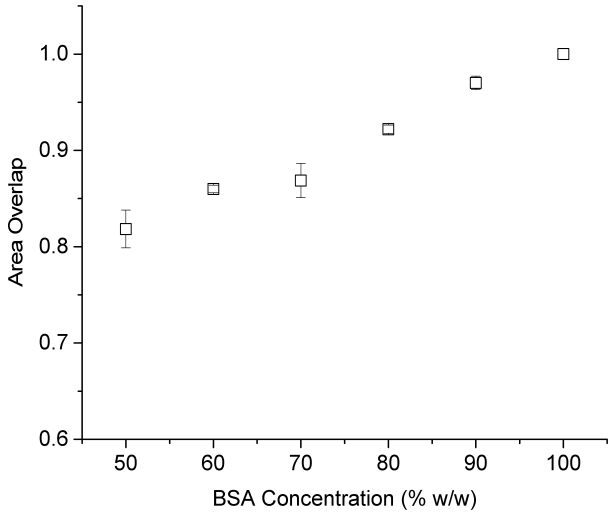

APPENDIX B.4: Figure represents the linear fit between fluorescence intensity and concentration of binary mixtures of BSA (1% w/w) (mean ± s.d.) (n=3).

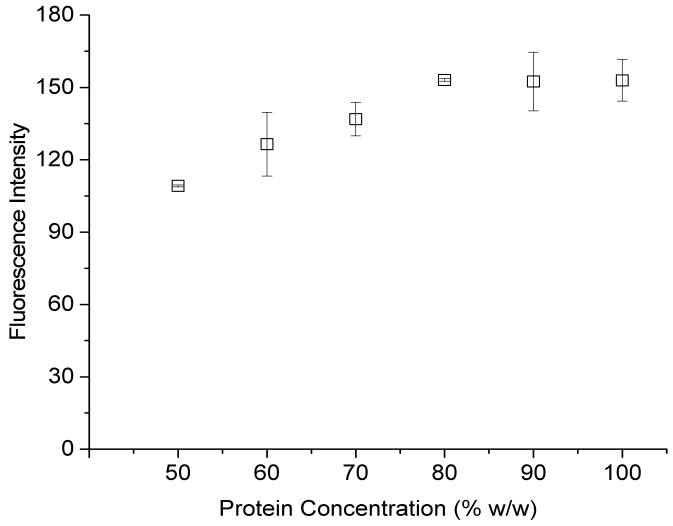

APPENDIX C: Friedman's test results for interfacial rheology measurements ((A) time to cross-over, (B) elastic (G') modulus, (C) oscillation torque for G" modulus and (D) power law exponent).

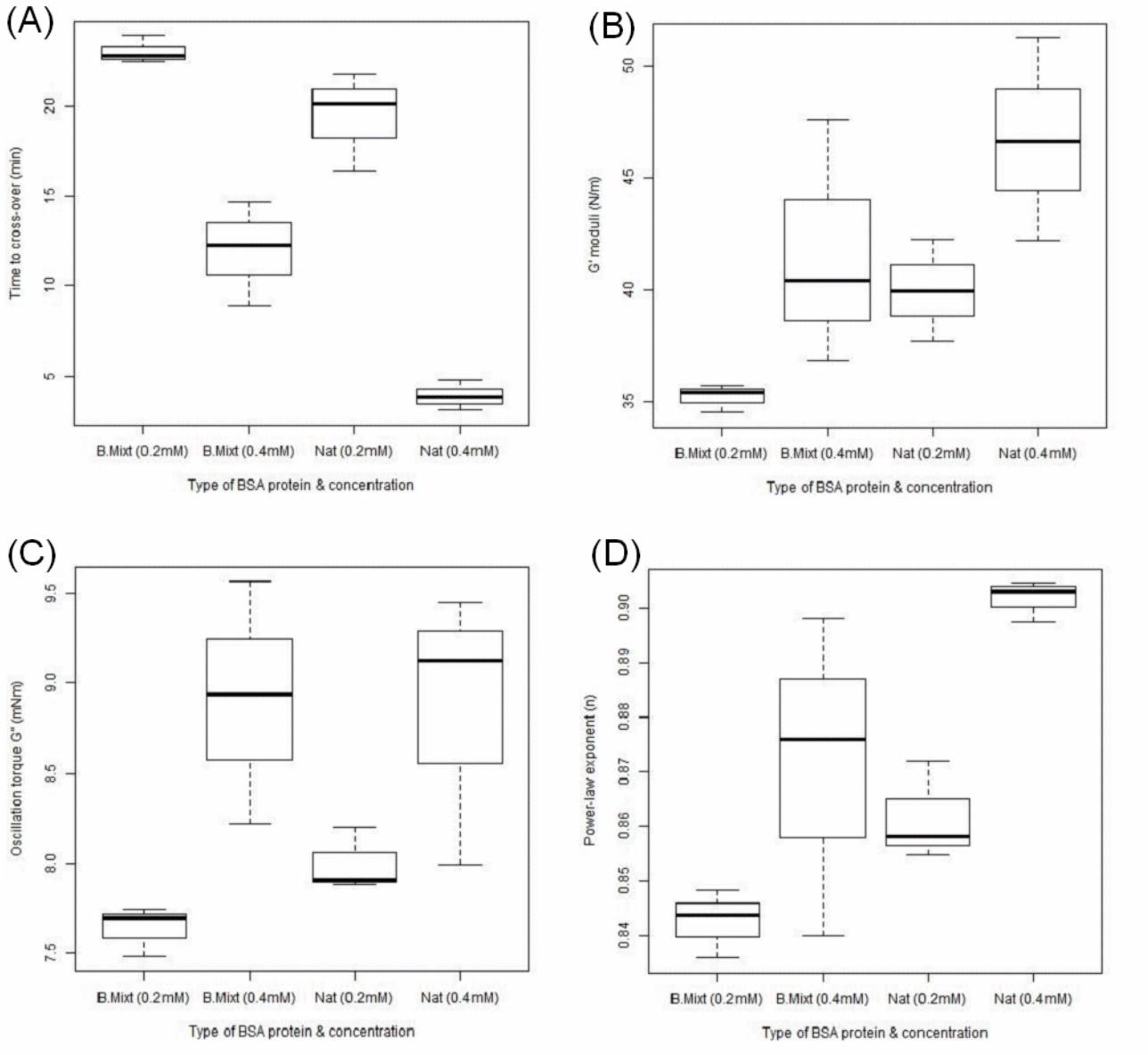

APPENDIX D: Friedman's test results for IFT measurements ((A) IFT_{30} and (B) initial slope).

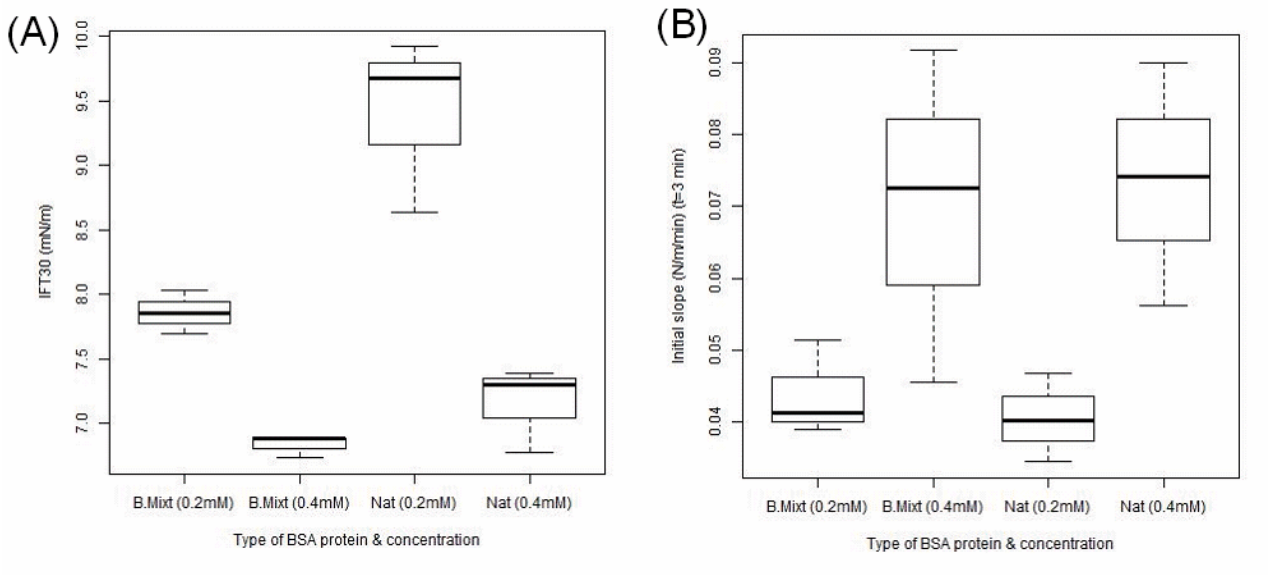

APPENDIX E: Plot of the complex viscosity (in Ns/m) vs. frequency (in rad/sec) for native BSA 0.5 mM alone after two hours of protein adsorption to the oil water interface. Slope corresponds to the power law exponent which was -0.812 ± 0.010 (mean ± s.d). Complex viscosity and frequency are in logarithmic scales.

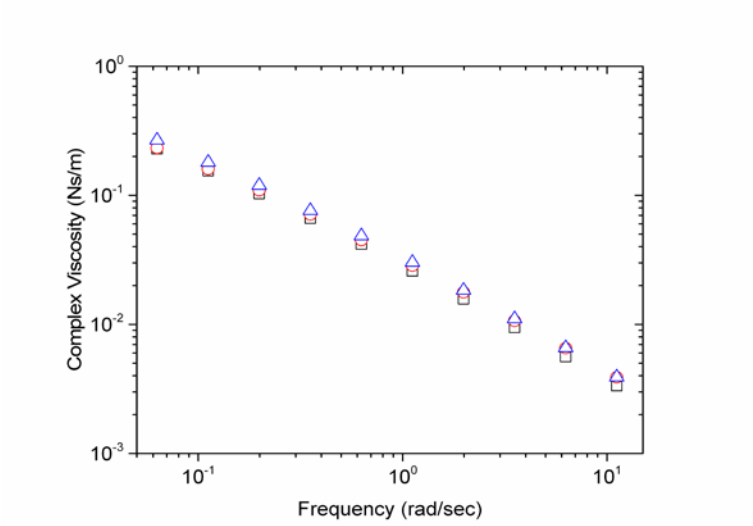

APPENDIX F: Typical example of elastic G' (solid symbols) and viscous G" (open symbols) moduli as a function of time for the oil and water interface (without protein). G' and G" moduli are in logarithmic scale.